# IDENTIFICATION AND CORRELATION OF THINLY BEDDED LATE QUATERNARY TEPHRAS OF COROMANDEL PENINSULA, NEW ZEALAND

by

A. G. Hogg

Thesis for the degree of

Doctor of Philosophy

in

Earth Sciences

University of Waikato

March, 1979

To Jacqueline

# ABSTRACT

The Coromandel Peninsula of North Island, New Zealand is covered by up to 2.5 m of thinly bedded Late Quaternary tephras. On the basis of their field characteristics, the tephras are divided into five field classes: the Recent bed (field class I) - a black, friable sandy loam; the Pumiceous bed (field class II) - reddish brown coarse lapilli and ash; the Silty bed (field class III) - a yellowish brown silt loam; the Lumpy bed (field class IV) - a brown sandy loam; and the Shower-bedded class (field class V) - shower bedded and massive sands and loamy sands.

The properties of the field classes were examined at 17 stratigraphic sections on the peninsula and indicate that classes I to IV each contain a mixture of at least two tephras. Individual tephras were characterised in the laboratory by multicomponent methods of analysis (particle size parameters, mineral assemblages), single component methods of analysis (chemical analysis of titanomagnetites by XRF), and single particle methods of analysis (microprobe analysis of titanomagnetite grains).

The Recent bed is composed of at least three tephras, including the Kaharoa Tephra (930 yrs B.P.), Taupo Pumice (1,819 yrs B.P.), and the fine upper portion of the Whangamata Tephra (6,280 yrs B.P.). The Pumiceous bed contains a thorough mixture of the coarser, basal component of the Whangamata Tephra and the finer grained Mamaku Ash (7,050 yrs B.P.) and Rotoma Ash (c. 9,000 yrs B.P.). The Silty bed, Lumpy bed and Shower-bedded class all contain a common tephra, the

Rotoehu Ash (41,700 yrs B.P.). The Shower-bedded class consists of pure Rotoehu Ash; the Lumpy bed is a composite of the upper part of the Rotoehu Ash and the Hauparu Tephra (30,000-40,000 yrs B.P.); the Silty bed is also a composite, but contains in addition to the upper part of the Rotoehu Ash and Hauparu Tephra, some unidentified hypersthene-bearing tephras of 20,000-11,000 yrs B.P. age, named "X" tephras.

The Whangamata Tephra Formation (symbol Wg) is dated at 6,280 $\pm$ 70 yrs B.P. (Wk 106), and is a brown, graded tephra deposited in two lobes, a coarse lobe of pumiceous ash and lapilli, up to 60 cm thick, extending between Whangamata and Thames on the Coromandel Peninsula, and a fine ash lobe, less than 10 cm in thickness, extending to the south and southwest of the Peninsula, in the Bay of Plenty and Waikato regions. The pumiceous lapilli have a peralkaline mineralogy with phenocrysts of anorthoclase, quartz, aegirine, cossyrite, olivine, riebeckite, and tuhualite, which identifies Mayor Island as the source volcano for the tephra.

It is suggested that the processes that have mixed the "X", Hauparu and Rotoehu tephras in the Katikati region (latitude 37° 30'S) are related to the vegetation pattern in the Late Otiran when the tephras became mixed under a forest cover north of about latitude 37° 30'S, but remained unmixed under scrubland south of this latitude, in the Katikati-Tauranga area.

# CONTENTS

# FIGURE CAPTIONS

Page

Page

CHAPTER 4

Page

# TABLE CAPTIONS

# ACKNOWLEDGEMENTS

I am particularly grateful to Professor J.D. McCraw, Earth Sciences Department, University of Waikato, for his guidance in all parts of this study and for his constructive criticism of the script.

Many people have been associated with the project. In particular, thanks are due to members of staff of the University of Waikato: Prof. H.S. Gibbs, Drs M.J. Selby, C.S. Nelson, and R.M. Briggs, for reviewing the manuscript; to Dr R.M. Briggs for his instruction in the use of the U-stage; to Dr C.K. Beltz for operating the SEM and Electron microprobe during analysis of titanomagnetite grains; to fellow students Messrs P. King and D. Lowe for their assistance and enthusiasm; to Dr W.A. Pullar, Soil Bureau, Rotorua for assistance in establishing the stratigraphic columns between Rotorua and Te Puke; and to Mr J. Boubee for supplying the Lake Mangahia sediment core. The author wishes to thank Mrs M. Henrickson for her excellent typing and Mr B. Fargher for printing the B and W photographs. Financial assistance was provided by a University Grants Committee Scholarship, together with a teaching fellowship for part of the time.

Finally, I am specially indebted to my fiancee Jacqueline, and my parents for their help, tolerance and encouragement in completing this study.

# CHAPTER 1

## INTRODUCTION

Early tephrostratigraphic studies were largely directed towards deposits consisting of individual tephras that could be identified and correlated over large distances by field mapping. The earliest work was carried out using field evidence such as colour and structure, the presence of paleosols or chalazoidites, or grain size and bedding characteristics (Baumgart 1954; Healy 1964; Vucetich and Pullar 1964, 1969). Later studies, also of individual tephras, have utilised tephra component properties, particularly ferromagnesian mineral assemblages, volcanic glass refractive indices and titanomagnetite and glass compositions to aid in correlating sites where field correlation is difficult or impossible (Cole 1970; Kohn 1970; Kittleman 1973; Rankin 1973; Howorth 1976; Westgate and Fulton 1975; Pullar et al. 1977; Kohn and Glasby 1978). As the mapping of major tephra units has proceeded, attention has turned to the deposits that are at the margins of the distributions shown on maps. At these large distances from the source, individual tephras are too thin to be preserved in the stratigraphic column as a unique tephra but tend to be incorporated into the deposit above or below. Some recent investigations have therefore been directed to the identification of components from deposits containing mixtures of tephras (Hodder and Wilson 1976; Hodder 1978).

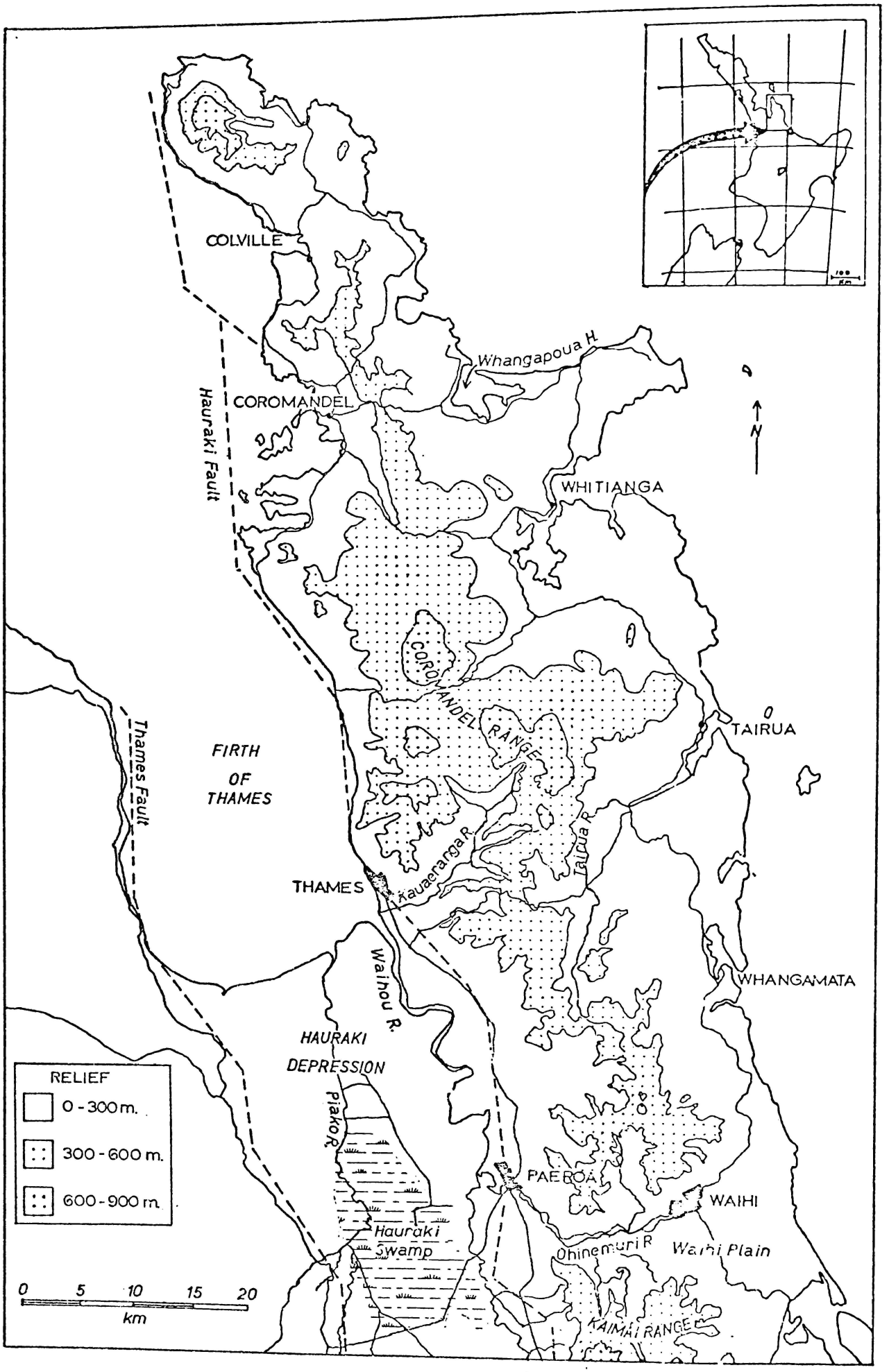


FIGURE 1.1 : Physiographic features of the Coromandel Peninsula

During the Holocene and Late Pleistocene the surface of the Coromandel Peninsula was mantled with a blanket of tephra, ranging in thickness from approximately two metres in the south to one metre in the north, of which only remnants now remain. The purpose of this thesis is to establish the stratigraphy and distribution of these thinly-bedded deposits and to devise suitable laboratory methods for use in characterising mixtures of tephras.

The area of study is the whole of the Coromandel Peninsula in the North Island of New Zealand (Fig. 1.1 inset). Although stratigraphic sections have been examined as far south as Rotorua, the region of principal interest is that bounded to the west by the Waihou River and to the south by the Kaimai Range (Fig. 1.1).

Physiographically, the entire region is dominated by the bush covered Coromandel Range whose peaks reach almost 900 m in the central part of the Peninsula. North of Thames, the west coast of the Peninsula is a steep-faced scarp which approximates the line of the Hauraki Fault. South of Thames, the fault separates the Coromandel Range from the Holocene fluviatile sediments and peats of the Hauraki Depression. Land of easy relief is largely confined to areas around the harbours of Whangapoua and Whitianga and the alluvial plains of the Tairua, Kauaeranga and Ohinemuri Rivers.

## Geological Setting

The basement rocks of the Coromandel Peninsula are indurated Jurassic sandstones and siltstones which have been subsequently

uplifted and deformed and overlain by Lower Oligocene sandstones, conglomerates, siltstones and limestones (Skinner 1976). Early Miocene times saw the onset of an extensive andesite-dacite-rhyolite eruptive period which lasted some 20 million years ending as late as the Early Pleistocene in some places. Although Late Pleistocene (? Holocene) vents have been located on the Peninsula (Dr D.N.B. Skinner, pers.comm.), no associated tephra has yet been identified.

Known possible sources for the tephras under study are shown in Fig. 1.2 and include the Tongariro, Taupo, Maroa, Okataina, Mayor Island and Auckland Volcanic Centres. Published information about tephras erupted from these vents is summarised in Table 1.1. Each of the tephras identified in this thesis is later deduced to have a source in the Okataina, Taupo or Mayor Island Volcanic Centres.

## Previous Work

Initial research into New Zealand's tephra cover began in the 1930's when the Soil Survey Section of Geological Survey undertook reconnaissance soil mapping which detailed the main soil forming tephras (Grange 1931; Taylor 1933). Investigations into the volcanic ash mantle have since been continued by Soil Bureau, Geological Survey and Waikato, Massey and Victoria Universities.

Descriptions of the tephra cover of the Coromandel region were first published by Taylor (1953) who recorded the distribution of Whangamata and Waihi Ashes (Fig. 1.3). He described the younger Whangamata Ash:

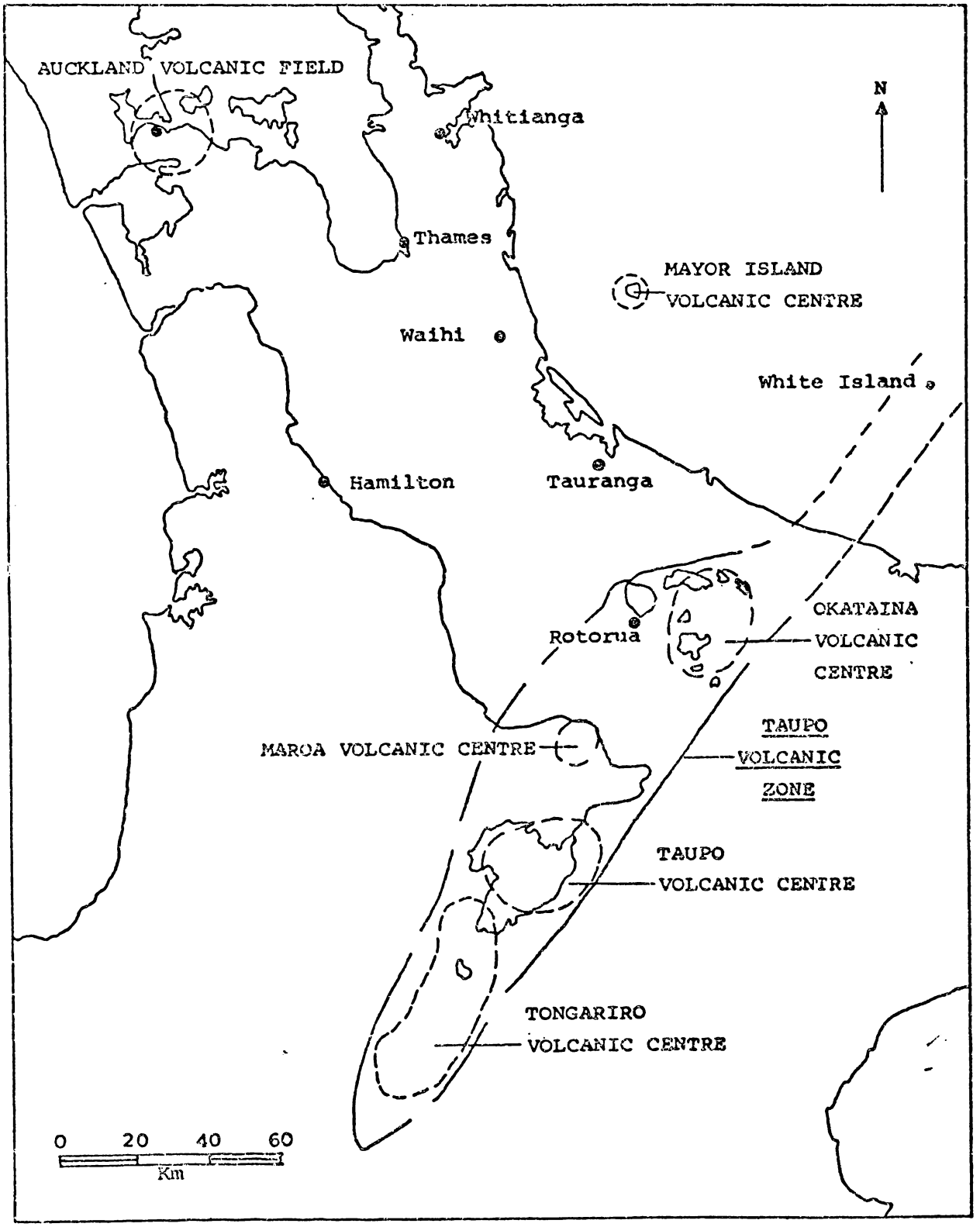


FIGURE 1.2 : Potential sources for tephras deposited upon the Coromandel Peninsula.

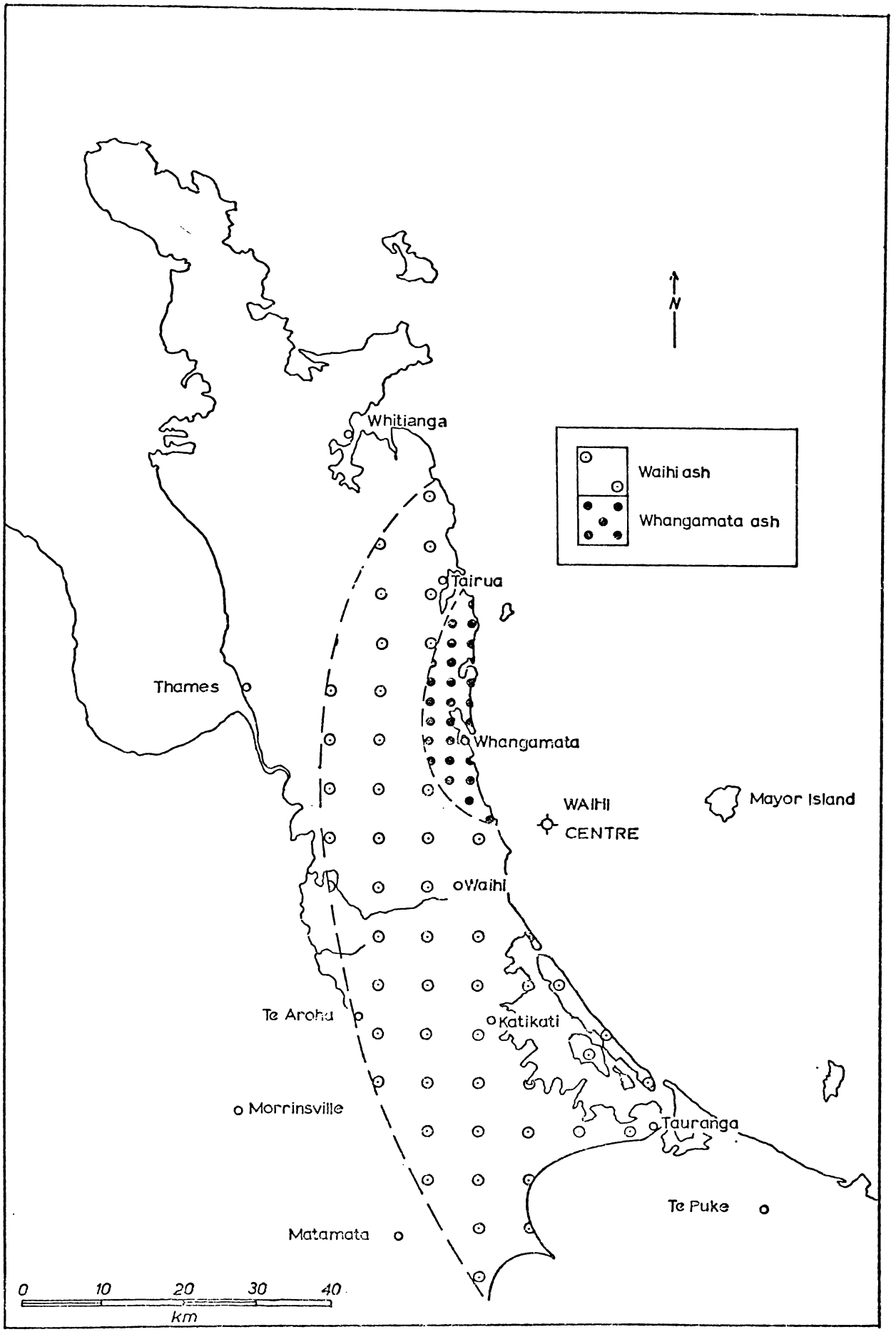


FIGURE 1.3 : Distribution of the Waihi and Whangamata Ashes (after Taylor 1953). Pullar et al. (1973) state that the tephras are derived from the Waihi Centre which they position as above.

"To the east of the Hauraki Depression the ash coarsens and thickens to five or six feet and the mineral assemblage changes to hornblende andesite. This is the Waihi Ash which margins the Bay of Plenty and East Cape areas, and consists of at least two separate beds" (p.12).

Owing to inadequate definition, the use of the term "Waihi Ash" in the literature has been confused. In an attempt to clarify the name, Pullar (1967) suggested that Taylor's definition was meant to include telescoped components of many tephras, ranging from Taupo Pumice to Rotoehu Ash (Table 1.1).

McCraw (1968,1975a) in soil surveys of the Ohinemuri and Thames/Coromandel counties, divided the tephra cover into the four ash units of Taylor and considered that the Waihi Ash comprised at least two and probably three showers. He records a profile at Waihi composed of:

18 in. (46 cm) friable sandy loam

24 in. (61 cm) compact silty loam

12 in. (30 cm) gritty greasy silt loam

10 in. (25 cm) compact fine sand.

Selby et al. (1971) described Quaternary surfaces in the Waihi area and recognised Taupo Pumice and Rotoehu Ash in the Holocene and Late Pleistocene sequence of tephras.

McCraw and Whitton (1971) compared the elemental content of a sample of the Whangamata Ash with five samples of pumice and obsidian from Mayor Island. They considered the Mayor Island samples were probably younger in age and comagmatic with Whangamata Ash but stressed that a Mayor Island source was not necessarily implied.

TABLE 1.1 : Summary of named tephras and published radiocarbon dates from five North Island Volcanic Centres.

| YEARS B.P. | OKATAINA CENTRE | MAROA-TAUPO CENTRE | OTHER CENTRES |
|---|---|---|---|
| 250 | Tarawera Fmn. (64BP) | | |
| 500 | | | |
| 750 | Kaharoa Tephra (930BP) | | Rangitoto Ash (750BP)[1] |
| 1,000 | | | |
| 1,500 | | Taupo Pumice Fmn. (1,850BP) | Ngauruhoe Tephra Fmn. (0-1,819BP)[3] |
| 2,000 | | Mapara Pumice (2,270BP) | Mangatawai Tephra Fmn. (2,500BP)[3] |
| 2,500 | | Whakaipo Tephra (2,800BP) | |
| 3,000 | Rotokawau Ash (no date) | Waimihia Formation (3,150BP) | Papakai Tephra (3,420BP)[3] |
| 4,000 | | | |
| 5,000 | Whakatane Ash (5,180BP) | Hinemaiaia Ash (5,085BP) | |
| 6,000 | | | Whangamata Tephra (6,280BP)[2] |
| 7,000 | Mamaku Ash (7,050BP) | | |
| | Rotoma Ash (7,330BP) | | |
| 8,000 | | Opepe Tephra (8,850BP) | |
| 9,000 | | Poronui Tephra (9,780BP) | Mangamate Tephra (9,700BP)[3] |
| | | | Okupata Tephra (9,790BP)[3] |
| 10,000 | Waiohau Tephra (11,250BP) | Puketarata Ash (no date) | |
| | Rotorua Ash (13,450BP) | | Rotoaira Tephra (13,800BP)[3] |
| | Rerewhakaaitu Tephra (14,700BP) | | |
| 15,000 | | | |
| 20,000 | Okareka Ash (20,700BP) | Kawakawa Fmn. (19,850BP) | |
| | Te Rere Ash (no date) | | |
| 30,000 | Omataroa Tephra (no date) | Poihipi Tephra (no date) | |
| | Awakeri Tephra (no date) | Okaia Tephra (no date) | |
| | Mangaone Tephra (no date) | Tihoi Tephra (no date) | |
| | Hauparu Tephra (no date) | Waihora Tephra (no date) | |
| | Te Mahoe Tephra (no date) | Otake Tephra (no date) | |
| | Maketu Tephra (no date) | | |
| | Tahuna Tephra (no date) | | |
| | Ngamotu Tephra (no date) | | |
| 40,000 | Rifle Range Ash (41,000BP) | | |
| | Earthquake Flat Breccia (41,000BP) | | |
| | Rotoiti Breccia Fmn. (41,000BP) | | |

Data from McCraw(1975)*;Howorth(1975);Vucetich and Howorth(1976);Cole(1970);and this thesis.

1 : Auckland Centre
2 : Mayor Island Centre
3 : Tongariro Centre
* : McCraw (1975b)

Pullar et al. (1973) published an estimated source of Whangamata Ash (Fig. 1.3) and assigned to it an age of approximately 1000 years B.P.

McCraw (1975b) described Whangamata Ash as having two members, an ash deposit overlying and surrounding a coarser lapilli deposit, and suggested that the eruption centre was in the western Bay of Plenty area.

Birrell et al. (1977) during investigations into the physical and chemical changes in the paleosol of Rotoehu Ash in the Bay of Plenty district, identified Rotoehu Ash a few kilometres north of Waihi. They suggested that the strong weathering gradient shown by the tephra in this region, was related to past environmental conditions and to the absence of an overlying tephra cover for a relatively long period of time, possibly until the deposition of Okareka Ash (c. 17 000 years B.P.). The authors also identified Whangamata Ash by spectrochemical methods and cited McCraw and Whitton (1971) in giving the tephra a tentative age of 8 390 $\pm$ 135 years B.P. It should be noted that this age was not applied to Whangamata Ash by McCraw and Whitton, but represents a charcoal sample collected from Mayor Island by Brothers (in Grant-Taylor and Rafter 1962).

Pullar et al. (1977) confirmed the presence of Kaharoa Ash and Taupo Pumice on the Peninsula and have shown that Wellman's Ohui Ash (Wellman 1962) is either Kaharoa Ash or Taupo Pumice.

The previous work on the Coromandel Late Pleistocene tephra deposits is summarised in Table 1.2.

TABLE 1.2 : Stratigraphy of the Coromandel Tephra deposits as determined by previous workers.

| | TAYLOR (1953) | McCRAW (1968) | SELBY, PULLAR & McCRAW (1971) | McCRAW (1975a+b) | BIRRELL, PULLAR & SEARLE (1977) | PULLAR, KOHN & COX (1977) | COMPOSITE TEPHRA COLUMN OF PREVIOUS WORK |
|---|---|---|---|---|---|---|---|
| HOLOCENE ASH BEDS | Second Period Ash | Whangamata Ash | Taupo Pumice | Taupo Pumice | Whangamata Ash | Kaharoa Ash | Kaharoa Ash |
| | | | | | | Taupo Pumice | Taupo Pumice |
| | Whangamata Ash | | Holocene Ash Beds | Whangamata Ash | | | Whangamata Ash |
| | | | | Whangamata Lapilli | | | Whangamata Lapilli |
| LATE PLEISTOCENE ASH BEDS | Third Period Ash | friable sandy loam | Late Pleistocene Ash Beds | friable silt loam | ? | | Waihi Ash |
| | | compact silty loam | | | ? | | |
| | Waihi Ash | gritty greasy silt loam (Waihi Ash) | | "Lumpy" Bed | ?Okareka Ash | | ?Okareka Ash |
| | | | | | Rotoehu Ash paleosol | | Rotoehu Ash paleosol |
| | | compact fine sand | Rotoehu Ash | compact fine sand | Rotoehu Ash | | Rotoehu Ash |
| EARLY TO MIDDLE PLEISTOCENE ASH BEDS | Hamilton Ash | Hamilton Ash | Hamilton Ash Formation | Hamilton Ash Formation | | | Hamilton Ash Formation |
| | Older Hamilton Ash | Old Ash | Kauroa Ash Formation | | | | Kauroa Ash Formation |

Terminology

Tephra is used in a broader sense than was originally implied by Thorarinsson (1954) in that it includes both airfall and airflow deposits (McCraw 1975b; Howorth 1975).

Ash, lapilli and blocks are used here to describe uncemented pyroclastic materials of varying grain sizes: ash, less than 2 mm; lapilli, 2-64 mm; blocks, coarser than 64 mm (Fisher 1961) - See Appendix B p.271.

Soil profile terminology is that of Taylor and Pohlen (1962).

Soil Colours utilise the Munsell Colour Notation (Japanese, JIS Z8721, 1964).

Tephrostratigraphy is concerned primarily with the definition, description and age of tephra layers (after Westgate and Fulton 1975).

Holocene when referring to tephras, follows the usage of Vucetich and Pullar (1969) and refers to the younger beds down to and including the Rerewhakaaitu Ash, dated at c. 14,700 years B.P.

Late Pleistocene with reference to tephras, also follows Vucetich and Pullar (1969) and includes tephras with ages between that of the Rerewhakaaitu Ash (c. 14,700 years B.P.) and the Rotoehu Ash (c. 42,000 years B.P.).

Upper Quaternary ) with reference to tephras indicates tephras
Late Quaternary ) younger than and including the Rotoehu Ash (c. 42,000 years B.P.)

Post- ) Terminology following Pullar et al. (1973).
Pre- ) e.g.: Post-Whangamata tephras - tephras younger than Whangamata Tephra
Pre-Rotoma tephras - tephras older than Rotoma Ash.

Heavy minerals - crystals which have a specific gravity exceeding 2.86 g/ml (e.g. opaque minerals, hypersthene etc).

Ferromagnesian minerals - Silicate minerals containing Fe and Al and having a specific gravity greater than 2.86 g/ml (e.g. hypersthene, aegirine etc).

This thesis has been subdivided into three main sections encompassing the field characteristics and distribution of the Coromandel tephra cover, characterisation of its component tephras by their grain size, mineralogical and chemical properties and finally identification of the tephras through correlation with established stratigraphic columns. Detailed petrological and mineralogical descriptions of tephra components and minerals have been removed from the text to improve its continuity and are presented in Appendix A. For similar reasons, full descriptions of laboratory procedure and analytical methods are confined to Appendix B. It should be stressed that this material is of fundamental importance to this research and is relegated to appendices solely to facilitate the reading of this thesis.

The map pocket at the back of this thesis contains a summary of the most important data on the Coromandel tephras and their correlatives, including the following:

(1) field characteristics of field classes I to V
(2) major stratigraphic columns and sample locations
(3) ferromagnesian mineral assemblages
(4) titanomagnetite element ratios.

The summary is presented in this manner to enable the reader to compare the data from different sections of this work.

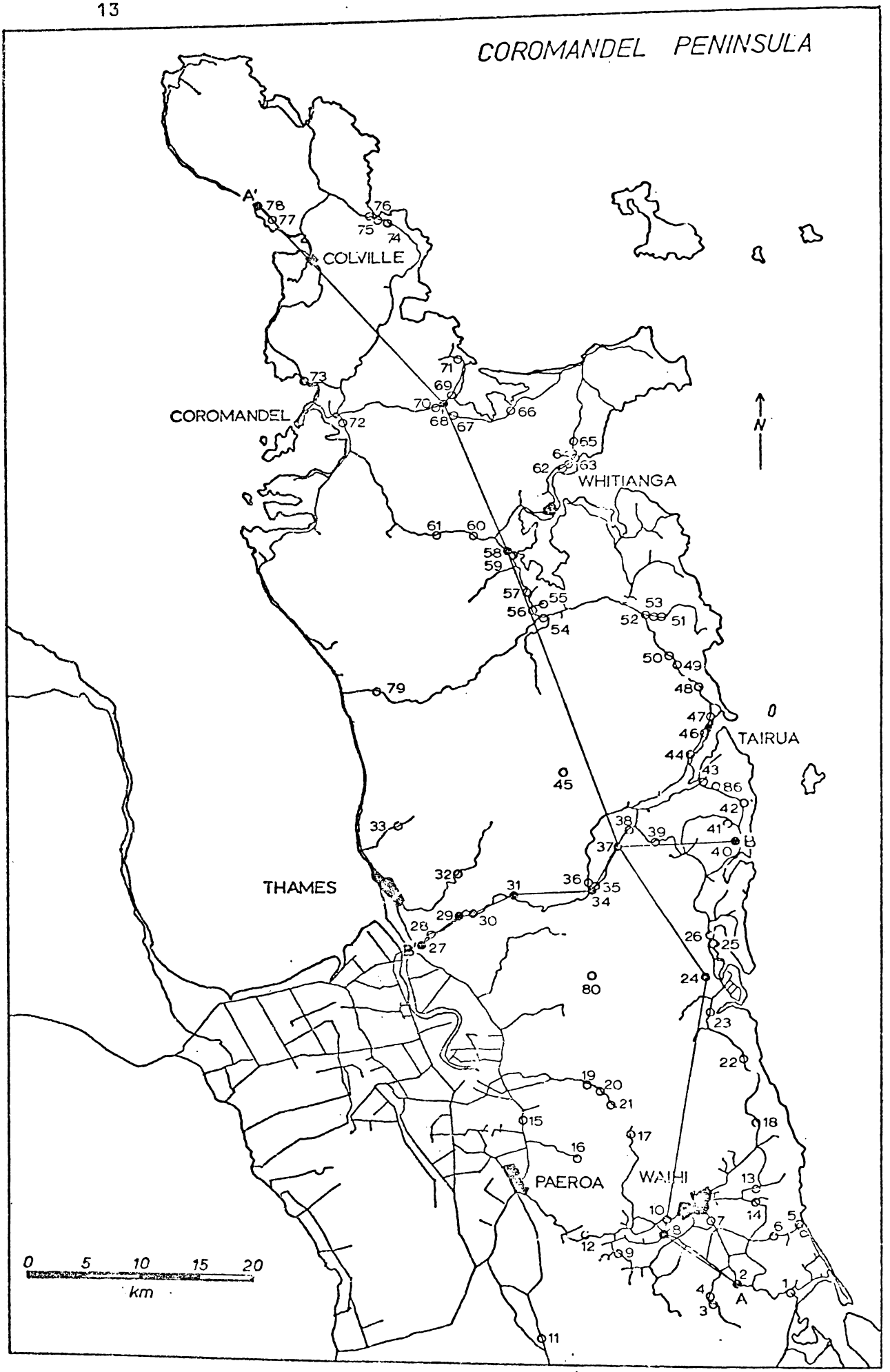


FIGURE 2.1 : Field site locations and correlation lines for the Late Quaternary tephra beds.

# CHAPTER 2

# FIELD INVESTIGATIONS

## Method of Study

In consideration of the degree of uniformity in thickness of the Coromandel tephras over the Peninsula, sections were established at intervals of approximately five kilometres at sites where deposits were preserved and where access was available (public roads, forestry tracks, farm tracks, foot tracks). After a preliminary reconnaissance, detailed field examinations were carried out beginning in the south where the deposits are thickest. A further investigation of all sites was made after detailed laboratory examinations had provided more information on individual tephras. Site descriptions and bed thicknesses were recorded at 80 stations shown on Fig. 2.1 - grid references for these stations are given in Appendix C.

## Mapping criteria

Criteria used for initial field mapping were derived from properties of the tephra, for example grain size, grading, shower-bedding and from characteristics arising from its subsequent modification, for example structure, clay content, colour and consistence.

## Stratigraphy

Initial investigations into Coromandel tephra stratigraphy provided a stratigraphic column subdivided into classes with

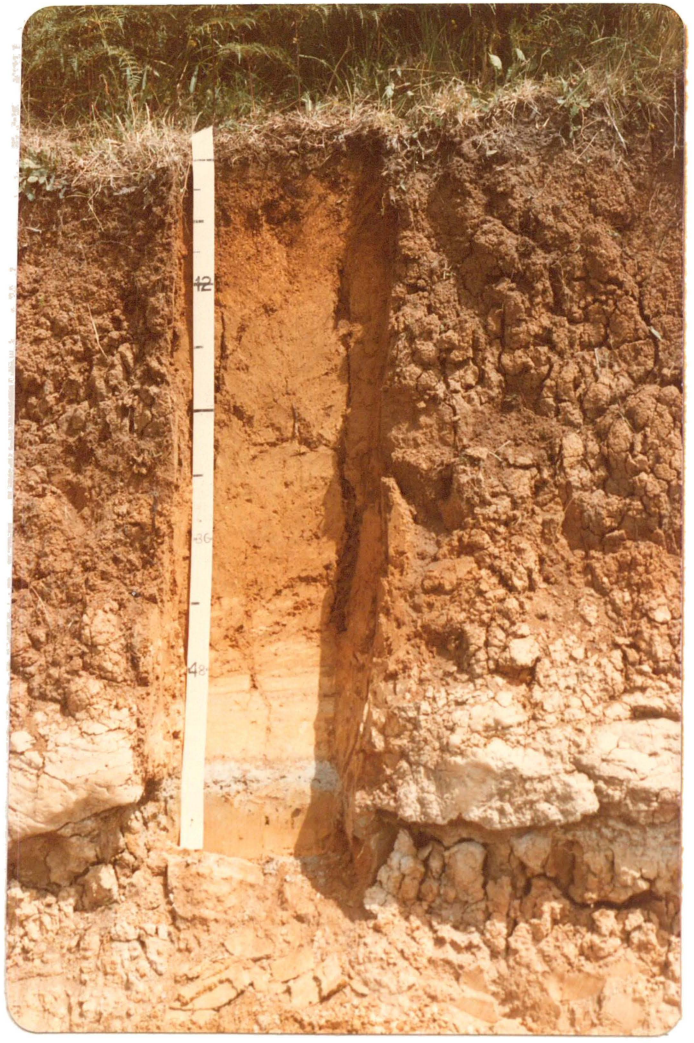

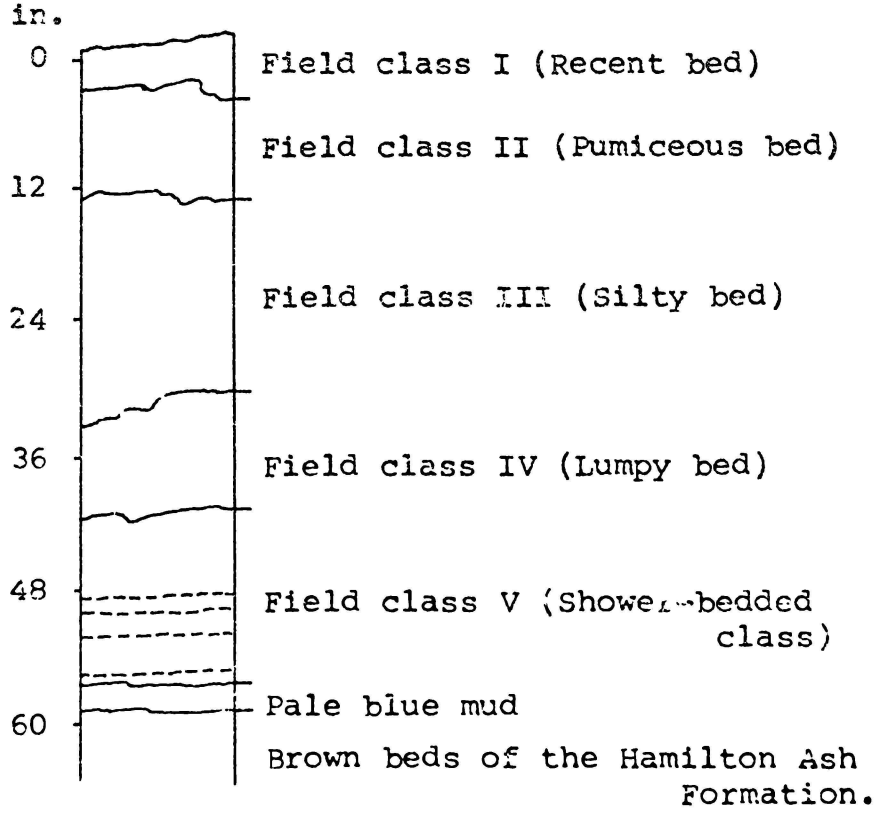


FIGURE 2.2 : Late Quaternary tephras, Kopu site (site 37,N49/252285) showing the boundaries of field classes I to V. Note the variations in the patterns exposed on weathered bank surfaces.

distinctive field properties. The field classes erected represent units that allow correlation between sites over large areas of the Peninsula. The five field classes, designated I, II, III, IV and V are termed the Recent bed, Pumiceous bed, Silty bed, Lumpy bed and Shower-bedded class respectively, as illustrated by the tephras at the Kopu site (Fig. 2.2). The distribution pattern of the total thickness of the Late Quaternary tephras found on the Peninsula is shown in Fig. 2.3. Recorded thicknesses of tephra deposits on the Coromandel Peninsula tend to be less regular than those for many other regions because of the dissected nature of the country and thinness of the deposits being studied. To improve the reliability of the data, the Peninsula was divided into six approximately equally spaced regions, two of which (regions 4 and 5) were subdivided to determine whether the Coromandel Range had influenced tephra deposition. The tephra mantle thickens southward from 75 cm in region 1 to 177 cm in the Whangamata region (region 5b) and then thins slightly to 174 cm in region 6. To the west of the Range the tephra cover is considerably thinner, suggesting that there may be some orographic control.

## Spatial distribution

Variation in the spatial distribution of the tephra deposits remaining on the surface of the Peninsula are related to both the nature and extent of the initial eruption and the degree of susceptibility of the site to mass wasting. The importance of the latter is demonstrated by the present day distribution pattern which is strongly influenced by slope angle. The tephras are preserved

FIGURE 2.3: Distribution pattern and thickness (cm) of the Upper Quaternary tephra column of the Coromandel Peninsula (field classes I to V)

| Region | Number of data sites (n) | Thickness mean ($\bar{X}$) | Standard deviation ($\theta$) | Coefficient of variation (c) % |
|---|---|---|---|---|
| 1 | 5 | 75 | 20 | 27 |
| 2 | 8 | 78 | 13 | 17 |
| 3 | 14 | 92 | 17 | 18 |
| 4a | 4 | 116 | 33 | 28 |
| 4b | 15 | 127 | 33 | 26 |
| 5a | 8 | 120 | 27 | 23 |
| 5b | 6 | 177 | 30 | 17 |
| 6 | 15 | 174 | 33 | 19 |

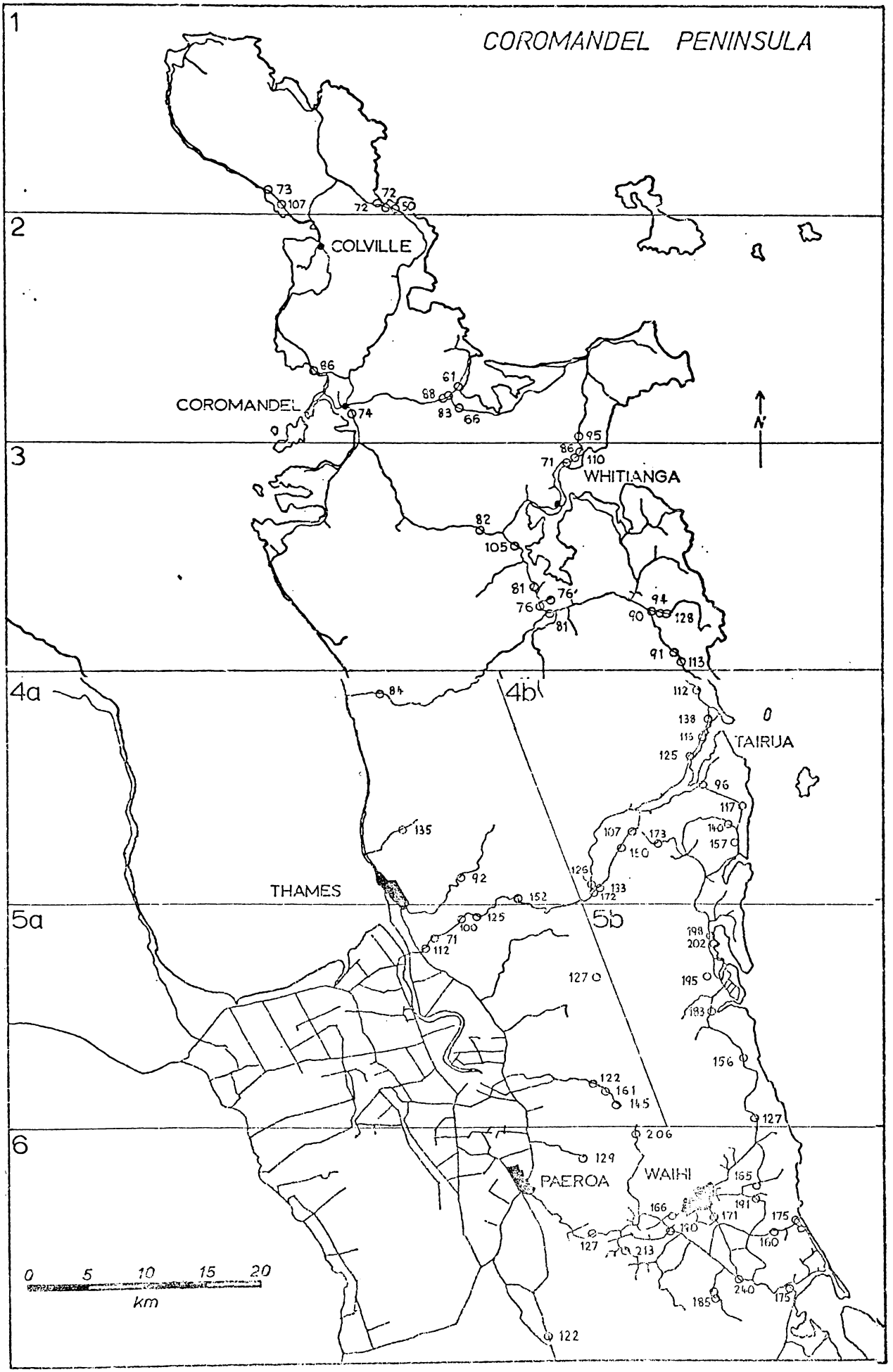
COROMANDEL PENINSULA
COLVILLE
COROMANDEL
WHITIANGA
TAIRUA
THAMES
PAEROA
WAIHI
1
2
3
4a
4b
5a
5b
6
N
0 5 10 15 20
km

on the low terraces and plains where they form a continuous mantle and at higher altitudes they occur only as isolated patches on ridge crests. In order to ensure against error caused by colluvial thickening, sites for detailed examination were chosen when slopes were less than $5^{o}$, most commonly on river terraces or plains, and distant from the base of moderately steep or steep slopes. Correlation lines A-A' (Fig. 2.4) show the main trends in field class thicknesses paralleling the length of the Peninsula, and B-B' (Fig. 2.5) at right angles to it across the Coromandel Range. Reference sections are described at the end of this thesis (Appendix F). All grid references are from the 1:63 360 topographical map series (NZMSI) and the national thousand-yard grid shown on this series; Map editions are summarised in Appendix C.

## FIELD CLASS CHARACTERISTICS

### 1. Field Class I (Recent bed)

Class I, containing the youngest of the tephras examined, overlies the Pumiceous bed and forms a distinct boundary with it when the older bed consists of abundant coarse pumiceous lapilli. Where the lapilli are less prominent and coarse ash grade predominates, the boundary is indistinct. The Recent bed, which is represented by 20 cm of sandy loam at Waihi, decreases in thickness northwards and gradually changes to a silt loam texture and merges with the underlying deposit (Fig. 2.6). At Whenuakite it is no longer recognisable. Around Whangamata it occurs as a very friable, distinctly gritty, sandy loam with a moderately developed fine crumb structure and contains abundant small lapilli

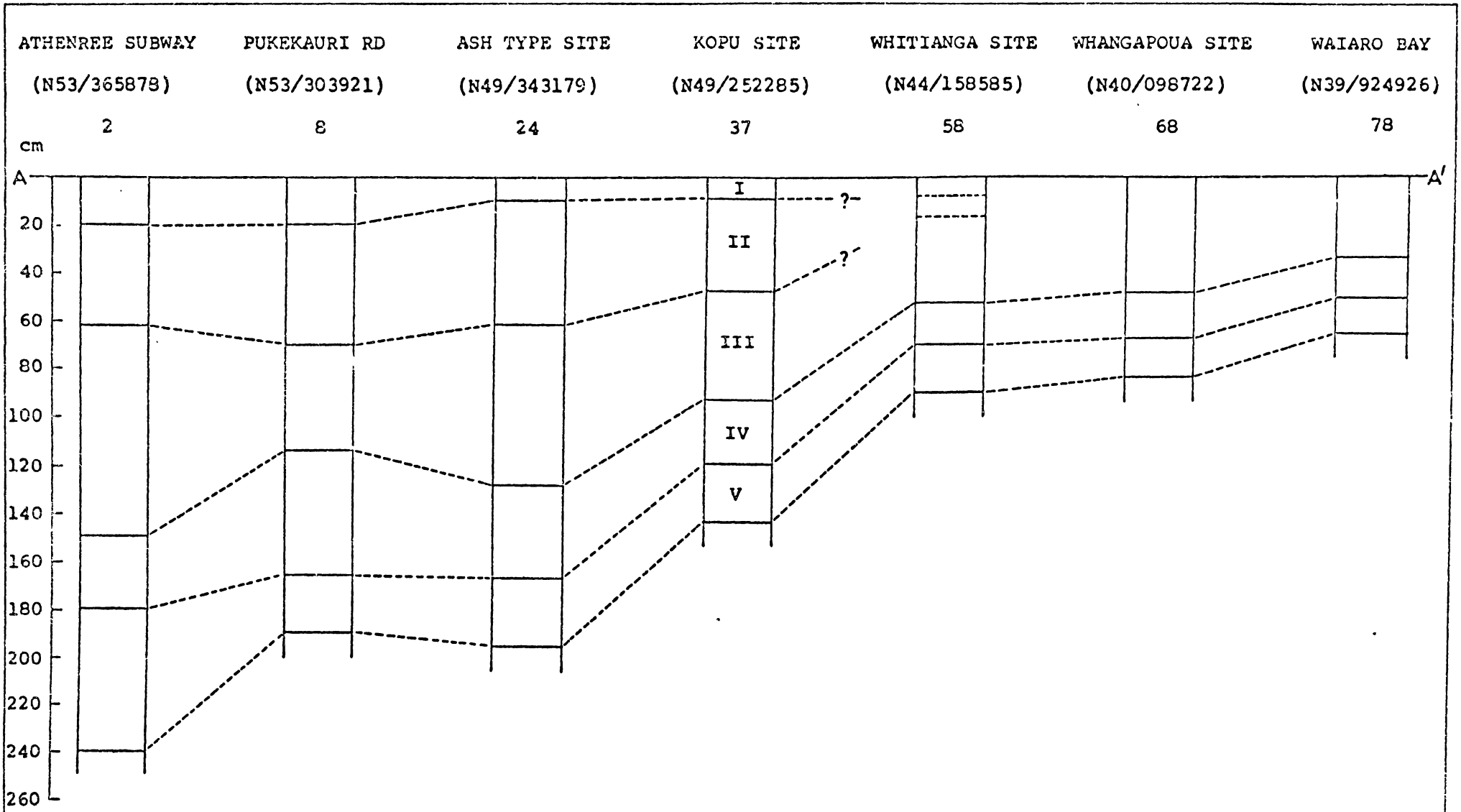


FIGURE 2.4 : Correlation line from Athenree Subway to Waiaro Bay (A-A'). For location of sections, see Fig.2.1

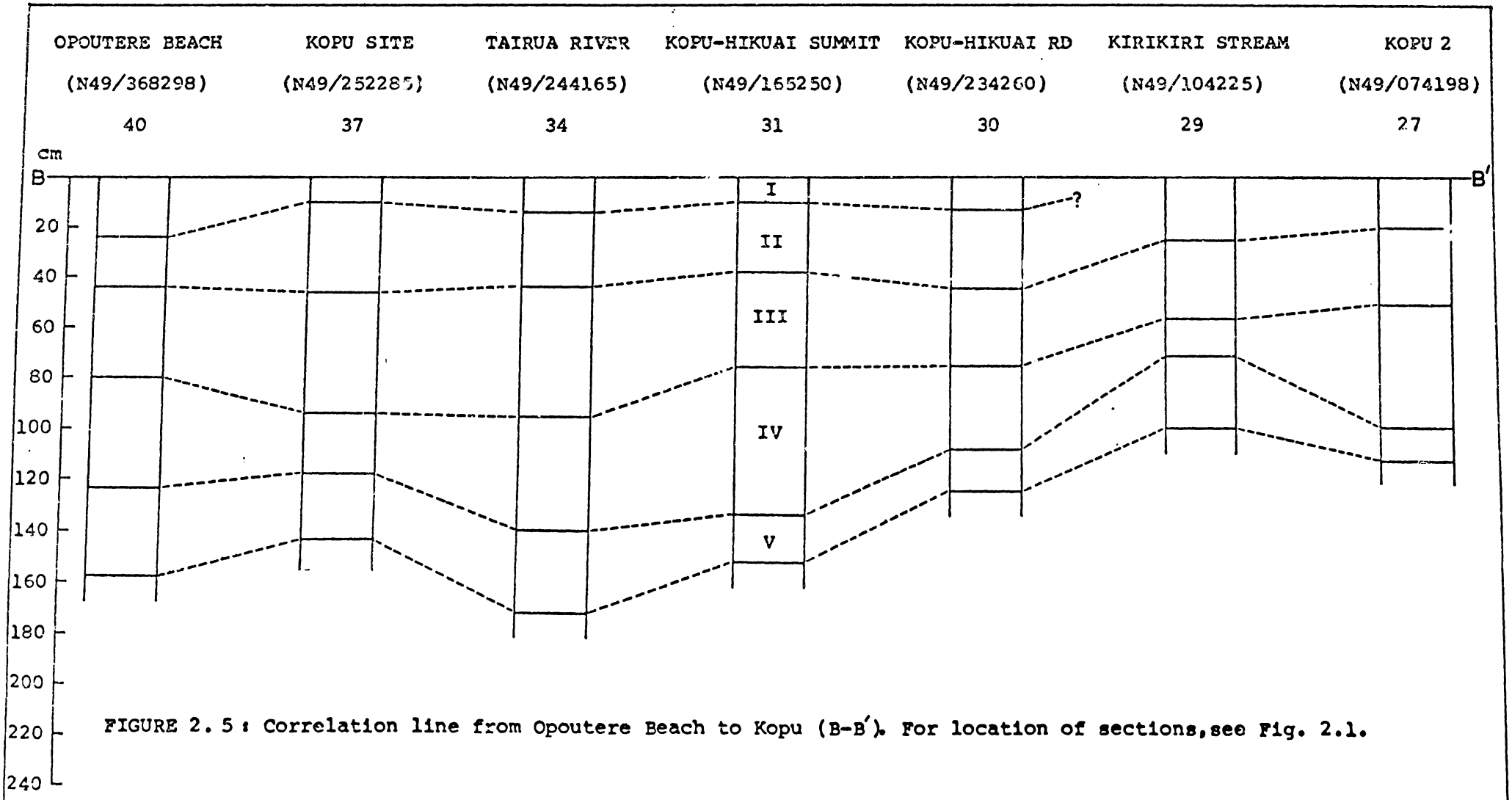


FIGURE 2.5 : Correlation line from Opoutere Beach to Kopu (B-B'). For location of sections, see Fig. 2.1.

of orange pumice which can be crushed readily. The grittiness is caused by many clear crystals between 1-2 mm in diameter. In the Waihi and Kopu regions, the Recent bed tends to be of finer grain size and consists of a friable sandy loam with a weakly developed fine granular structure. The grittiness noted above is lacking in these regions though the pumice content appears to be slightly higher.

Two types of pumice fragments have been identified in field class I. One type, a fine pumice (generally less than 5 mm in diameter) is white, offers considerable resistance to crushing and is found in highest concentration in the south of the Peninsula. The other pumice type is finer (less than 2 mm in diameter), orange yellow or occasionally grey in colour, and crushes readily suggesting that it has been derived from an older eruption. The tephras forming the Recent bed occupy the present day soil A horizon and have undergone thorough biological mixing.

2. Field Class II (Pumiceous bed)

Field class II consists of 60 cm of coarse pumice lapilli at Whangamata decreasing in thickness to 30 cm of coarse pumiceous ash at Waihi (Fig. 2.7). The area of deposition covered by the Pumiceous bed is oblate and asymmetrical and is defined by a northern limit of less than 10 cm at Tairua but maintaining a thickness of approximately 30 cm south of Waihi, which may indicate either wind direction variation with altitude at the time of deposition or a multi-tephra origin for the deposit. The distribution, though asymmetrical, is approximately centred around

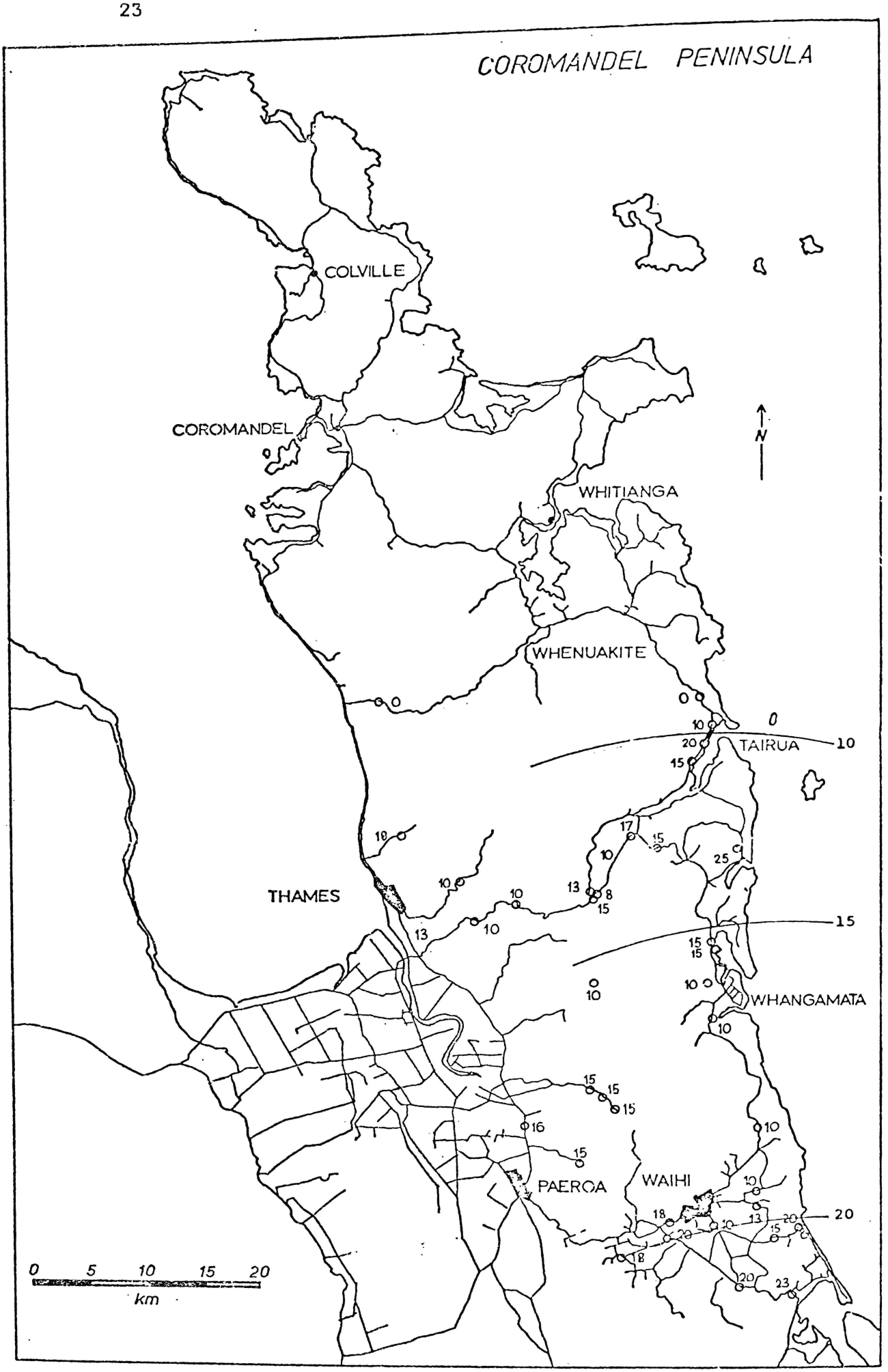


FIGURE 2.6 : Distribution pattern and thickness (cm) of field class I (Recent bed).

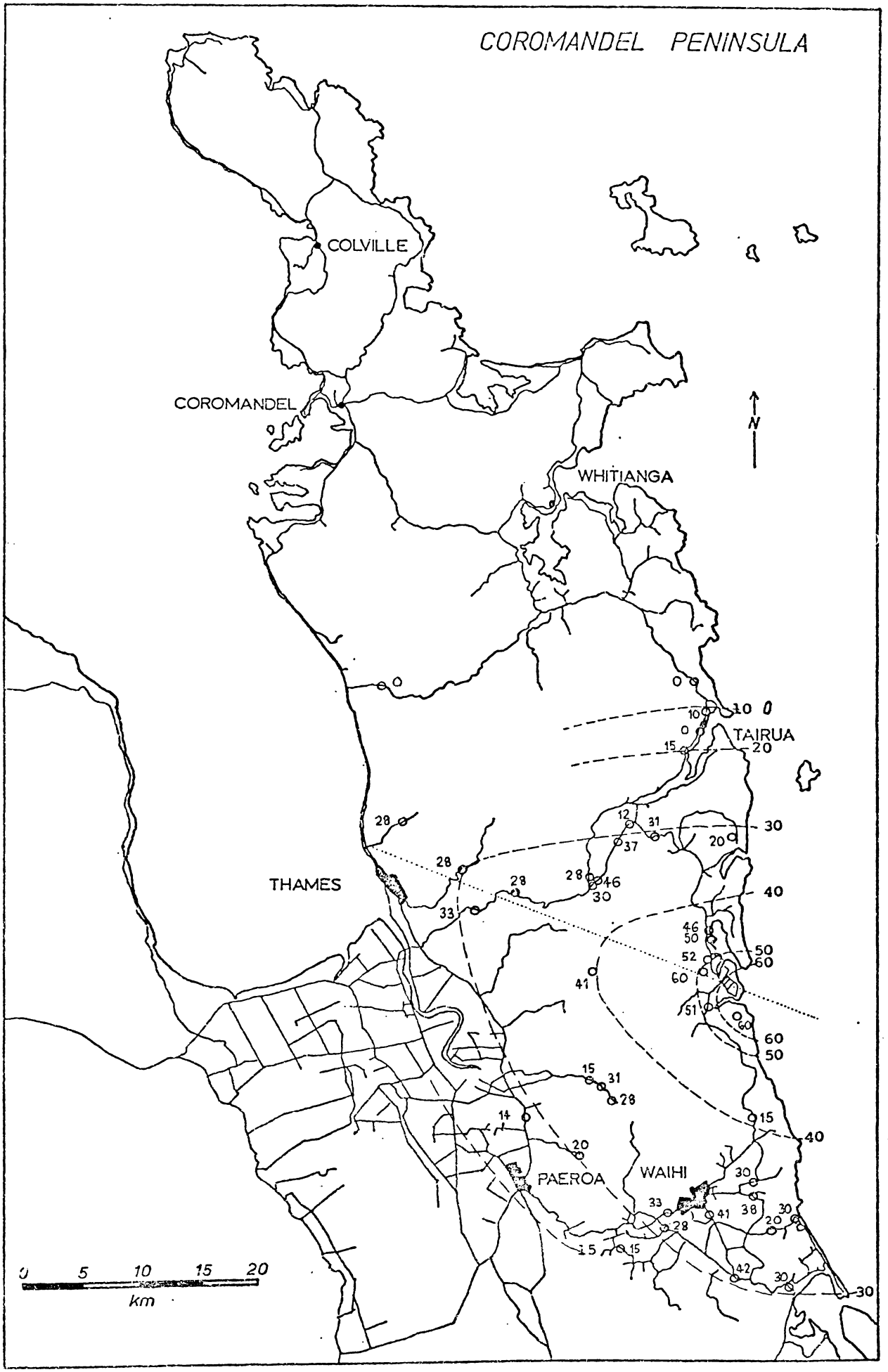


FIGURE 2.7 : Distribution pattern and thickness (cm) of field class II (Pumiceous bed).

an axis lying east-south-east between Thames and Whangamata thus suggesting a source off the Whangamata coast in the western Bay of Plenty.

The coarse, pumiceous lapilli are conspicuous having a dark reddish brown colour, which is concentrated on the surface of the grains and changes to bright brown when the lapilli are crushed. The deposit is normally graded with lapilli up to 30 mm in diameter and with the coarsest lapilli being firm to very firm and weakly cemented but loose when dug (Fig. 2.9). Green obsidian fragments are commonly present and average 3-8 mm in diameter. Occasionally, coarse dull yellowish brown lapilli occupy an "egg-cup" form, which is under lain by discontinuous iron pans and reddish brown lapilli (Fig. 2.8). Although the boundary between the coarse class II pumices and the underlying Silty bed is generally a distinct one (as in Fig. 2.9), isolated lapilli are incorporated into the upper 10 cm of the Silty bed.

The characteristics of the Pumiceous bed change with a decrease in grain size from lapilli to coarse ash. In the Waihi region, class II is represented by approximately 30 cm of bright brown to yellowish brown sandy loam and although of considerably finer grain size, the correlatives of the dark reddish brown pumice lapilli are present in the form of very abundant, small ($< 3$ mm) orange yellow pumice fragments; the bed is friable and has a moderately developed fine crumb and medium nutty structure and is separated from the Silty bed by an indistinct boundary.

FIGURE 2.8 : Stratigraphic relationship between the dull yellowish brown and dark reddish brown lapilli of field class II at site 84, Whangamata South. (Spade is 1 metre in length).

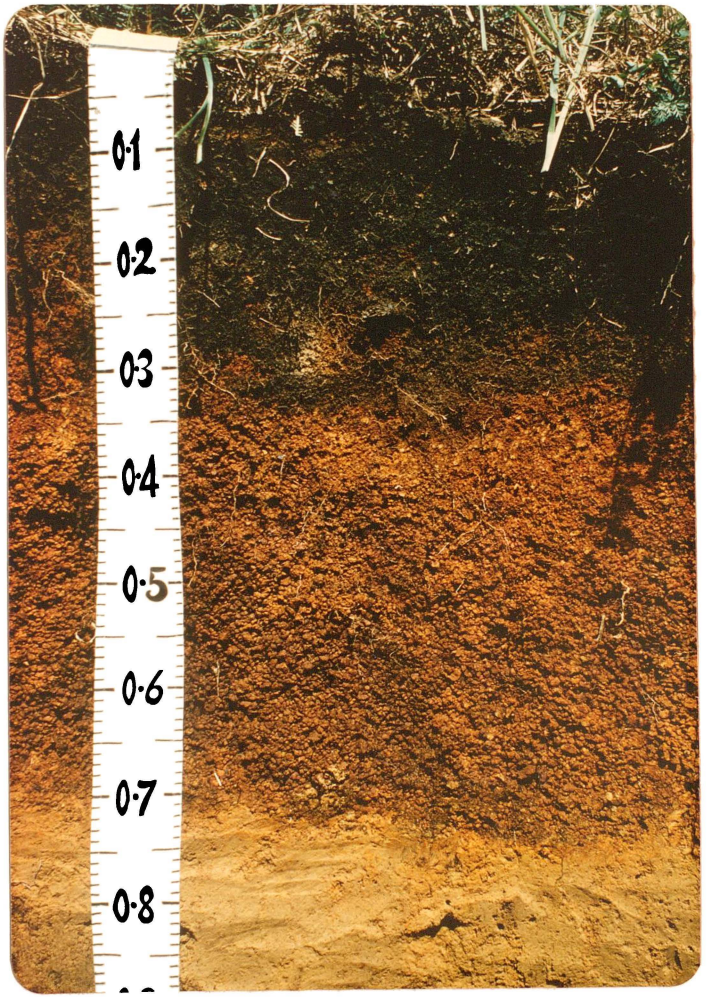


FIGURE 2.9 : Coarse reddish brown lapilli of field class II at site 25 (Old Mill). 30 cm of black sandy loam (class I), overlies 40cm of normally graded coarse lapilli of class II. A distinct boundary separates classes II and III.

## 3. Field Class III (Silty bed)

The Silty bed is characterised by its fine grain size and occupies the central portion of the stratigraphic column, lying between two coarser beds, the Pumiceous bed above and Lumpy bed beneath. Class III extends the full length of the Peninsula with its thickness decreasing from over 60 cm in the south to 40 cm at Colville in the north (Fig. 2.10). In region 3 some sites show the Silty bed to be thicker than in region 4. This disruption to the gradual decrease in thickness northward probably does not mean an actual increase in thickness of class III but is due to an inclusion of some material from field classes I and II in amounts too small to be recognised separately. There is a decrease in bed thickness from the eastern side of the Coromandel Range to the western side.

The Silty bed generally supports the soil A horizon in the northernmost part of the Peninsula owing to the more limited distribution of the overlying tephras. The upper part of the tephra layer in these regions therefore has dark brown or brownish black soil colours and more friable consistencies than in the buried correlatives further south.

Geographically, textures become finer from south to north with silt loams fining to clayey silt loams and clay loams in the north. The Silty bed also shows gradations within the actual deposit, with the upper and lower parts varying mainly in colouration and consistency. Colours vary from yellowish brown to bright yellowish brown and the bed generally becomes firmer with depth, ranging in consistence from friable to firm. Structures are generally

moderately developed medium nutty or blocky and are expressed on the weathered surfaces of banks as a frittered pattern, similar to that shown by the Lumpy bed. The boundary between the Silty and Lumpy beds is indistinct.

4. Field Class IV (Lumpy bed)

The Lumpy bed extends into the far north of the Peninsula and decreases in thickness from 40 cm in the south to 20 cm in the north (Fig. 2.11). A decrease in grain size accompanies the decrease in bed thickness northwards, with silty sandy loams predominating in the south and sandy silt and clay loams further north. Colours range from yellowish brown to bright brown, with distinctly paler colours in the Whitianga and Colville areas. The matrix consistence is generally firm but the moderately abundant creampuffs[1] are very firm. The Lumpy bed has a characteristic weakly to moderately developed coarse blocky structure which produces a frittered pattern upon weathered surfaces exposed in road cuttings. These surfaces are also characterised by distinctly reddish hues (bright brown) and abundant colourless crystals flecking the exposed beds.

On the western side of the Coromandel Range the class IV deposit loses many of its characteristic properties, particularly its blocky structure (see Site 32: Kauaeranga Valley p.324). Here the bed is yellowish brown in colour, has a friable to firm consistence and a strongly developed fine to medium nutty structure

---

[1] "Creampuff" - For their definition and discussion on their origin, see p.38.

FIGURE 2.10: Distribution pattern and thickness (cm) of field class III (Silty bed)

| Region | Number of data sites (n) | Thickness mean ($\bar{X}$) | Standard deviation ($\sigma$) | Coefficient of variation (c) % |
|---|---|---|---|---|
| 1 | 4 | 38 | 13 | 35 |
| 2 | 6 | 36 | 12 | 34 |
| 3 | 6 | 45 | 8 | 18 |
| 4a | 4 | 42 | 13 | 31 |
| 4b | 14 | 35 | 15 | 41 |
| 5a | 7 | 32 | 5 | 15 |
| 5b | 6 | 57 | 11 | 20 |
| 6 | 13 | 55 | 15 | 28 |

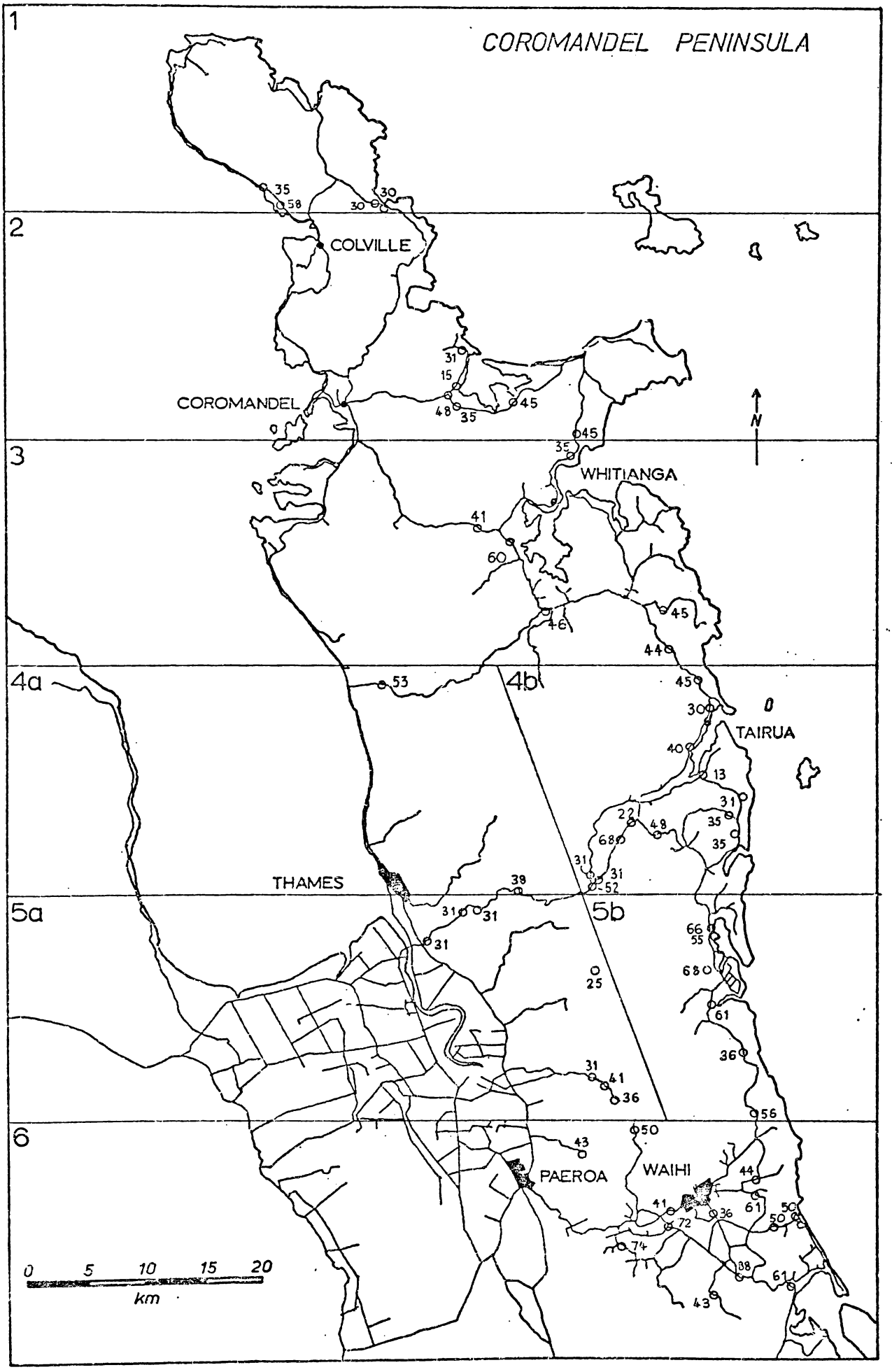
COROMANDEL PENINSULA
COLVILLE
COROMANDEL
WHITIANGA
TAIRUA
THAMES
PAEROA
WAIHI
N
0 5 10 15 20
km

FIGURE 2.11: Distribution pattern and thickness (cm) of field class IV (Lumpy bed)

| Region | Number of data sites (n) | Thickness mean ($\bar{X}$) | Standard deviation ($\sigma$) | Coefficient of variation (c) |
|---|---|---|---|---|
| 1 | 4 | 25 | 11 | 43 |
| 2 | 6 | 18 | 2 | 14 |
| 3 | 7 | 29 | 10 | 34 |
| 4a | 3 | 35 | 20 | 56 |
| 4b | 13 | 39 | 10 | 25 |
| 5a | 7 | 35 | 10 | 30 |
| 5b | 4 | 29 | 7 | 23 |
| 6 | 13 | 40 | 9 | 23 |

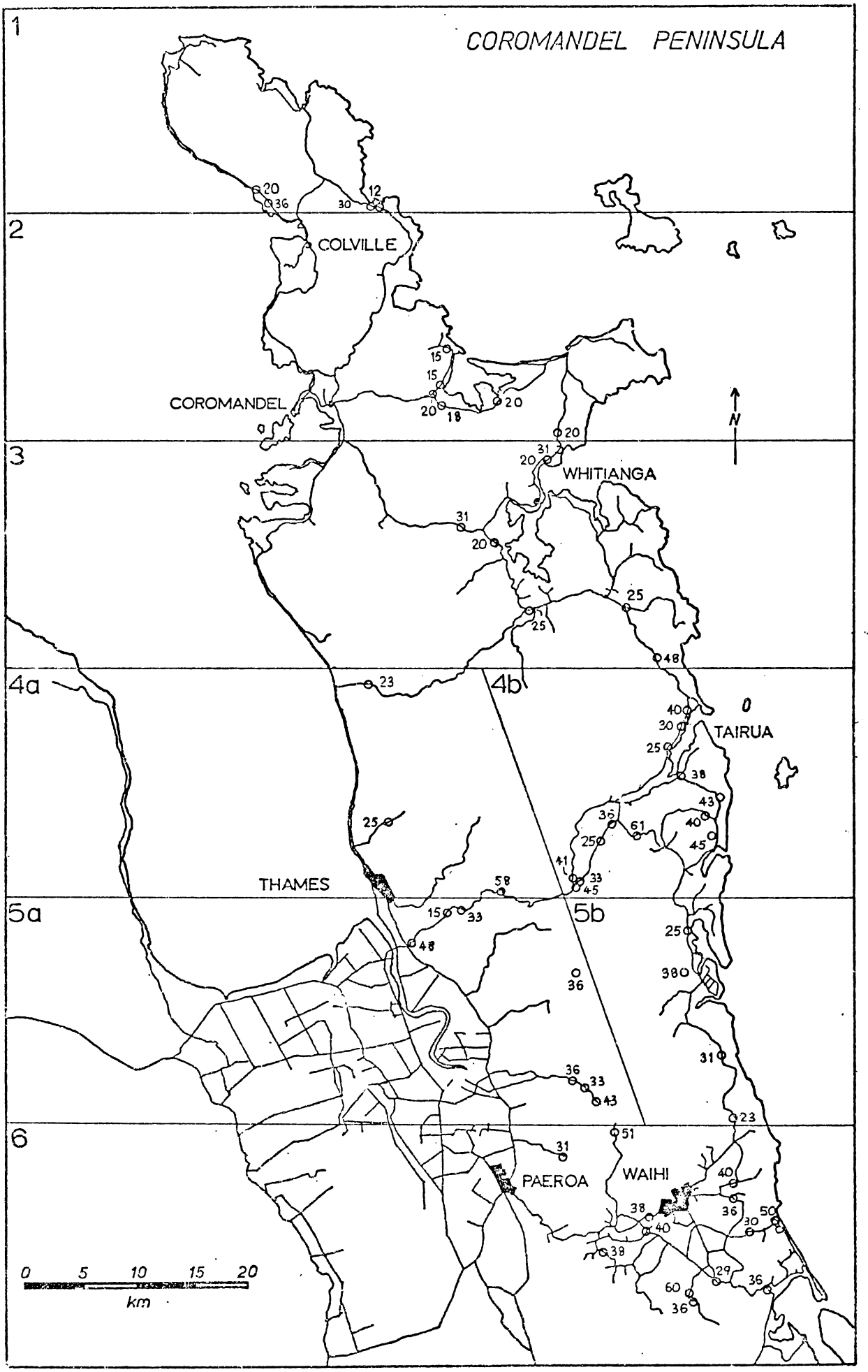
COROMANDEL PENINSULA
1
2
3
4a
4b
5a
5b
6
COLVILLE
COROMANDEL
WHITIANGA
TAIRUA
THAMES
PAEROA
WAIHI
N
0 5 10 15 20
km

FIGURE 2.12: Distribution pattern and thickness (cm) of field class V (Shower-bedded class)

| Region | Number of data sites (n) | Thickness mean ($\bar{X}$) | Standard deviation ($\theta$) | Coefficient of variation (c) % |
|---|---|---|---|---|
| 1 | 5 | 17 | 8 | 44 |
| 2 | 9 | 24 | 10 | 43 |
| 3 | 10 | 22 | 12 | 57 |
| 4a | 3 | 13 | 5 | 38 |
| 4b | 13 | 27 | 9 | 34 |
| 5a | 7 | 26 | 11 | 41 |
| 5b | 5 | 32 | 9 | 27 |
| 6 | 14 | 40 | 15 | 39 |

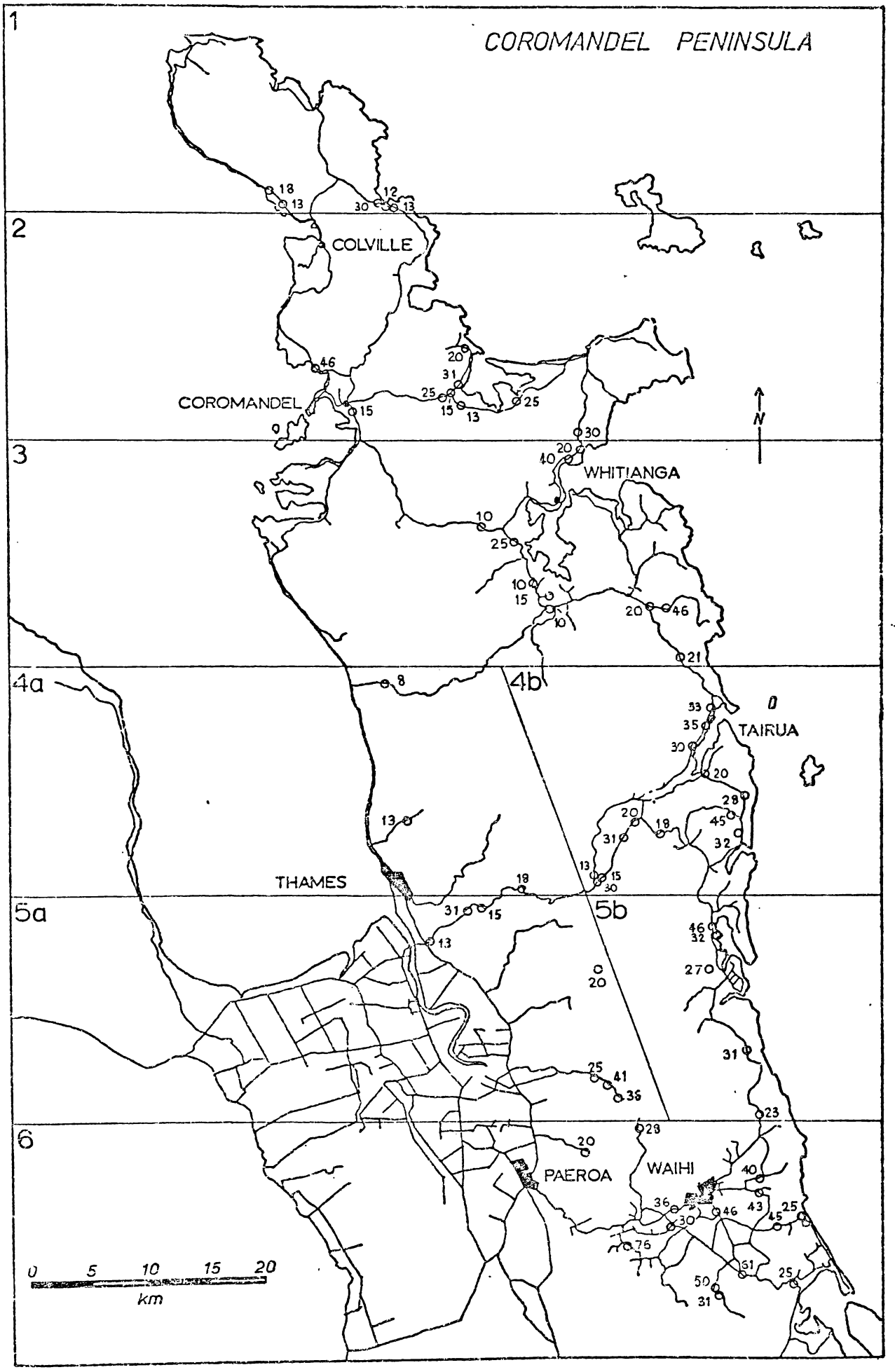
COROMANDEL PENINSULA
COLVILLE
COROMANDEL
WHITIANGA
TAIRUA
THAMES
PAEROA
WAIHI
1
2
3
4a
4b
5a
5b
6
N
0 5 10 15 20
km

with some fine crumb. There is no clear distinction between field classes IV and V - the latter is probably represented by a high density of creampuffs at the base of the Upper Quaternary tephra column. The absence of a blocky structure in the Lumpy bed west of the Coromandel Range, may be related to the fine grain size of the associated creampuffs (sandy silt loams) which are in turn, influenced by the Shower-bedded deposit beneath.

5. Field Class V (Shower-bedded class)

The lowermost tephra deposits studied in this thesis are represented by Shower-bedded and undifferentiated sands and loamy sands which merge into and accompany the overlying Lumpy bed as far north as the Colville region. As Fig. 2.12 indicates, the deposit decreases regularly in thickness northwards from approximately 40 cm in the south to approximately 20 cm at Waiaro Bay.

Field classes IV and V can be subdivided into five zones as illustrated in Figs. 2.13 and 2.14. The basal shower-bedded zone is characterised by alternating fine and coarse sands, ranging in colour from bright yellowish to grey, green and orange. Individual events can be identified within the zone and some, only a few centimetres thick, can be traced for tens of kilometres up the Peninsula. The zone of undifferentiated sands consists of bright yellowish brown homogeneous sands which lack the shower-bedding characteristic of the zone below. The undifferentiated sands contain irregular fractures which increase in abundance upwards until the uppermost zone of field class V consists of

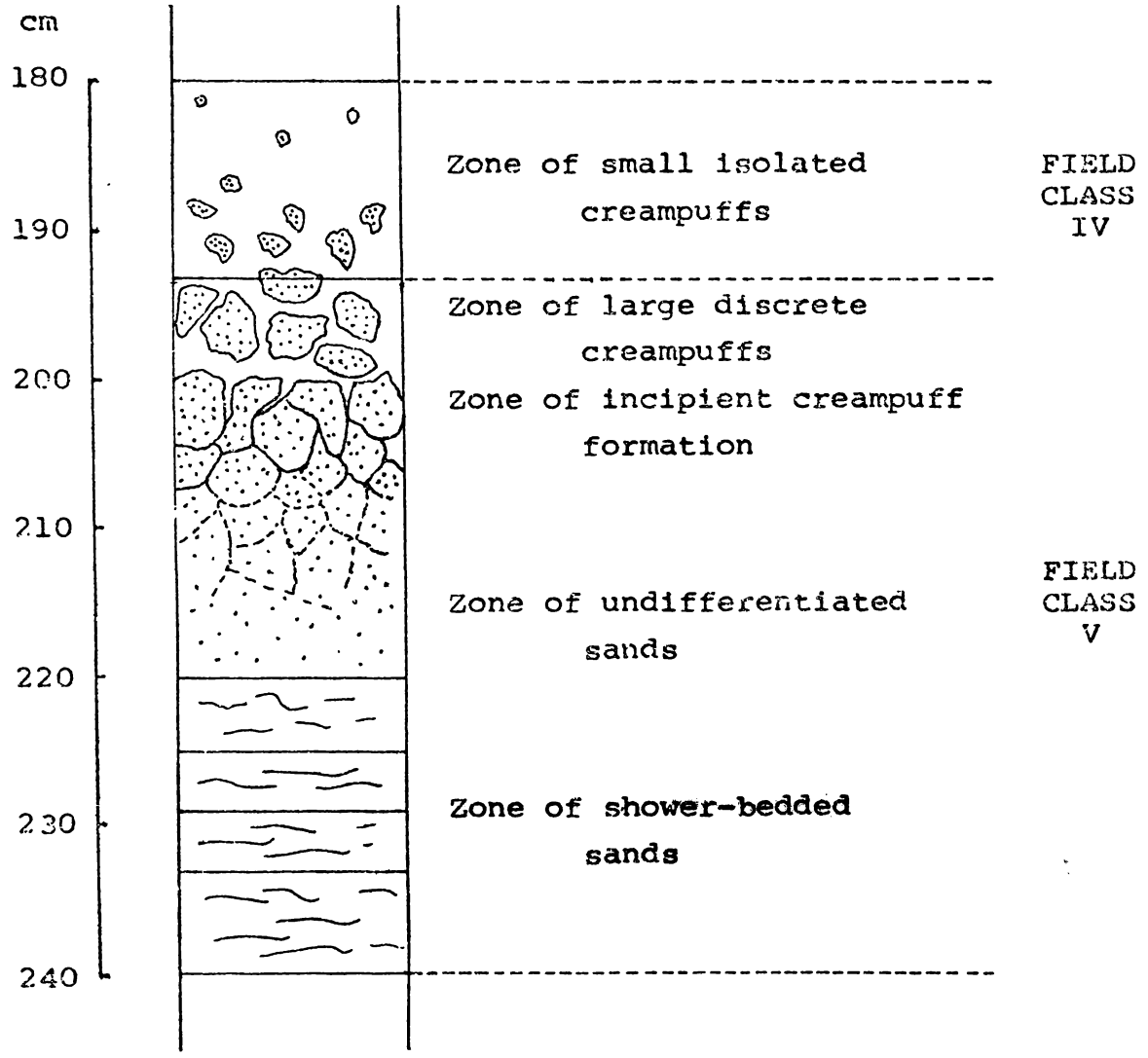


FIGURE 2.13 : Zones in field classes IV and V at site 2 (Athenree subway).


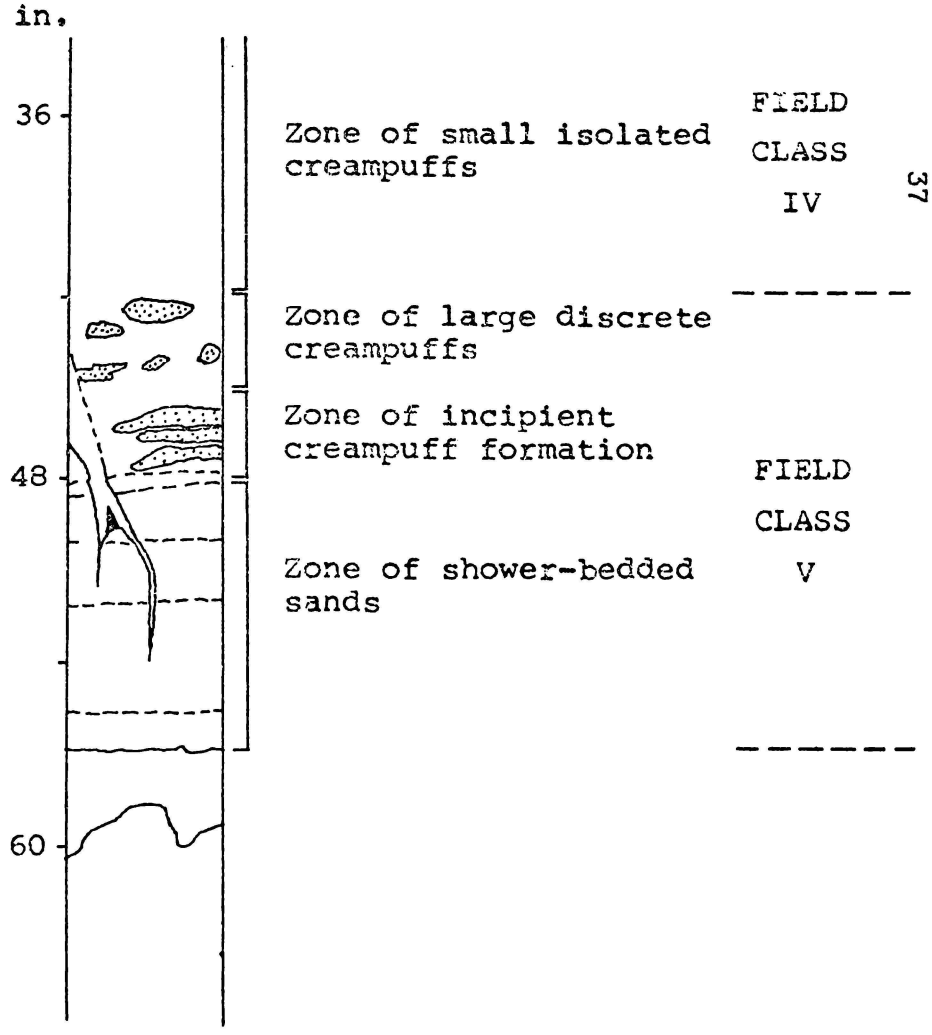


FIGURE 2.14 : Field classes IV and V at the Kopu site (site 37). Four zones within the Lumpy bed and Shower-bedded class are shown. The "zone of undifferentiated sands" is not present at the Kopu site.

discrete, relatively unweathered lumps of primary material surrounded by a sandy loam matrix including a considerable amount of secondary material. Field class IV is dominated by the sandy loam matrix into which small, subspherical, isolated remnants of primary material (here called "creampuffs") are scattered. The progression from undifferentiated sands and fractured, discrete lumps of sand to small isolated creampuffs suggests the influence of normal weathering processes operating in a soil prior to the deposition of the tephras composing field classes I to III. The presence of creampuffs in class IV, and their apparent relationship with the sands of class V, suggests that class IV may be the paleosol of class V. This view is strengthened by the combined thicknesses for field classes IV and V, which have lower coefficients of variation within each region than the separate class IV and V measurements (c.f. Fig. 2.15 with Figs. 2.11 and 2.12).

The Shower-bedded class forms a sharp boundary with the underlying deposits, which are generally either older tephra beds belonging to the Hamilton Ash Formation or blue mud-textured beds.

FIGURE 2.15: Distribution pattern and thickness (cm) of field classes IV and V

| Region | Number of data sites (n) | Thickness mean ($\bar{X}$) | Standard deviation ($\theta$) | Coefficient of variation (c) |
|---|---|---|---|---|
| 1 | 4 | 43 | 5 | 11 |
| 2 | 6 | 40 | 8 | 19 |
| 3 | 7 | 48 | 12 | 26 |
| 4a | 4 | 43 | 22 | 51 |
| 4b | 14 | 62 | 18 | 28 |
| 5a | 8 | 60 | 11 | 19 |
| 5b | 6 | 65 | 12 | 18 |
| 6 | 14 | 78 | 17 | 22 |

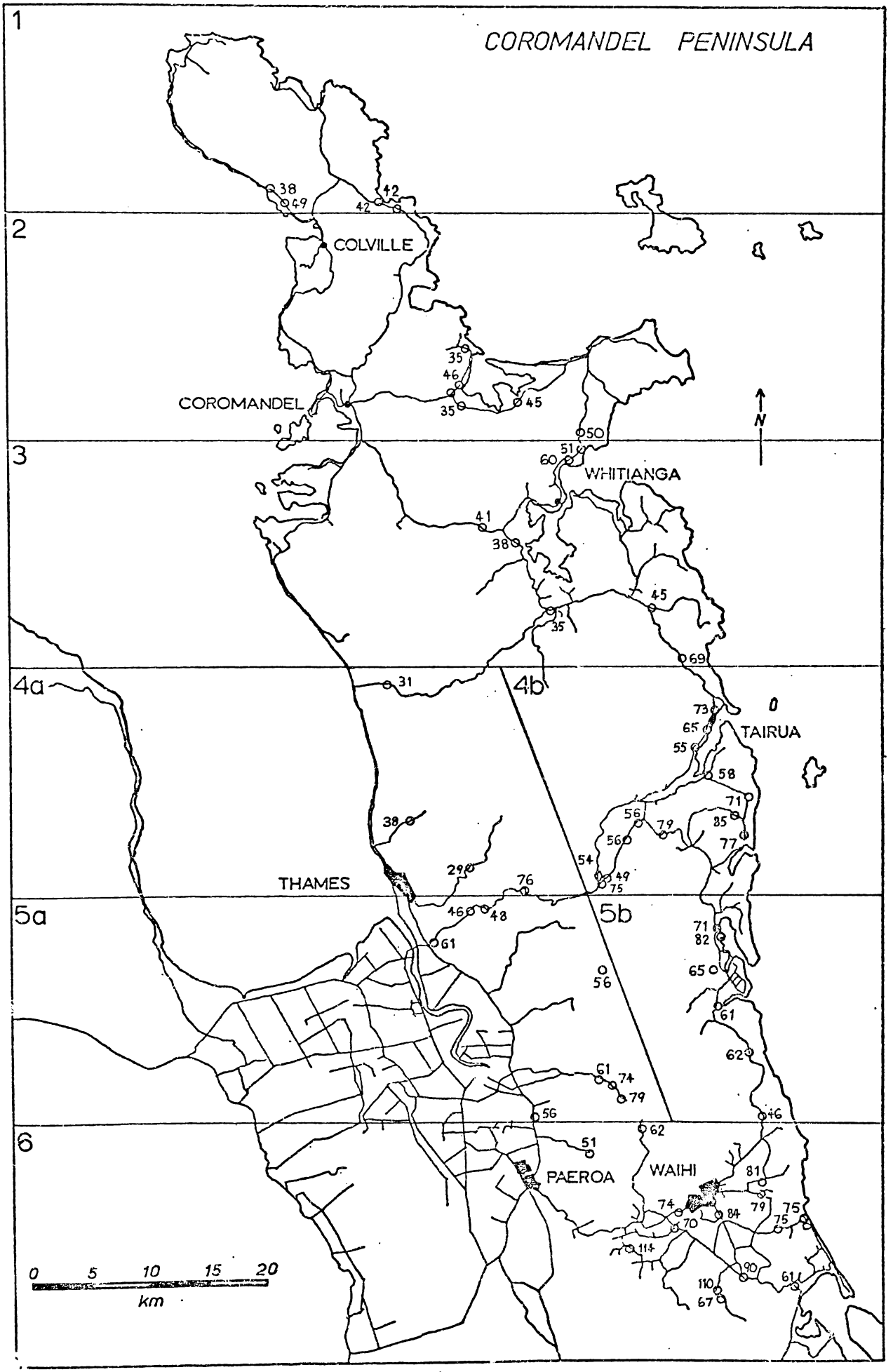
COROMANDEL PENINSULA
1
2
3
4a
4b
5a
5b
6
COLVILLE
COROMANDEL
WHITIANGA
TAIRUA
THAMES
PAEROA
WAIHI
N
0 5 10 15 20
km

# CHAPTER 3

## CHARACTERISATION OF THE TEPHRAS OF THE FIVE FIELD CLASSES AT A REFERENCE SITE FOR THE SOUTHERN PART OF THE COROMANDEL PENINSULA

### INTRODUCTION

In this chapter the particle size, mineralogical and chemical properties of the tephras occurring at a reference site in the Waihi region are described, to aid in the characterisation of individual tephras contained within the five field classes.

A site on the Waihi Plain (Pukekauri Rd., Site 8) about four kilometres southwest of Waihi with well defined field class boundaries, was selected as a reference site for detailed sampling. Samples, approximately three kilograms in weight and taken at least 75 cm back from the weathered bank surface, were obtained from the two metre thickness of tephra exposed in the road cutting (Fig. 3.1). Three samples from class V were collected at Waimata Rd. (Site 4), eight kilometres to the southeast of Pukekauri Rd, where the shower-bedded zone of field class V is more clearly exposed.

Many of the tephras deposited upon the Coromandel Peninsula are comparatively thin and since deposition have become mixed with older deposits by soil forming processes. Laboratory investigations attempt to recognise and "finger-print" tephra units within these mixed deposits. Methods applicable to the examination of mixed tephra deposits can be broadly grouped as multicomponent, single component-multiparticle and single component-single particle (Hodder

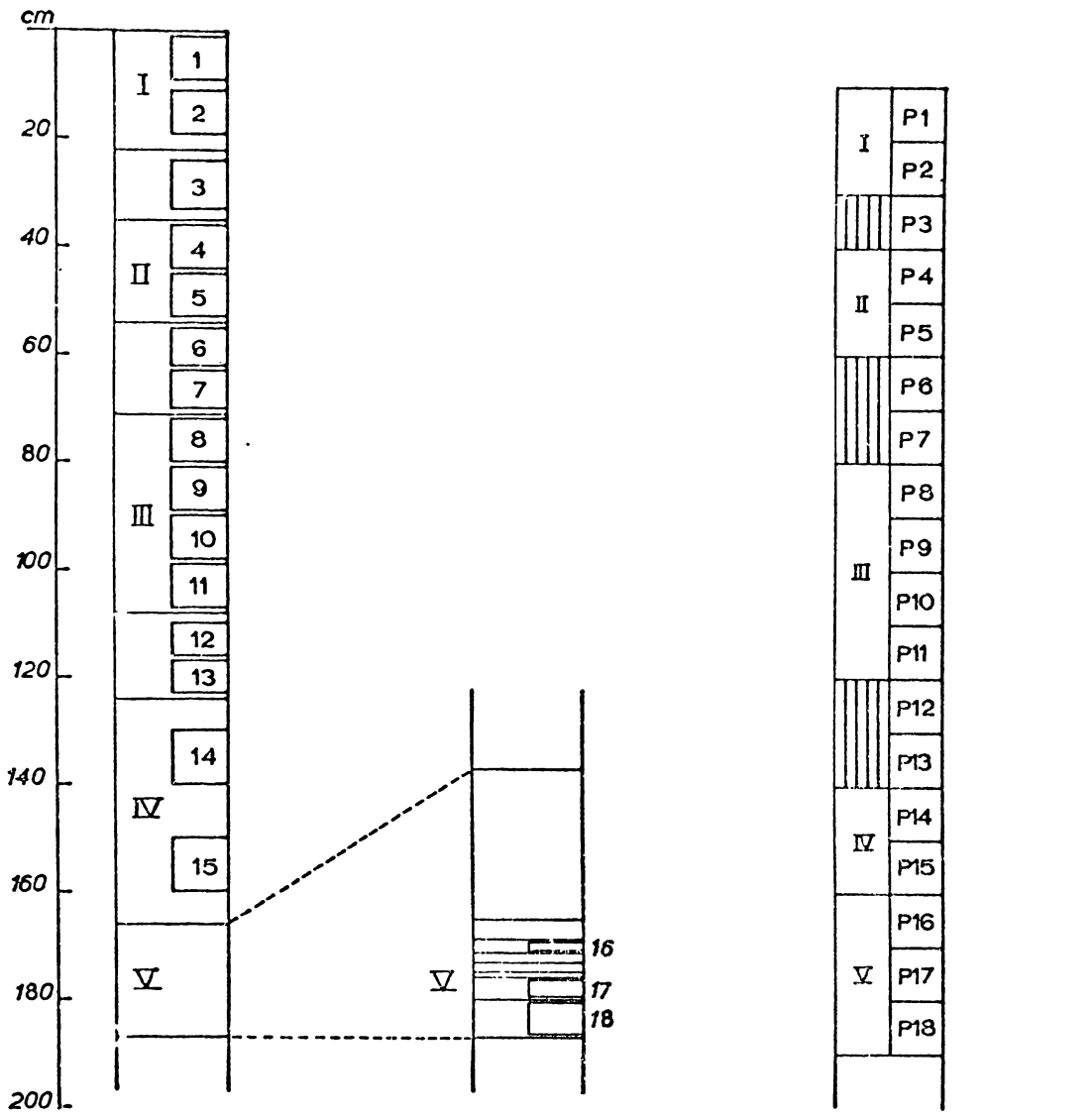


FIGURE 3.1 : Field classes and sample locations for the reference sections on the Waihi Plain. Field classes are represented by Roman Numerals e.g. I and tephras considered intermediate between two field classes are designated: e.g. I/II, or shown by cross hatching. The Waimata Rd samples are labelled P16 to P18 in the composite tephra column and are included in the term "Pukekauri Rd samples" when it is used in the text.

and Wilson 1976). Multicomponent techniques encompass a range of mineral types and in this thesis include mineralogical studies and the determination of particle size parameters for both whole tephra samples and sand fractions. Single-component methods apply to analytical methods for specific minerals and are subdivided into either techniques involving many grains (multiparticle), for example chemical analysis of titanomagnetite, or techniques applied to a single grain of a particular mineral (single particle), as with electron microprobe analysis of single titanomagnetite grains. A flow chart summarising physical separation techniques, analytical methods, and techniques for the characterisation of tephras is presented in Fig. 3.2.

MULTICOMPONENT METHOD OF CHARACTERISATION

1. Particle Size parameters

Tephra particle size properties, especially grain size, sorting and grading, are commonly used to characterise tephras in field correlation studies (e.g. Vucetich and Pullar 1964). The use of grain size parameters derived from laboratory analyses for characterising tephras is less well documented in the literature, although the parameters of mean grain size and standard deviation (or sorting) have been utilised for correlation purposes with some success (e.g. Fisher 1964; 1966).

Particle size parameters were calculated for both whole tephra samples (i.e. sand, silt and clay) and for the sand fraction (coarser than 4 $\emptyset$) following standard hydrometer and sieve analyses (see Appendix B, p.269). The statistical parameters used include

the phi mean grain size of Folk and Ward (1957) and the phi deviation measure of Inman (1952). Because many of the samples analysed contained a considerable proportion of very fine clay particles (12-14 ∅), extrapolation to the 84th percentile was occasionally necessary.

(a) Particle size parameters for whole tephra samples

Particle size data and parameters for sixteen Pukekauri Rd samples are presented in Appendix E (Figs. E.1 and E.2 and Table E.1) and summarised graphically in Figs. 3.3 and 3.4 using both soil (Taylor and Pohlen (1962) and sedimentary (Folk 1968) size classes.

The samples are mainly clay loams or sandy loams according to the soil particle size classes and sandy muds using the sedimentary scheme. Field and laboratory textural classes are compared in Table 3.1, which indicates that the field estimations underestimate the clay content in all except the coarsest samples. Two separate factors produced this inconsistency. The first occurs in the two youngest field classes and involves pumice grains which cannot be physically separated and are therefore exposed to the vibration treatment necessary to disperse the samples. Whereas the pumice in class I is fresh and relatively unaffected by exposure to ultra-sonic waves, that in class II is strongly weathered and the severe abrasion results in an artificial contribution to the silt and clay fraction. The second factor, operating in the three older field classes, is related to the tendency for amorphous clay minerals to be aggregated in their natural field states. Field textural determinations therefore measure these aggregates rather than

FIGURE 3.2: Flow chart summarising the techniques used for isolating components from the Coromandel tephras. Multicomponent and single component (multiparticle and single particle) methods of characterisation are also indicated.

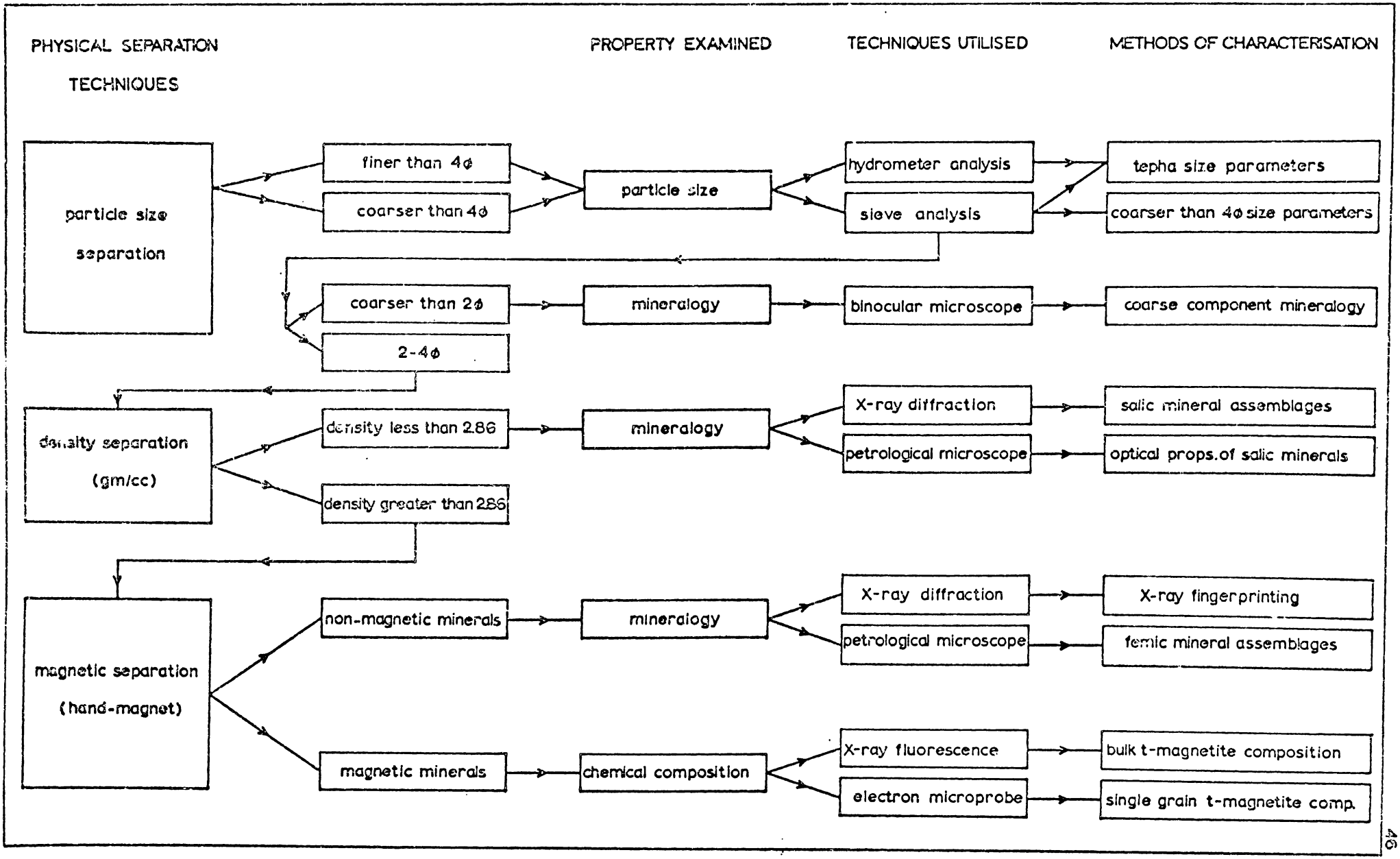
PHYSICAL SEPARATION TECHNIQUES
PROPERTY EXAMINED
TECHNIQUES UTILISED
METHODS OF CHARACTERISATION
particle size separation
finer than 4ϕ
coarser than 4ϕ
particle size
hydrometer analysis
sieve analysis
tepha size parameters
coarser than 4ϕ size parameters
coarser than 2ϕ
2-4ϕ
mineralogy
binocular microscope
coarse component mineralogy
density separation (gm/cc)
density less than 2.86
density greater than 2.86
mineralogy
X-ray diffraction
petrological microscope
salic mineral assemblages
optical props. of salic minerals
magnetic separation (hand-magnet)
non-magnetic minerals
magnetic minerals
mineralogy
chemical composition
X-ray diffraction
petrological microscope
X-ray fluorescence
electron microprobe
X-ray fingerprinting
femic mineral assemblages
bulk t-magnetite composition
single grain t-magnetite comp.

FIGURE 3.3: Percentage sand, silt, and clay and the mean grain size for the Pukekauri Rd tephra samples.

A : The Sedimentary scheme of Folk.

B : The New Zealand soil particle size classes.

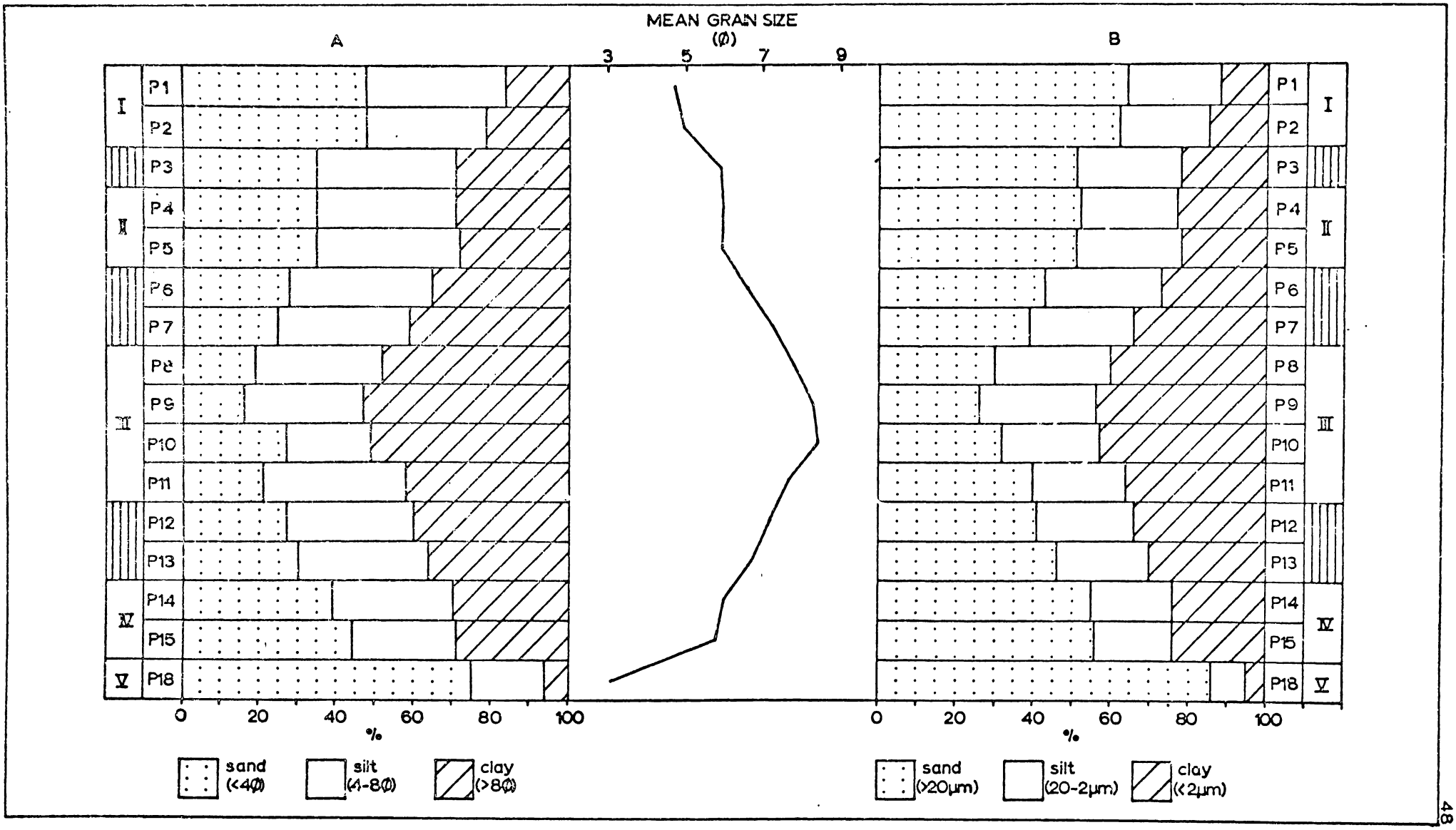
MEAN GRAIN SIZE
(Ø)
3
5
7
9
A
B
I
II
III
IV
V
P1
P2
P3
P4
P5
P6
P7
P8
P9
P10
P11
P12
P13
P14
P15
P18
0
20
40
60
80
100
%
sand
(<4Ø)
silt
(4-8Ø)
clay
(>8Ø)
sand
(>20µm)
silt
(20-2µm)
clay
(<2µm)

A : New Zealand Soil Particle Size Classes

Sand : < 5.65ϕ (20μm)
Silt : 5.65-9ϕ (20-2μm)
Clay : > 9ϕ (2μm)
(Taylor and Pohlen 1962)

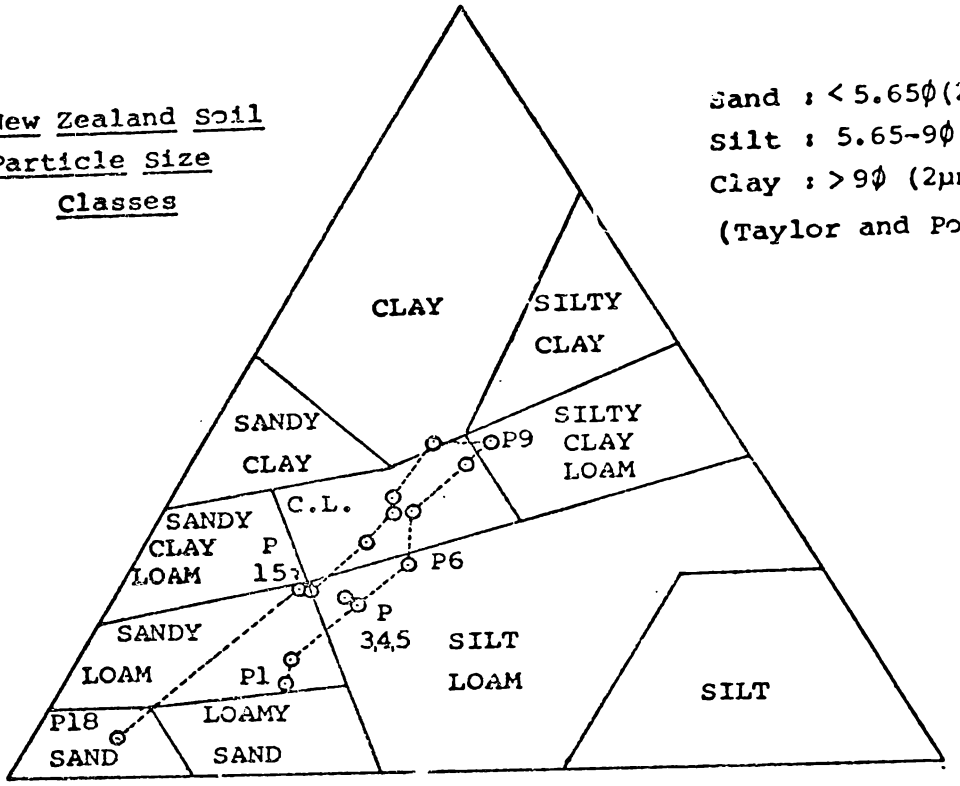


B : Sedimentary Scheme of Folk (1968)

Sand : < 4ϕ (63μm)
Silt : 4-8ϕ (63-4μm)
Clay : > 8ϕ (4μm)
(Folk 1968)

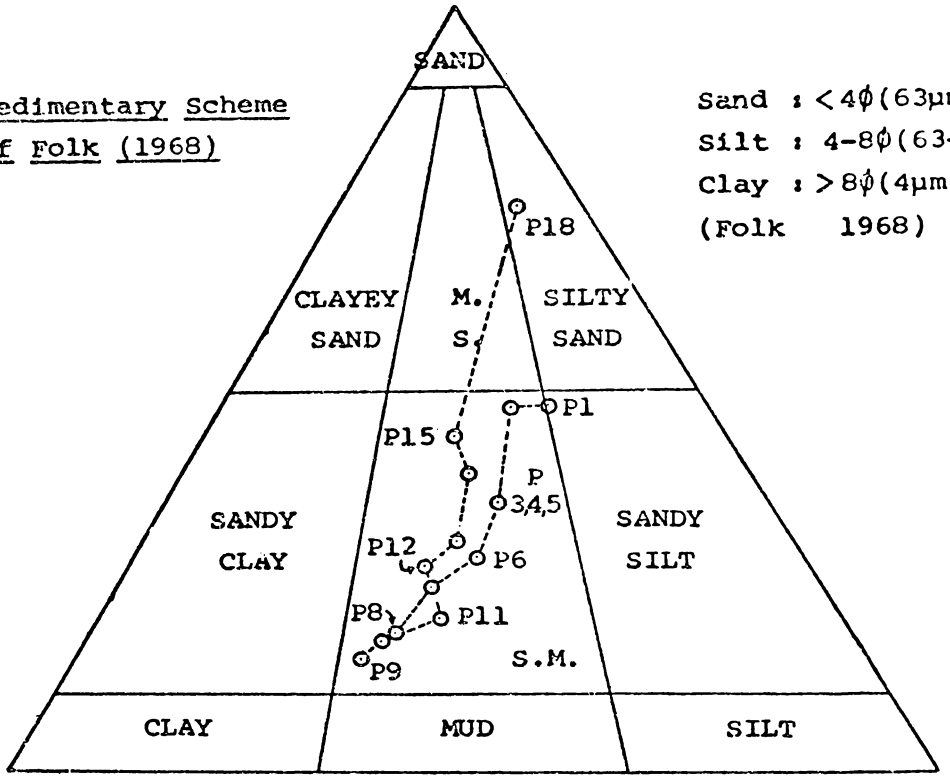


FIGURE 3.4 : Triangular textural plots for tephras from Pukekauri Rd.

discrete particles with the result that the field textures are consistently coarser than laboratory ones.

TABLE 3.1: A comparison of field textural classes and particle size classes for the Pukekauri Rd Stratigraphic column

| | | Textural class determined in the field (see p.321) | Particle Size class determined in the laboratory. (N.Z. soil particle size classes) |
|---|---|---|---|
| I | P1<br>P2 | Sandy loam | Sandy loam |
| I/II | P3 | Coarse sandy loam | |
| II | P4<br>P5 | Silty sandy loam | Silt loam |
| II/III | P6<br>P7 | Fine sandy silt loam | Clay loam |
| IV | P8<br>P9<br>P10<br>P11 | Silt loam | Silty clay loam<br>Clay |
| III/IV | P12<br>P13 | Silt loam | Clay loam |
| IV | P14<br>P15 | Silty sandy loam | Sandy loam |
| V | P18 | Sand | Sand |

The most important particle size characteristics of individual tephra field classes are as follows. The Recent bed contains young tephras, having a low clay content and a high percentage of sand. The particle size distribution is unimodal with the mode between 1-2 $\phi$ (see Fig. E.2 p.306). Samples from the Pumiceous bed vary

from unimodal to trimodal distributions, with the polymodality probably relating to abrasion of weathered pumice grains through vibration treatment. The Silty bed is characterised by a high clay content and a bimodal grain size distribution with modes at approximately 4 ϕ and 7 ϕ. The Lumpy bed is coarser than the Silty bed and changes from a bimodal distribution in its upper parts to a unimodal distribution lower in the bed, with a mode at approximately 3 ϕ. The Shower-bedded class, represented by P18, contains a high proportion of sand-sized material with a unimodal distribution centred on 1-2 ϕ. The particle size distributions of whole tephra samples are insufficiently sensitive to define field class boundaries.

(b) Particle size parameters for the tephra sand fractions (coarser than 4 ϕ).

Because the high clay content of some samples masks the grain size properties of the primary material remaining from the original tephra deposit, particle size parameters were calculated for the sand fractions (coarser than 4 ϕ). Particle size data and parameters for the coarser than 4 ϕ material at Pukekauri Rd are given in Appendix E (Figs. E.3 and E.4 and Table E.2) and summarised in Fig. 3.5.

In Fig. 3.5 the samples have been grouped into three sand-sized categories [coarser than 2 ϕ, fine sand (2-3 ϕ), and very fine sand (3-4 ϕ)] in an attempt to distinguish samples whose grain size has been influenced by addition of pumiceous material. Field classes I and II have a large coarse component with a relatively small fine sand fraction. Although field classes I and

II have similar proportions of the coarse fraction, the very fine sand component is much greater in class II and the samples are more poorly sorted. Samples P3 and P4 are strongly bimodal with a coarse mode at 1-1.5 ϕ and a finer one at 3-3.5 ϕ (Fig. E.4); the fine mode probably contains fragments of weathered yellow orange pumice grains which decomposed during vibration treatment. Samples P5 and P6 are transitional in nature, with P7 having a particle size distribution like those of class III. Samples from field class III exhibit the finest mean grain sizes, are moderately sorted and coarsen regularly with depth (Fig. 3.5). No assistance in locating the boundary between field classes III and IV could be obtained from particle size data, as P8 grades uniformly down the stratigraphic column to P14. However an indication of the boundary is obtained from the mode of the unimodal class III and IV samples: while samples P6 to P11 have a mode between 3-3.5 ϕ, a steady coarsening occurs below this depth with P12 having a mode at 2.5-3 ϕ and P13, P14 and P15 at 2-2.5 ϕ, thus indicating that P12 is a mixed sample. The Shower-bedded class is characteristically better sorted than the younger tephras and is strongly unimodal, with mean grain sizes varying markedly within the zone of shower-bedding.

Variations in grain size parameters through the stratigraphic column for both whole tephra samples and their sand fractions confirm the tephric classes established on the basis of field characteristics. They further indicate that transitional samples exist between classes II and III (P5?, P6, P7?) and between classes III and IV (P12).

FIGURE 3.5 : Particle size distribution, mean grain size and sorting coefficient for the coarser than 4 Ø fraction of the tephras at Pukekauri Rd. Boundaries between field classes, inferred from the data, are shown on the right hand side of the diagram. Particle size data are recorded in Appendix E (Figs. E.3 and E.4 and Table E.2) in the form of cumulative frequency curves and histograms of selected samples.

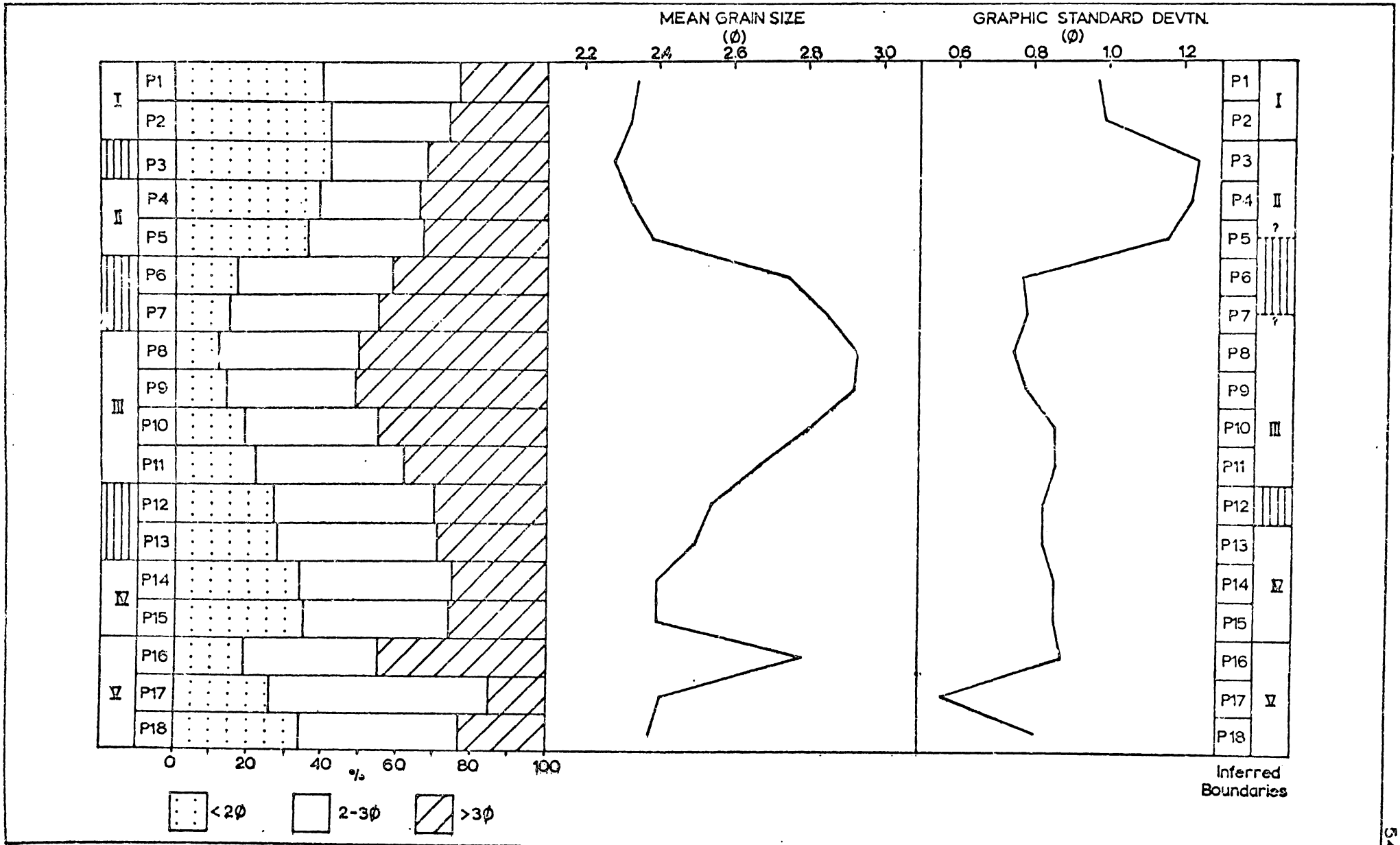
MEAN GRAIN SIZE
(Ø)
2.2
2.4
2.6
2.8
3.0
GRAPHIC STANDARD DEVTN.
(Ø)
0.6
0.8
1.0
1.2
I
II
III
IV
V
P1
P2
P3
P4
P5
P6
P7
P8
P9
P10
P11
P12
P13
P14
P15
P16
P17
P18
0
20
40
%
60
80
100
<2Ø
2-3Ø
>3Ø
Inferred
Boundaries

## 2. Mineral assemblages

Petrological characteristics form one of the oldest and most useful multicomponent techniques for characterising volcanic tephra deposits. For example, Ewart (1971) divided the acidic rocks of the Taupo Volcanic Zone into five main groupings, on the basis of their ferromagnesian mineral assemblages (see also Cole 1970). Rapid methods of "finger-printing" heavy minerals by X-ray diffraction have supplemented traditional studies utilising the petrological microscope (e.g. Pryor and Hester 1969). Salic mineral assemblages have been used less commonly to characterise tephras. Abundances of feldspar, quartz and glass have been determined in tephras by petrological microscope (e.g. Ewart 1963), and infra-red analysis (e.g. Hodder and Wilson 1976) and in loose sediments by X-ray diffraction analysis (e.g. Nelson and Cochrane 1970). The Central North Island tephras have also been classified into broad categories by their clay contents, particularly the proportions of allophane and hydrated halloysite (Kirkman 1975).

To aid in the characterisation of the Coromandel tephras, the mineralogy of the coarser than 0 $\phi$ size fraction has been examined, along with modal analyses of the salic minerals, X-ray "finger-printing" of the ferromagnesian minerals and modal analysis of the ferromagnesian minerals.

### (a) Mineralogical examination of the coarser than 0 $\phi$ (1 mm) size fraction

The coarse fractions ($<0\ \phi$) of the tephras at Pukekauri Rd are composed of quartz, rock fragments and volcanic glass in the

form of glassy fragments, pumice and obsidian (Table 3.2). The rock fragments are grey and white in colour and composed of a glassy groundmass with isolated anhedral zones of devitrified glass and scarce altered plagioclase phenocrysts. The pumiceous grains of field classes I and II are subdivided into two categories on the basis of colour (Appendix A p.240). Yellow orange pumice grains are strongly flow-banded and have a low phenocryst content dominated by anorthoclase. White pumiceous grains, less weathered than those described above, have a predominantly plagioclase phenocryst content.

TABLE 3.2: Relative abundances of quartz, rock fragments and volcanic glass in the coarser than 0 Ø fraction of the tephras at Pukekauri Rd, determined by binocular microscope

| Sample | | Quartz | Rock Fragments | Volcanic Glass | | |
|---|---|---|---|---|---|---|
| | | | | Glassy Fragments | Pumice | Obsidian |
| I | P1,P2 | S[+] | S | - | EA | S |
| I/II & III | P3,P4,P5 | S | C | - | EA | C |
| II/III | P6,P7 | VC | VC | - | A | C-r |
| III | P8-P11 | A-VA | A | C | - | - |
| III/IV | P12,P13 | VA | VC | C | - | - |

+ EA (Extremely abundant) >70%
VA (Very abundant) 50-70
A (Abundant) 30-49
VC (Very common) 10-29
C (Common) 5-9
S (Scarce) 1-4
r (rare) < 1%

Table 3.2 shows that the content of rock fragments and quartz is relatively low in field classes I and II while in field classes III and III/IV it is very common to very abundant, at the expense of the modal percentage of volcanic glass. The volcanic glass fraction of classes I and II is dominated by pumiceous glass with minor obsidian, which contrasts with the glass fragment-rich content of other field classes.

(b) Modal analyses of the salic mineral assemblage

Proportions of quartz, plagioclase and anorthoclase were determined semi-quantitatively in the 2-4 Ø fraction of the Pukekauri Rd tephras using the X-ray diffraction technique of Nelson and Cochrane (1970) - Table 3.3. The heavy mineral fraction was determined by weighing separates obtained by heavy liquid techniques, and volcanic glass contents were obtained by difference. All samples were analysed in triplicate to provide an estimation of error (standard deviations are shown in Table 3.3). Errors were found to be greater than the $\pm$ 10% of true value obtained by Nelson and Cochrane. Figure 3.6 summarises the data and allows tentative stratigraphic boundaries to be constructed, as described below. Two major stratigraphic boundaries can be defined in Fig. 3.6. Field class II is clearly distinguished from class III at the depth represented by samples P6 and P7. Class II is characterised by high amounts of glass and anorthoclase, and low amounts of plagioclase and heavy minerals. In class III, anorthoclase is absent, the glass content is lower and decreases with depth, and the heavy mineral and plagioclase content becomes increasingly abundant in the lower parts of the bed. The second

TABLE 3.3: Modal analysis of the 2-4 ϕ fraction of the Coromandel tephras at Pukekauri Rd

| Samples | | Plagioclase (Wt %) | Quartz (Wt %) | Anorthoclase (Wt %) | Volcanic glass (Wt %) | Heavy minerals (Wt %) |
|---|---|---|---|---|---|---|
| I | P1 | 14±0.5 | 9±2.5 | 6±1.3 | 69 | 2 |
| | P2 | 16±0.4 | 13±1.4 | 5±0.2 | 64 | 2 |
| I/II | P3 | 12±1.5 | 11±2.5 | 9±1.2 | 66 | 2 |
| II | P4 | 15±0.8 | 9±1.2 | 9±0.5 | 65 | 2 |
| | P5 | 14±1.2 | 9±1.2 | 7±0 | 67 | 3 |
| II/III | P6 | 14±1.5 | 9±0 | 5±0.7 | 69 | 3 |
| | P7 | 16±0.7 | 9±2.0 | - | 70 | 5 |
| III | P8 | 20±0.5 | 9±1.2 | - | 65 | 6 |
| | P9 | 22±2.3 | 9±1.2 | - | 58 | 11 |
| | P10 | 22±1.8 | 9±1.2 | - | 55 | 14 |
| | P11 | 25±1.9 | 9±0 | - | 49 | 17 |
| III/IV | P12 | 33±5.0 | 5±0.5 | - | 41 | 21 |
| | P13 | 31±2.0 | 11±3.0 | - | 36 | 22 |
| IV | P14 | 37±5.0 | 11±3.2 | - | 34 | 18 |
| | P15 | 28±1.9 | 11±1.2 | - | 45 | 16 |
| V | P16 | 18±1.8 | 11±1.2 | - | 67 | 4 |
| | P17 | 30±2.9 | 21±1.6 | - | 40 | 9 |
| | P18 | 38±5.2 | 5±2.6 | - | 40 | 17 |

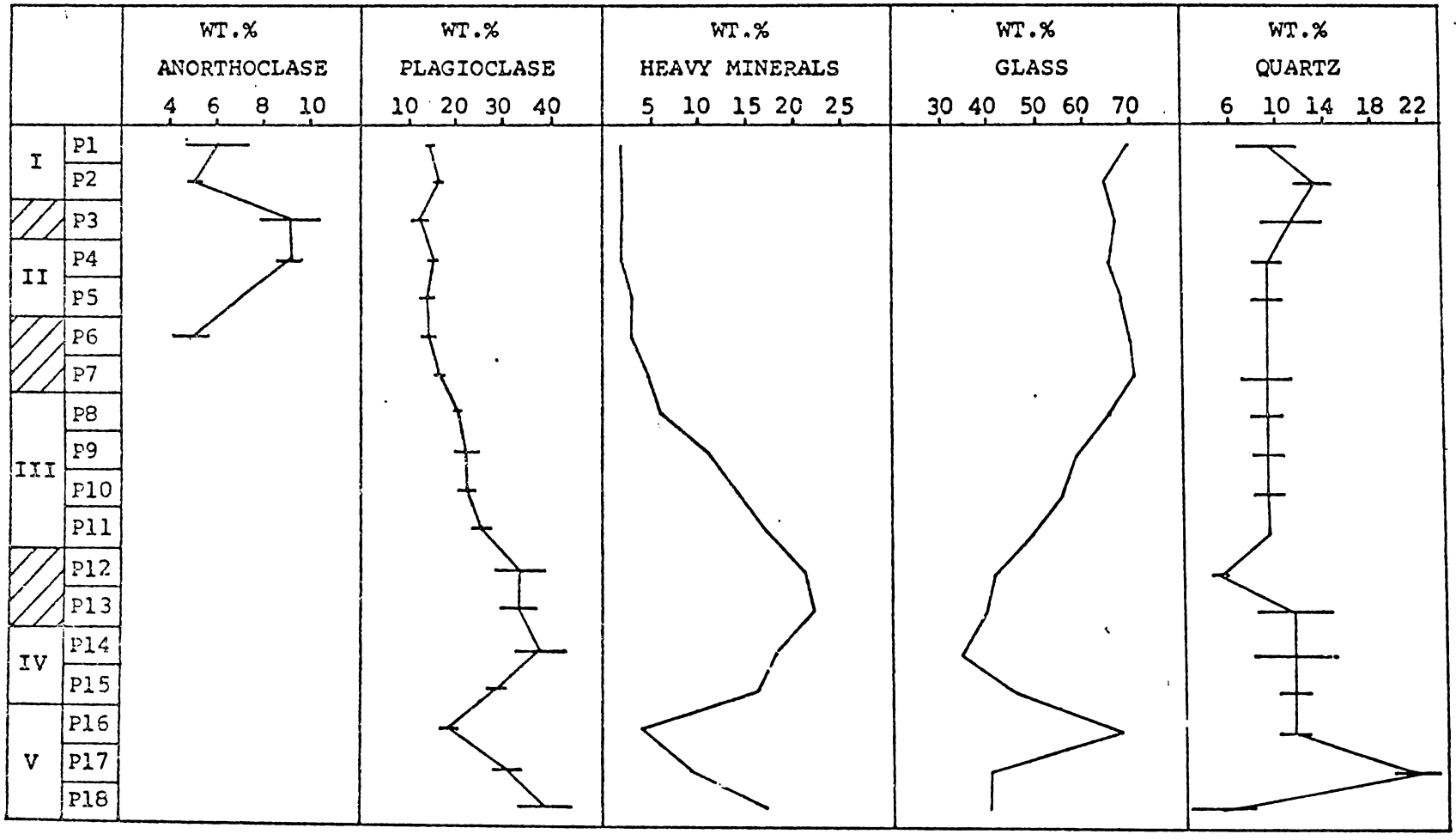


FIGURE 3.6 : The felsic and heavy mineral contents of the 2-4$\phi$ fraction of the Coromandel tephras at Pukekauri Rd. Anorthoclase, plagioclase and quartz values were determined by XRD and include the standard deviation.

major stratigraphic boundary lies between classes IV and V with class V being distinguished from class IV by its extremely variable properties.

Considerable mineralogical variation exists within, as well as between, field classes, particularly for classes III and V. Class III shows an increasing content of plagioclase and heavy minerals with depth, at the expense of volcanic glass. These changes could possibly be due to preferential gravitational settling of plagioclase and glass following eruption (plagioclase density = 2.65, rhyolitic glass = 2.30), or to a gradual change in magma composition as eruption progresses (c.f. the Hekla eruption of 1947, Thorarinsson 1954), or to the mixing of a younger, glass-rich rephra with an older plagioclase-rich tephra. The latter alternative is preferred because 2V measurements of plagioclase in field class III show an unusually high coefficient of variation, suggesting a mixture of two populations of different compositions (see Appendix A p.249). Field class V shows extreme mineralogical diversity although its field properties indicate that the zone of shower-bedding has been derived from closely spaced eruptive pulses from a single source. To test the hypothesis that the mineralogical diversity is associated with variations in particle size, two samples from the zone of shower-bedding in field class V were sieved and their mineralogy examined for each grain size interval within the 2-4 $\phi$ range (Table 3.4). Plagioclase and quartz dominate the coarser intervals and volcanic glass and the heavy minerals the finer ones. Table 3.4 shows that the mineralogical diversity within the zone of shower-bedding is related

TABLE 3.4: Relationship between mineralogy and particle size in the 2-4 ϕ fraction of two field class V samples from the zone of shower-bedding

| Sample | | Particle size fraction | | | |
|---|---|---|---|---|---|
| | | 2.0-2.5 ϕ (Wt %) | 2.5-3.0 ϕ (Wt %) | 3.0-3.5 ϕ (Wt %) | 3.5-4.0 ϕ (Wt %) |
| P17 | Quartz | 24 | 21 | 13 | 13 |
| | Plagioclase | 43 | 30 | 21 | 17 |
| | Glass and heavy minerals | 33 | 49 | 66 | 70 |
| P18 | Quartz | 16 | 14 | 11 | 11 |
| | Plagioclase | 55 | 41 | 35 | 34 |
| | Glass and heavy minerals | 29 | 45 | 54 | 55 |

to the mean grain size and not to real differences in composition within field class V. Thus sample P16 has a mean of 2.69 and is therefore comparatively rich in volcanic glass. In contrast, sample P18 is coarser (mean = 2.38) and is therefore dominated by quartz and plagioclase.

(c) Finger-printing by X-ray diffraction of the ferromagnesian mineral assemblage

Smear mounts of ferromagnesian mineral separates from five samples of the tephras at Pukekauri Rd were X-rayed and compared with samples from two tephras of known composition, the Tahuna Tephra (Howorth, pers.comm.) and the Rotoiti Breccia (Ewart 1968).

Figure 3.7 indicates that for the Coromandel tephras at Pukekauri Rd, cummingtonite increases in concentration with depth at the expense of hypersthene and hornblende. While the youngest and oldest tephras (classes I and V respectively) show distinct differences using this method, the variations between adjacent field classes are on too small a scale to permit easy distinction between them.

(d) Modal analysis of the ferromagnesian mineral assemblage

Modal analyses of the ferromagnesian minerals were carried out by optical methods and the reliability of the analyses assessed by the chart of Van der Plas and Tobi (1965). Between 300 and 500 grains were counted on each slide to maintain an error for the major constituent of better than $\pm$ 5% (at the 95% confidence level).

Data on the ferromagnesian mineral abundances for the tephras at Pukekauri Rd are shown in Table 3.5 and summarised in Fig. 3.8. The Pukekauri Rd column can be subdivided into five units on the basis of hypersthene to amphibole ratios (Fig. 3.8).

(1) Low hypersthene/amphibole (P1-P4).

(2) Increasing hyposthene/amphibole (P5-P7).

(3) High hypersthene/amphibole (P8-P12)

(4) Decreasing hypersthene/amphibole (P13-P15).

(5) Very low hypersthene/amphibole (P16-P18).

The youngest tephras, represented by P1-P4, are distinguished from the samples below by their high aegirine and augite contents. The two categories of pumiceous grains occurring in field classes I and II have distinctive ferromagnesian mineral assemblages (Table 3.6).

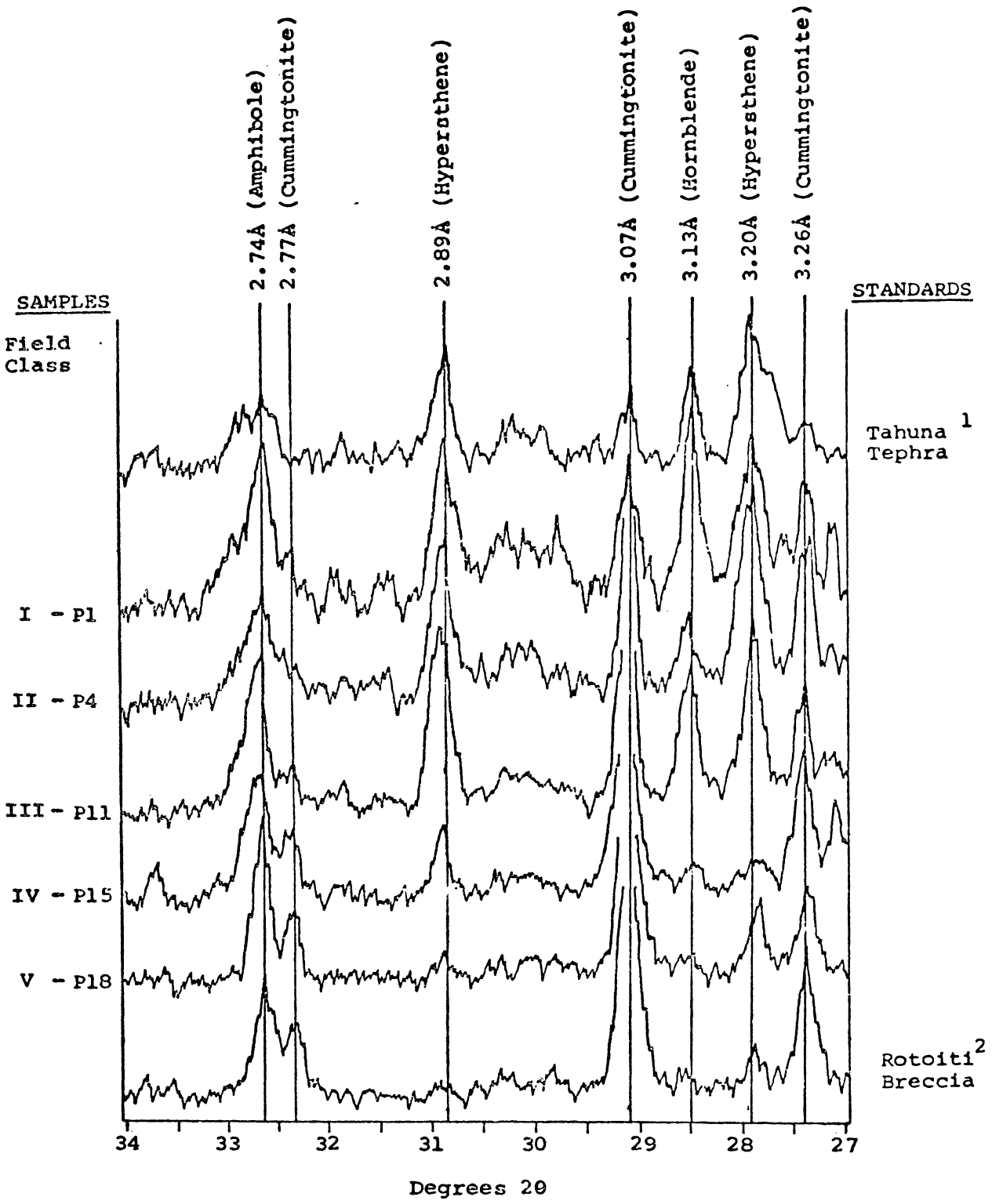


FIGURE 3.7 : Finger-printing of the Coromandel tephras by X-ray diffraction analysis of their ferromagnesian mineral assemblages.

1. Tahuna Tephra: hornblende (48-62%)
hypersthene (32-46%).
augite (2-10%)

2. Rotoiti Breccia : cummingtonite (65-95%)
hypersthene (10-35%)
augite (0-5%)

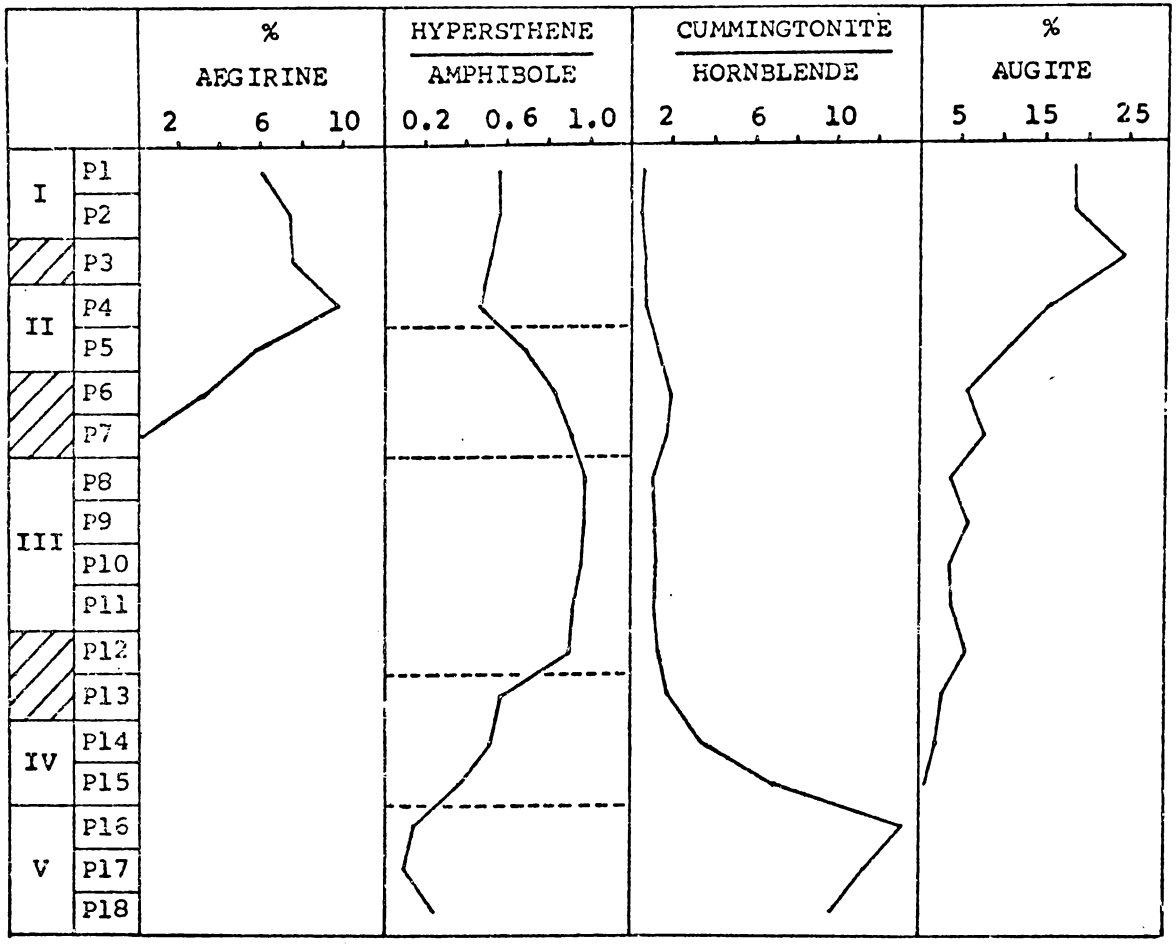


FIGURE 3.8 : Ferromagnesian mineral ratios in the 2-4ϕ fraction of the Coromandel tephras at Pukekauri Rd. The hypersthene to amphibole ratio can be divided into five units.
For further explanation see text.

TABLE 3.5 : Modal analyses of the ferromagnesian minerals in the 2–4 Ø fraction of the Coromandel tephras at Pukekauri Rd

| Field class | Sample | % Hypersthene | % Cummingtonite | % Hornblende | % Augite | % Aegirine | Additional minerals[1] |
|---|---|---|---|---|---|---|---|
| I | P1 | 28 | 19 | 30 | 17 | 6 | titanomagnetite, zircon, cossyrite, olivine, riebeckite, oxyhornblende |
| | P2 | 27 | 14 | 34 | 18 | 7 | |
| I/II | P3 | 23 | 20 | 26 | 24 | 7 | titanomagnetite, zircon, cossyrite, olivine, riebeckite, oxyhornblende, ? hedenbergite, tuhualite |
| II | P4 | 24 | 22 | 30 | 14 | 10 | |
| | P5 | 34 | 28 | 22 | 10 | 6 | titanomagnetite, zircon |
| II/III | P6 | 41 | 33 | 17 | 6 | 3 | |
| | P7 | 43 | 31 | 17 | 8 | 1 | |
| III | P8 | 47 | 25 | 24 | 4 | | titanomagnetite, zircon |
| | P9 | 46 | 26 | 22 | 6 | | |
| | P10 | 47 | 27 | 22 | 4 | | |
| | P11 | 46 | 26 | 24 | 4 | | |

| | | | | | | |
|---|---|---|---|---|---|---|
| III/IV | P12 | 45 | 29 | 20 | 6 | |
| | P13 | 35 | 40 | 22 | 3 | titanomagnetite |
| IV | P14 | 33 | 50 | 15 | 2 | zircon, |
| | P15 | 27 | 63 | 9 | 1 | vermiculite |
| V | P16 | 9 | 85 | 6 | | |
| | P17 | 8 | 86 | 6 | | |
| | P18 | 11 | 82 | 7 | | |

[1] See Appendix A for descriptions of minerals

TABLE 3.6: Ferromagnesian mineral abundances in the pumiceous lapilli and 2-4 ϕ fraction of field classes I and II at Pukekauri Rd

| Field class | Sample | Size fraction | % Hyper-sthene | % Cumming-tonite | % Horn-blende | % Augite | % Aegirine | % Cossyrite |
|---|---|---|---|---|---|---|---|---|
| I | P1 | White pumiceous lapilli[1] | 96 | 2 | - | 2 | - | - |
| | | 2-4 ϕ | 28 | 19 | 30 | 17 | 6 | trace |
| II | P4 | Yellow orange pumiceous lapilli[1] | 12 | 1 | 2 | - | 71 | 14 |
| | | 2-4 ϕ | 24 | 22 | 30 | 14 | 10 | trace |

1. Lapilli crushed and passed through a 2-4 ϕ sieve before heavy mineral extraction

The white pumiceous grains which occur in field class I, are dominated by hypersthene and have a ferromagnesian assemblage quite unlike that of the 2-4 Ø fraction. The yellow orange pumice grains in field class II contain aegirine, cossyrite and hypersthene in different proportions to the accompanying 2-4 Ø fraction. The ferromagnesian mineralogy therefore indicates that at least three separate tephras are present in field classes I and II. One tephra is represented by the hypersthene-rich white pumiceous lapilli, a second by the yellow orange pumiceous lapilli which contains aegirine and cossyrite, and at least one other fine grained tephra, characterised by the large amounts of cummingtonite and hornblende in the 2-4 Ø fractions. It is probable that the hypersthene, cummingtonite and hornblende associated with the yellow orange pumiceous lapilli are derived from a fine grained tephra of different composition, whose crystals have become lodged within surface vesicles of the pumice. This conclusion is based upon the peralkaline nature of aegirine and cossyrite, which do not crystalise from the same magma as calc-alkaline minerals such as hypersthene, cummingtonite or hornblende (Carmichael et al. 1974).

A more accurate division between field classes may be obtained by using a triangular plot of the three main ferromagnesian minerals (Fig. 3.9). The diagram indicates that a number of changes in the positions of the field class boundaries should be made: sample P3 has class II properties; samples P5, P6 and P7 are transitional between classes II and III although the low hornblende content of P6 and P7 suggests that the samples may have been influenced by another tephra; sample P12 has class III properties; and sample P13 has class IV properties.

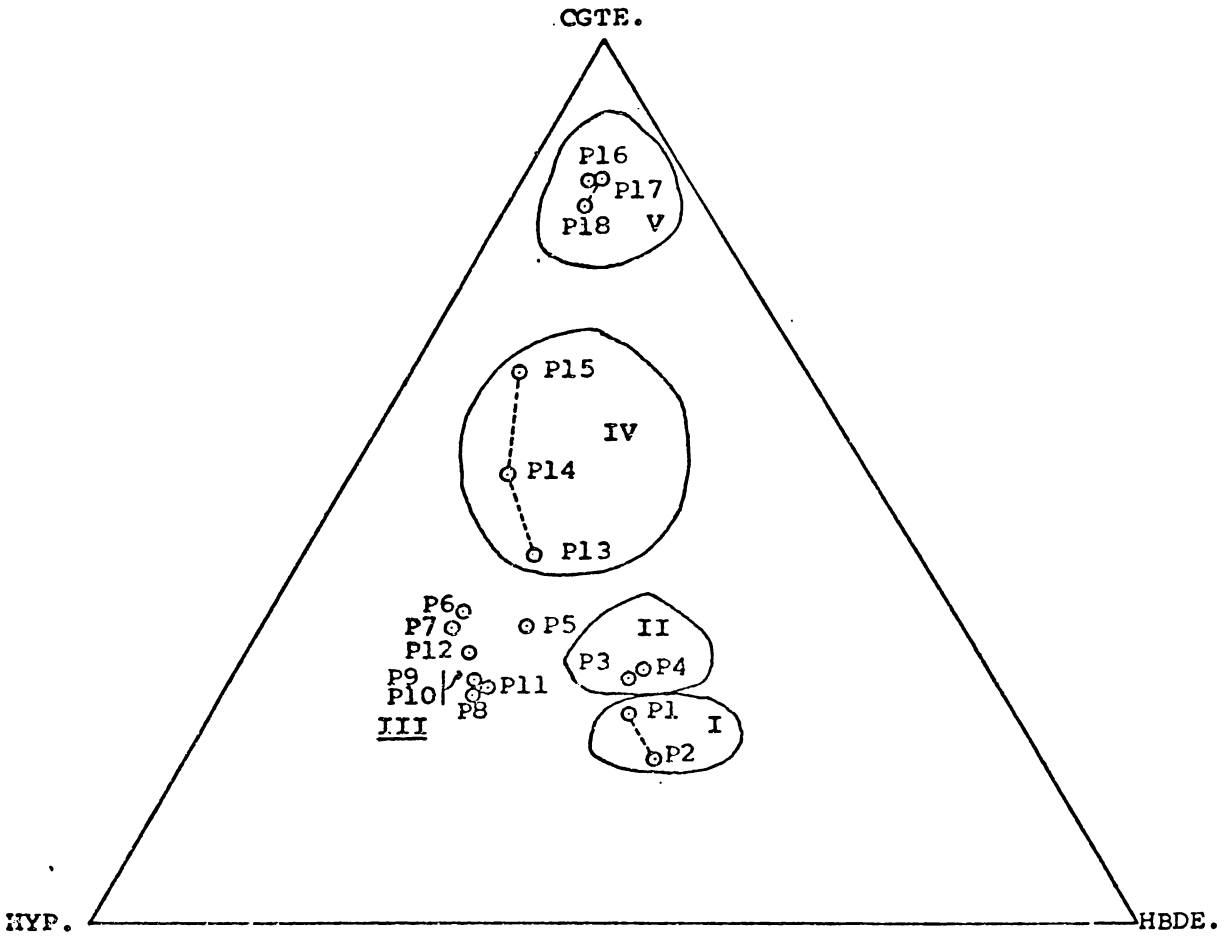


FIGURE 3.9 : Triangular plot of the three main ferromagnesian minerals from the Coromandel tephras at Pukekauri Rd. Suggested field class boundary limits are represented by enclosed areas.

CGTE = Cummingtonite
HBDE = Hornblende
HYP = Hypersthene

(e) Summary of the mineralogical characteristics of the Coromandel tephras at Pukekauri Rd

The mineralogy of the Coromandel tephras at Pukekauri Rd substantiates the fivefold division established in the field, and enables the field class boundaries to be positioned more accurately (Table 3.7).

TABLE 3.7: Repositioning of field class boundaries in the Pukekauri Rd stratigraphic column on the basis of mineralogical data

| Field class | Designation | Original field class boundaries | Field class boundaries inferred from mineralogical data |
|---|---|---|---|
| I | Recent bed | P1, P2 | P1, P2 |
| I/II | | P3 | - |
| II | Pumiceous bed | P4, P5 | P3, P4, ? P5 |
| II/III | | P6, P7 | ? P5, P6, P7 |
| III | Silty bed | P8, P9, P10, P11 | P8, P9, P10, P11, P12 |
| III/IV | | P12, P13 | - |
| IV | Lumpy bed | P14, P15 | P13, P14, P15 |
| V | Shower-bedded class | P16, P17, P18 | P16, P17, P18 |

The mineralogical characteristics of each of the five field classes are summarised below.

The Recent bed represented by samples P1 and P2, is dominated by pumiceous lapilli in the coarser size fractions and volcanic glass, mainly in the form of curved and pumiceous fragments, in

the finer. Clear and brown shards are both present, exhibiting a wide range of refractive indices (Appendix A) suggesting that the Recent bed is a composite tephra unit containing a number of tephras mixed by soil forming processes. The ferromagnesian mineral assemblage indicates the presence of at least three tephras. Two of these tephras are represented in the lapilli size fraction where one consists of white pumice containing plagioclase and hypersthene, and the other is a yellow orange pumice dominated by anorthoclase, aegirine and cossyrite. The third tephra is contained within the 2-4 $\phi$ fraction and characterised by minerals not common in the pumiceous lapilli, namely cummingtonite and hornblende.

The Pumiceous bed (samples P3 and P4) is dominantly glassy in nature and contains an abundance of the yellow orange pumiceous lapilli described above. The yellow orange pumices have a phanocrystic assemblage of anorthoclase, aegirine and cossyrite, with minor olivine, riebeckite, and tuhualite, which indicates that it has a peralkaline composition; it is subsequently referred to as "peralkaline pumice". At least one other tephra is present in the class II sand fraction and is represented by plagioclase, hypersthene, cummingtonite, hornblende and augite. The tephras comprising the Pumiceous bed had undergone substantial mixing with other tephras, resulting in a non-homogeneous deposit with gradational boundaries above and below - i.e. P2 grades into P3, and P4 grades into P5. Although P5 has class III properties, it also has strong affinities with field class II and has therefore been placed in both class II and with the transition samples P6 and P7.

The Silty bed is calc-alkaline and rhyolitic in composition (Appendix A) and though still dominated by glass, it contains greater amounts of quartz and plagioclase. The high hypersthene content, with lesser amounts of cummingtonite and hornblende, enables distinction of this class from other tephras. The most significant characteristic of the Silty bed is its gradational nature, with properties varying uniformly from the top of the bed into the Lumpy bed beneath, as exemplified by the increasing plagioclase concentration with depth. The possibility that class III represents a mixture of two tephras is supported by the optic axial angles of hypersthene and plagioclase, the former showing two distinct populations and the latter an unusually wide range of values (Appendix A).

The Lumpy bed is comparatively enriched in plagioclase and quartz relative to volcanic glass, a feature found in all the older deposits. Like the Silty bed, it exhibits vertical gradations with plagioclase decreasing while cummingtonite increases in concentration with depth. The trend of increasing cummingtonite concentration at the expense of hypersthene and hornblende continues into field class V, emphasising the gradational nature of the lower boundary.

The Shower-bedded class is also rhyolitic in composition and shows both mineralogical diversity in terms of its salic mineral fraction and homogeneity as indicated by the ferromagnesian mineral assemblages. The plagioclase, quartz and volcanic glass contents are controlled largely by grain size and hence show considerable variation within the individual shower-bedded units of class V. Cummingtonite comprises over 80% of the ferromagnesian mineral

assemblages of all class V samples, which indicates a common origin for the many shower-bedded units in the basal part of this field class.

## SINGLE COMPONENT METHODS OF CHARACTERISATION

### 1. Multiparticle

#### (a) Introduction

The characteristics of a tephra deposit result from the summation of the properties of the numerous discrete components comprising that tephra. The measurement of bulk composition and bulk mineralogy in multicomponent systems such as tephras is often unsuitable for correlation purposes because of the tendency for individual components to vary in their geographical distributions. Heavy minerals which are denser than the bulk of the deposit tend to fall closer to the volcanic vent while salic minerals and glass increase in abundance with increasing distance from source (Eaton 1964).

The usefulness of single components in the identification and correlation of tephras has been demonstrated by many workers (e.g. Smith and Westgate 1969; Kohn 1970; Rankin 1973; Westgate and Fulton 1975; Hodder and Wilson 1976; Smith et al. 1977a and b). Smith et al. (1977b) list three criteria for testing the usefulness of a single component for correlation purposes: it should exhibit maximum uniformity; its composition must be attributable with certainty to contemporaneous volcanic action; and the component must persist with distance from the volcano. A fourth criterion

could well be added, namely that the component should have remained largely unaltered in the weathering regime.

Volcanic glass has been proposed by many workers as the most useful single component for correlation purposes (e.g. Steen and Fryxell 1965; Smith and Westgate 1969; Borchardt and Harward 1971; Howorth and Rankin 1975; Smith et al. 1977a and b). However, in this study, glasses were avoided, because of the weathered pumiceous lapilli in classes I and II.

The use of the chemical composition of oxide minerals, particularly titanomagnetites, for correlation purposes has only received attention comparatively recently (e.g. Kohn 1970; Westgate and Fulton 1975). Kohn (1970) working on central North Island volcanic deposits pointed out that titanomagnetites are attractive for correlation purposes because they are ubiquitous in these deposits, they are stable during weathering, their range in chemical composition is considerable, and they can be relatively easily extracted and purified by magnetic methods. Moreover, because titanomagnetites crystalise early in a silicate melt, their chemical composition is characteristic of the parent magma (Carmichael 1967). Wright and Lovering (1965) have demonstrated that exsolution in titanomagnetite grains (Appendix A p.259) does not change their overall composition but merely redistributes the elements within the exsolved phases. Exsolved titanomagnetite grains can therefore be ignored in analyses of bulk titanomagnetite samples.

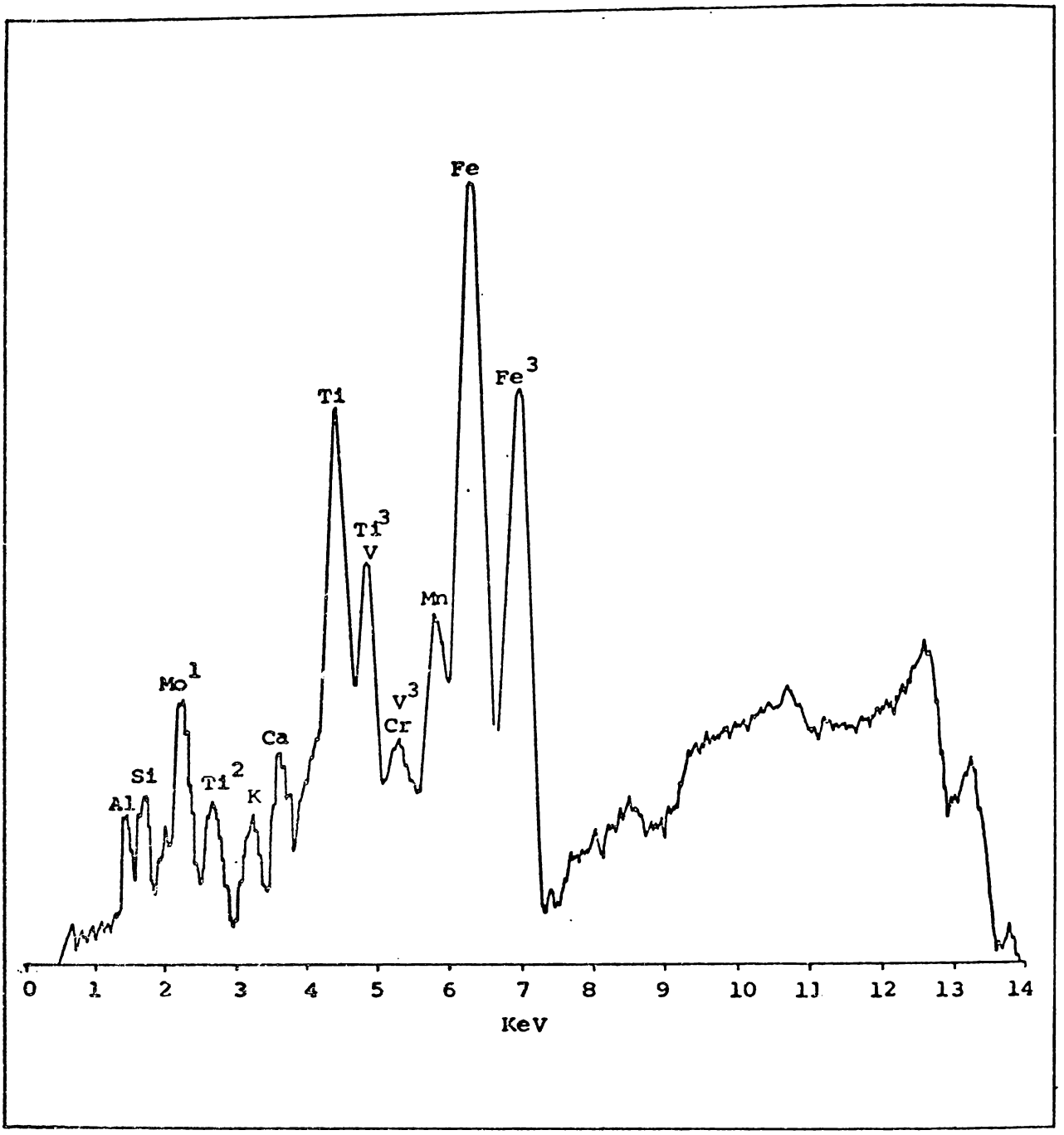


FIGURE 3.10 : Typical XRF spectrum of titanomagnetite from the Coromandel tephras. Sample P18.

1. Mo (Lα)
2. Ti escape peak
3. Element K (β)

All peaks are K (α) unless otherwise indicated.

(b) Titanomagnetite element content

Titanomagnetite was extracted by hand magnet, ground and concentrated to a purity estimated to exceed 99% and analysed under mylar film by XRF (see experimental procedure in Appendix B). It should be noted that because of the possibility of machine drift, all samples that are to be compared were analysed within a single 24 hour period.

The fluorescent intensities from nine elements were recorded (in counts per second) (Fig. 3.10) from eighteen samples representing the five field classes at Pukekauri Rd. The data for Ti, V, Mn and Fe are presented in Fig. 3.11 and as ratios in the form of an X - Y plot in Fig. 3.12. Seven of the nine elements analysed are represented within either the titanomagnetite or ilmenite phases (Al, Ca, Ti, V, Cr, Mn and Fe); the remaining two elements (Si and K) are contained within contaminating minerals such as volcanic glass or included crystals. Ti occurs in both titanomagnetite and hematite phases and shows important variation throughout the tephra column (for P1 to P18; C = 10.7%), which makes it the most useful element for characterising individual field classes. V is generally associated with the titanomagnetite phase (Carmichael 1967) and shows significant variation throughout the stratigraphic column (C = 14.7%); the Ti/V ratio is particularly important for categorising tephra samples. Mn in titanomagnetite is recommended by Kohn (1970) for the characterisation of tephras and exhibits moderate variability (C = 5.9%) and forms a useful ratio with Ti (Ti/Mn). Fe is present in both the titanomagnetite and hematite phases and shows the highest count rates of all the elements examined. However, it was not

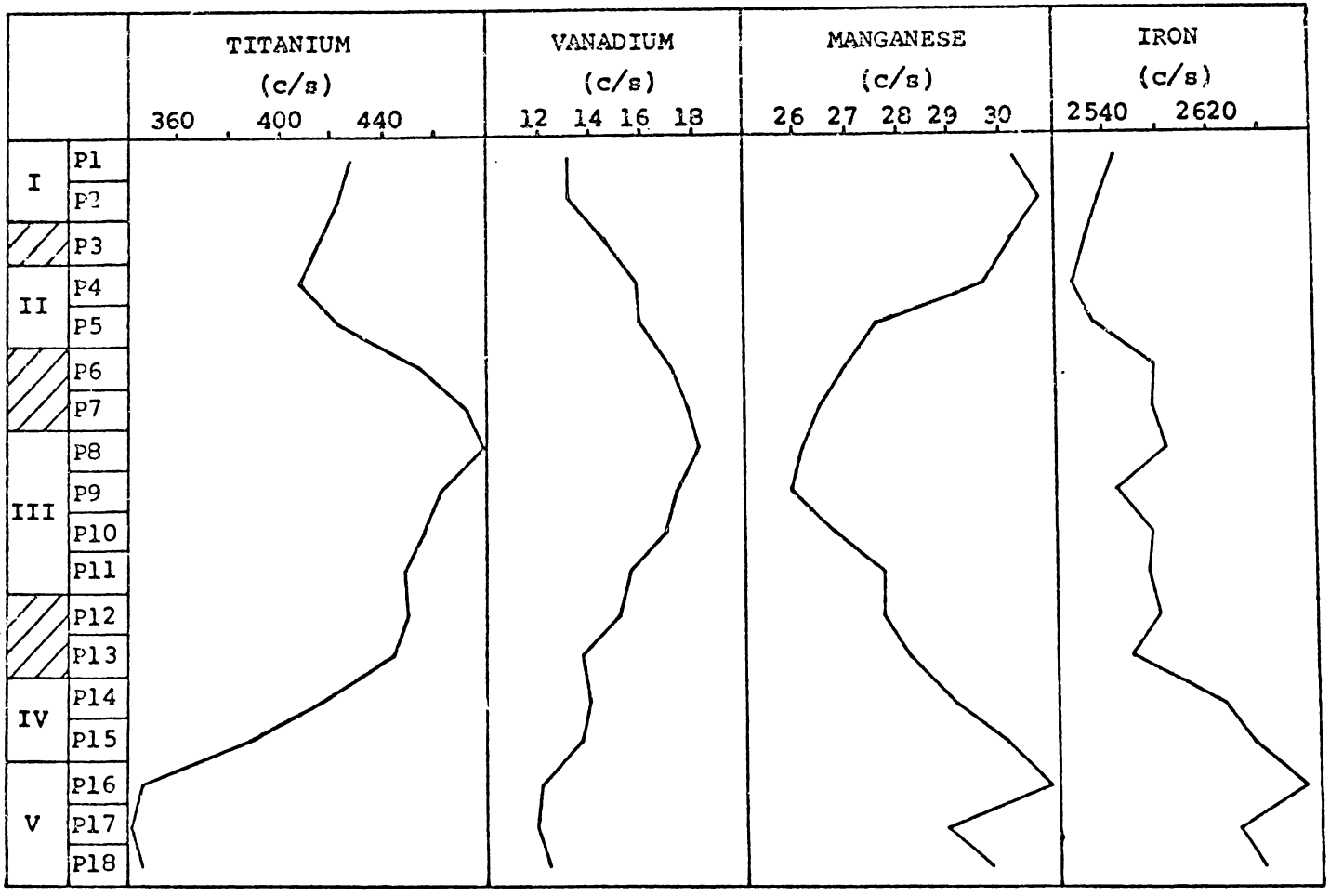


FIGURE 3.11 : Count rates for Ti,V,Mn and Fe from titanomagnetite extracted from the Coromandel tephras at Pukekauri Rd., and analysed by XRF.

utilised for characterisation purposes because of its low variability (P1 to P18; C = 2.1%). In all XRF spectra small quantities of Al and Ca occur; Al is derived from titanomagnetite, aluminous spinels, hematite and aluminosilicates, while Ca is present in both the titanomagnetite structure (Carmichael 1963, 1967) and in accessory minerals such as apatite and aluminosilicates (Wright and Lovering 1965). The high Ca count rates for samples P1 and P2 indicate significant contamination by volcanic glass and inclusions within the oxide minerals. Al and Ca were not used for correlation purposes because of variable contributions of these elements from extraneous materials. Carmichael (1963) and Wright and Lovering (1965) found that there was no Si or K in titanomagnetite so that the Si and K in this work are probably derived from volcanic glass and inclusions within the oxide minerals. Cr, although detectable by XRF, is masked by V ($CrK\alpha$ = 5.41 KeV; $VK\beta$ = 4.95 KeV). The concentrations of Cr are too low to permit the application of peak-stripping techniques.

X - Y plots of the ratios of Ti/V, Ti/Mn, V/Mn, V/Ti, Mn/V and Mn/Ti from titanomagnetites of all field classes indicate that Ti/V and Ti/Mn give the most satisfactory results for distinguishing between samples (Fig. 3.12).

(c) Discussion of results

From Fig. 3.12 it is apparent that the samples from any field class can be placed into one of three categories:

(i) those that have similar elemental ratios, forming a group e.g. F.C. V (P16, P17, P18);

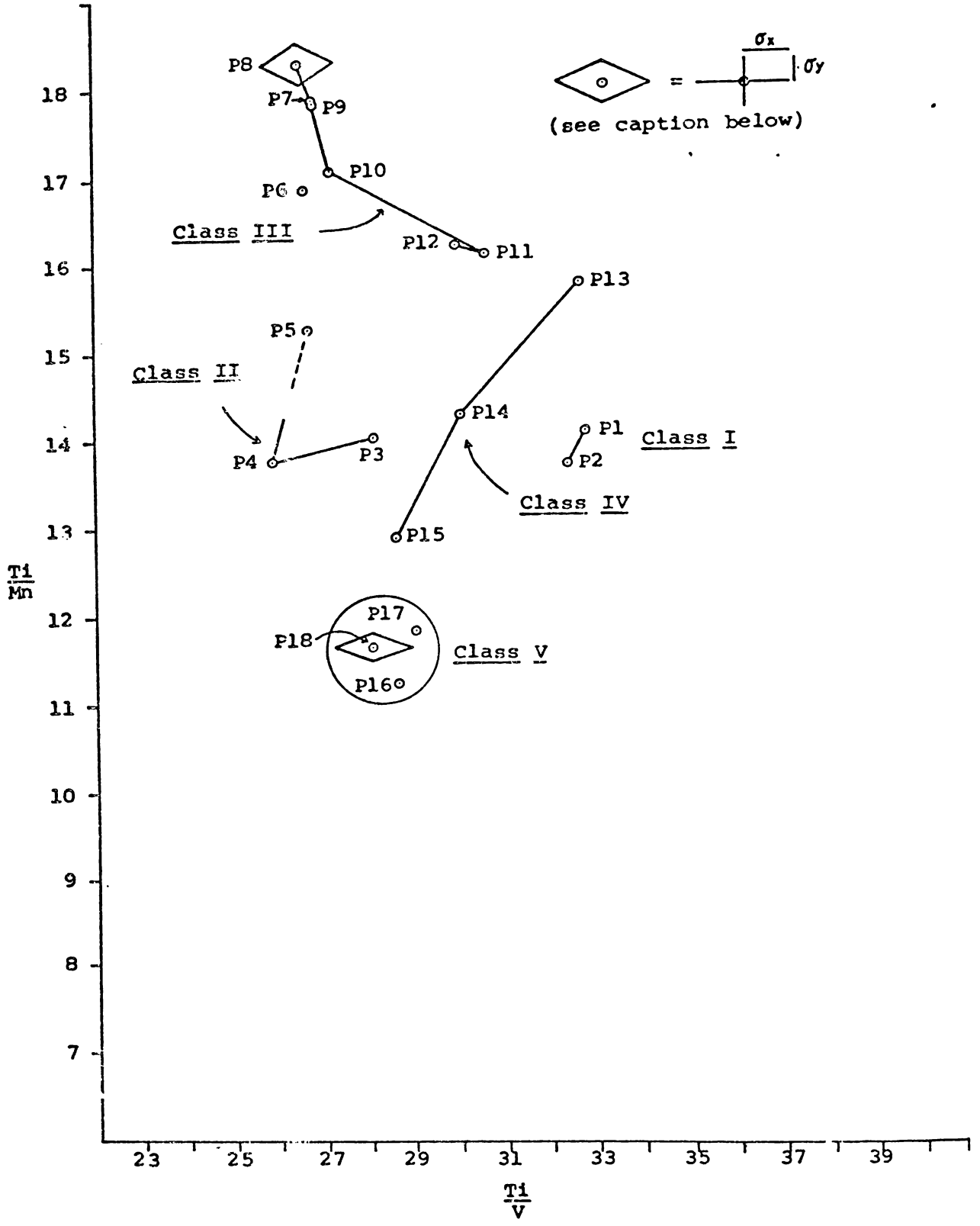


FIGURE 3.12 : Ratios of count rates of Ti, Mn and V from titanomagnetites extracted from the Holocene and Late Pleistocene tephras at Pukekauri Rd. Solid lines connect samples in stratigraphic succession. The standard deviations for samples P8 and P18 are calculated from repeated analyses of the two samples (see Appendix B, p.286 ).

(ii) those that form a linear relationship with each other e.g. F.C. III (P8, P9, P10, P11, P12) and F.C. IV (P13, P14, P15);

(iii) those that do not fit into either category e.g. F.C. I (P1, P2); F.C. II (P3, P4) and intermediate samples (P5, P6, P7).

Kohn (1970) found that samples from any one tephra clustered in a similar manner to that shown by category (i) so that field class V probably represents a pure tephra

The linear relationships formed by field classes III and IV (category ii) could result from compositional zonation within the class, or the field class may contain a mixture of two or more tephras. Lipman (1971) found that compositional zonation occurred within a single ash flow sheet in Southern Nevada, and Ewart (1965) showed there was a compositional variation in the Whakamaru Ignimbrite. Compositional zonation within a single tephra unit is less common, but does occur (Dr G.P.L. Walker, pers. comm., 1978). Utilising data from Kohn (1973), the variability in the Ti, V and Mn element contents throughout the Kawakawa, Waiohau and Kaharoa tephras has been examined (Kohn's analysis numbers 241-245, 196-201, and 10-14 respectively). No variation consistent with compositional zonation occurs and although this is insufficient reason to abandon this hypothesis as it relates to the Coromandel tephras, it does suggest that compositional zonation is an unlikely explanation for the chemical and mineralogical variations shown by classes III and IV.

Mixing of two or more pure tephras would result in a sequence of samples with compositions intermediate between the end members (Fig. 3.13). The mechanism shown is considered most likely to

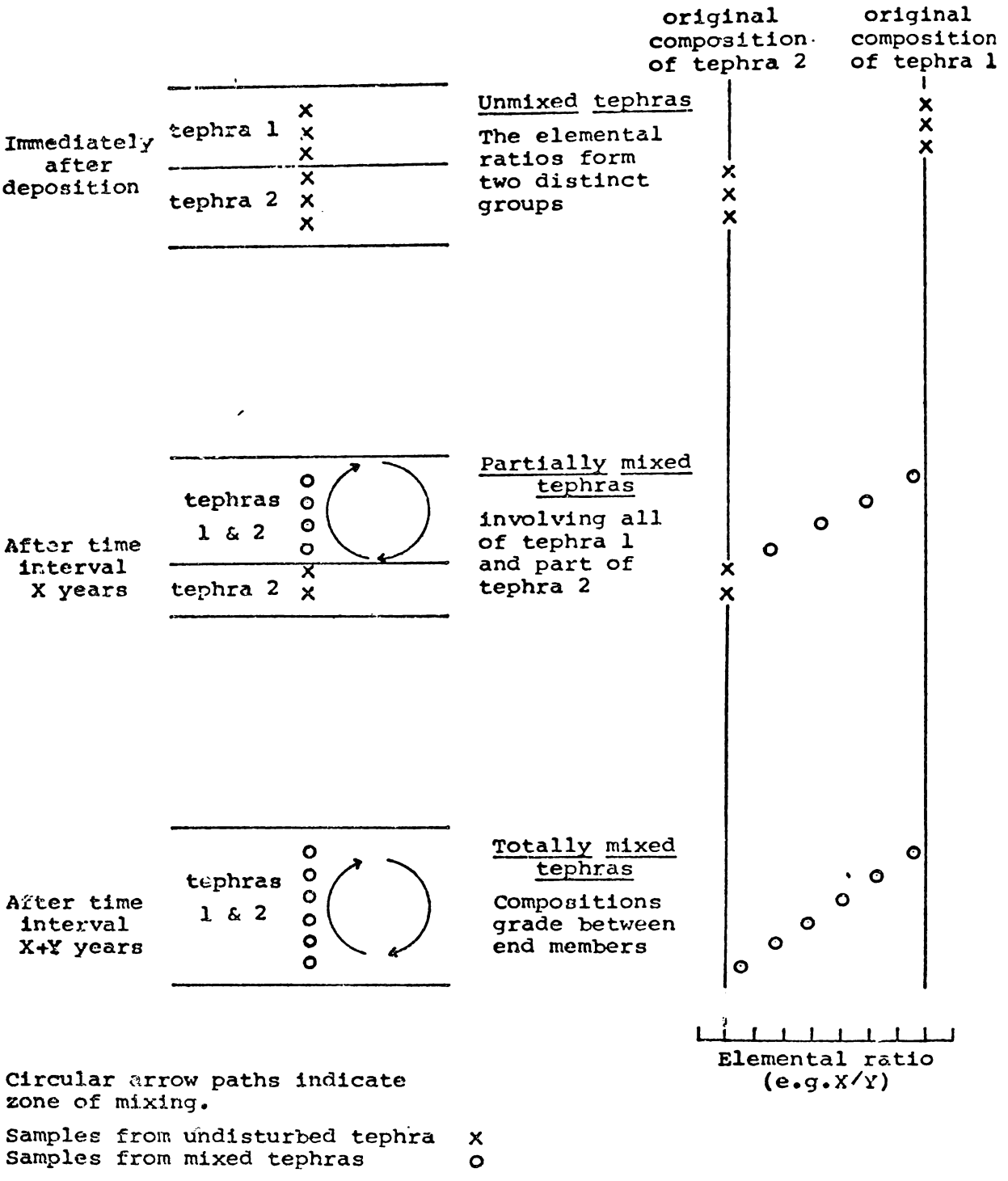


FIGURE 3.13 : Model explaining linear trends in properties throughout a field class as the result of the mixing of two tephras.

explain the relationships exhibited by field classes III and IV. It is beyond the capacity of single component (multiparticle) methods to distinguish between these two hypotheses; this can only be achieved by single component (single particle techniques). Electron microprobe analysis of a number of single titanomagnetite grains concentrated from samples of either classes III or IV could provide insight into this problem. Fig. 3.14 depicts schematically the results of microprobe analysis that would be expected from a compositional zonation hypothesis and an hypothesis involving the mixing of two tephras. For compositional zonation, one population of titanomagnetite grains varies gradationally from the top to the base of the deposit; when mixtures of tephras are involved, two distinct populations should be detectable.

Analyses of the titanomagnetites by XRF support the relocated boundaries of the field classes presented in the mineralogical section (Table 3.7). In particular, P5, P6 and P7 have titanomagnetite characteristics transitional between field classes II and III. Samples P1 and P2 have closely spaced elemental ratios, indicating the homogeneous nature of class I, a property consistent with the field class corresponding to the soil A horizon. The Recent bed is clearly separated from class II by its high Ti/V values. Class II (P3,P4) is characterised by a low Ti/V ratio and a medium Ti/Mn ratio, thus distinguishing it clearly from both classes I and III. Class II is internally variable, with the upper parts (e.g. P3) grading into the overlying field class and the lower parts (e.g. P4, ?P5) into the underlying Silty bed. Samples P8 to P12 show a linear relationship which is possibly the result of

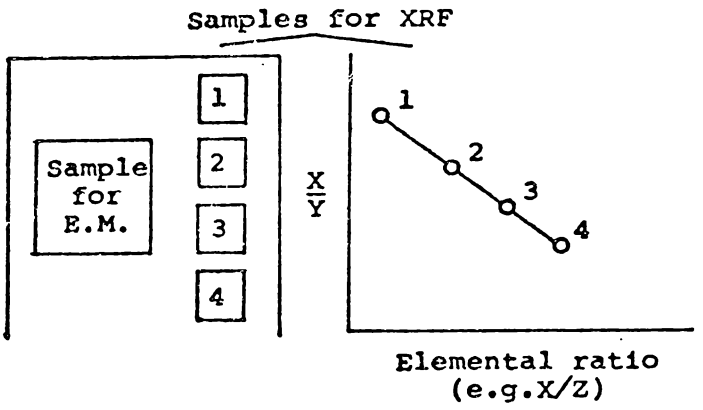


Elemental analyses of bulk titanomagnetite by XRF exhibit a linear relationship. (e.g. in F.C.III)

ANTICIPATED RESULT IF THE HYPOTHESIS IS CORRECT

Elemental analyses of single titanomagnetite grains by E.M.

Hypothesis 1 : Compositional zonation

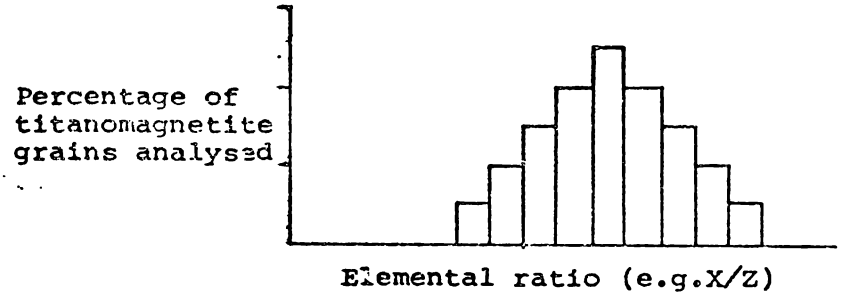


A unimodal distribution with a high standard deviation.

Hypothesis 2 : The mixing of two tephras

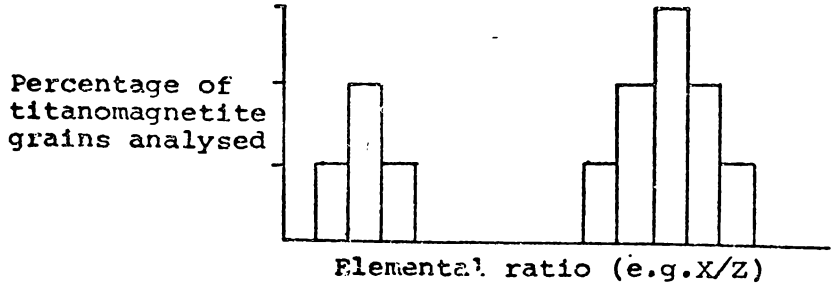


A bimodal distribution with low standard deviations.

FIGURE 3.14 : Experimental procedure involving electron microprobe (E.M.) analysis of single titanomagnetite grains utilised to explain linear relationships shown by the XRF analyses of bulk titanomagnetite.

mixing of two tephras to form a composite deposit. The Silty bed is characterised by a higher Ti/Mn ratio than the classes above and below. Class IV (P13,P14,P15) exhibits moderate Ti/Mn and Ti/V values and samples show a linear relationship with the lowermost sample (P15) having a similar titanomagnetite chemistry to samples from the underlying Shower-bedded class. Very low Ti/Mn values and intermediate Ti/V ratios of field class V titanomagnetites demonstrate that this class is a compositionally homogeneous deposit probably representing a single tephra.

2. Single particle

(a) Introduction

The second type of single component method is one in which attention is focused on discrete particles. Single particle methods grade continuously into the single component (multiparticle) methods, depending upon whether results obtained from analysis of one mineral grain are averaged with those of others. Hodder and Wilson (1976) point out that averaging a set of measurements from discrete grains may be at the expense of detection of real variation between mineral grains. They measured accurately the refractive index of volcanic glasses from a tephra deposit and obtained a high average residual associated with the mean. By regrouping the raw data from the individual shards to give mean values with associated average residuals typical of those for uncontaminated glass, they showed that there was a mixture of two tephras in the deposit they studied.

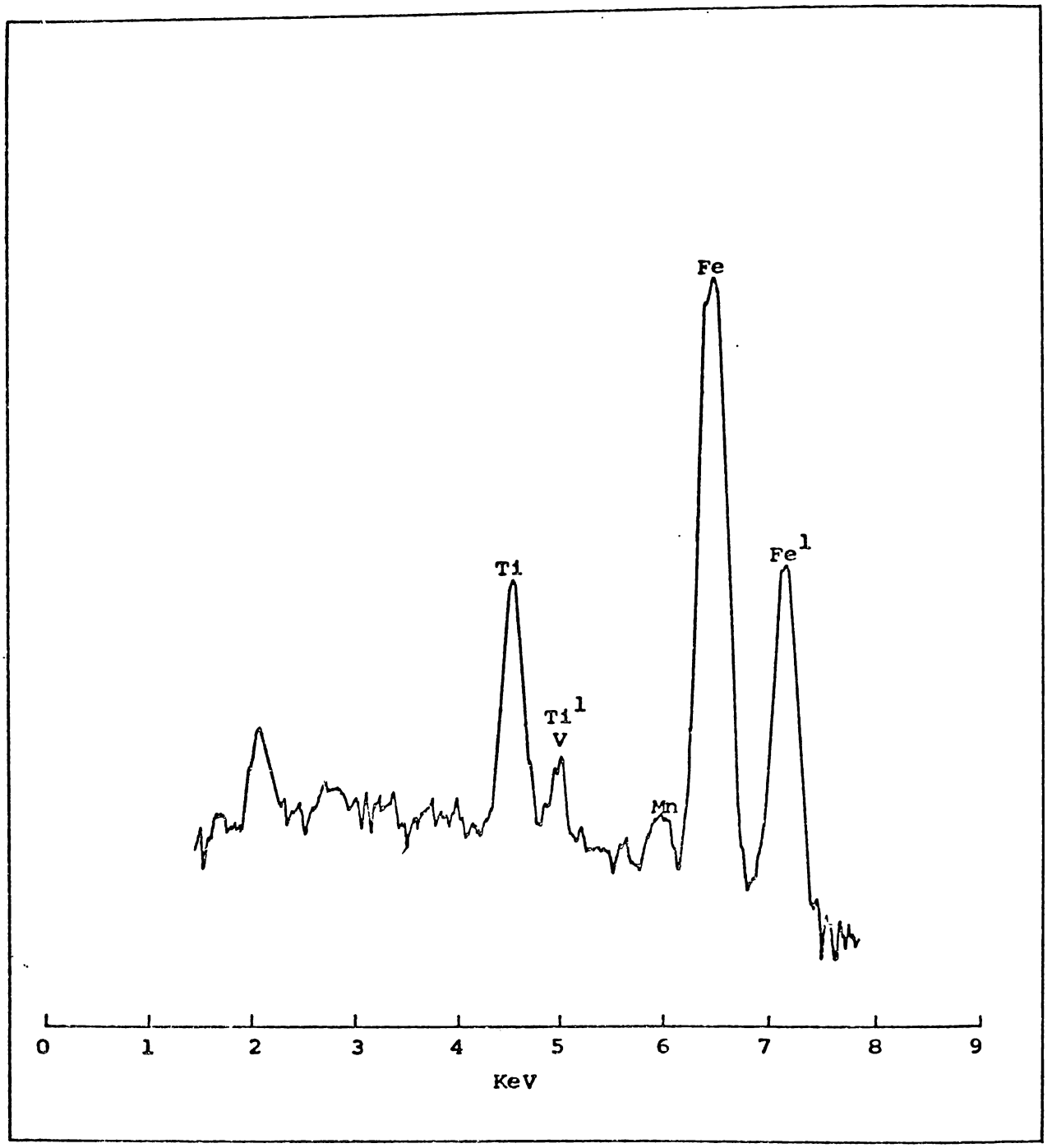


FIGURE 3.15 : Typical electron microprobe spectrum of titanomagnetite from the Coromandel tephras. Sample K10.
1. Element K(β)
All peaks are K(α) unless otherwise indicated.

Although electron microprobe analysis (E.M.) provides a similar potential for recognising mixtures of tephras within apparently homogeneous deposits, the technique has been confined to obtaining average analyses of particular components, such as volcanic glass (Smith and Westgate 1969; Smith et al. 1977a, b) or titanomagnetite (Westgate and Fulton 1975).

Bulk titanomagnetite analyses using X.R.F. have defined individual field classes and have shown trends within classes. However, they cannot provide information on the number of tephras contributing to individual samples, for which E.M. analysis of single titanomagnetite grains has been employed. In addition the technique has been instrumental in indicating whether classes III and IV are compositionally zoned or are composite deposits.

Five samples (K1; the finer than 2 mm fraction of K3; K6; K7; K10), representing field classes I to V, were collected from the Kopu site (site 37, N49/252285) where field class boundaries are more clearly defined than at Pukekauri Rd (see Fig. 4.15 p.137). Individual titanomagnetite grains were analysed using a Scanning Electron microscope with an E.M. attachment (see Appendix 8). Various combinations of the ratios of the total counts over 40 seconds for the three main elements Fe, Ti, and Mn indicated that the Fe/Ti ratio gave the most satisfactory results for characterising titanomagnetite from different tephras. A typical plot of the element intensities from a titanomagnetite grain illustrates the reduced sensitivity of the S.E.M.-E.M. system for the elements examined compared with X.R.F. spectra from bulk titanomagnetite analyses (Fig. 3.15). Exsolved grains identified

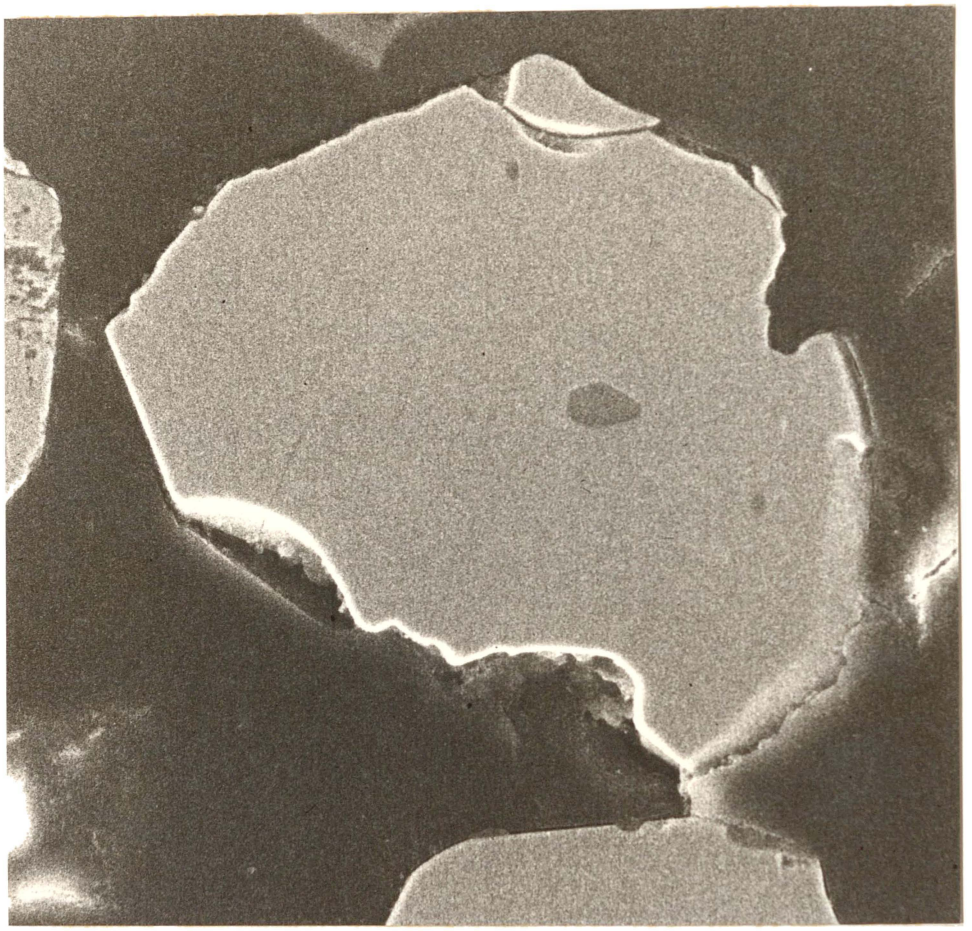

FIGURE 3.16 : Scanning electron micrograph of a polished, gold-coated, homogeneous titanomagnetite grain (light grey) with included apatite crystal (medium grey). The apatite crystal is grey because of its lower conductivity compared with the surrounding titanomagnetite crystal.

by the method indicated in Appendix B p.289, and included crystals which were visible on the screen (Fig. 3.16), were avoided during the analyses. The analyses for the five samples are presented in Table 3.8.

TABLE 3.8: Mean Fe/Ti ratios of titanomagnetites extracted from the Coromandel tephras at the Kopu site and analysed by E.M.

| | | No.of grains of titano-magnetite analysed | Mean counts Fe / counts Ti | Standard deviation | Coefficient of variation % | Equivalent Pukekauri Rd samples |
|---|---|---|---|---|---|---|
| I | K1 | 26 | 6.29 | 0.83 | 13.17 | P1,P2 |
| II | K3 (<2 mm) | 37 | 6.37 | 0.98 | 15.33 | P3,P4 |
| III | K6 | 37 | 6.56 | 0.97 | 14.81 | P10,P11 |
| IV | K7 | 28 | 7.01 | 0.74 | 10.58 | P14,P15 |
| V | K10 | 23 | 7.37 | 0.10 | 1.35 | P18 |

(b) Discussion of results

The very low coefficient of variation for field class V is consistent with the mineralogical and chemical data which indicates it is a pure tephra. In comparison, the high coefficients of variation associated with field classes I to IV suggest they all contain more than one tephra. Confirmation of this suggestion is indicated by Fig. 3.17 in which the Fe/Ti ratios are grouped into 0.05 intervals. Regrouping of the data reveals polymodal titanomagnetite compositions in all samples except field class V (K10). Data on each of the main modes are presented in Table 3.9.

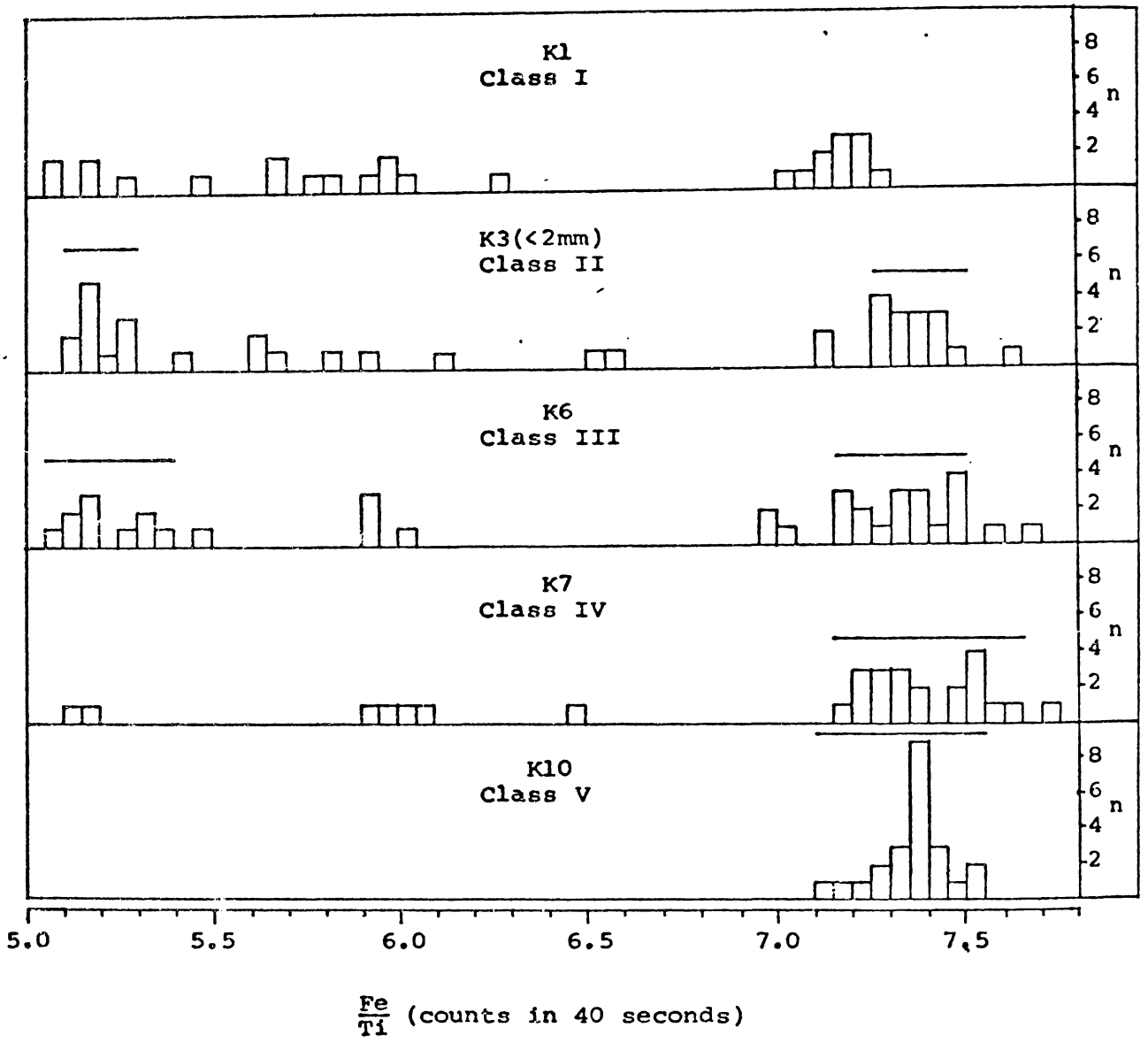


FIGURE 3.17 : Range in Fe/Ti ratios for titanomagnetites extracted from the Coromandel tephras at the Kopu site and analysed by electron microprobe. The dominant modes are indicated by lines overlying the data points. Statistical parameters for these modes are given in Table 3.9. "n" equals the number of titanomagnetite grains in any particular 0.05 interval.

Table 3.9: Modal grouping of the Fe/Ti ratios of titanomagnetites extracted from the Coromandel tephras at the Kopu site

| | | Range counts Fe / counts Ti | No. of grains contained within the modal range | % of grains contained within the modal range | Total % of samples accounted for | Median counts Fe / counts Ti | Mean counts Fe / counts Ti | Standard deviation of the mean | Coefficient of variation of the mean (%) |
|---|---|---|---|---|---|---|---|---|---|
| I | K1 | 5.08 – 5.30 | 5 | 19.2 | | 5.17 | 5.17 | 0.09 | 1.64 |
| | | 5.70 – 6.09 | 8 | 30.8 | 92.3 | 5.88 | 5.88 | 0.14 | 2.45 |
| | | 7.05 – 7.30 | 11 | 42.3 | | 7.18 | 7.18 | 0.07 | 1.00 |
| II | K3 < 2 mm | 5.14 – 5.31 | 11 | 29.7 | | 5.20 | 5.21 | 0.06 | 1.13 |
| | | 7.27 – 7.47 | 14 | 37.8 | 67.6 | 7.35 | 7.36 | 0.06 | 0.85 |
| III | K6 | 5.07 – 5.37 | 10 | 27.0 | | 5.18 | 5.23 | 0.10 | 1.99 |
| | | 7.16 – 7.48 | 17 | 45.9 | 72.9 | 7.35 | 7.34 | 0.11 | 1.48 |
| IV | K7 | 7.18 – 7.62 | 20 | 71.4 | 71.4 | 7.36 | 7.39 | 0.14 | 1.86 |
| V | K10 | 7.13 – 7.56 | 23 | 100.0 | 100.0 | 7.37 | 7.37 | 0.10 | 1.35 |

The median is the best statistical measure for comparing the Fe/Ti ratios of the modes, as it ignores the extremes of the distribution and reduces the possibility of erratic results being incorporated into the parameter.

Field class I (K1) contains titanomagnetites with highly variable compositions. The class coincides with the modern soil A horizon and hence experiences subaerial additions in the form of aeolian dust or distal fallout of very fine grained products of Central North Island volcanism. The division into three modes, although somewhat arbitrary, demonstrates the multiple nature of this field class. The Pumiceous bed, represented by the finer than 2 mm fraction of K3, is characterised by titanomagnetites having a narrower compositional range, capable of being grouped into two distinct modes which together account for 68% of the grains analysed. Both modes represent tephras that are calc-alkaline in composition, as titanomagnetites from peralkaline tephras have higher Fe/Ti ratios than those shown in Fig. 3.17. Coarse reddish brown lapilli of peralkaline composition from field class II at the Old Mill site (site 25), contained rare phenocrystic titanomagnetite with an Fe/Ti ratio of 9.2. Field class II must therefore contain at least three tephras, two calc-alkaline and one peralkaline in composition. The Silty bed (K6) is also composed of titanomagnetites with two dominant modal Fe/Ti ratios having medians at 5.18 and 7.35 respectively; together these modes account for about 73% of the grains examined. The marked bimodality supports class III being a mixture of two tephras rather than representing a single deposit exhibiting compositional zonation. The Lumpy bed, represented by K7,

exhibits both class III characteristics, in that an important fraction (29%) of the titanomagnetite grains lie outside the principal mode, and also class V characteristics, in its tendency towards unimodality. The Shower-bedded class (K10) is strongly unimodal and the distribution is consistent with a single tephra origin, devoid of contaminating material.

E.M. analysis of titanomagnetites has revealed that all field classes except the oldest are composed of multiple tephras, thereby demonstrating the significance of post-depositional changes that must be anticipated when considering the origins of thin tephra beds.

## DISCUSSION

### 1. Field class I (Recent bed)

Most of the data obtained indicate class I represents a unique combination of tephras, distinct from class II beneath. Involvement in modern soil-forming activities has resulted in a homogenised deposit containing at least three tephras, one of which also occurs in class II. At least one tephra is contained within the finer part of the sand fraction (2-4 Ø) and is characterised by volcanic glass, plagioclase, hypersthene, cummingtonite, hornblende and augite. Another is represented by white, fresh, pumiceous lapilli containing hypersthene and plagioclase phenocrysts. The third tephra, which is more abundant in the underlying Pumiceous bed, contains yellow orange, highly altered pumiceous lapilli with a peralkaline phenocrystic assemblage.

Sample P2 has many properties in common with P3 indicating mixing between classes I and II. However, there are sufficient differences between these samples to allocate them to separate field classes rather than placing P3 into an intermediate class, as was suggested by initial field work.

2. Field class II (Pumiceous bed)

The Pumiceous bed is clearly distinguished from the Silty bed by its coarser grain size and peralkaline component. It is dominated by the peralkaline, yellow orange pumiceous lapilli mentioned above which contain phenocrystic anorthoclase, quartz, aegirine, cossyrite, olivine, riebeckite and tuhualite. Two tephras having calc-alkaline mineral assemblages dominated by glass, plagioclase, quartz, hypersthene, cummingtonite, hornblende and augite occur within the sand fraction of the Pumiceous bed.
The lower boundary of field class II is uncertain; some parameters such as particle size suggest that it lies between P5 and P6, while others, such as mineralogy, indicate that P5 is also transitional in nature. There is some evidence to suggest that the transition between classes II and III (occupied by ?P5, P6 and P7) may be influenced by another tephra.

3. Field class III (Silty bed)

Clay-rich class III samples near the centre of the stratigraphic column are sandwiched between coarser deposits above and below. Grain size parameters, salic and ferromagnesian mineralogy, and titanomagnetite chemistry are examples of parameters

which change uniformly through the bed in response to varying contributions from tephras forming an intimate mixture within class III. The bed appears to be a mixture of two tephras: a younger, fine-grained, glass-rich tephra, and an older, comparatively coarse-grained deposit having greater amounts of plagioclase and quartz. Both tephras have a calc-alkaline ferromagnesian assemblage dominated by hypersthene, cummingtonite and hornblende. Many of the properties associated with grain size, mineralogy and titanomagnetite chemistry grade uniformly from P8 to P15 and although the boundary between class III and class IV is an indistinct one, most parameters support a division in the region of sample P12. The Silty bed is easily distinguished from the underlying Lumpy bed by its finer grain size, hypersthene-dominated ferromagnesian mineral assemblage, and titanomagnetite chemistry.

4. Field class IV (Lumpy bed)

The Lumpy bed is also non-homogeneous, with textural, mineralogical and chemical properties changing uniformly between its top (P14) and the Shower-bedded class beneath (i.e. P16, P17, and P18). Class IV samples are distinguished from class V by their finer grain sizes, their higher clay and hypersthene contents, and their titanomagnetite chemistry. About 70% of the deposit is occupied by a single tephra with the remainder containing subaerial additions, probably distal components of Central North Island volcanism.

5. Field class V (Shower-bedded class)

The oldest group of samples in the column are the non-bedded sandy loams and shower-bedded sands of class V (P16,P17 and P18). Although particle size parameters and salic mineral assemblages vary with the explosive strength of each eruptive cycle, the cummingtonite-dominated ferromagnesian mineral assemblage and titanomagnetite chemistry show remarkable constancy between successive pulses, indicating a common origin from a single, prolonged, eruptive event.

Figure 3.18 summarises the relationships between field class boundaries, samples and component tephras. Some of the five tephras found in field classes III to V occur in more than one field class, with the number of different tephras contributing to the three older classes probably not exceeding three (see Chapter 4 p.160).

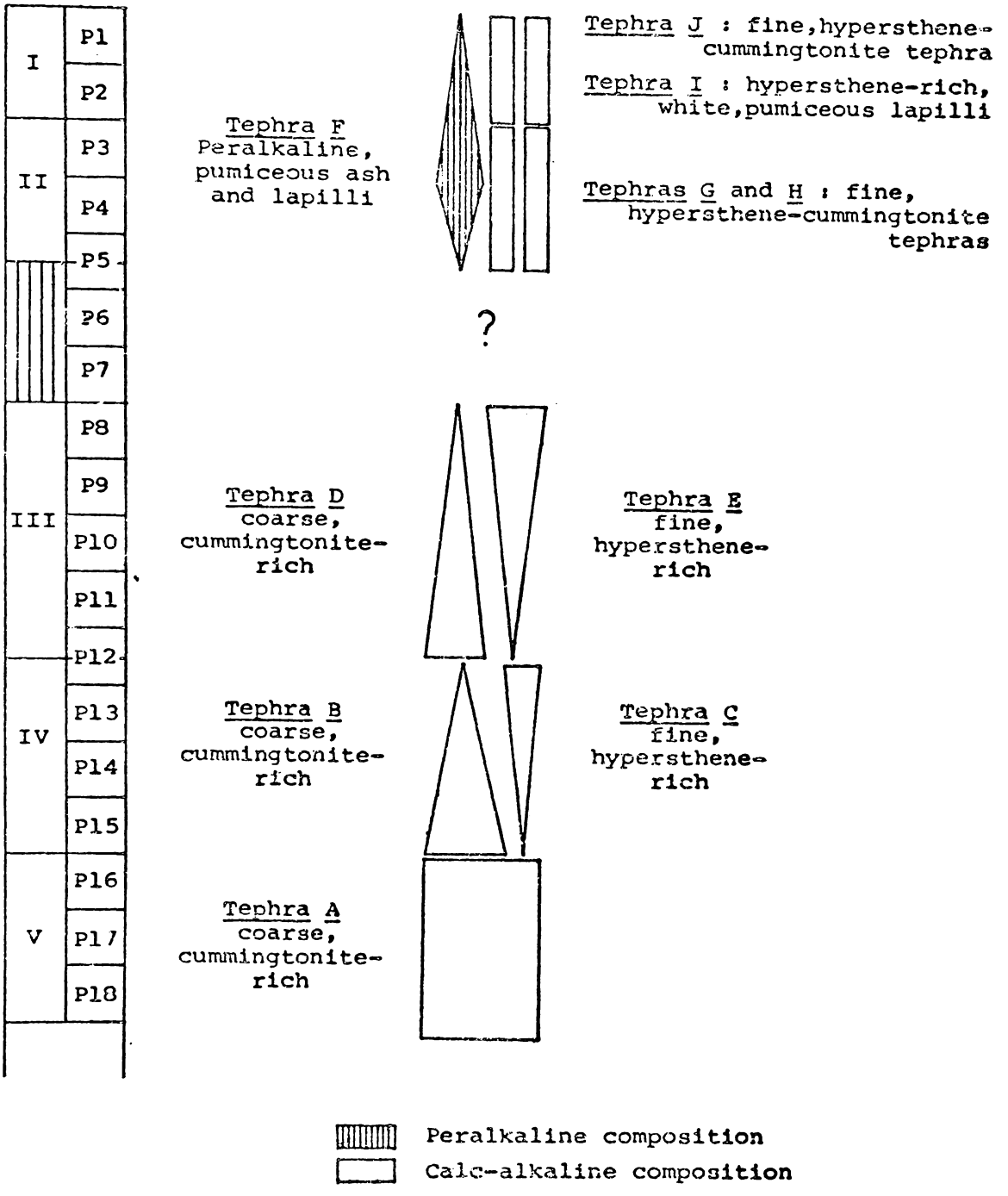


FIGURE 3.18 : Relationships between the Field classes, samples, and the number and vertical distribution of component tephras in the Coromandel tephra sequence at Pukekauri Rd. Width of individual tephra symbol denotes the approximate content of that tephra in any particular sample (e.g. P3:50%F,25%G,25%H). It should be noted that some of the tephras occurring in field classes III to V are common to more than one field class.

# CHAPTER 4

## VARIATION IN THE PROPERTIES OF FIELD CLASSES I TO V WITH GEOGRAPHICAL DISTRIBUTION OVER THE COROMANDEL PENINSULA.

### INTRODUCTION

In chapter three, individual field classes within the two metre thick Late Pleistocene and Holocene tephra cover at Pukekauri Rd, Waihi, were investigated by various tephrostratigraphic techniques and a number of component tephras recognised. This chapter describes the properties of the field classes in stratigraphic sections over the remainder of the Peninsula and aims at testing the usefulness of some of the tephra characteristics of the reference section for correlation purposes, and elucidating further the number and properties of tephras contained within the various field classes.

Field and laboratory data indicate that the five field classes representing the Coromandel tephras can be considered in two groups, classes I and II, and classes III, IV and V, with each group containing closely related tephras. This chapter follows this grouping with the first section discussing the Recent and Pumiceous beds and the second the three older field classes.

## A. FIELD CLASSES I AND II (THE RECENT AND PUMICEOUS BEDS)

### 1. Introduction

Detailed examination of the stratigraphic column at Pukekauri Rd has indicated that field classes I and II contain multiple tephras (Fig. 3.18 p.96). Of these, at least four tephras are calc-alkaline and represented by both lapilli and ash deposits, and one is a peralkaline, pumiceous lapilli and ash-sized tephra. Northwards from Waihi, field observations show a gradual change in the characteristics of these tephras. The influence of the peralkaline component in class II increases with the coarse pumiceous ash and very fine yellow orange pumiceous lapilli of the Pukekauri Rd site passing laterally into coarse, reddish brown, lapilli at Whangamata. The Recent bed (Class I) also changes character between Waihi and Whangamata, with the tephras unique to class I being mixed with the fine-grained, upper part of the underlying peralkaline pumice deposit. The mixing is a consequence of soil forming processes and North of Waihi is the major reason for discussing class I in conjunction with class II with which it is intimately associated. Fig. 4.1 illustrates the variation in the combined thicknesses of the class I and II deposits over the southern end of the Coromandel Peninsula.

### 2. Field relations

The Recent bed thins from approximately 20 cm on the Waihi Plain to 10 cm at Tairua (Fig. 4.1) and is no longer detectable at Whenuakite. It changes from a very friable, distinctly gritty,

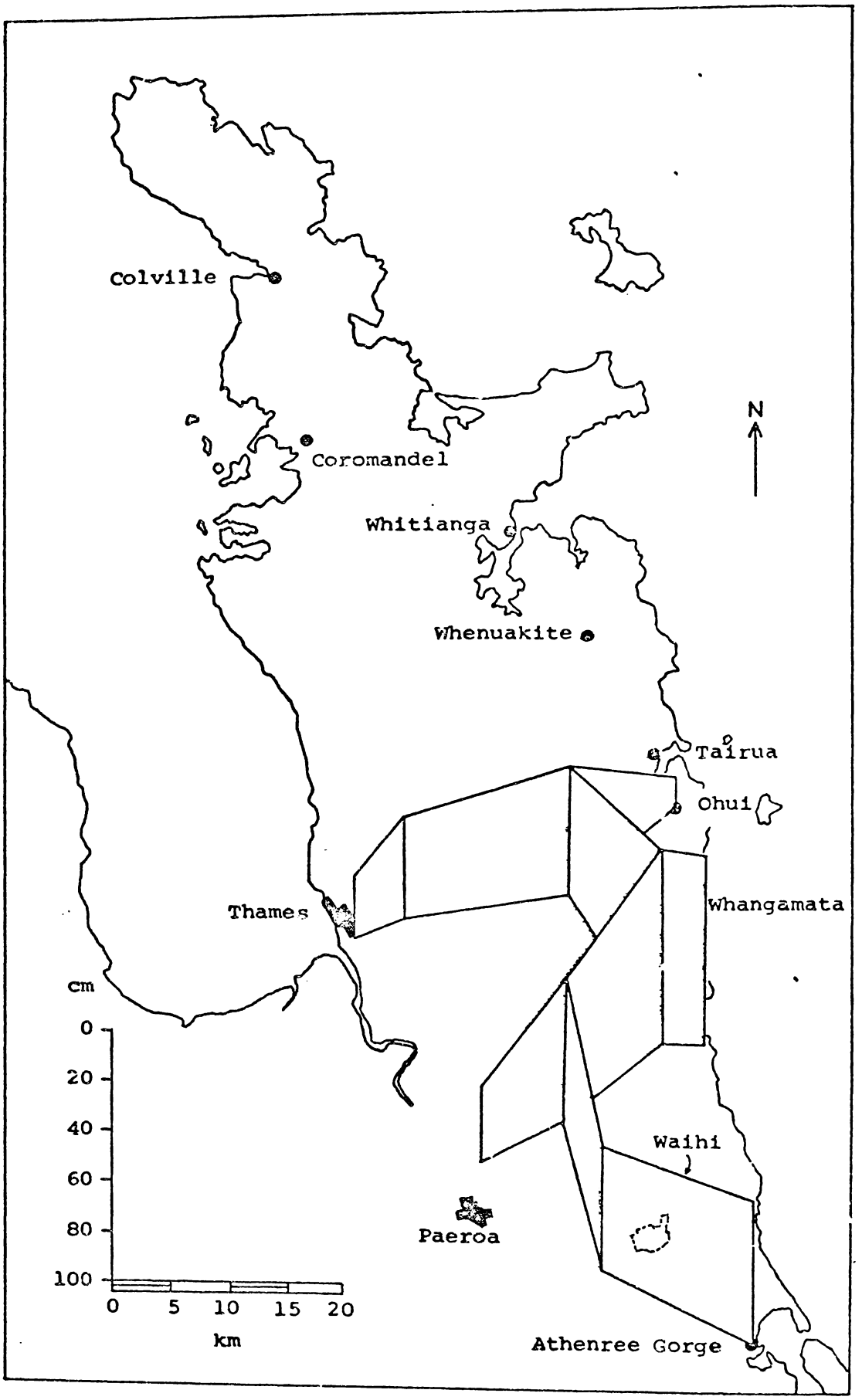


FIGURE 4.1 : Fence diagram showing the variation in the combined thicknesses of field classes I and II.

sandy loam at Whangamata to a finer-grained, sandy loam further south.

Near Whangamata the Pumiceous bed consists of 60 cm of loose, reddish brown pumiceous lapilli with fragments up to 35 mm in diameter. The pumice is strongly weathered as is demonstrated by the ease with which it may be crushed, and by its reddish brown colour, which is more intense on the surface of the grains and which becomes pale yellow towards their centres. The reddish brown lapilli are sometimes overlain by dull yellowish brown lapilli (Fig. 2.8 p.26) which otherwise appears to be similar material. The different coloured lapilli are separated by a diffuse boundary suggesting that the colour variations may be the result of soil forming processes (see p.117). In the Whangamata district the Pumiceous bed consists of coarse, normally graded lapilli showing a sharp lower boundary with the Silty bed (Fig. 2.9 p.26). Extending radially away from Whangamata the deposit becomes progressively finer and is of coarse ash grade at Waihi and Ohui. With decreasing size, the lapilli lose their identity and become incorporated into a yellowish brown, friable, sandy loam (similar to that occurring at the Pukekauri Rd site), which has a diffuse boundary with field class III. Hilly relief combined with the weathered nature of the Pumiceous bed has limited the number of good exposures of these younger tephras in the Whangamata region. Most data on classes I and II have come from the 15 localities shown in Fig. 4.2.

The area covered by the Pumiceous bed is oblate and asymmetrical around the eruption axis, and is considerably thicker

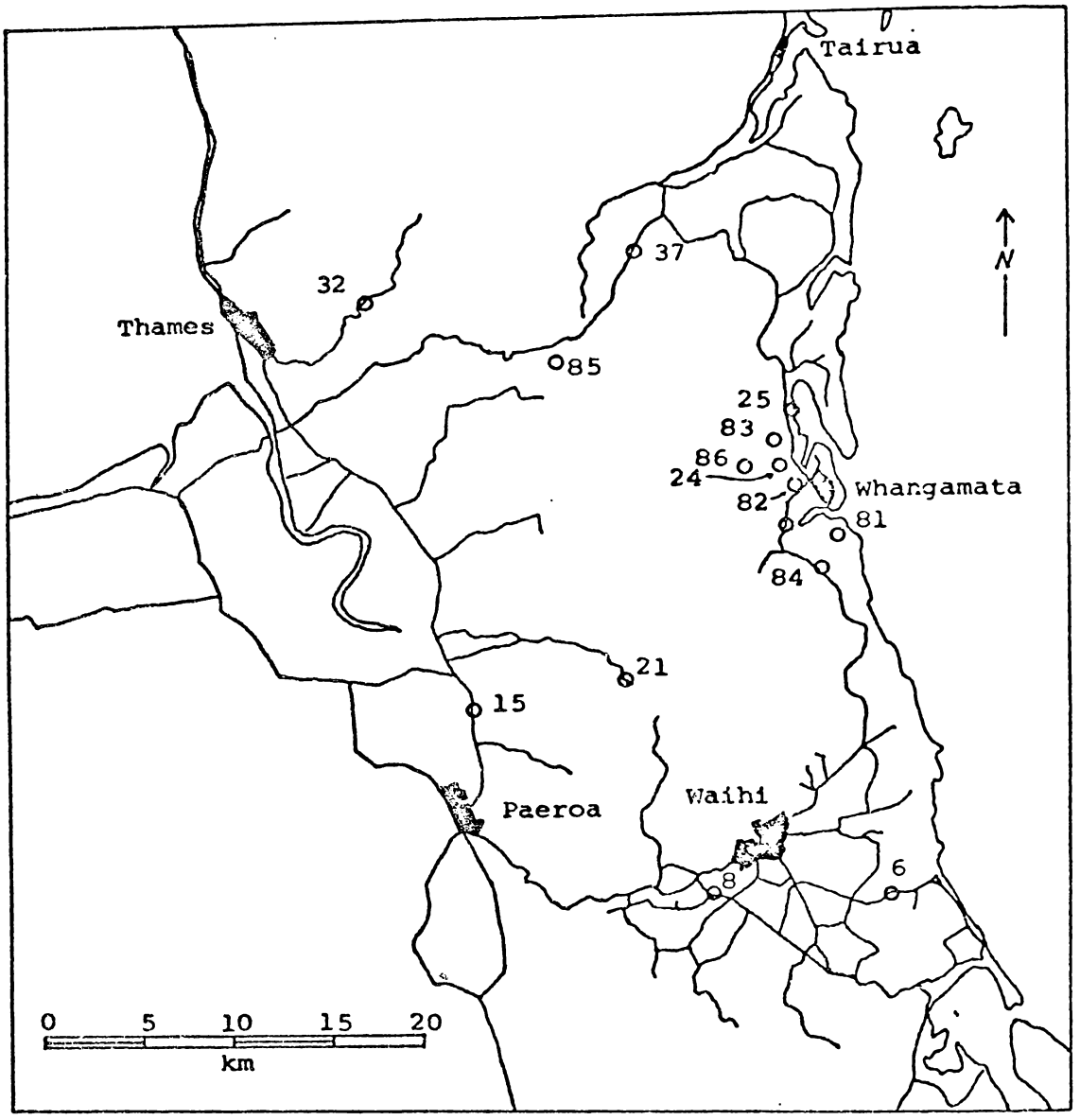


FIGURE 4.2 : Reference sites for the Recent and Pumiceous beds in the southern Coromandel Peninsula.

Site number : 6 - Waihi Beach
8 - Pukekauri Rd.
15 - Thames-Paeroa highway
21 - Maratoto Valley
23 - Whangamata dump
24 - Ash type site
25 - Old mill site
32 - Kauaeranga Valley
37 - Kopu
81 - Mayor farm
82 - Whangamata reservoir
83 - Moana point
84 - Whangamata south
85 - Neavesville
86 - Tairua forest

in the south than in the north (Fig. 2.7 p.24). This may reflect the influence of the class II calc-alkaline components or it may indicate deposition of the peralkaline component in two lobes, one striking ESE/WNW and the other NE/SW, or perhaps a combination of both factors. Discrete yellow orange pumice grains are detected in field class II as far south as the Athenree Gorge and as far north as Ohui (Fig. 4.1), although laboratory evidence indicates that the influence of the peralkaline tephra is more extensive than this (see p.125).

## 3. Granulometric study

### (a) Lateral variations in the particle size distribution of the Pumiceous bed.

Grain size parameters employed to characterise the beds include those mentioned in Chapter 3 (p.44) together with the maximum diameter of Kuno et al. (1964) and the modal size of Folk (1966). The changes in particle size distribution with geographical location were investigated using channel samples (i.e. samples representing material collected continuously from the top of a tephra unit, to its base) of class II material from seven sites in the Whangamata region (Table 4.1 and Fig. 4.3). Data were obtained from the coarser than 4 Ø fraction of channel samples in order to allow a comparison of parameters applicable to primary material unaffected by internal properties of the bed, such as grading. As Fig. 4.3 indicates, all samples are bimodal with four showing a third mode in the 2-4 Ø region, possibly the result of "artificial" abrasion of the strongly weathered pumice fragments.

FIGURE 4.3 : Histograms of the particle size distributions of the coarser than 4 Ø fractions of field class II channel samples collected from seven sites in the greater Whangamata region. Data in the form of cumulative frequency curves are shown in Appendix E (Fig. E.5).

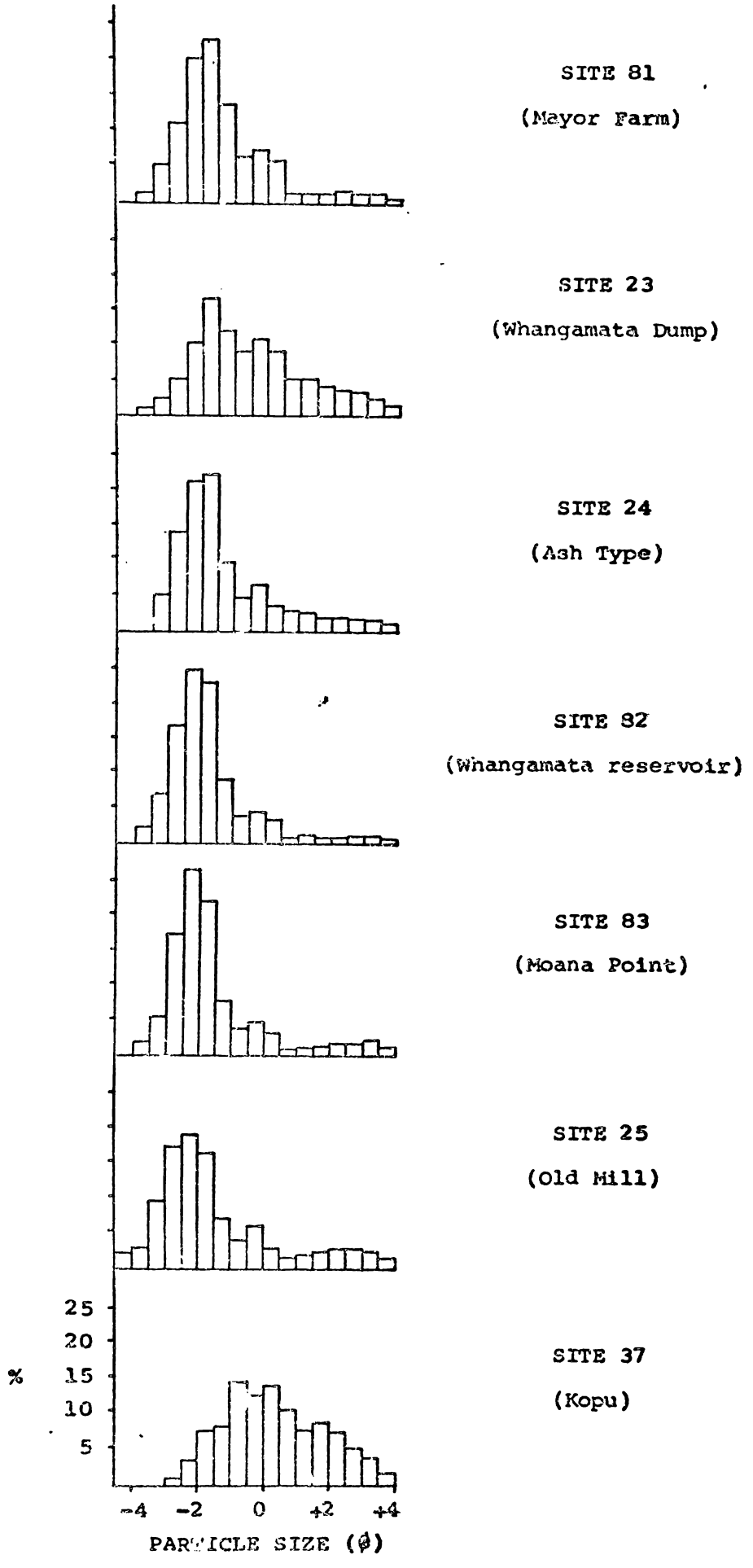
SITE 81
(Mayor Farm)
SITE 23
(Whangamata Dump)
SITE 24
(Ash Type)
SITE 82
(Whangamata reservoir)
SITE 83
(Moana Point)
SITE 25
(Old Mill)
SITE 37
(Kopu)
25
20
%
15
10
5
-4
-2
0
+2
+4
PARTICLE SIZE (ϕ)

TABLE 4.1 : Grain size parameters of channel samples from the Pumiceous bed at seven sites in the greater Whangamata region

| Site No. | Site locality | Mean diam. of the five largest particles (mm) | Coarser than 4 Ø fraction [1] | | | |
|---|---|---|---|---|---|---|
| | | | Median (Ø) | Mean (Ø) | Sorting Coefficient (Ø) | Primary mode [2] (Ø) |
| 25 | Old Mill | 27.8 | -1.99 | -1.57 | 1.56 | -2.25 |
| 81 | Mayor farm | 27.2 | -1.71 | -1.49 | 1.16 | -1.70 |
| 82 | Whangamata reservoir | 26.4 | -2.02 | -1.87 | 0.97 | -2.03 |
| 24 | Ash type | 24.6 | -1.82 | -1.49 | 1.30 | -1.79 |
| 83 | Moana Point | 21.6 | -1.99 | -1.68 | 1.14 | -2.10 |
| 23 | Whangamata dump | 19.6 | -0.82 | -0.51 | 1.73 | -1.60 |
| 37 | Kopu | 9.6 | +0.21 | +0.37 | 1.58 | -0.58 |

1 To ensure particle disaggregation, samples were gently wet-sieved through -1 Ø, 0 Ø, 1 Ø and 4 Ø sieves and then subjected to two minutes of dry, hand-sieving.

2 The mode, the most frequently occurring grain diameter (Folk 1966) here refers to the majority of the grains only (primary mode - Fig. 4.3). It is calculated by the method of Folk and Ward (1957).

Grain size parameters such as the median, mean and sorting coefficient only have real significance for normal distributions (Bond and Sparks 1976); these parameters have therefore been used to a limited extent only, with more emphasis being placed upon the modal size value. The Old Mill site (number 25) contains both the coarsest primary modal value and the maximum diameter grains (Table 4.1) and hence it is most likely to be the closest on-land site to the eruptive centre (cf. Walker 1971). A comparison of maximum diameters with parameters derived from sieve analyses suggests reworking has occurred at some sites; for example, at Moana Point (site 83), the deposit has both a coarse primary modal value and mean grain size but the maximum diameter is considerably finer than at many of the other sites.

(b) Variations in the particle size distributions within the Recent and Pumiceous beds

The graded bedded appearance of class II material in the field is confirmed by particle size characteristics of the coarser than 4 $\emptyset$ fraction of deposits from the Old Mill (site 25) and Whangamata South (site 84) sites (Fig. 4.5). The field class and sample locations for these sites and others used in this chapter are shown in Fig. 4.4. The Pumiceous bed is normally graded (Fig. 4.5) and considerably coarser than the Recent bed above (cf. OM3 and OM1). The dull yellowish brown lapilli in the upper part of the Pumiceous bed (e.g. Wg 1) has modes in the coarse and very fine sand fractions, in common with the reddish brown lapilli beneath (Wg 2), but lacks the granule mode of the lower sample. This suggests that the dull

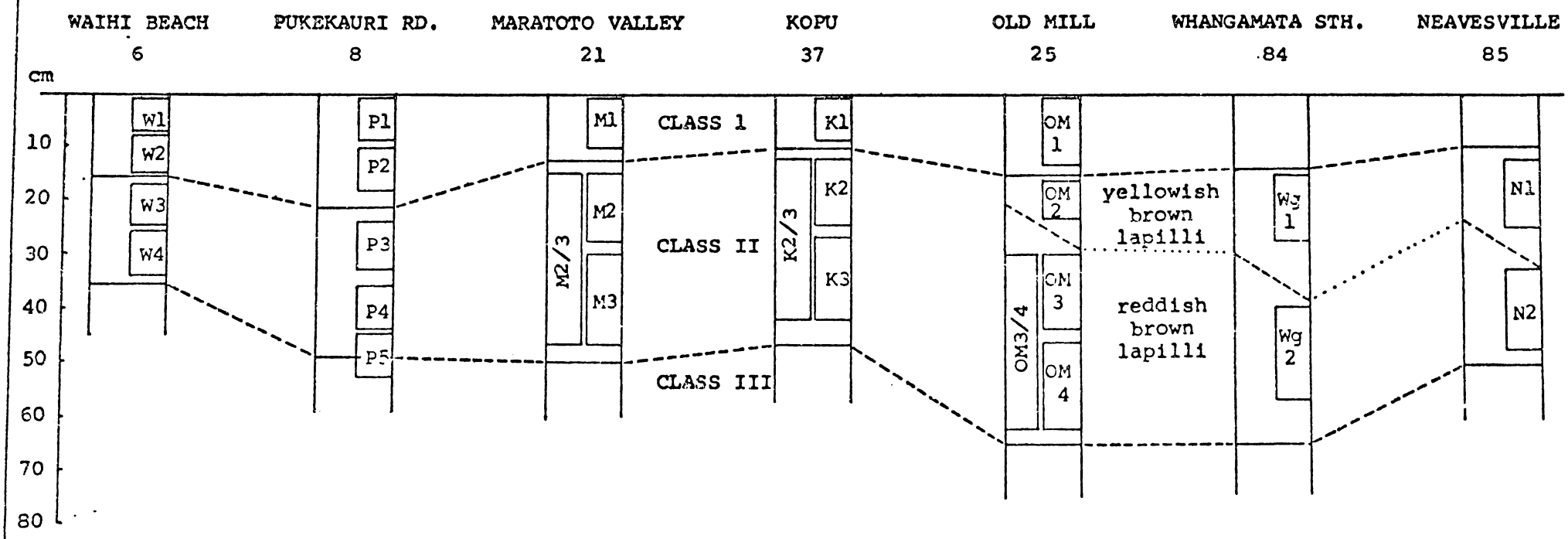


FIGURE 4.4 : Field class and sample locations for sites discussed in chapter 4.

Note : Two types of samples were collected from these sites ; channel samples representing the entire field class (eg.OM 3/4)

samples representing parts of a field class (eg.OM 3)

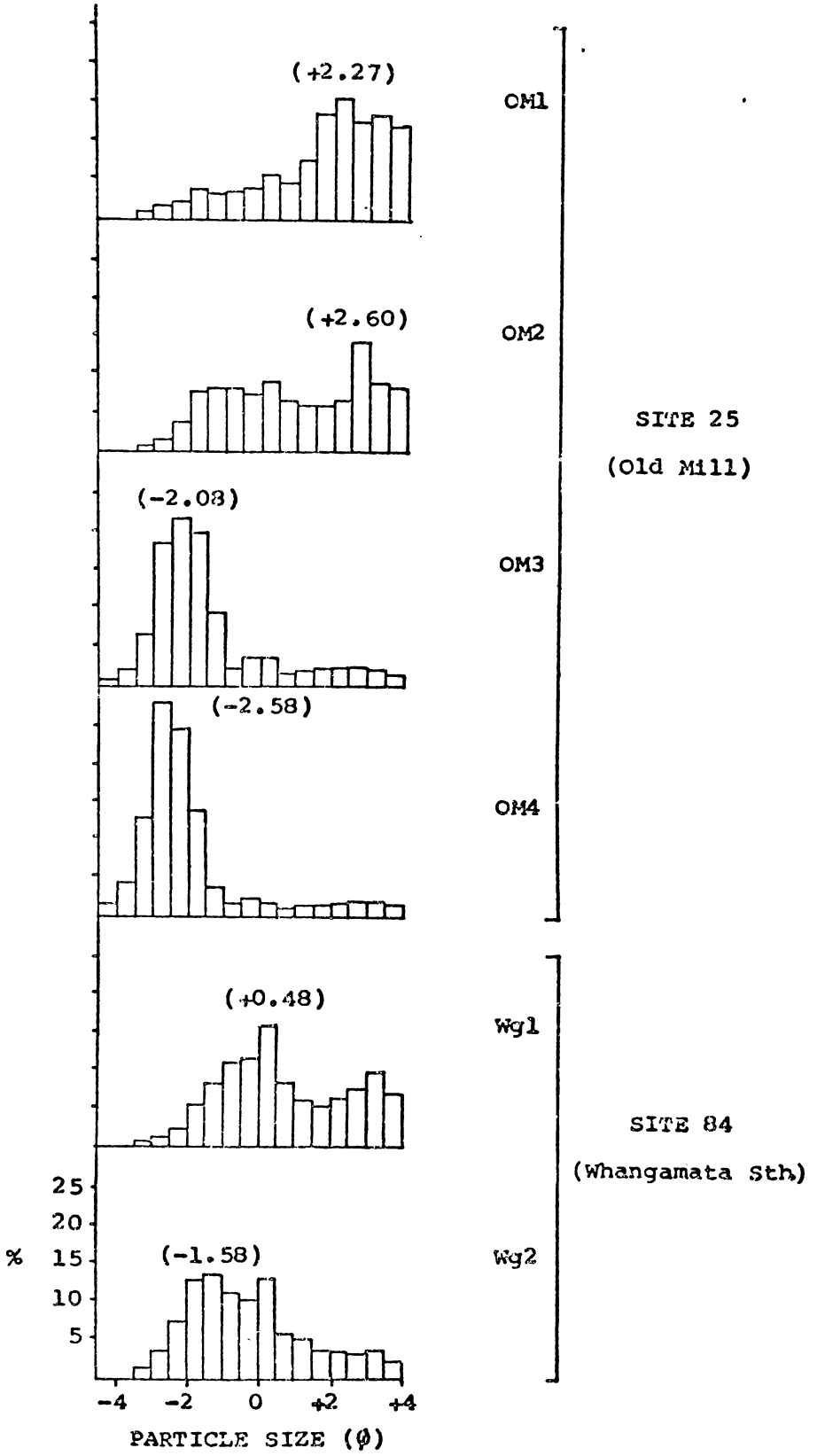


FIGURE 4.5: Histograms of the coarser than 4Ø fraction of field class I&II samples from sites 25 (Old Mill) and 84 (Whangamata South). Data are summarised in Appendix E (Fig.E.6)

(Note : Primary modal values are given in parentheses)

yellowish brown lapilli represent simply the upper part of the Pumiceous bed and that it is not a separate tephra with the colour differences being of post-depositional origin (see p.117). The large difference in the primary modal diameters between the dull yellowish brown and reddish brown lapilli is related partly to the normally graded nature of the deposit and also to the tendency for the softer, dull yellowish brown lapilli to abrade more during hand sieving.

Textural analyses emphasise the polymodal grain size distributions in the Recent and Pumiceous beds, even when any artificially created modes are excluded. The relationship between mineralogy and size classes was determined from the coarser than 2 Ø fraction of field class II samples at sites 25 (Old Mill) and 37 (Kopu), with the results shown in Fig. 4.6. The coarser grain size (2 Ø) was selected to avoid sand-sized aggregates of secondary material and to enable identification of the tephra components by binocular microscope. The deposits are polycomponent being composed of three types of pyroclastic materials (cf. Walker 1971): vitric components (pumiceous lapilli); crystal components (anorthoclase crystals); and lithic components (glassy rock fragments containing minor devitrified glass and altered feldspar phenocrysts). The polymodal nature of the grain size histograms in Fig. 4.6 results therefore from a combination of the particle size distributions of these three components. As the grain size fines, as for example from site 25 to site 37, the crystal and lithic components increase in abundance compared with the vitric components so that site 37 shows stronger bimodality. While the

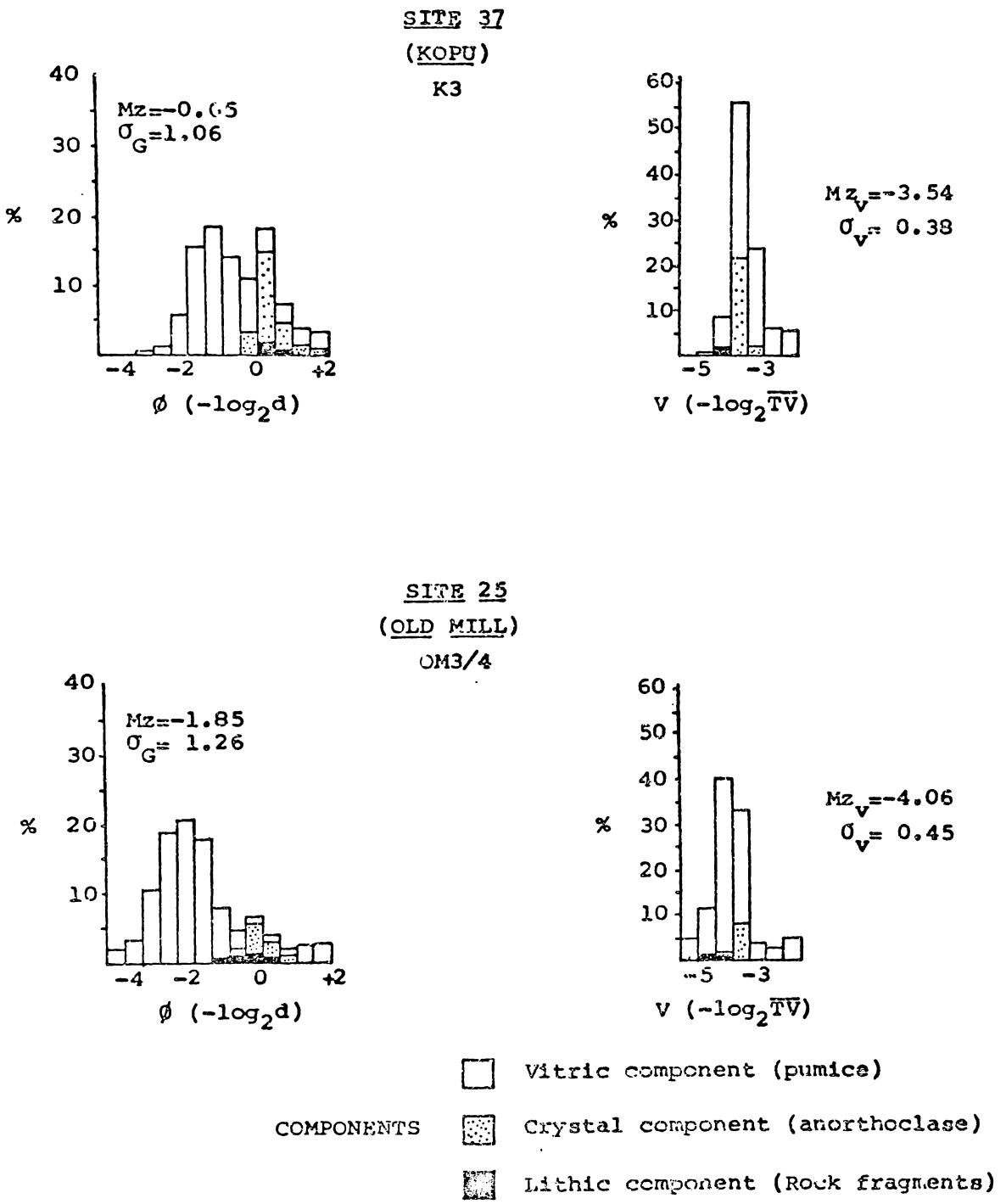


FIGURE 4.6 : Particle size and Fall velocity distributions and tephra components for the coarser than 2ø fraction of field class II at sites 25 and 37. Data from Appendix E (Fig. E.7).

Note : Terminal velocity classes, calculated using data on fragment size, density, shape and surface roughness and the curves of Walker et al.(1971), are treated in a similar manner to the grain size classes of Krumbein (1936). $\overline{TV}$ is the terminal velocity in metres per sec.

samples as a whole are typically poorly sorted, the particle size distributions for the individual components constituting sample OM3/4 are either moderately sorted or very well sorted (Table 4.2).

TABLE 4.2: A comparison of the grain size properties of a polycomponent tephra sample and its three constituents, the vitric, crystal and lithic components Sample OM3/4.

| | | Percentage of total sample | Median (Ø) | Mean (Ø) | Sorting Coefficient (ØG Ø) |
|---|---|---|---|---|---|
| Whole sample (OM3/4) (coarser than 2 Ø) | | 100.0 | -2.10 | -1.85 | 1.26 |
| OM3/4 coarser than 2 Ø | Vitric component | 90.1 | -2.23 | -2.18 | 0.87 |
| | Crystal component | 8.7 | -0.15 | -0.13 | 0.34 |
| | Lithic component | 1.3 | -0.40 | -0.40 | 0.21 |

Walker (1971) found that polycomponent deposits were best characterised by plotting weight percentages against terminal fall velocities rather than particle diameters, since fall velocities take into account fragment density, shape and surface roughness in addition to grain size and thereby group in the same class all particles which fall at the same rate. He demonstrated that small dense crystals would have the same fall velocity, and hence accumulate at the same time, as pumice fragments of much larger size. This would produce the type of bimodal size distributions shown in Figs. 4.5 and 4.6. The particle densities of the three components of samples from the Pumiceous bed were determined in mixtures of

bromoform and acetone and classified according to the scheme of Walker et al. (1971); the vitric component occurs as rough spheres with a density of 0.30-0.50 g/l; the crystal component as cylinders with a density of 2.60 g/l; and the lithic component as rough spheres with a density of 2.60 g/l. The particle size distributions of the Pumiceous bed at sites 25 and 37 shown in Fig. 4.6, were converted to terminal velocity distributions utilising the curves of Walker et al. (1971) and are shown as plots of weight percent of the tephra components against terminal velocity class in Fig. 4.6. The terminal velocity distributions are strongly unimodal and have a standard deviation ($\theta v$) that is considerably less than that obtained from the equivalent particle size curves ($\theta G$ $\phi$). The unimodal fall velocity distributions shown in Fig. 4.6 demonstrate that the particle size distribution of the coarser than 2 $\phi$ material from the Pumiceous bed in the Whangamata region is controlled by the peralkaline lapilli, with the polymodality being a function of the components comprising the tephra.

Mineralogical and chemical examinations of samples from field classes I and II at Pukekauri Rd revealed that the field classes contain a mixture of both peralkaline and calc-alkaline tephras (see p.96). To investigate the influence of the calc-alkaline tephras on the particle size and fall velocity distributions, five samples from sites 37 (Kopu) and 21 (Maratoto Valley) were examined (Fig. 4.7). The fall velocity distributions of the coarser samples of class II (K2 and K3) are strongly unimodal and the crystal component is represented by pure anorthoclase, which indicates the predominance of the peralkaline lapilli in those samples. However,

FIGURE 4.7 : Particle size and fall velocity distributions and tephra components for the coarser than 2 $\emptyset$ fraction from field classes I and II at sites 37 and 21.

Data from Appendix E (Fig. E7).

Note: Because of the fine grain size of the five samples above, each sample contained a large proportion of lapilli-sized aggregates of fine material which could not be removed by wet sieving. The samples were therefore suspended in dilute HCl (pH3) and slowly rotated in an end-over-end shaker for seven hours. Examination of individual size classes by binocular microscope enabled adjustments to be made for the minor amounts of aggregates particles still remaining as well as determining the percentages of each of the three components as indicated above.

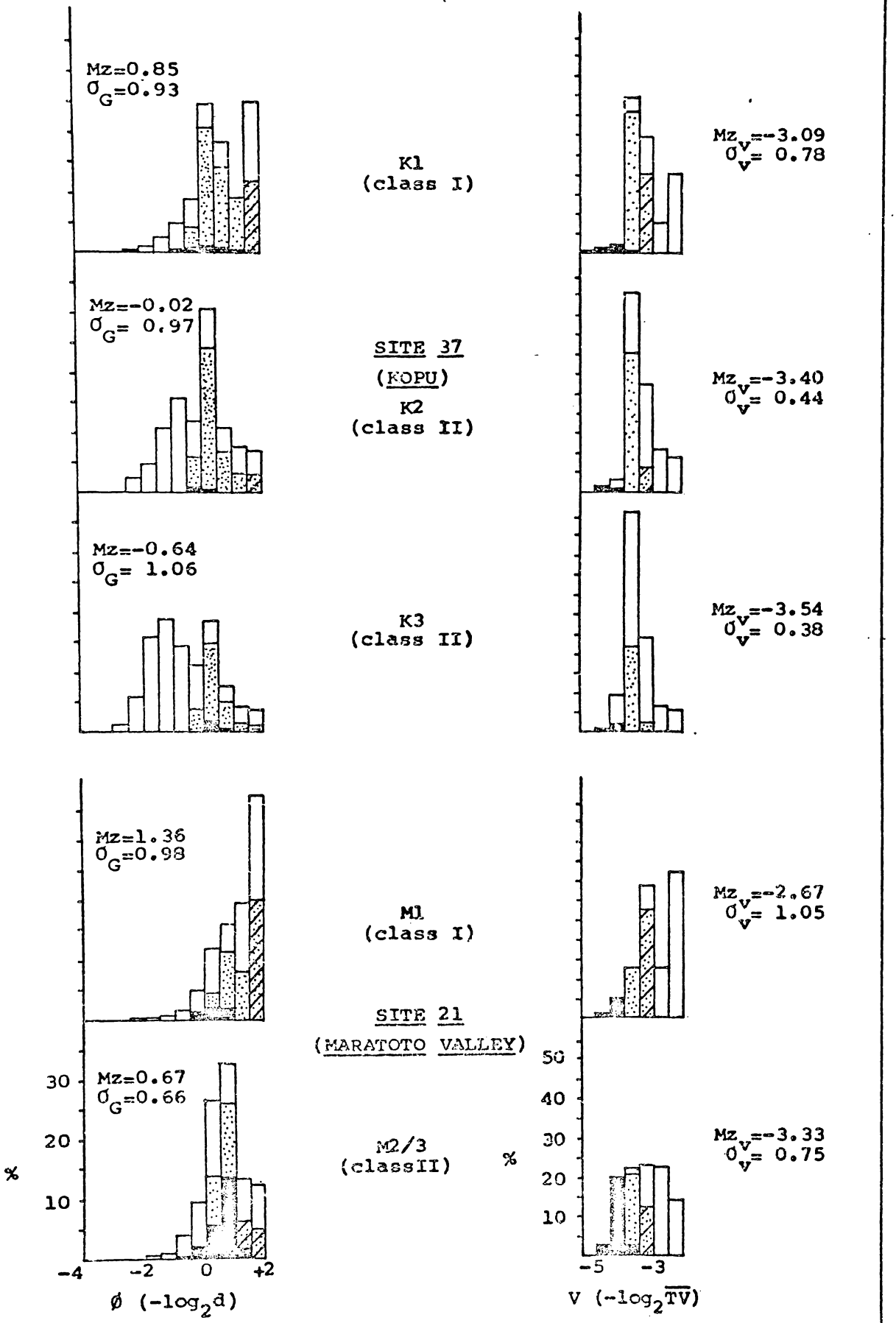
Mz=0.85
σG=0.93
K1
(class I)
Mz=-3.09
σv= 0.78
Mz=-0.02
σG= 0.97
SITE 37
(KOPU)
K2
(class II)
Mz=-3.40
σv= 0.44
Mz=-0.64
σG= 1.06
K3
(class II)
Mz=-3.54
σv= 0.38
Mz=1.36
σG=0.98
M1
(class I)
Mz=-2.67
σv= 1.05
SITE 21
(MARATOTO VALLEY)
Mz=0.67
σG=0.66
M2/3
(classII)
Mz=-3.33
σv= 0.75
%
30
20
10
50
40
30
20
10
-4
-2
0
+2
-5
-3
ø (-log2d)
V (-log2TV)
TEPHRA
COMPONENTS
Vitric component (pumice)
Crystal component
anorthoclase
anorth. + plag.
Lithic component (rock fragments)

the finer class II (M2/3) and class I (K1,M1) samples have comparatively poorly sorted fall velocity distributions and a crystal component containing equal amounts of plagioclase and anorthoclase, which identifies the presence of calc-alkaline material in these samples. The fall velocity distributions of the Recent and Pumiceous beds therefore demonstrate that when the Pumiceous bed is coarse, the particle size distribution of the coarser than 2 Ø fraction is controlled completely by the peralkaline lapilli; in the Recent bed and when the Pumiceous bed is finer, the calc-alkaline tephras exert an influence in the 0-2 Ø size range.

## 4. Petrography and mineralogy

### (a) Pumice

A major constituent of classes I and II is altered pumiceous volcanic glass which occurs as discrete shards in the Waihi region and as coarse, sparsely porphyritic pumiceous lapilli accompanied by minor amounts of free crystals and lithic fragments near Whangamata. The proportions of pumice, free crystals and lithic fragments in field classes I and II for three sites are shown in Fig. 4.8. In the coarser samples, for example OM3/4 and K3, pumice predominates, but free crystals and lithic fragments become increasingly abundant with finer grain size, as in samples K1, K2, M1 and M2/3. The coarse, reddish brown pumiceous lapilli have a moderate concentration of vesicles and many are prominently flow-banded. Thin sections of the coarser particles (coarser than 30 mm) show phenocrystic anorthoclase; other phenocrysts are detectable only after crushing and concentration techniques.

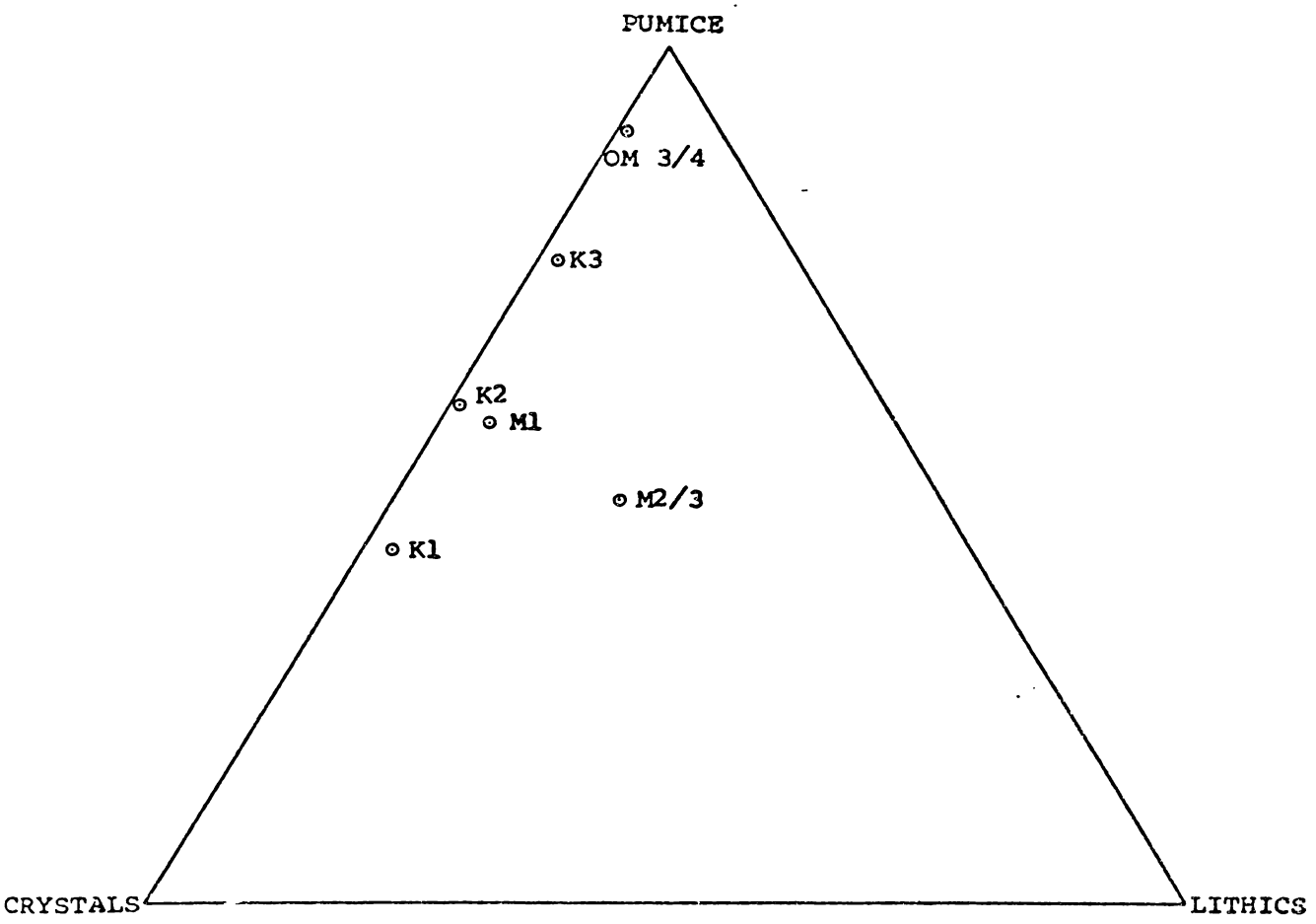


FIGURE 4.8 : Percentage of Pumice, Crystals and Lithic fragments in the Recent and Pumiceous beds in the greater Whangamata region. Percent of the coarser than 2Ø fraction at sites 25 (OM 3/4), 37 (K1,K2,K3) and 21 (M1,M2/3).

A unique feature of the Pumiceous bed in the Whangamata region is the intense reddish brown colour of its pumice fragments. Nicholls and Carmichael (1969) have noted that despite the iron-rich nature of peralkaline deposits, ferromagnesian phenocrysts are usually very scarce so that residual glasses are typically enriched in Fe. It is therefore likely that the reddish brown colour has resulted from oxidation of the Fe contained within the glasses under the soil forming environment of the Coromandel Peninsula. The proportion of selected elements was determined using XRF for the coarser than -1 $\phi$ fraction of thirteen samples of reddish brown and dull yellowish brown pumiceous lapilli occurring in the Whangamata region (Fig. 4.9). The data indicate a relationship between colour and the Si and Fe contents, with Fe being more concentrated in the reddish brown lapilli, and Si in the dull yellowish brown lapilli. Considering the colour of the deposits and the susceptibility of Fe to oxidation and mobilisation, it seems likely that the colour differences have resulted from the movement and deposition of Fe through the profile. The lapilli have probably undergone the following sequences of changes:

(i) Intense chemical weathering under the influence of the soil forming processes which resulted in physical decomposition of the glass and oxidation of Fe, producing a change in colour of the lapilli from grey to red brown.

(ii) Local mobilisation of $Fe^{3+}$ under the influence of certain forest trees such as Kauri and Rimu, resulting in the removal of the reddish brown colour in the upper parts of some profiles to form the dull yellowish brown lapilli (cf. the podsolization of tephras described by Singer et al. 1978).

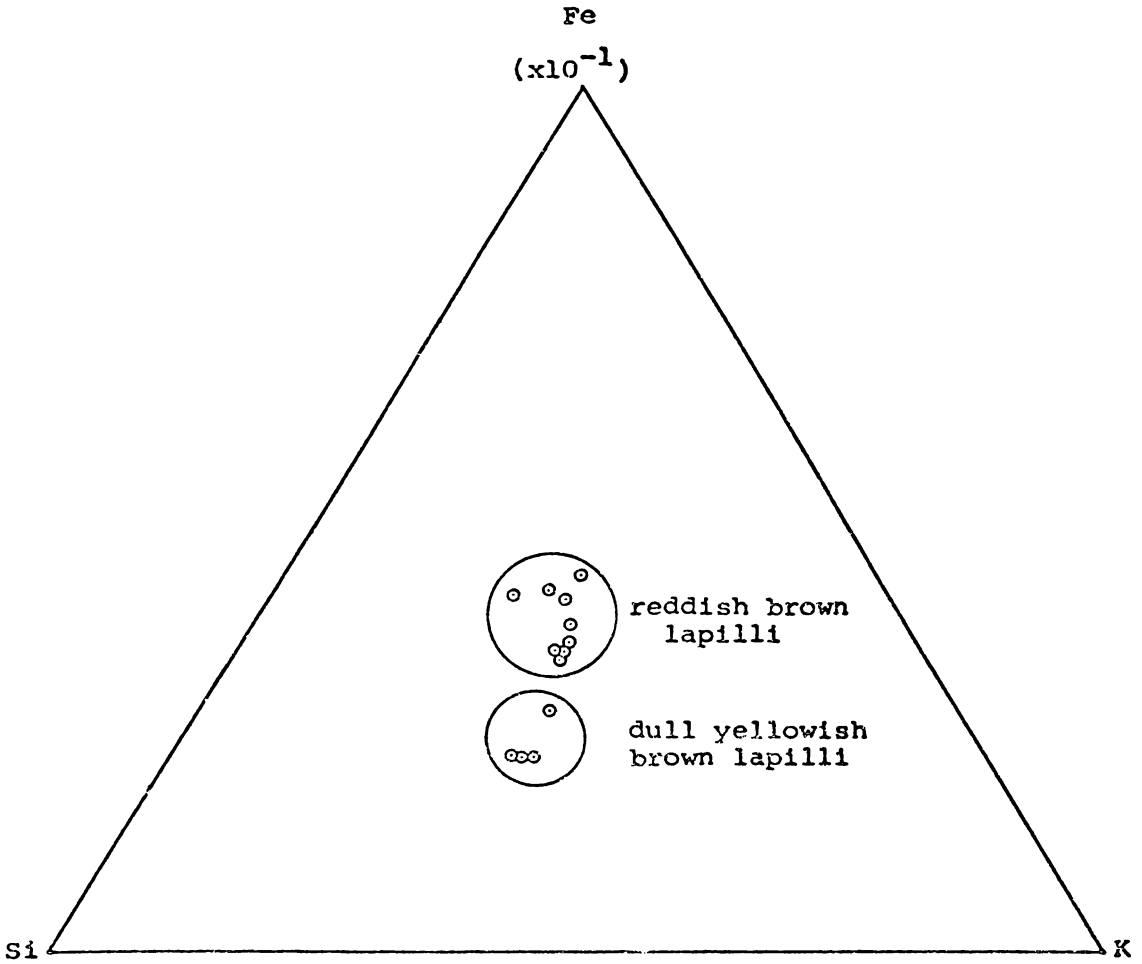


FIGURE 4.9 : Relative amounts of Si, K and Fe in the coarser than -1Ø fraction of the reddish brown and dull yellowish brown lapilli in field class II, in the Whangamata region. Units are Si (cps %); K (cps %); and Fe ( cpsx10$^{-1}$ %).

(b) Quartz and feldspar

The felsic minerals of field classes I and II have been described previously in Chapter 3 and Appendix A, and include quartz, plagioclase and anorthoclase. The felsic mineral contents of the 2-4 Ø fractions of the Recent and Pumiceous beds were determined at four sites (Table 4.3). The table shows the influence of the class II calc-alkaline tephras (identified by their plagioclase content), particularly at the sites in the southern part of the region (e.g. M1, M2/3). The similarity in the felsic mineral contents of the dull yellowish brown and reddish brown lapilli at the Whangamata south and Neavesville sites reinforces the view that these two lapilli in fact represent a single deposit which has undergone post-depositional changes.

TABLE 4.3 : Felsic mineral content of the Recent and Pumiceous beds. Weight % in the 2-4 Ø fraction, determined by XRD

| Site | Field class | Sample | Plagioclase | Quartz | Anorthoclase |
|---|---|---|---|---|---|
| 37 (Kopu) | I | K1 | 17 | 11 | 7 |
| | II | K2 | 11 | 5 | 7 |
| | | K3 | 10 | 5 | 7 |
| 21 (Maratoto Valley) | I | M1 | 15 | 9 | 7 |
| | II | M2/3 | 11 | 11 | 7 |
| 84 (Whangamata south) | II | Wg1(yell. brown lap.) | 10 | 5 | 10 |
| | | Wg2(red brown lapilli) | 10 | 5 | 7 |
| 85 (Neavesville) | II | N1(yell. brown lap.) | 13 | 9 | 10 |
| | | N2(red brown lapilli) | 13 | 5 | 11 |
| 8 (Pukekauri Rd) | II | P3 | 12 | 11 | 9 |

For site locations and the stratigraphic position of samples, see Fig.4.4 p. 107.

(c) Ferromagnesian mineralogy

The ferromagnesian mineral assemblages of the coarser class I and II deposits from the Kopu site are compared with the finer-grained Pukekauri Rd samples in Table 4.4 and Fig. 4.10. It is clear from Table 4.4 that even the coarser samples of the Pumiceous bed (e.g. K3) contain significant amounts of calc-alkaline material which is concentrated in the finer size fractions and increases in

TABLE 4.4 : Ferromagnesian mineral assemblages in the 2-4 $\phi$ fraction of the Recent and Pumiceous beds

| Site | Field class | Sample | Calc-alkaline mineral suite | | | | Peralkaline minerals |
|---|---|---|---|---|---|---|---|
| | | | Hypersthene (%) | Cummingtonite (%) | Hornblende (%) | Augite (%) | Aegirine (%) |
| 8 (Pukekauri Rd) | I | P1 | 28 | 19 | 30 | 17 | 6 |
| | | P2 | 27 | 14 | 34 | 18 | 7 |
| | II | P3 | 23 | 20 | 26 | 24 | 7 |
| | | P4 | 24 | 22 | 30 | 14 | 10 |
| 6 (Waihi Beach) | I | W1 | 36 | 20 | 25 | 10 | 9 |
| | | W2 | 29 | 17 | 31 | 14 | 9 |
| | II | W3 | 36 | 17 | 25 | 11 | 11 |
| | | W4 | 45 | 29 | 11 | 8 | 7 |
| 37 (Kopu) | I | K1 | 44 | 20 | 24 | 8 | 4 |
| | II | K2 | 41 | 18 | 15 | 7 | 19 |
| | | K3 | 49 | 32 | 8 | - | 11 |

For site locations and the stratigraphic position of samples, see Fig. 4.4 p.107.

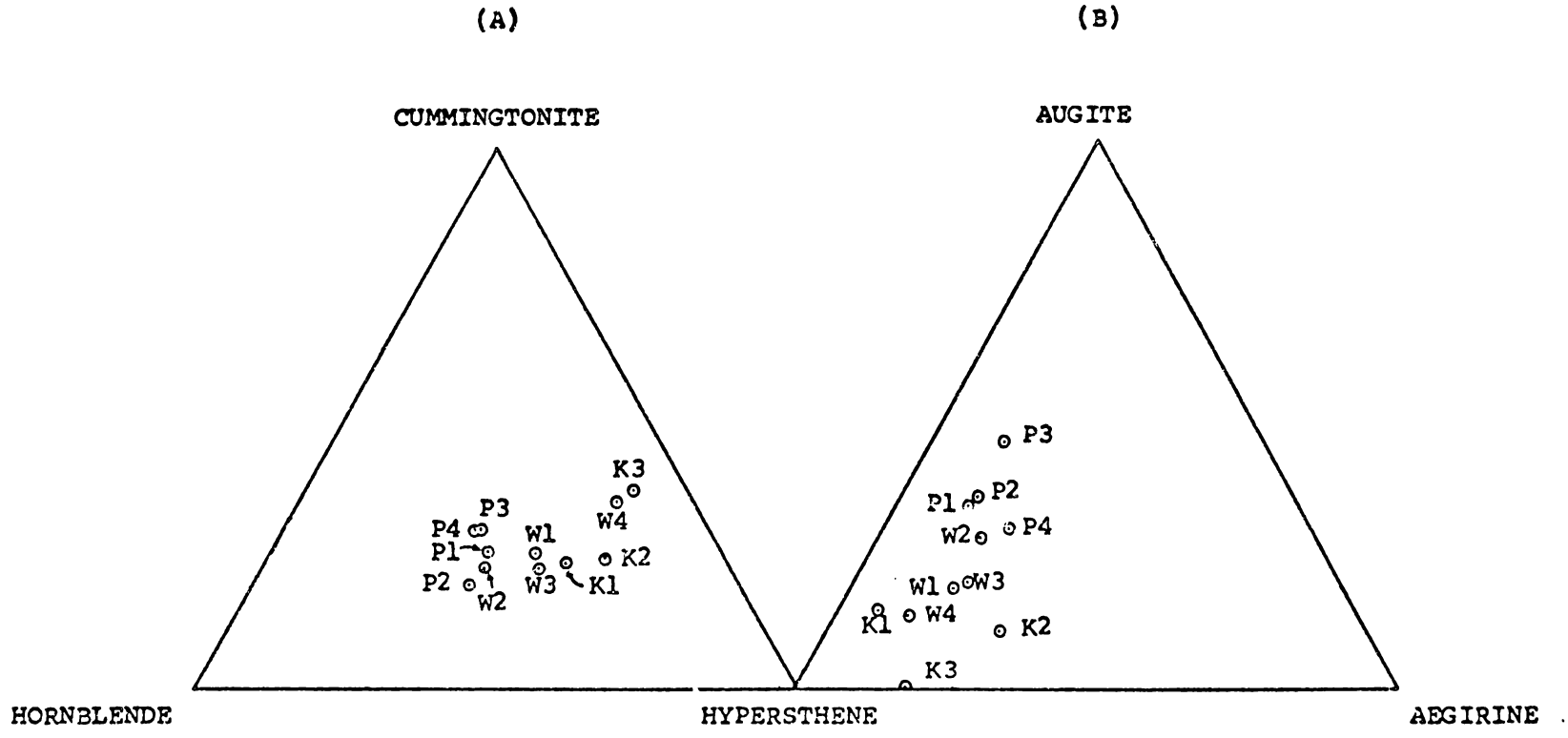


FIGURE 4.10 : Ferromagnesian mineral assemblages in the 2-4Ø fraction of the Recent and Pumiceous beds at sites 8 (Pukekauri Rd), 6 (Waihi Beach), and 37 (Kopu).
A : Triangular diagram of the cummingtonite, hornblende and hypersthene contents.
B : Triangular diagram of the augite, aegirine and hypersthene contents.

concentration south of Whangamata. The four main calc-alkaline minerals represented at the Pukekauri Rd site, namely cummingtonite, hornblende, hypersthene and augite, are also present at the Kopu site but in different proportions. The major difference involves the pyroxenes, the Kopu samples being dominated by hypersthene while those from Pukekauri Rd contain subequal amounts of hypersthene and augite. Samples from the Recent and Pumiceous beds were analysed from a site on the Waihi-Waihi Beach highway (site 6, Waihi Beach -- see Fig. 4.4) to establish if the Pukekauri Rd site is representative of the Waihi region (Table 4.4 and Figure 4.10). It is apparent that the ferromagnesian mineral assemblage of the class II Waihi Beach samples (W3,W4) show more affinity with the Kopu samples than do P3 and P4 from Pukekauri Rd. This is particularly noticeable if the augite is excluded, as in Fig. 4.10A. These data suggest that the Recent and Pumiceous beds from sites on the Waihi Plain have been influenced by an augite-bearing tephra, the influence of which has been less significant at the Waihi Beach site and absent at the Kopu site.

In many of the sites examined, the field class I and II peralkaline minerals occur as phenocrysts in the pumiceous lapilli and therefore are present only in low concentration in the sand fraction. To provide a more reliable estimate of the relative proportions of the calc-alkaline and peralkaline tephras, the coarser than 1 $\emptyset$ fraction was examined (Table 4.5). Class I samples are completely dominated by hypersthene with lesser amounts of aegirine and cossyrite. Class II samples are dominated by either hypersthene or aegirine, with minor cossyrite and cummingtonite. In all five localities shown in Table 4.5, the proportions of aegirine and

TABLE 4.5 : Ferromagnesian mineral content (2-4 Ø fraction) extracted from crushed lapilli (coarser than 1 Ø) of field classes I and II

| Site | Field class | Sample | Calc-alkaline minerals | | | Peralkaline minerals | | |
|---|---|---|---|---|---|---|---|---|
| | | | Hypersthene (%) | Cummingtonite (%) | Hornblende (%) | Aegirine (%) | Cossyrite (%) | Riebeckite (%) |
| 37 (Kopu) | I | K1 | 81 | 1 | 2 | 8 | 8 | - |
| | II | K2 | 48 | 12 | 5 | 30 | 4 | 1 |
| | | K3 | 15 | 6 | 3 | 76 | - | - |
| 21 (Maratoto Valley) | I | M1 | 91 | 1 | 1 | 6 | 1 | - |
| | II | M2 | 65 | 7 | 1 | 24 | 1 | 2 |
| | | M3 | 16 | 14 | 2 | 57 | 7 | 4 |
| 84 (Whangamata south) | II | Wg1 | 59 | 2 | 1 | 33 | 5 | - |
| | | Wg2 | 12 | 7 | 2 | 68 | 10 | - |
| 85 (Neavesville) | II | N1 | 86 | - | 1 | 10 | 3 | - |
| | | N2 | 66 | - | 1 | 33 | - | - |
| 25 (Old Mill) | II | OM2 | 34 | 8 | 9 | 49 | - | - |
| | | OM3 | 1 | - | - | 96 | 2 | 1 |
| | | OM4 | 1 | - | - | 98 | 1 | - |

To estimate phenocrystic assemblages, the coarser than 1 Ø fraction was subjected to severe mechanical abrasion by ultrasonic vibrations to dislodge any fine material from pumice cavities which might otherwise affect results.

hypersthene vary inversely with depth, the aegirine replacing hypersthene as the deposit coarsens. This relationship between mineralogy and texture also occurs within individual samples where aegirine is concentrated in the coarser fractions and hypersthene

and cummingtonite in the finer (e.g. in sample K3, Table 4.6).

TABLE 4.6 : Relationship between ferromagnesian mineral content and grain size in a sample of the Pumiceous bed (sample K3).

| | | Calc-alkaline minerals | | | Peralkaline minerals | |
|---|---|---|---|---|---|---|
| | | Hypers-thene | Cumming-tonite | Horn-blende | Aegirine | Cossyrite |
| % mineral in the size fraction shown | coarser than -0.5Ø | 30 | 15 | 5 | 49 | 1 |
| | -0.5-2 Ø | 33 | 29 | 5 | 32 | 1 |
| | 2-4 Ø | 48 | 32 | 8 | 11 | 1 |

Sample K3 was wet-sieved into the three fractions shown above, severely probed to remove superficial crystals lodged within pumice cavities, crushed, and the 2-4 Ø ferromagnesian mineral fraction analysed.

In conclusion, hypersthene, cummingtonite, hornblende, and augite are considered to represent calc-alkaline tephras which become increasingly important in class I and the upper parts of class II, and in the southern parts of the region. The ferromagnesian mineral assemblage of the peralkaline pumiceous lapilli contains aegirine, cossyrite, olivine, ? hedenbergite, riebeckite and tuhualite and is most prominent when the Pumiceous bed is coarsest.

The only recorded Late Quaternary volcanic sources of aegirine in New Zealand are the peralkaline eruptives of Mayor Island (Marshall 1932; Buck 1978). As the peralkaline tephra of field classes I and II occurs in a stratigraphic column that is otherwise calc-alkaline in composition, aegirine provides an excellent marker

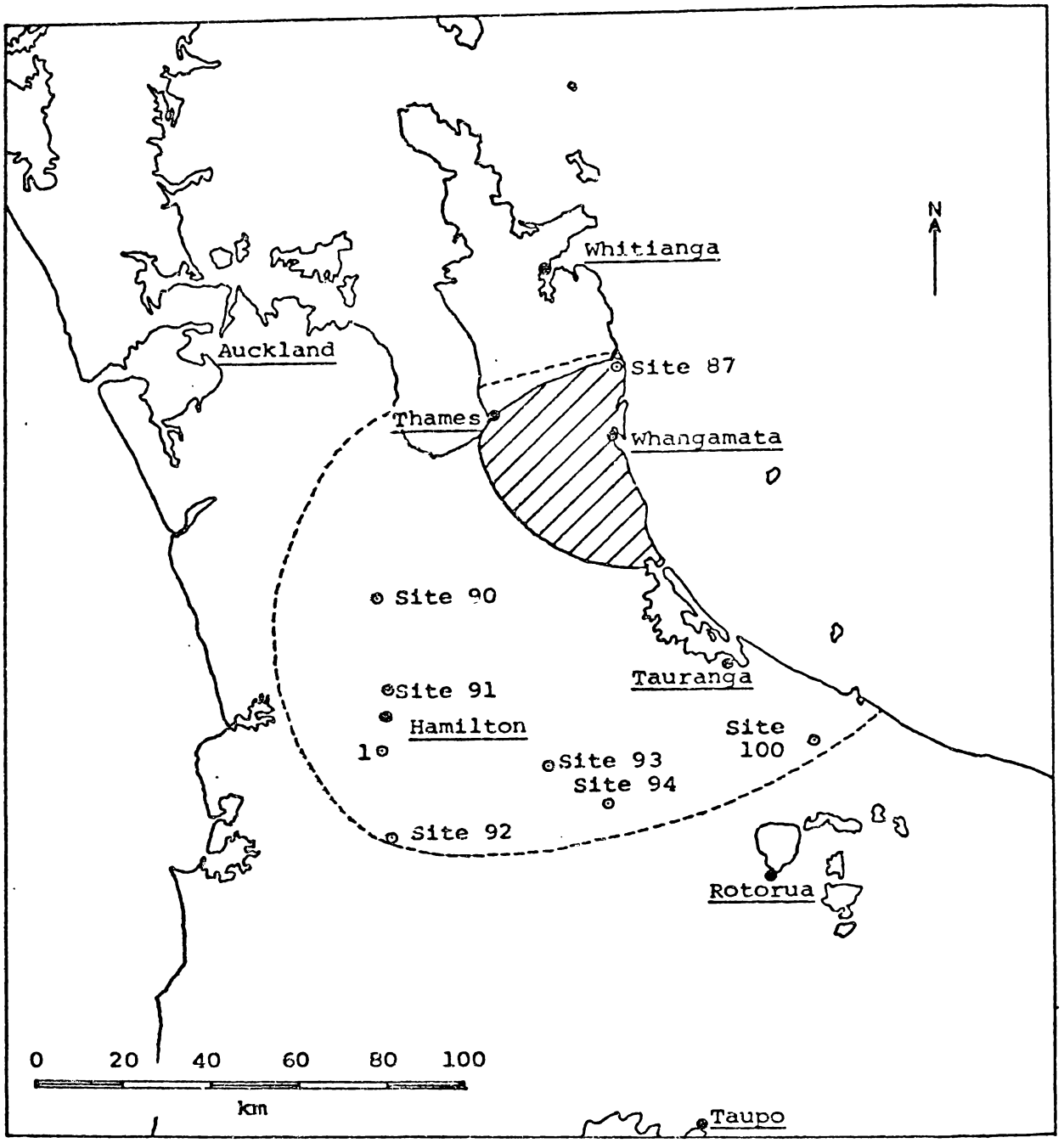


FIGURE 4.11 : Areas of deposition of the peralkaline pumiceous ash and lapilli of field classes I and II .

Area of the deposit identified by field observation

Area of the deposit identified by the aegirine content.

1 : Lake Mangahia : Lake cores contain a 5mm thick layer of the peralkaline tephra (see Fig.4.12).

of the peralkaline lapilli, because of its distinctive optical properties. On this basis, the peralkaline tephra has been detected in tephra columns over 100 km distance from Whangamata (Fig. 4.11), with aegirine contents varying from less than 1% in the south (e.g. site 92) to more than 8% at sites further north (e.g. site 90) - Table 4.7.

TABLE 4.7 : Percent aegirine in the ferromagnesian mineral assemblages extracted from Upper Quaternary tephras in the Coromandel - Bay of Plenty - Waikato regions

| Site No. | Location | % aegirine in the 2-4Ø fraction of the ferromagnesian mineral assemblage | Depth of the sample from the surface (cm) | Source of data |
|---|---|---|---|---|
| 87 | Ohui site | 3 | 0-15 | this thesis |
| 90 | Welches Rd | 8 | 0-20 | ibid |
| 91 | Rototuna | 2-5 | 0-55 | Mr D. Lowe (M.Sc., in prep.) |
| 92 | Kakepuku | 1 | 25-45 | |
| 93 | Taotaoroa | 1 | 29-50 | |
| 95 | Tapapa | 1 | 40-95 | |
| 100 | Te Matai Rd | 1 | 60-70 | this thesis |

The presence of the peralkaline pumiceous tephra in the Waikato region was confirmed by locating it in a core collected from the sediment accumulated in a peat lake near Hamilton (Fig. 4.12). The 2 m core contains mineral layers ranging in thickness from 2 mm to 50 mm, separated by finely disseminated black organic muds. All the mineral layers are dominated by volcanic glass, much of which is in the form of pumiceous ash and lapilli ranging in appearance from dark grey to white and varying in their degree of vesiculation

and phenocryst content. The ferromagnesian mineral assemblages commonly contain hypersthene, hornblende, and augite, and in particular layers, aegirine, cummingtonite, olivine and biotite. Layer X, only 5 mm in thickness, contains a ferromagnesian mineral fraction including aegirine with minor cossyrite, olivine and riebeckite, which identifies it as the peralkaline pumiceous deposit of field class II (Table 4.8). The relatively high proportion of accompanying calc-alkaline minerals, suggests that layer X has been contaminated after deposition on the lake bed.

TABLE 4.8 : The ferromagnesian mineral assemblage of Layer X from the Waikato lake sediment core (2-4 Ø fraction)

| | Calc-alkaline minerals | | | Peralkaline minerals | | | |
|---|---|---|---|---|---|---|---|
| | Hypersthene (%) | Hornblende (%) | Augite (%) | Aegirine (%) | Cossyrite (%) | Riebeckite (%) | Olivine (%) |
| Layer X | 26 | 16 | 26 | 28 | 2 | 1 | 1 |

For the stratigraphic position of Layer X, see Fig. 4.12.

The area covered by the peralkaline pumiceous lapilli and ash that has been mapped in the field is approximately 1300 $km^2$ and has a northwesterly-trending axis (see Fig. 2.7 p. 24). The presence of free aegirine crystals in the Bay of Plenty - Waikato region indicates a very much wider dispersion area of some 10,000 $km^2$ having a southwesterly axis (Fig. 4.11). On the basis of this, and the grain size distribution of samples from class II, it appears that the main eruption was distributed along a northwesterly-trending axis,

while the finer material was deposited further to the south, along a more southwesterly axis. The divergence in axial directions could have originated in at least four ways:

(i) A northeasterly wind may have prevailed during eruption from a vent inclined in a northwesterly direction (e.g. Fisher 1964 ).

(ii) The wind may have changed direction from the southeast to the northeast at the end of the eruption, as it did during the Crater Lake pumice eruption (Fisher 1964 ).

(iii) The wind direction may have varied with altitude, with the lower part of the atmosphere bearing northwest and the upper atmosphere distributing the finer material in a southwesterly direction (cf. Topping 1972).

(iv) There may have been a series of lapilli and ash eruptions within a single eruptive episode that were distributed by winds from different directions.

There is presently insufficient evidence to decide between these alternatives.

## 5. Titanomagnetite chemistry

Analyses of seven titanomagnetite concentrates (Fig. 4.13) show that a close relationship exists between the class II tephras of the Waihi Beach and Kopu sites. Two samples from the Kopu site (K2 and K3) were wet-sieved into coarser and finer than −1 Ø fractions and their titanomagnetites extracted and analysed with the aim of testing the hypothesis that the coarser fraction is dominated by the peralkaline tephra and the finer by the calc-alkaline

FIGURE 4.12 : Mineral layers exposed in a 2 m core of lake deposits near Hamilton (Lake Mangahia, N65/738357 - see Fig. 4.11). Layer X, 5 mm thick, is a grey, pumiceous coarse ash which correlates with the field class I and II peralkaline tephra. The base of the column is approximately 15,000 years B.P.

The Lake Mangahia core was collected by Mr J. Boubee, Biological Sciences, University of Waikato.

1. % heavy minerals in the 2-4 Ø fraction
2. When more than one ferromagnesian mineral is present the mineral in highest concentration is typed in capital letters.

| Wt.% Heavy Minerals 1 | Dominant Ferromagnesian Minerals 2 | cm | | Petrographical descriptions |
|---|---|---|---|---|
| 3.3 | HYPERSTHENE | 0 | XIV | White, poorly vesiculated, sparsely porphyritic, pumiceous coarse ash and very fine lapilli. |
| | | 10 | | |
| 0.4 | HYPERSTHENE | | XIII | White, fine ash composed of pumiceous glass shards. |
| | | 20 | | |
| 22.4 | hornblende augite | 30 | XII | White, extremely vesiculated, highly porphyritic, pumiceous coarse ash. |
| | | 40 | | |
| | | 50 | | |
| | | 60 | | |
| | | 70 | | |
| 28.2 | AUGITE | | XI | White, poorly vesiculated, highly porphyritic, pumiceous coarse ash. |
| 0.3 | aegirine hypersthene hornblende augite | 80 | X | Grey, extremely vesiculated, sparsely porphyritic, normally graded, pumiceous coarse ash. |
| | | | IX | White to pale brownish yellow, moderately vesiculated, sparsely porphyritic, pumiceous coarse ash. |
| 0.1 | hypersthene cummingtonite hornblende augite | 90 | | |
| | | 100 | VIII | Pale yellowish brown and white, fine pumiceous ash. |
| | | 110 | | |
| | | 120 | | |
| 2.5 | hornblende augite | | VII | White, fine ash composed of pumiceous glass shards. |
| | | 130 | | |
| 13.0 | hypersthene augite olivine | 140 | VI | Dark grey and white, poorly vesiculated, sparsely porphyritic, coarse ash (andesitic). |
| | | 150 | V | Pale grey, fine ash. |
| | | 160 | | |
| 0.1 | HYPERSTHENE | 170 | IV | White, fine ash composed of pumiceous glass shards, multiple-bedded. |
| 1.7 | hypersthene augite | 180 | III | Very dark grey, fine ash. |
| | | 190 | | |
| 2.2 | HYPERSTHENE hornblende | 200 | II | White, moderately vesiculated, sparsely porphyritic, normally graded coarse ash and very fine lapilli. |
| | | 210 | | |
| 0.2 | BIOTITE hornblende | | I | White, fine ash composed of pumiceous glass shards. |
| | | 220 | | |

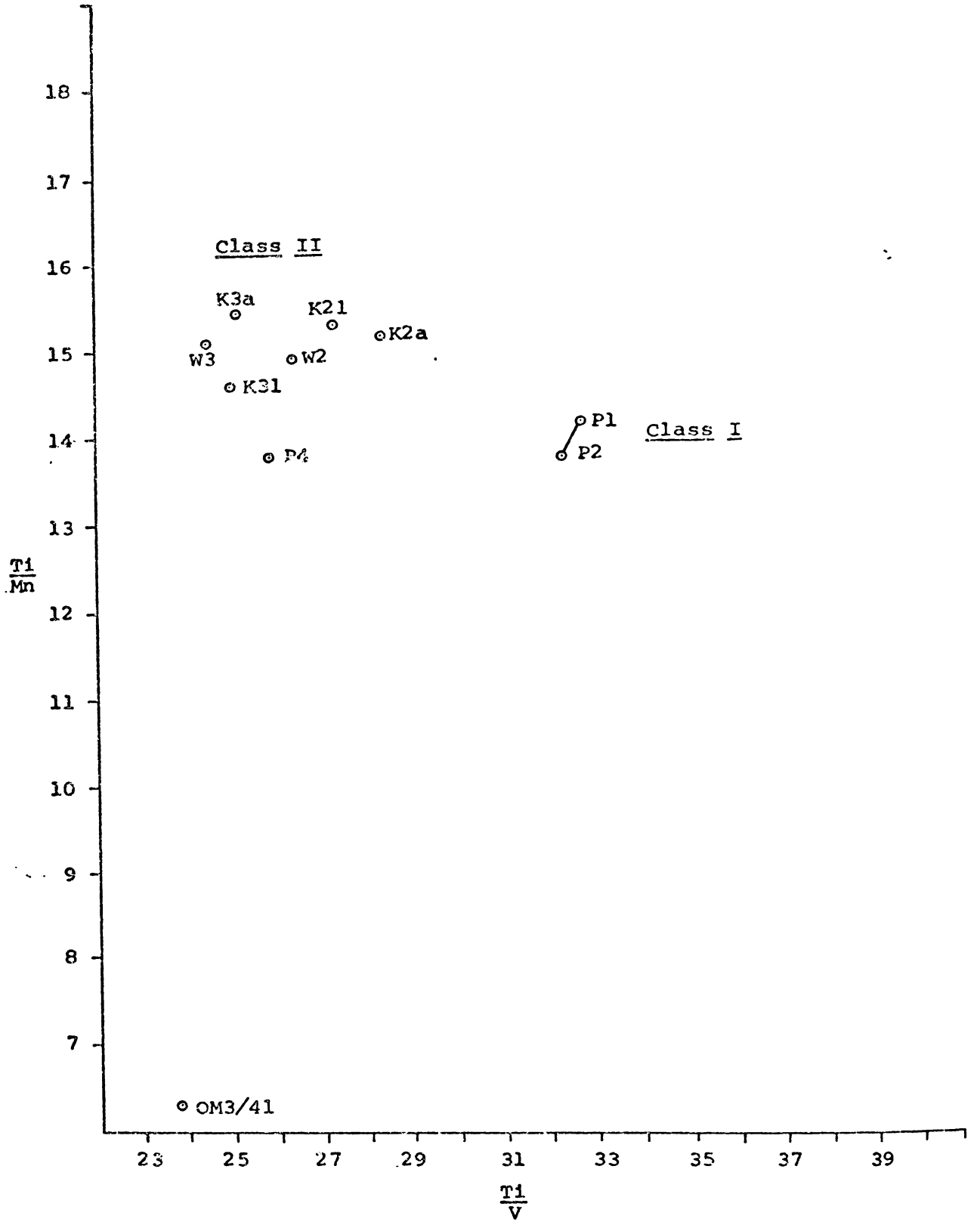


FIGURE 4.13 : Ratios of count rates of Ti, Mn and V from titanomagnetites extracted from field classes I and II at Pukekauri Rd (P1,P2,P4), Waihi Beach (W2,W3), Kopu (K2a,K21,K3a,K31), and Old Mill(OM3/41) sites.
K21,K31,OM3/41 samples represent the coarser than -1Ø fraction of the Kopu and Old Mill sites.
K2a and K3a represent the finer than -1Ø fraction of the Kopu samples K2 and K3 respectively.

tephra and to try and establish the original stratigraphic relationship between the peralkaline and calc-alkaline deposits. Fig. 4.13 shows that there is very little difference between the two size fractions from the Kopu samples (i.e. K2L and K2A; K3L and K3A). The titanomagnetites analysed from OM3/4L are more representative of the peralkaline tephra titanomagnetite chemistry since the coarse fraction of that sample is known from the silicate mineralogy to contain only minor amounts of the calc-alkaline component (see Table 4.5 p.123). The considerable difference in the Ti/Mn ratios between the Kopu samples and OM3/4L demonstrates the extent to which the lapilli at the Kopu site have been influenced by the calc-alkaline tephra, whose fine grain size and high proportion of titanomagnetite gives the sparsely porphyritic peralkaline lapilli a considerable calc-alkaline character. It is therefore concluded from the titanomagnetite chemistry that only sites containing coarse lapilli (coarser than 16 mm) in the Pumiceous bed have a predominantly peralkaline composition; where the Pumiceous bed is of medium, fine and very fine lapilli, an important calc-alkaline component is also present.

## 6. Discussion of the Calc-alkaline and Peralkaline tephras in classes I and II

### (a) The Calc-alkaline tephras

Four calc-alkaline tephras (tephras G, H, I and J in Fig. 3.18 p. 96) may be recognised in field classes I and II north of Waihi. With the exception of Tephra I, they have fine grain sizes ($M_z$ finer than 2 $\phi$) and contain volcanic glass, plagioclase, quartz,

titanomagnetite, hypersthene, cummingtonite, hornblende and augite. The tephras decrease in thickness and have finer grain sizes north of Waihi, indicating they were erupted from vents to the south of the Coromandel Peninsula.

(b) The peralkaline tephra (tephra F of Fig. 3.18)

This tephra is represented by an extensive ash and lapilli deposit covering at least 10,000 $km^2$ from a source off the east coast of Whangamata. Deposition appears to have occurred in two lobes: a coarse, pumice-rich unit covering some 1300 $km^2$ lying to the northeast of Whangamata and extending over the Coromandel Range at least as far as Thames; and a finer glass and crystal-rich lobe spreading over more than 8,000 $km^2$ to the southwest, beyond Hamilton City where it is 5 mm thick.

The lapilli exhibit a polymodal grain size distribution resulting from the interaction of vitric, crystal and lithic components of varying size, shape and density. Where the deposit is coarsest, it is dominated by weathered, iron-rich, reddish brown, sparsely porphyritic pumiceous lapilli with the associated crystal and lithic fragments (represented by anorthoclase and glassy rock fragments respectively) being only of minor importance. The tephra occurs in both field classes I and II, with class I containing abundant glass and free crystals and representing the finer part of the eruption, and class II containing the reddish brown lapilli forming the base of the deposit. Free anorthoclase crystals also occur in class II and these decrease in abundance from the top to the bottom of the deposit, as the lapilli grain size coarsens.

South and west of Whangamata, the lapilli grade into a deposit of ash-sized material which contains larger amounts of free crystals, namely anorthoclase, quartz, titanomagnetite, aegirine, cossyrite, riebeckite, olivine, tuhualite and ? hedenbergite. A similar mineral suite, which indicates the tephra is derived from an over-saturated, peralkaline magma, can be found as phenocrysts within the dull yellowish brown and reddish brown lapalli. Iron contained in the glasses has probably been oxidised by weathering processes intensified in the soil forming regime, giving the reddish brown colouration presently displayed by most of the lapilli. The local areas of dull yellowish brown lapilli have been leached of their iron under the influence of mor-forming vegetation associated with trees such as the kauri and rimu.

## B. FIELD CLASSES III, IV AND V (THE SILTY AND LUMPY BEDS, AND SHOWER-BEDDED CLASS)

### 1. Introduction

Field classes III to V contain calc-alkaline tephras whose sources lie to the south of the Coromandel Peninsula, as indicated by decreasing bed thicknesses northwards. The Silty and Lumpy beds are non-homogeneous, exhibiting properties that change systematically from the top of the Silty bed to the base of the Lumpy bed in response to varying contributions from mixtures of tephras. In comparison, the Shower-bedded class (class V) has uniform compositional properties, but variable particle size characteristics at any

particular site, indicating that this material was deposited during a continuous period of volcanism consisting of a number of discrete eruptions.

The following section examines some properties of field classes III to V as they vary with geographical location, in particular the particle size parameters of the coarser than 4 ∅ material, the ferromagnesian mineralogy, and the titanomagnetite chemistry.

## 2. Field relations

The properties of field classes III to V on the Peninsula, have been investigated using samples collected from Kopu (site 37), Whitianga (site 58), and Waiaro Bay (site 78) (Figs. 4.14 and 4.15).

At Kopu, the reddish brown lapilli of class II clearly delineate the boundary between classes II and III, a distinction not found at Whitianga where field work has been unable to recognise the fine-grained distal parts of the class I and II tephras (if present) separately from class III material. Also, at Waiaro Bay there is no clear separation between the Silty and Lumpy beds, but the thickness of the Silty bed at Whitianga suggests that it should be present. In the upper part of the Waiaro Bay 'A' horizon some coarse (less than 20 mm) pebbles are present indicating that colluvium has been added to the top of the tephra column. The Shower-bedded class is readily identified by its prominent shower-bedding at the Kopu and Whitianga sites, but is less well defined at Waiaro Bay because of the very fine grain size of the individual units.

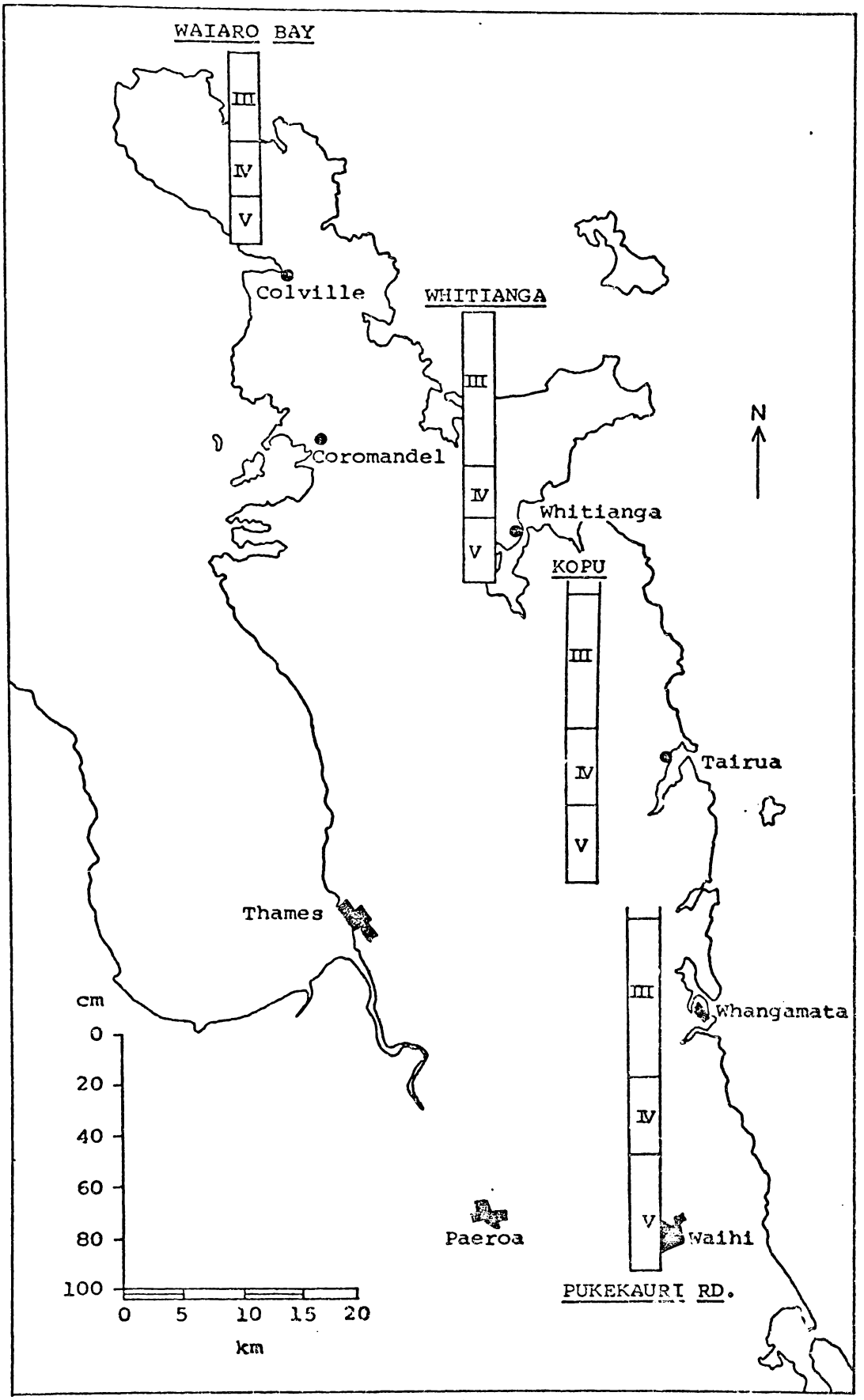


FIGURE 4.14 : Site locations and bed thicknesses of field classes III to V for the sites discussed in Chapter 4, section B. Field classes I and II may be present at the Whitianga site, but could not be distinguished by field examinations.

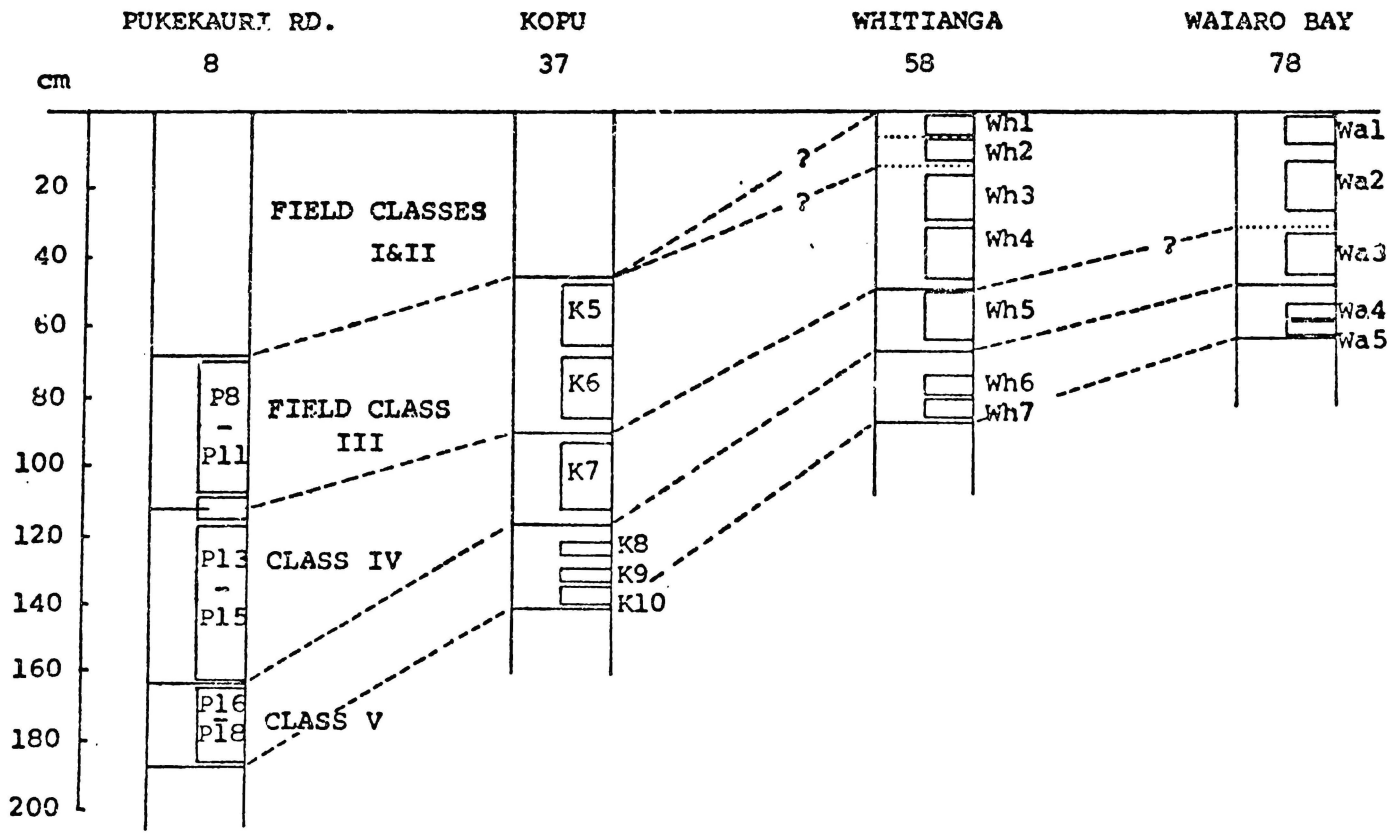


FIGURE 4.15 : Field class and sample locations for sites discussed in chapter 4, section B.

Note : Samples P17,K9,Wh6,Wa4 from field class V are hereafter known as the 'middle orange'unit. Samples P18,K10,Wh7,Wa5 from class V are hereafter known as the 'basal grey' unit.

## 3. Particle size distribution of the coarser than 4 ∅ fraction

Particle size data for nineteen samples from field classes III to V are given in Appendix E (Fig. E.9) and statistical parameters are summarised in Fig. 4.16 and Table 4.9.

TABLE 4.9 : Particle size parameters for field classes III to V at the Kopu, Whitianga, and Waiaro Bay sites (Coarser than 4 ∅).

| | Field class | Sample | Mz (∅) | ϑG (∅) |
|---|---|---|---|---|
| Site 37 (Kopu) | III | K5 | 2.95 | 0.69 |
| | | K6 | 2.87 | 0.73 |
| | IV | K7 | 2.72 | 0.73 |
| | | Kcmpf | 2.74 | 0.75 |
| | V | K8 | 3.24 | 0.48 |
| | | K9 | 2.98 | 0.46 |
| | | K10 | 2.82 | 0.58 |
| Site 58 (Whitianga) | ? | Wh1 | 3.06 | 0.53 |
| | III | Wh2 | 2.97 | 0.56 |
| | | Wh3 | 3.01 | 0.57 |
| | | Wh4 | 2.98 | 0.58 |
| | IV | Wh5 | 2.95 | 0.57 |
| | V | Wh6 | 3.25 | 0.38 |
| | | Wh7 | 3.07 | 0.47 |
| Site 78 (Waiaro Bay) | ? | Wa1 | 2.75 | 1.02 |
| | | Wa2 | 3.01 | 0.57 |
| | IV | Wa3 | 3.07 | 0.54 |
| | V | Wa4 | 3.42 | 0.38 |
| | | Wa5 | 3.34 | 0.44 |

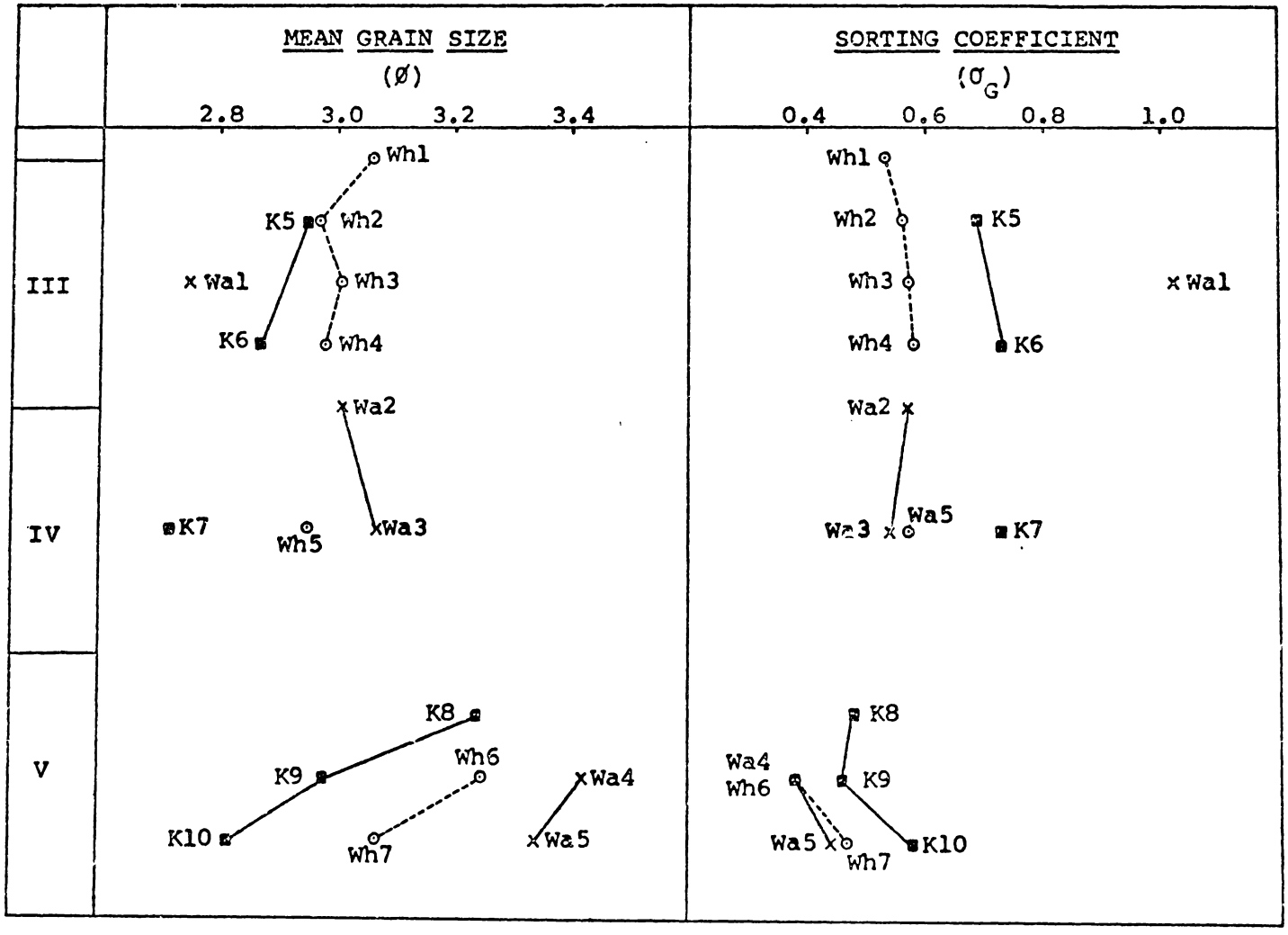


FIGURE 4.16 : Mean grain size and sorting coefficient for samples from field classes III to V from the Kopu, Whitianga and Waiaro Bay sites. Particle size parameters are from the coarser than 4Ø fraction. Data from Appendix E (Fig. E.9).

At the Kopu site the mean grain size coarsens and the sorting deteriorates with depth from the upper part of the Silty bed (K5) to the Lumpy bed (K7) before becoming finer in the basal, well sorted, Shower-bedded class. The particle size parameters of "creampuffs" from the Lumpy bed are very similar to those in the surrounding matrix deposit (sample Kcmpf in Table 4.9). The Whitianga site also exhibits a progressive coarsening from the topsoil (Wh1) to the Lumpy bed (Wh5). The data are not sufficiently sensitive to indicate which field class Wh 1 and Wh2 belong to (i.e. classes I, II or III). The topsoil at Waiaro Bay (Wa1) has a poorly sorted bimodal particle size distribution, and a coarse mean grain size, explained by the addition of colluvial material. At the Kopu and Whitianga sites, the lowest sample from class III (K6) has a finer mean grain size than the underlying class IV sample (K7). This trend is discontinued at the Waiaro Bay site with Wa2 being coarser than Wa3, thus suggesting that Wa2 possibly belongs to class IV rather than to class III (as is shown on Figs. 4.14 and 4.15).

The mean grain size and sorting coefficients for samples from field classes III to V are plotted against distance from the Pukekauri Rd site in Figs. 4.17 and 4.18. For each of the field classes the mean grain size and sorting coefficient changes in a systematic manner from Pukekauri Rd northwards to Waiaro Bay with the samples becoming progressively finer and better sorted up the Peninsula, indicative of sources to the south.

FIGURE 4.17 : Variation in the mean grain size of the coarser than 4 Ø fraction of field classes III to V with distance north of Pukekauri Rd.

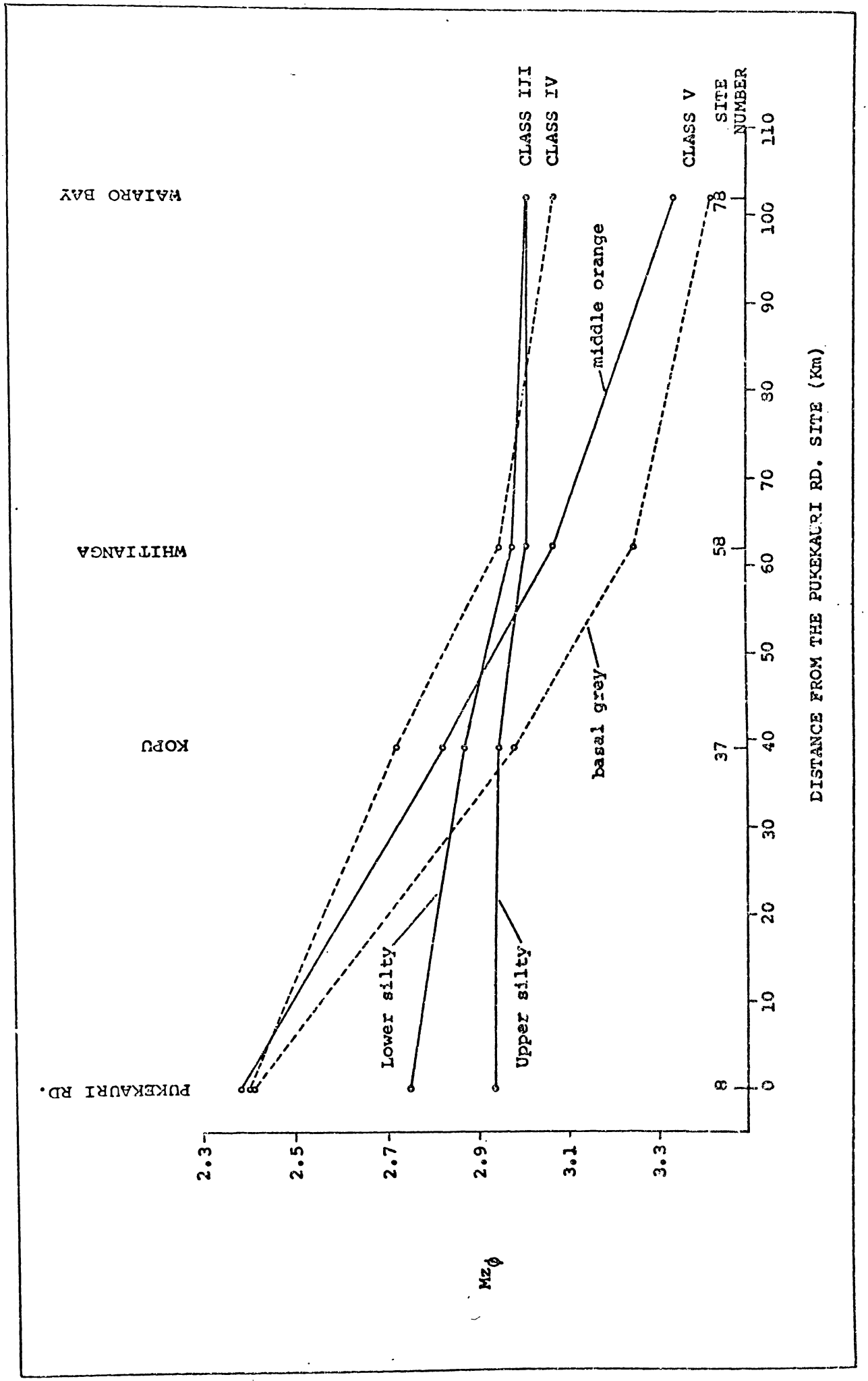
PUKEKAURI RD.
KOPU
WHITIANGA
WAIARO BAY
Lower silty
Upper silty
basal grey
middle orange
CLASS III
CLASS IV
CLASS V
SITE NUMBER
8
37
58
78
0
10
20
30
40
50
60
70
80
90
100
110
DISTANCE FROM THE PUKEKAURI RD. SITE (Km)
Mz ϕ
2.3
2.5
2.7
2.9
3.1
3.3

FIGURE 4.18 : Variation in the sorting coefficient of the coarser than 4 Ø fraction of field classes III to V with distance north of Pukekauri Rd.

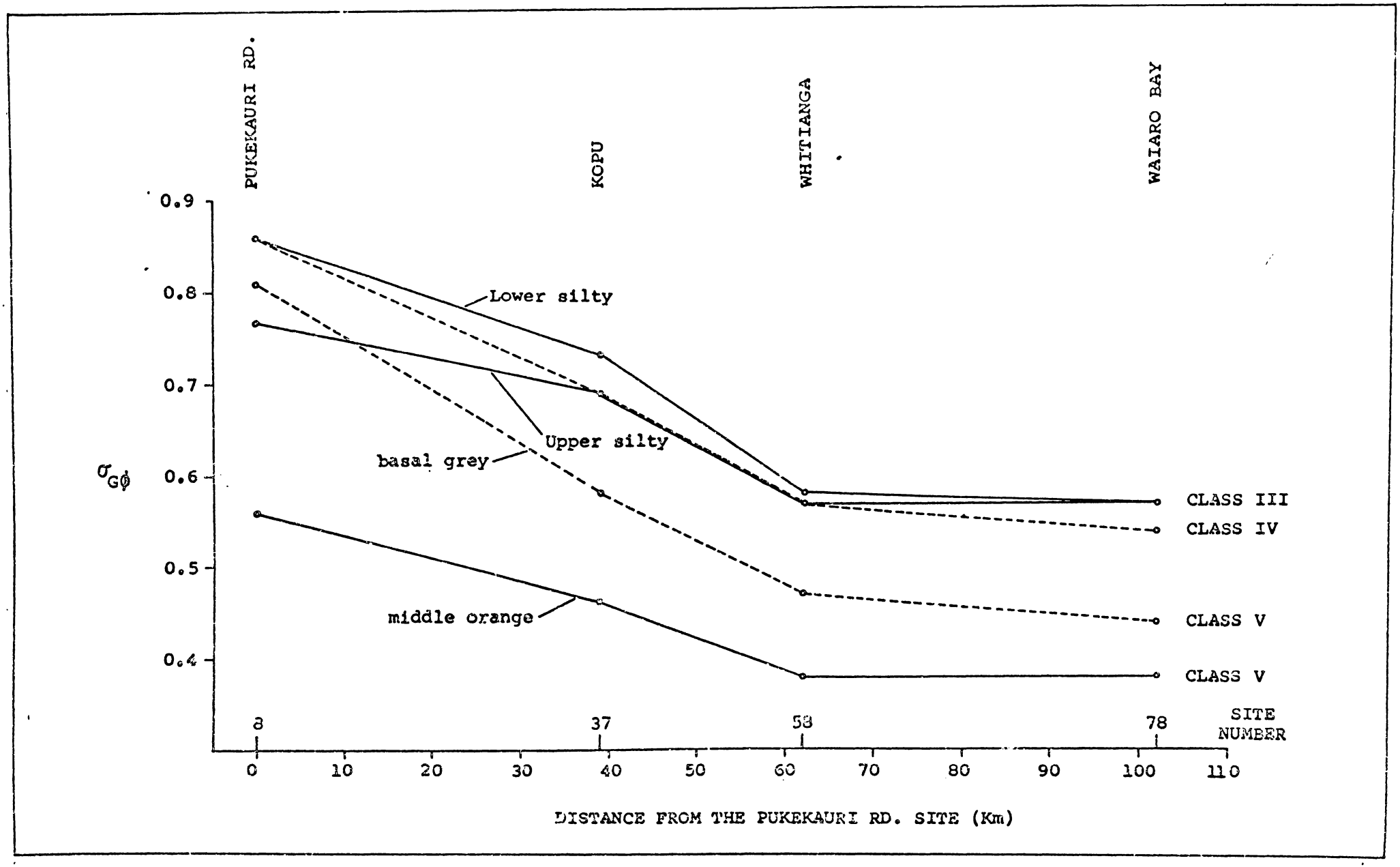
PUKEKAURI RD.
KOPU
WHITIANGA
WAIARO BAY
0.9
0.8
0.7
0.6
0.5
0.4
$\sigma_{G\phi}$
Lower silty
Upper silty
basal grey
middle orange
CLASS III
CLASS IV
CLASS V
CLASS V
8
37
58
78
SITE NUMBER
0
10
20
30
40
50
60
70
80
90
100
110
DISTANCE FROM THE PUKEKAURI RD. SITE (Km)

4. Ferromagnesian mineralogy

The 2-4 ϕ fractions of the Kopu, Whitianga and Waiaro Bay samples are calc-alkaline in composition and dominated by cummingtonite, hypersthene and hornblende, with minor augite (Table 4.10 and Fig. 4.19).

Data from the Kopu site allow a three-fold subdivision into low, medium and high cummingtonite, corresponding with field classes III, IV and V respectively. The hypersthene/amphibole ratio declines progressively from the top of the Silty bed (K5) into the Lumpy bed (K7), with the amount of cummingtonite increasing substantially from around 50% to over 70%. The ferromagnesian mineral assemblage of the creampuffs which were collected from the Lumpy bed at Kopu (Kcmpf in Table 4.10) is significantly different from the surrounding matrix and mineralogically is more like the underlying Shower-bedded class.

At Whitianga the hypersthene/amphibole ratio also decreases steadily throughout classes III and IV (Wh2 to Wh5), reflecting an increasing cummingtonite and decreasing hypersthene and hornblende content with depth. The A horizon at Whitianga does not conform to this pattern which suggests that it may contain the distal remnants of field class I and/or II tephras, and should therefore be assigned class I/II status.

The very high proportion of cummingtonite in the Waiaro Bay topsoil (Wa1), considered to be partly colluvial from its particle size characteristics, indicates that the finer fraction of the sample (finer than 1.5 ϕ) is totally composed of tephric material similar to the sample below, into which a coarse fraction has been

TABLE 4.10 : The ferromagnesian mineral assemblages of field classes III to V at the Kopu, Whitianga and Waiaro Bay sites (2–4 ∅ fraction).

| | Field class | Sample | hypers-thene (%) | cumming-tonite (%) | horn-blende (%) | augite (%) | hypersthene / amphibole |
|---|---|---|---|---|---|---|---|
| Site 37 (Kopu) | III | K5 | 41 | 43 | 13 | 3 | 0.73 |
| | | K6 | 38 | 52 | 8 | 2 | 0.66 |
| | IV | K7 | 21 | 72 | 7 | - | 0.27 |
| | | Kcmpf | 11 | 85 | 4 | - | 0.12 |
| | V | K8 | 7 | 88 | 5 | - | 0.08 |
| | | K9 | 7 | 91 | 2 | - | 0.07 |
| | | K10 | 11 | 87 | 2 | - | 0.12 |
| Site 58 (Whitianga) | ?I/II | Wh1 | 32 | 44 | 19 | 5 | 0.51 |
| | III | Wh2 | 35 | 44 | 16 | 5 | 0.59 |
| | | Wh3 | 34 | 49 | 15 | 2 | 0.52 |
| | | Wh4 | 25 | 62 | 12 | 1 | 0.33 |
| | IV | Wh5 | 25 | 66 | 9 | - | 0.33 |
| | V | Wh6 | 8 | 88 | 4 | - | 0.09 |
| | | Wh7 | 9 | 88 | 3 | - | 0.10 |
| Site 78 (Waiaro Bay) | ?III | Wa1 | 11 | 82 | 7 | - | 0.13 |
| | IV | Wa2 | 13 | 81 | 6 | - | 0.15 |
| | | Wa3 | 14 | 81 | 5 | - | 0.16 |
| | V | Wa4 | 11 | 86 | 3 | - | 0.12 |
| | | Wa5 | 11 | 84 | 5 | - | 0.13 |

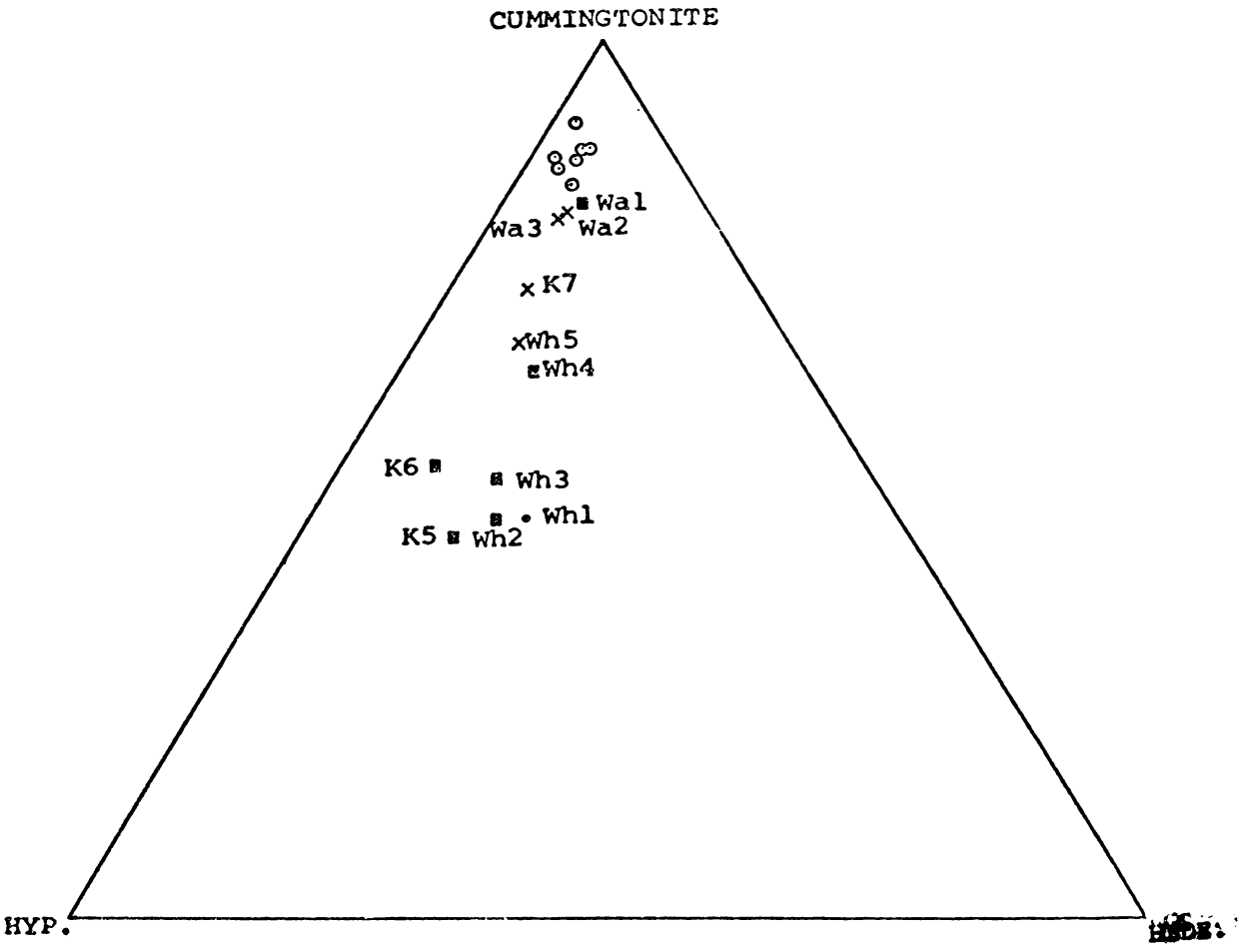


- Field class III
- x Field class IV
- o Field class V

FIGURE 4.19 : The ferromagnesian mineral assemblages of field classes III to V at Kopu, Whitianga and Waiaro Bay.(2-4Ø fraction). Sample Wh1 is thought to be an intermediate sample and is therefore not included in classes III to V.

incorporated. Although field classes IV and V can be identified at Waiaro Bay and the distribution pattern indicates that class III should also be present, the ferromagnesian mineral assemblages for all the Waiaro Bay samples are similar and contain over 80% cummingtonite, with the hypersthene characteristic of classes III and IV being absent. As the Waiaro Bay column appears too thick to represent field class V only and the colluvial addition to the topsoil has been confined to coarse material, it is likely that field classes III and IV are present but characterised by significantly different ferromagnesian mineral assemblages. This sudden decrease in the hypersthene/cummingtonite ratio of classes III and IV at Waiaro Bay (Fig. 4.21), probably indicates a significant change in the number of tephras comprising these classes as the deposits have thinned north of Whitianga.

The weight percentage of heavy minerals in the 2-4 $\phi$ fraction of classes III to V is plotted against geographical location on the Peninsula in Fig. 4.20. The general trend is a progressive decrease in the content of heavy minerals on moving north up the Peninsula, shown particularly by the samples from the Lumpy bed and Shower-bedded class. The tendency for the proportion of heavy minerals to decrease away from the source is typical of tephras (Eaton 1964; Williams and McBurney 1969), but is not demonstrated by the Silty bed which increases slightly in its heavy mineral content between Pukekauri Rd and Whitianga, before decreasing in a more usual manner north of Whitianga. This once again supports the contention that the Silty bed is composed of two main tephras, one tephra being poor in heavy minerals and losing influence between Pukekauri Rd and Whitianga, and the other tephra comparatively rich in heavy

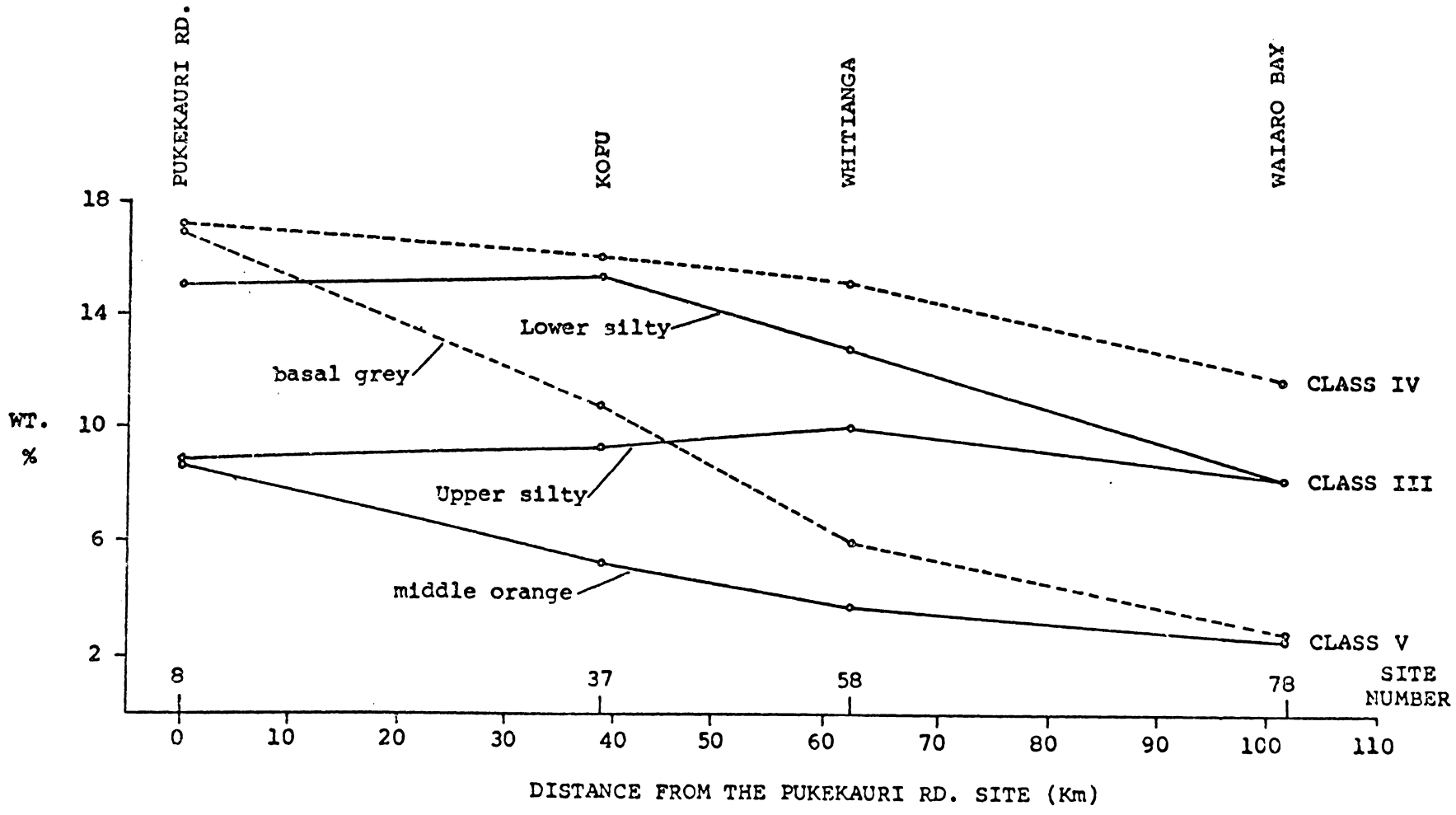


FIGURE 4.20: Change in the percentage of Heavy Minerals in the 2-4ϕ fraction of field classes III - V with distance north of Pukekauri Rd.

minerals, so that it increases in importance in this region. The heavy mineral content repeats the common tendency for properties to change in a gradational manner between field classes III and IV at all sites shown on Fig. 4.20, with the samples from the upper part of the Silty bed having comparatively low heavy mineral contents and the Lumpy bed showing higher values.

The hypersthene/amphibole ratios, when plotted against distance up the Peninsula (Fig. 4.21), are constant in class V and decrease in classes III and IV. The irregular trend shown by class IV in Fig. 4.21, is probably related to the varying concentration of creampuffs in the Lumpy bed, with cummingtonite being in higher proportion when the site is rich in creampuffs (as at Kopu, K7). From the examination of the ferromagnesian assemblages of the Silty bed at Kopu, Whitianga and Waiaro Bay it is apparent that the two tephras constituting the Silty bed have the following characteristics:

(i) a heavy mineral - poor tephra containing hypersthene and hornblende, which progressively loses its influence northwards;

(ii) a tephra comparatively rich in heavy minerals, with a ferromagnesian assemblage dominated by cummingtonite which becomes increasingly influential in the northern parts of the Peninsula.

5. Titanomagnetite chemistry

The third technique used to study the lateral variations of field classes III to V is the composition of the titanomagnetites, summarised in Fig. 4.22. The two pairs of class III samples from

FIGURE 4.21 : Change in the hypersthene/amphibole ratio in field classes III to V with distance north of Pukekauri Rd.

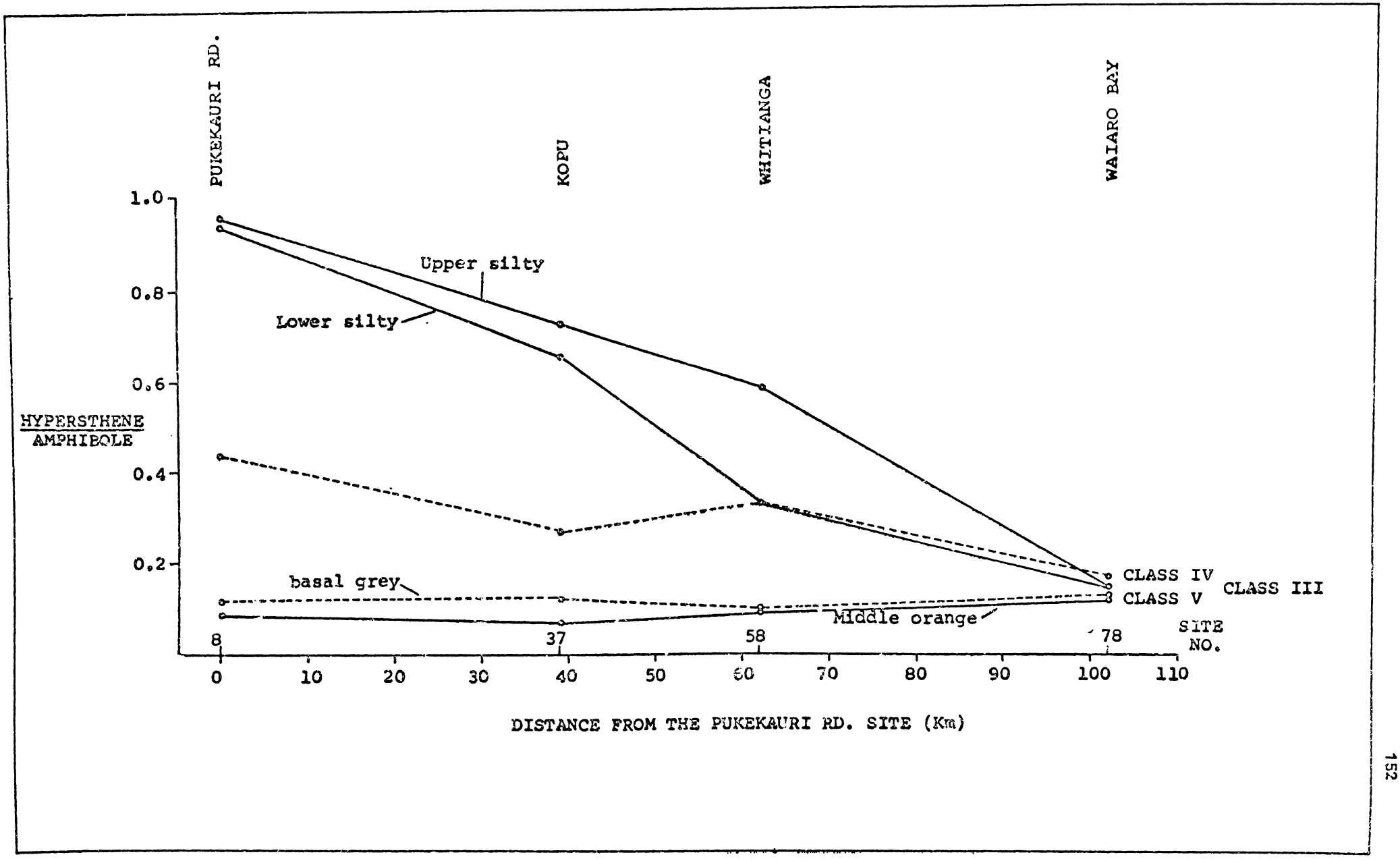
PUKEKAURI RD.
KOPU
WHITIANGA
WAIARO BAY
1.0
0.8
0.6
0.4
0.2
HYPERSTHENE
AMPHIBOLE
Upper silty
Lower silty
basal grey
Middle orange
CLASS IV
CLASS V
CLASS III
8
37
58
78
SITE
NO.
0
10
20
30
40
50
60
70
80
90
100
110
DISTANCE FROM THE PUKEKAURI RD. SITE (Km)

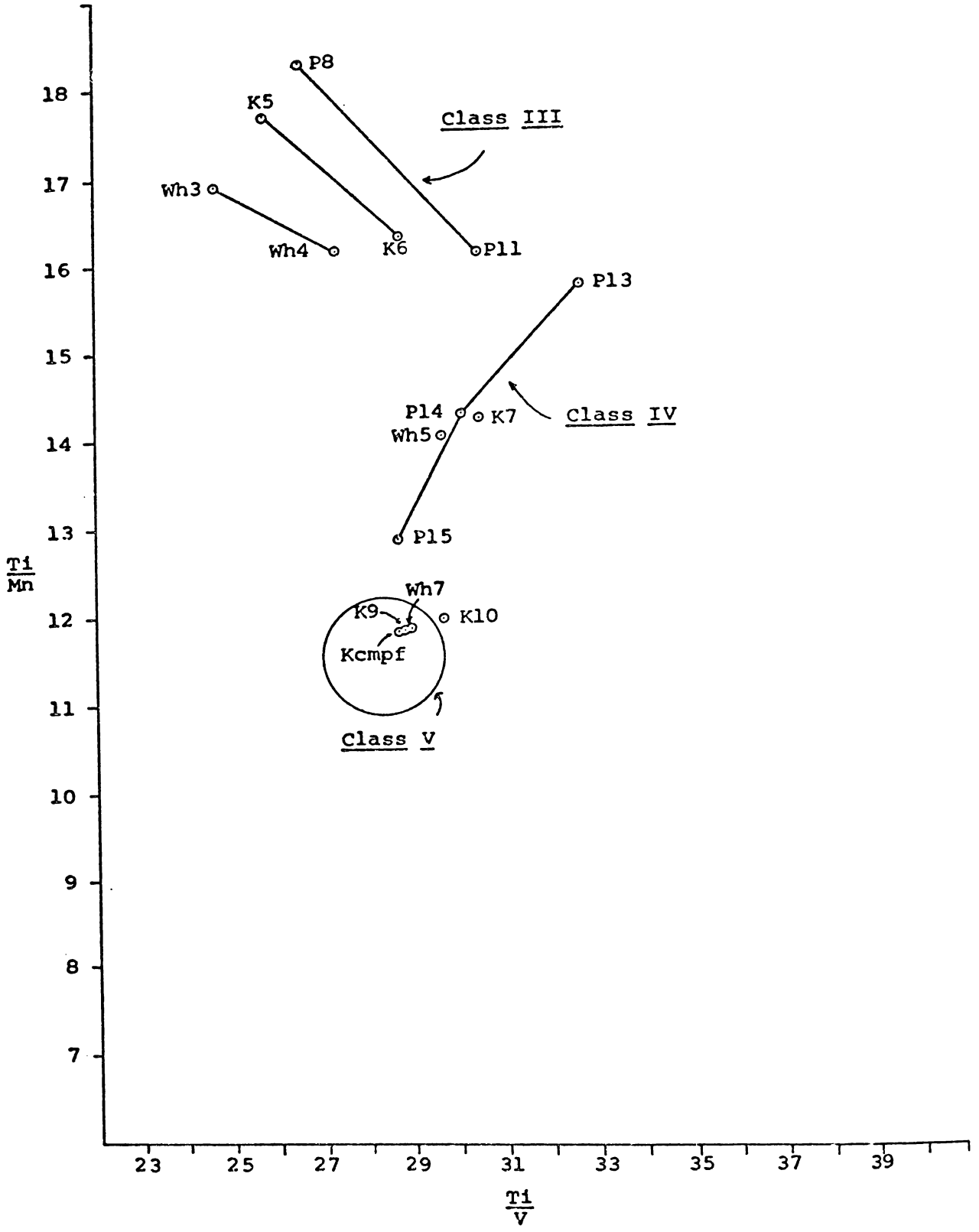


FIGURE 4.22 : Ratios of count rates of Ti, Mn and V from titanomagnetites extracted from the Holocene and Late Pleistocene tephras on the Coromandel Peninsula. Samples are from : Pukekauri Rd (P8,P11,P13,P14,P15); Kopu (K5, K6,K7,K9,KCmpf,K10); and Whitianga (Wh3,Wh4,Wh5,Wh7).

Kopu and Whitianga exhibit a similar pattern to that at the Pukekauri Rd site, with the upper half of the deposit having a higher Ti/Mn ratio and lower Ti/V ratio than the lower half. The displacement of the class III samples towards lower Ti/Mn and Ti/V ratios with increasing distance north of Pukekauri Rd reinforces the hypothesis that class III contains tephras whose contributions vary up the Peninsula.

The field class IV and V analyses do not vary significantly between Pukekauri Rd and Whitianga, indicating that the tephra or tephras composing each field class maintain their individual contributions at least as far north as Whitianga. The creampuffs extracted from the Kopu Lumpy bed (sample K7) have titanomagnetite compositions identical with those of field class V, and are considerably different from the matrix which surrounds them (matrix represented in Fig. 4.22 by K7).

## 6. Discussion

The non-bedded sandy loams and shower-bedded sands of class V at Pukekauri Rd can be traced for more than 100 km up the Peninsula and show both a variation in thickness from more than 40 cm in the south to less than 20 cm in the north and also a decreasing mean grain size, indicating that the source of the tephra lies to the south of the region. The cummingtonite-bearing ferromagnesian mineral assemblage and the titanomagnetite compositions show little variation either between the individual units constituting the zone of shower-bedding or between the sites at the extreme ends of the Peninsula, indicating the field class V is comprised of a single tephra only.

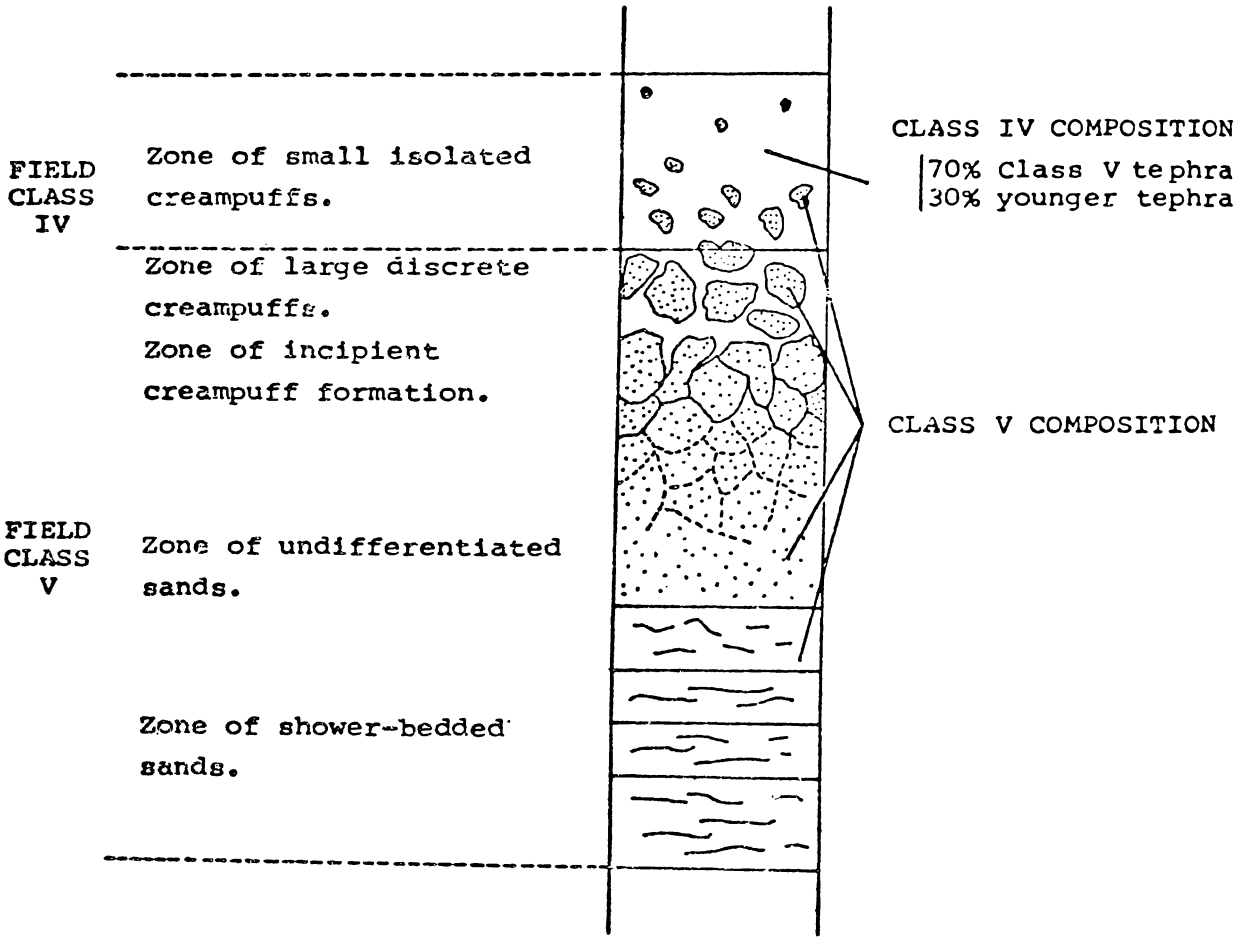


FIGURE 4.23 : Relationship between the compositions of the creampuffs and matrix of field class IV and the composition of field class V.
Zones of field class V as shown on Fig. 2.13 p.36.

Field class IV has properties which vary more from site to site, particularly its particle size characteristics, ferromagnesian mineralogy and to a lesser extent, titanomagnetite chemistry. All these variations are probably related to the concentration of creampuffs in the Lumpy bed. It was suggested in Chapter 2 (p.38) that the creampuffs in class IV represent subspherical remnants of primary material of class V not altered by weathering processes that have operated in the past. This suggestion is supported by the titanomagnetite chemistry and ferromagnesian mineralogy of the creampuffs, which demonstrates they have similar compositions to the underlying Shower-bedded class. The titanomagnetite grain compositions indicate that the matrix of field class IV contains two tephras (Fig. 3.17 p. 89), with the main tephra occupying approximately 70% of the class. The high cummingtonite content of class IV identifies this tephra as that contained within field class V below, which has been diluted by small amounts (approximately 30%) of a hypersthene and hornblende-bearing tephra. Fig. 4.23 summarises the relationship between the compositions of the creampuffs and matrix of class IV and the composition of class V.

Data from the Pukekauri Rd, Kopu and Whitianga sites indicate that there is a relationship between field classes III and IV, with such parameters as the mean grain size, hypersthene/amphibole ratio and percentage of heavy minerals varying systematically from the top of the Silty bed to the Lumpy bed beneath (Fig. 4.24). It was concluded in Chapter 3 (p.96) that field class III consists of a mixture of two tephras, a younger, fine-grained one which is rich in glass, hypersthene and hornblende and an older tephra which is comparatively coarse-grained and contains quartz, feldspar and

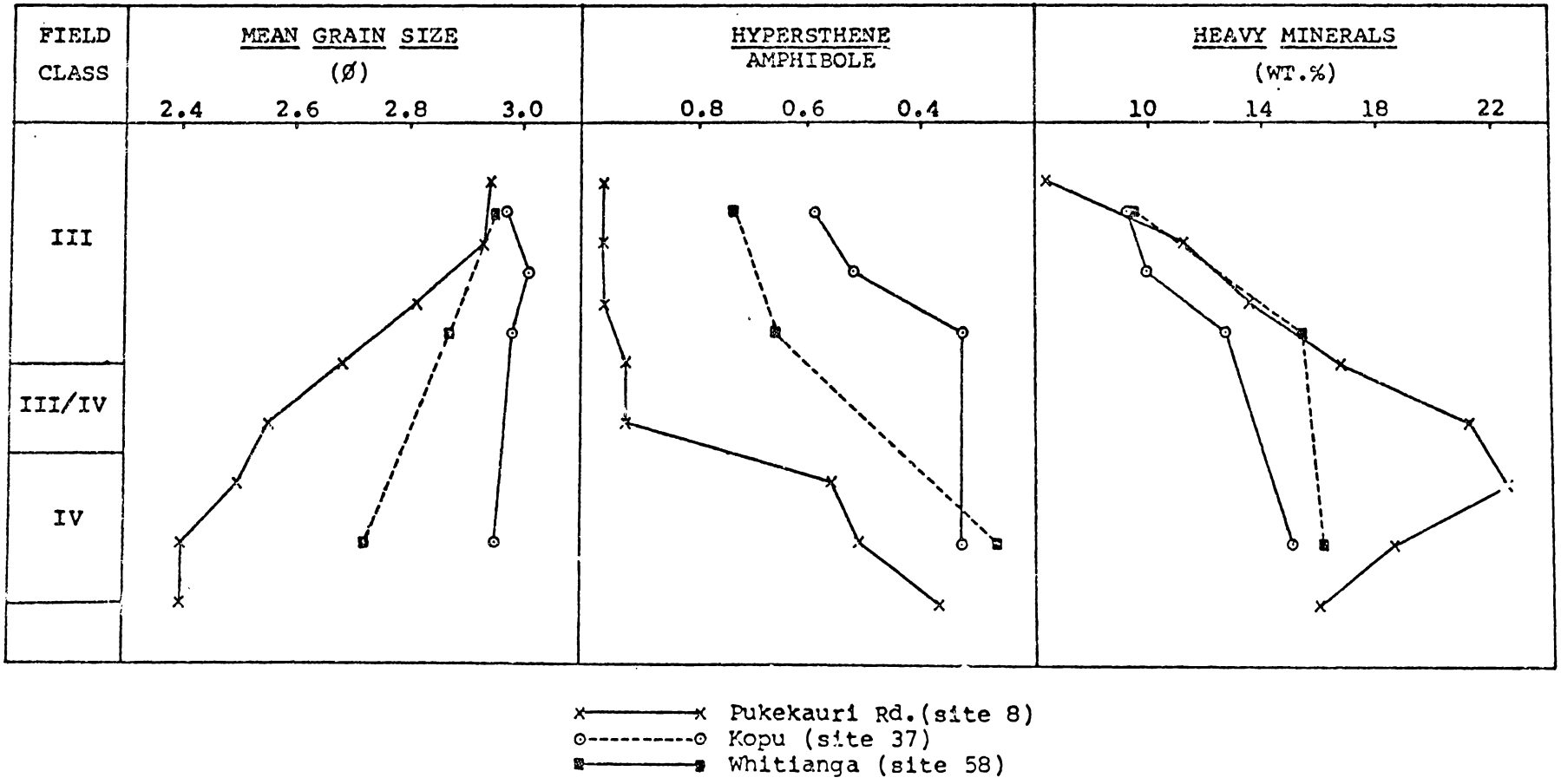


FIGURE 4.24 : Three examples of parameters varying systematically from the top of field class III to the top of field class IV. All parameters are based upon the coarser than 4Ø fraction.

cummingtonite. It is proposed that the systematic variations between field classes III and IV noted above, are the result of mixing of these tephras.

A model attempting to explain the origin of field classes III to V and their inter-relationships is outlined in Fig. 4.25. The oldest of the field classes studied (class V) - Fig. 4.25 (a), resulted from a series of closely related eruptions and formed a prominent shower-bedded tephra. Individual eruptive layers have variable mean grain sizes but exhibit uniformity in their ferromagnesian mineral assemblages and titanomagnetite compositions. Under the influence of the paleo-soil regime, weathering of the sands resulted in the formation of creampuffs of sand texture in a sandy loam matrix; both creampuffs and matrix had a similar mineral composition and were characterised by cummingtonite.

After some time interval, class V was buried by a thin, comparatively fine-grained deposit (Tephra A in Fig. 4.25(a)), with a hypersthene plus hornblende ferromagnesian mineral assemblage. Subaerial mixing processes, effective where tephras are relatively thin, fine-grained, and exposed to soil forming processes for a few thousand years, resulted from the activities of flora and fauna or of climatic phenomena. These processes operated most efficiently between Tephra A and the upper part of class V to eventually form a mixed tephra deposit, class IV, whose matrix had properties grading into the class V tephra beneath (Fig. 4.25(b)). The titanomagnetites from class IV show a range in composition dependent upon the relative influences of each of the two mixed tephras, as explained in Chapter 3 (Fig. 3.13 p.81). While a remnant of pure class V tephra

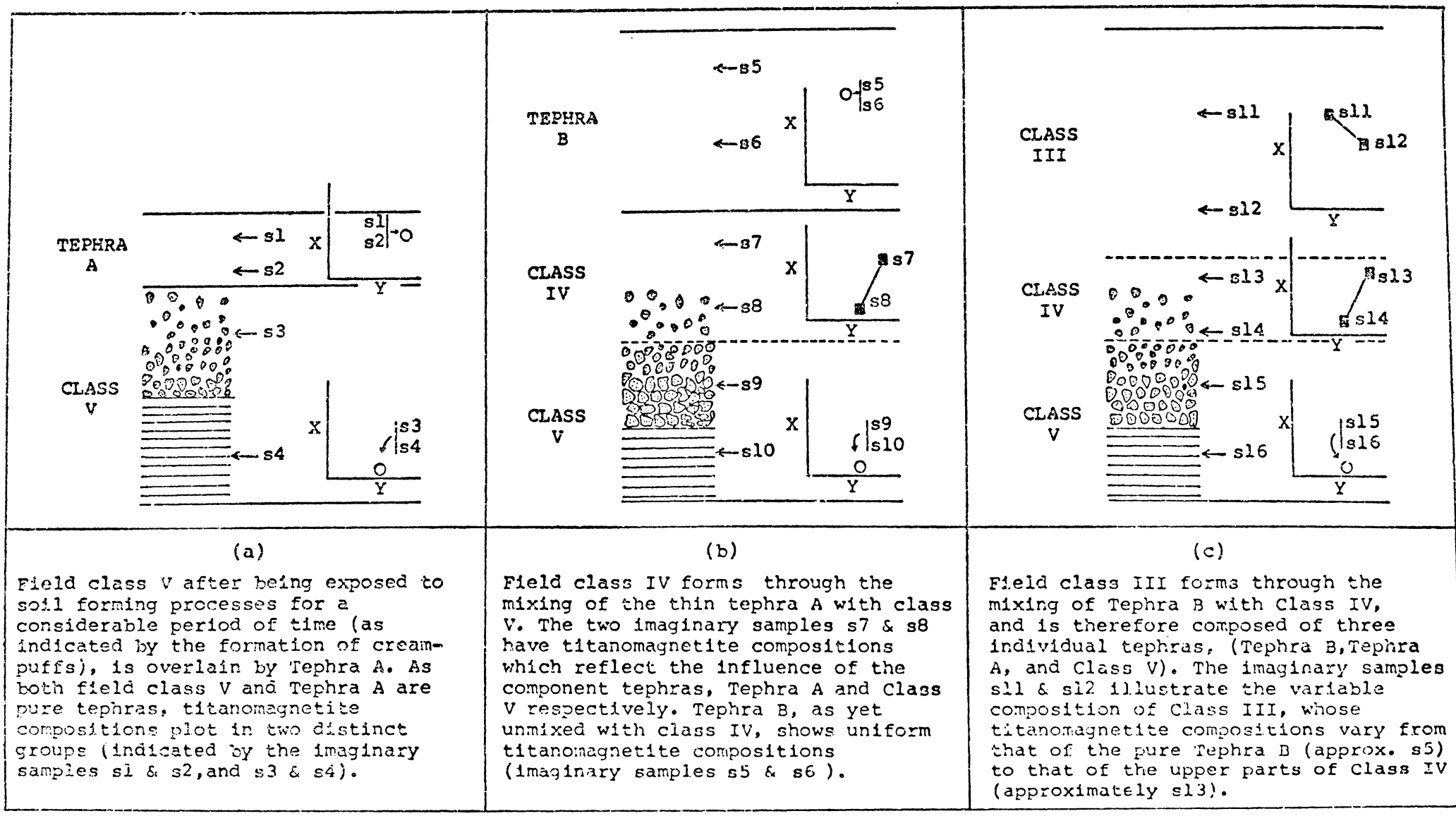


(a)

Field class V after being exposed to soil forming processes for a considerable period of time (as indicated by the formation of cream-puffs), is overlain by Tephra A. As both field class V and Tephra A are pure tephras, titanomagnetite compositions plot in two distinct groups (indicated by the imaginary samples s1 & s2, and s3 & s4).

(b)

Field class IV forms through the mixing of the thin tephra A with class V. The two imaginary samples s7 & s8 have titanomagnetite compositions which reflect the influence of the component tephras, Tephra A and Class V respectively. Tephra B, as yet unmixed with class IV, shows uniform titanomagnetite compositions (imaginary samples s5 & s6 ).

(c)

Field class III forms through the mixing of Tephra B with Class IV, and is therefore composed of three individual tephras, (Tephra B, Tephra A, and Class V). The imaginary samples s11 & s12 illustrate the variable composition of Class III, whose titanomagnetite compositions vary from that of the pure Tephra B (approx. s5) to that of the upper parts of Class IV (approximately s13).

FIGURE 4.25 : Proposed model of tephra deposition and subsequent modification for the tephras comprising field classes III to V. The X/Y graphs shown above represent estimated titanomagnetite compositions for imaginary samples denoted by an arrow ; Y = Ti/Mn , X = Ti/V.

has been preserved because of its thickness, Tephra A has been completely incorporated into the mixed class IV deposit.

After a further time interval, a second tephra (Tephra B) was deposited upon class IV and mixed with the upper part of the deposit to form field class III (Fig. 4.25(c)). Class III therefore has properties which vary systematically from its upper part (which is more like Tephra B) to class IV below, as exemplified by its coarsening mean grain size and increasing cummingtonite content with depth.

In Fig. 4.26 the composition of the ferromagnesian mineral assemblages of Tephras A and B have been calculated. The approximate composition of Tephra A can be calculated knowing the approximate relative proportions of the two tephras comprising field class IV (from titanomagnetite grain compositions) i.e. 70% class V and 30% Tephra A, and the composition of the resulting mixed deposit (class IV). Similarly the composition of Tephra B can be calculated knowing the approximate proportions of field class IV with which it combines to form field class III.

According to this model of tephra deposition and modification, field classes III to V should be comprised of three tephras only:

Field class III
- (i) Tephra B (equals Tephra E in Fig. 3.18 p.96 )
- (ii) Tephra A
- (iii) Class V tephra (equals Tephra D in Fig. 3.18).

Field class IV
- (ii) Tephra A (equals Tephra C in Fig. 3.18)
- (iii) Class V tephra (equals Tephra B in Fig. 3.18).

Field class V
- (iii) Class V tephra (equals Tephra A in Fig. 3.18).

The compositions of titanomagnetite grains for field classes III to V

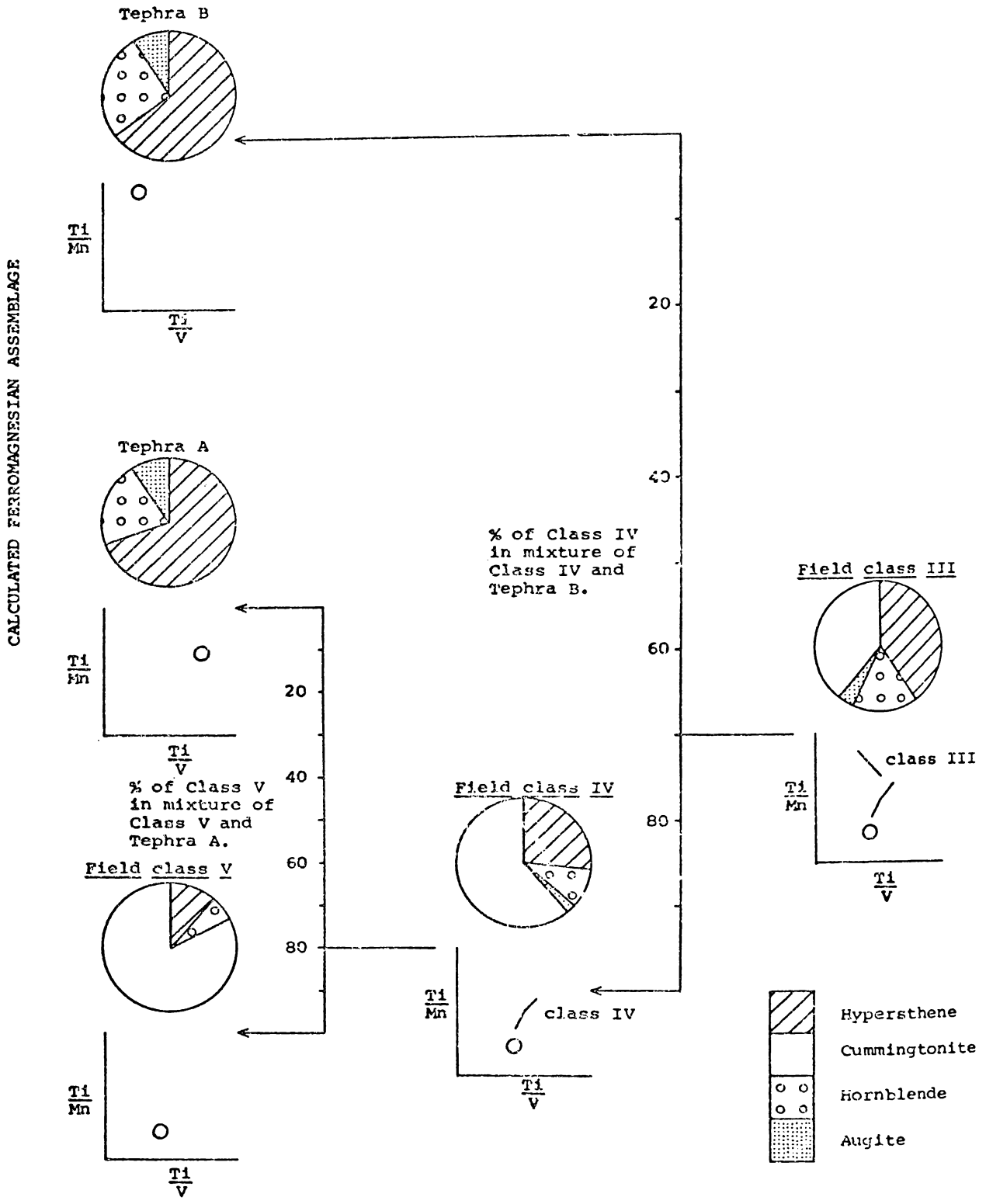


FIGURE 4.26 : Ferromagnesian mineralogy and titanomagnetite compositions for field classes III to V, and calculated characteristics of component tephras A and B. For further explanation see text.

support this model by demonstrating the presence of three separate tephras in these field classes (Fig. 4.27).

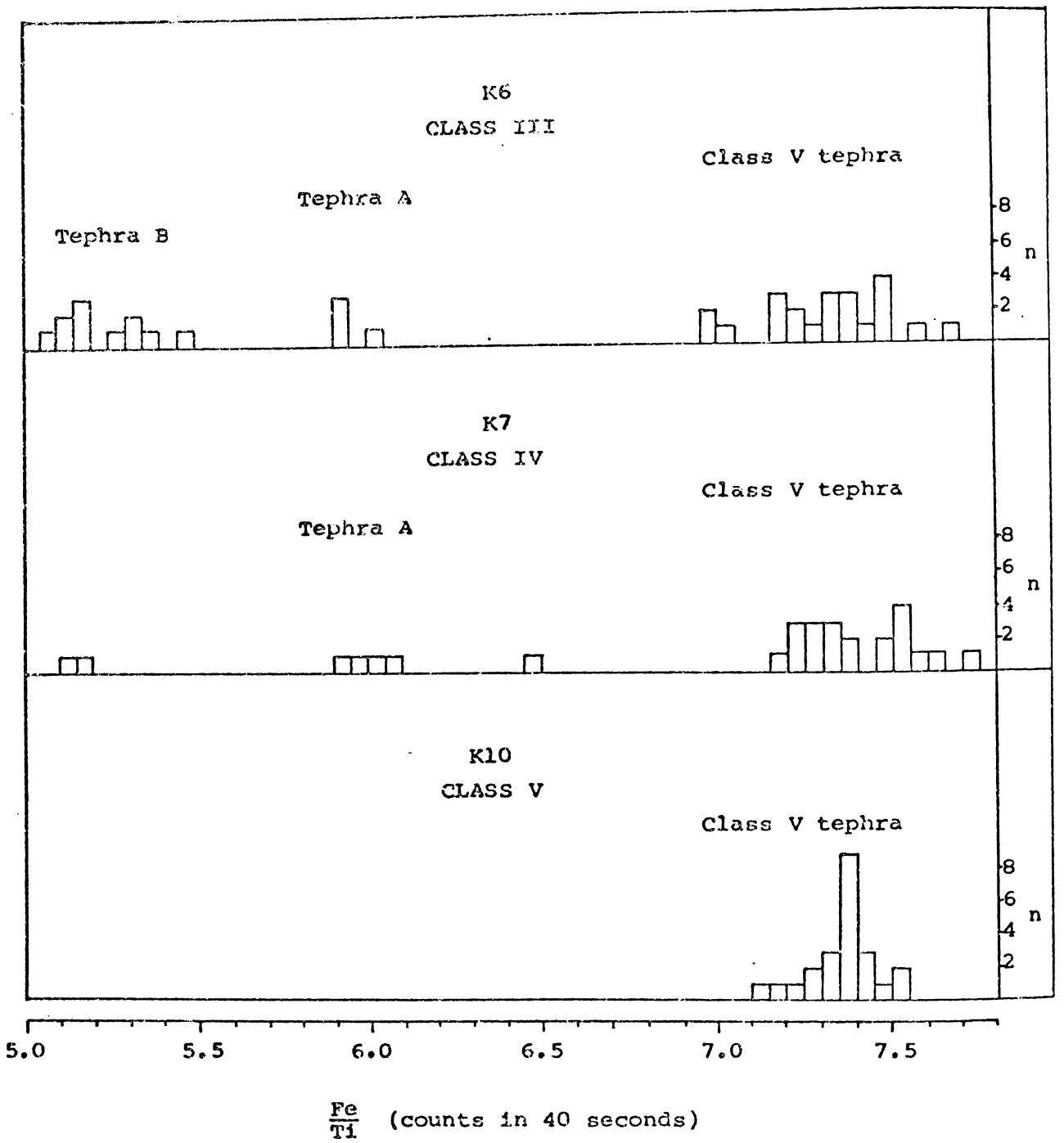


FIGURE 4.27 : Range in Fe/Ti ratios for titanomagnetites extracted from the Coromandel tephras at the Kopu site. Field classes III to V shown above contain three tephras which correspond to Tephra B, Tephra A, and the Class V tephra outlined in the model of tephra deposition and modification.

# CHAPTER 5

# CORRELATION AND IDENTIFICATION OF THE COROMANDEL TEPHRAS

## INTRODUCTION

In Chapters 3 and 4 the properties of the Holocene and Late Pleistocene tephra cover of the Coromandel Peninsula were examined to determine the number of tephras characterising the five field classes, and the stratigraphic relationships and geographical distribution of these tephras on the Peninsula. This chapter deals with their correlation with known deposits in the Bay of Plenty region. This correlation is hampered by both the composite nature of field classes I to IV and the lack of an established stratigraphic column for the Holocene tephras in the northern Bay of Plenty.

The stratigraphy of the Late Pleistocene tephra cover in the Bay of Plenty has been recently established in some detail by Howorth (1976). The Holocene stratigraphy of the region is far less reliable with the nearest useful stratigraphic column occurring at Tikitere Hill, 85 km south of Pukekauri Rd (Vucetich and Pullar 1964). This column has been constructed entirely by field mapping techniques, and lacks the detail provided by an associated laboratory examination and may contain tephras not visible in the field.

Identification of the component tephras within the field classes of the Coromandel Peninsula has been deduced in three ways:

(A) Examination of a peat core record of the depositional history of the Holocene tephras.

(B) Construction of a composite stratigraphic column of known tephras in the Te Puke region.

(C) Correlation of the unknown tephras from the Coromandel Peninsula with those comprising the Te Puke column.

## (A) HOLOCENE TEPHRA DEPOSITS AS IDENTIFIED WITHIN THE HAURAKI PEAT BOG

Interpretation of the Holocene tephra stratigraphy on a dry land surface is obscured by biological mixing in the active region of the soil, particularly where deposits are shallow and distant from their sources. However, their stratigraphy may be obtained from peat swamps where individual tephras are separated by layers of organic matter deposited in the intervals between eruptions, and their ages can be established by radio-carbon dating (e.g. Rigg and Gould 1957; Nasmith et al. 1967).

Using an "Aberdeen" type peat sampler (Jowsey 1966), a continuous peat core 10 m long was extracted from a site approximately 1 km from the Elstow canal on the oligotrophic, high moor swamp of the Hauraki Plains (Fig. 5.1). The swamp covers approximately 240 $km^2$ and reaches depths of up to 11 m (Davoren 1978). A peat sample collected at the base of the peat column was dated by the Radio-carbon Laboratory, University of Waikato, at 9360 years ($\theta$ = 100), which supplies a maximum age of the swamp at this site. The core revealed three visible tephras; a white, "sugar-like"

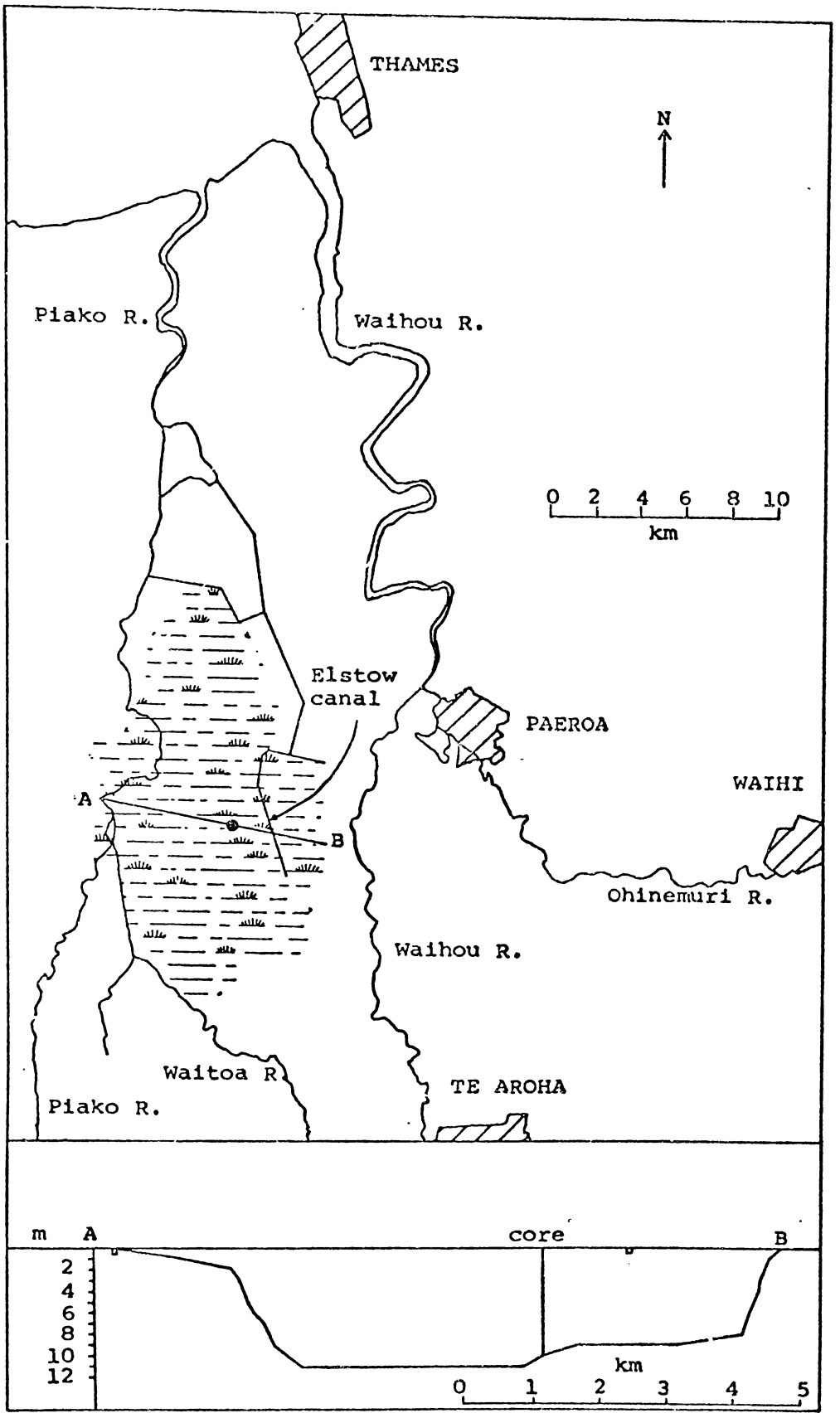


FIGURE 5.1 : Hauraki Peat Bog, Hauraki Plains. The profile of the bog is shown along the section A-B, with the depth contours from Davoren (1978). The section is based upon a horizontal surface, though in reality, doming is considerable. The core site is shown as a black circle on the section A-B above.

deposit interspersed with peat between 1.3-1.7 m deep, a 20 cm layer of white pumiceous ash and lapilli at 2.2-2.4 m depth, and a brown coloured tephra of normally graded ash and lapilli averaging 10 cm in thickness at a depth of 5.9-6.0 m (Fig. 5.2).

A more thorough investigation of the peat core was made by slicing the air-dried core into sections 4 cm long and analysing the crushed material by XRF for K, Si and Fe, since these elements gave the highest count rates when analysing mineral-rich sections (Fig. 5.3). The elemental count rates, particularly the K and Si contents, indicate nine concentrations of inorganic material within the core (numbered "a" to "i" in Fig. 5.3). Three of the layers are clearly tephras, identified by their relatively coarse grain sizes (deposits a, b and e on Fig. 5.3), and a fourth (layer c) may be a tephra as it contains a sizable heavy mineral fraction. The remaining layers (d, f, g, h and i in Fig. 5.3) in comparison with the tephras, have extremely fine grain sizes, no heavy mineral fraction and are dominated by volcanic glass, suggesting that they represent over-bank silt deposits from the nearby Waitoa or Waihou rivers. A stratigraphic column incorporating these new data is shown in Fig. 5.4.

Mineralogical data on the tephras contained within the core are presented in Tables 5.1 and 5.2. Layer "a" (the "sugar-like" tephra) is characterised by a high crystalline content, with quartz and plagioclase constituting nearly 70 modal percent and a ferromagnesian mineral assemblage containing hypersthene and hornblende. The white, pumiceous ash and lapilli (layer b) contains a higher percentage of glass and heavy minerals with quartz and plagioclase

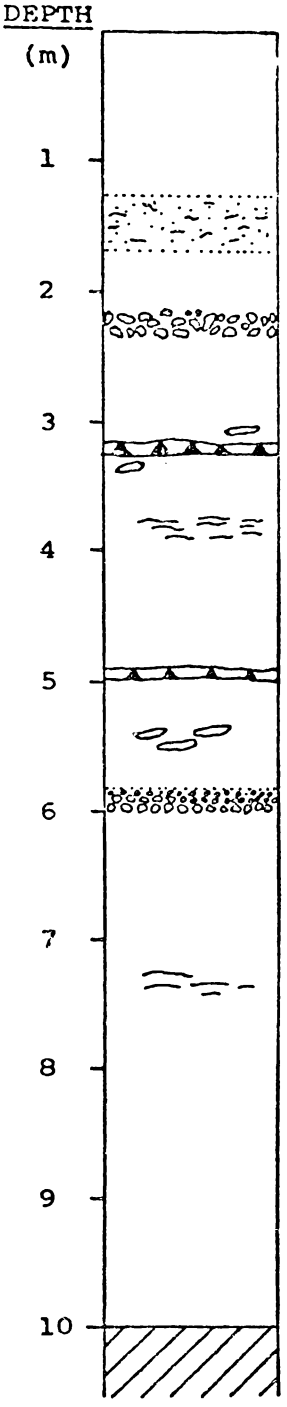


| VEGETATION | TEPHRAS |
|---|---|
| Very wet, difficult to sample. Calorophus minor, Baumea spp., Sphagnum spp., Gleichenia dicarpa, and wood twigs.and | |
| Calorophus minor (up to 80%), some Sphagnum spp.(mod. decomposed), Baumea spp., Sporodanthus traversii and wood. Very wet, charcoal, poorly to moderately decomposed. | abundant, sugar-like, white,pum. coarse ash. |
| Baumea spp.(70-80%), some Calorophus minor, Sporodanthus traversii, Gleichenia dicarpa and woody roots and fragments. Very wet, slushy, moderately decomposed. | White,poorly vesiculated, sparsely porphyritic, pum. coarse ash & fine lapilli. |
| Gleichenia dicarpa, some Calorophus minor and Baumea spp., very slushy, moderately to well decomposed. | |
| Bands of charcoal common down to 5m. Wood throughout profile. | |
| | Brown,extrem. vesiculated, sparsely porphyritic, normally graded,coarse ash and very fine lapilli. |
| Resistant, difficult to penetrate root mats of Gleichenia/Baumea or Gleichenia/Calorophus common throughout profile. | |
| Brown, fine-grained sediment. | |

KEY

- Tephra layers
- Resistant root mats
- Wood or timber
- Charcoal layer

FIGURE 5.2 : Profile of the Hauraki Peat Bog, Southern Dome. Vegetation after Davoren (1978). Core location N53/074907-see Fig. 5.1.

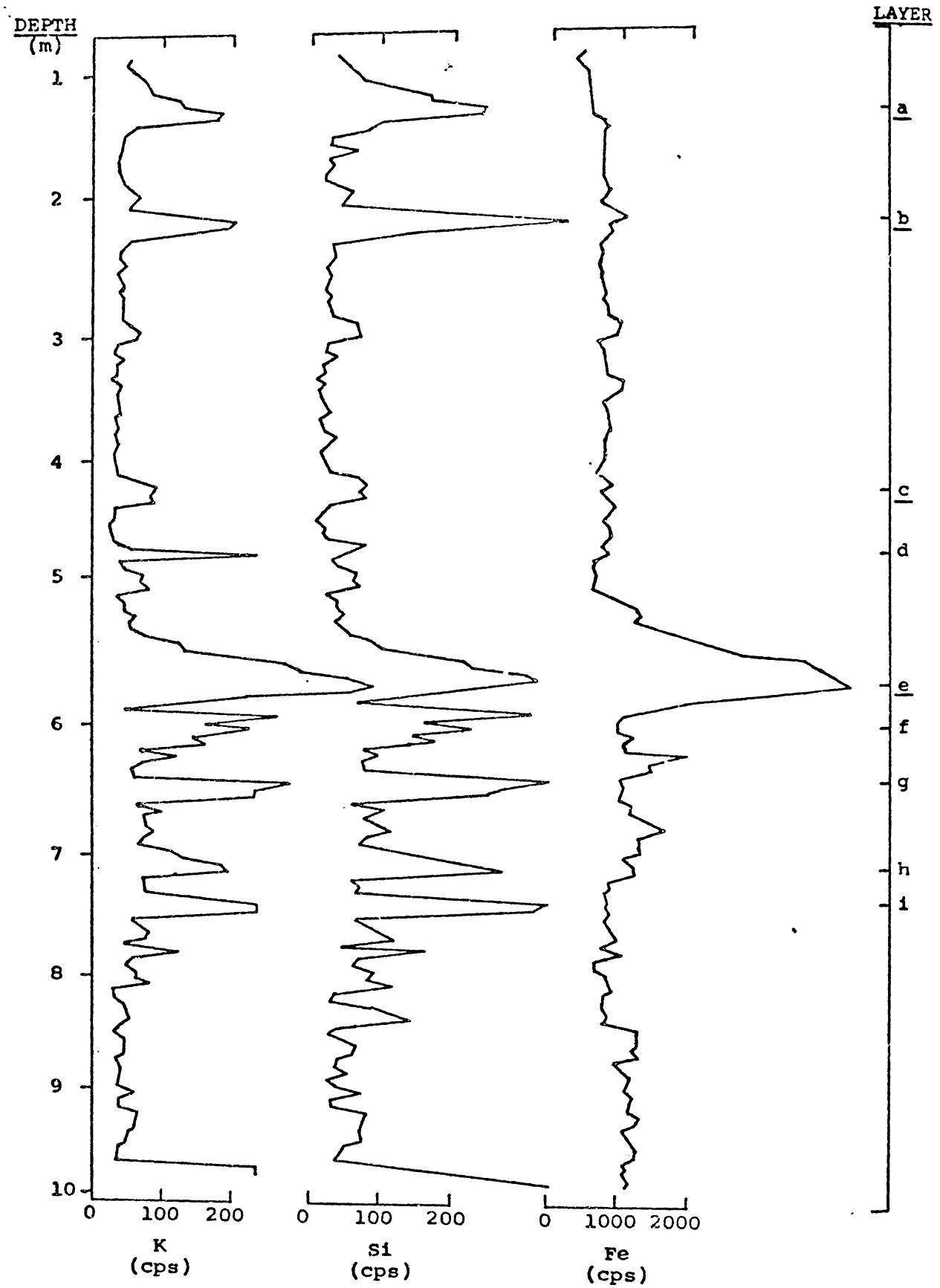


FIGURE 5.3 : Elemental count rates for K, Si and Fe from 4cm sections of the Hauraki Plains peat core, determined by XRF. Mineral layers are labeled "a" to "i", with tephra layers marked by underlining. The axis marked "DEPTH" is not a regular scale. The metre spacings are irregular because the number of 4cm sections varies in any metre interval; this has resulted from changes in the mineral content and degree of compaction of the core.

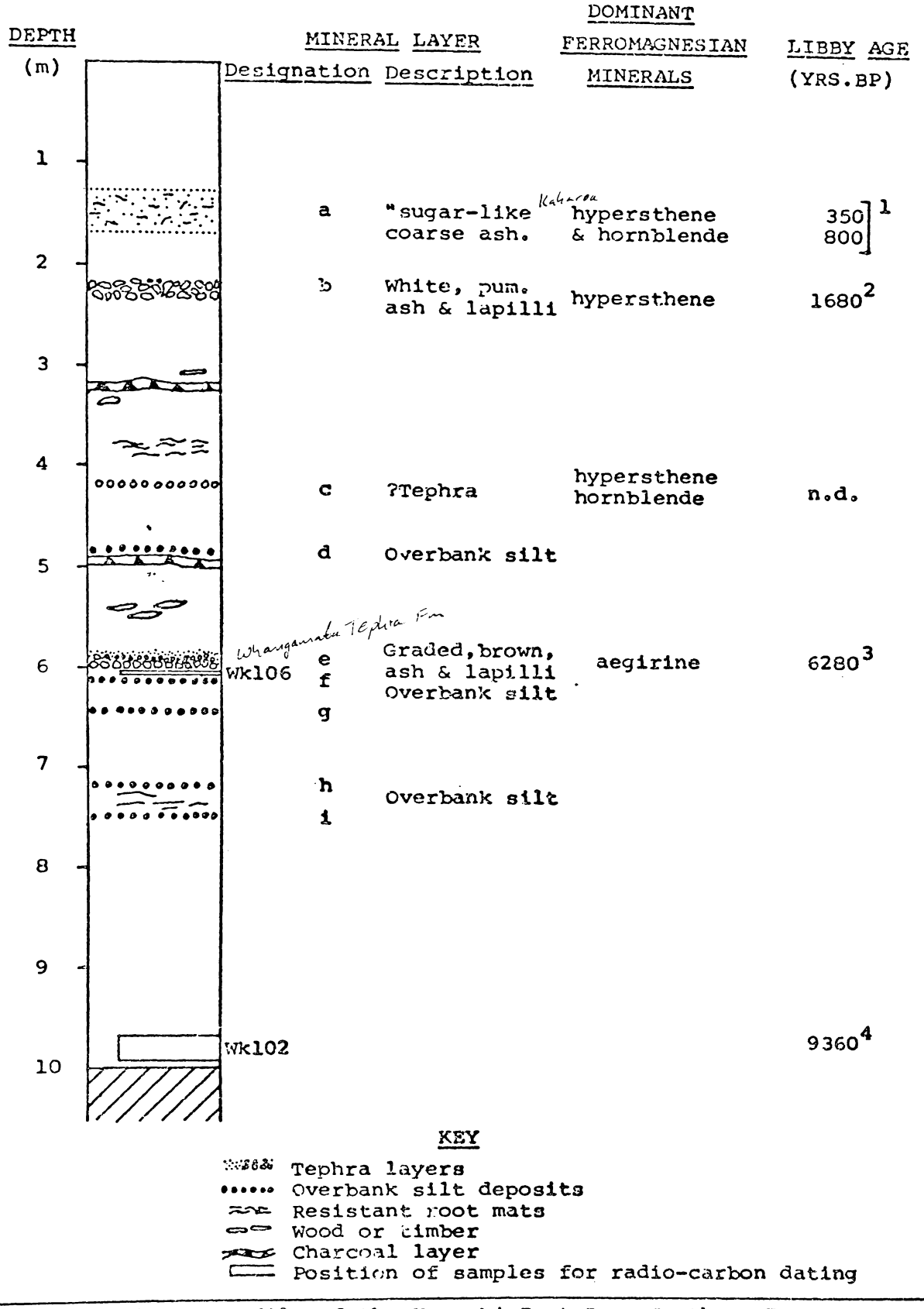


FIGURE 5.4 : Profile of the Hauraki Peat Bog, Southern Dome, showing mineral layers and tephra characteristics.

1 : From Pullar et al.(1977)-350, from peat enclosing ash
800, from wood underlying ash

2 : From Pullar et al.(1977).

3 : W.K.106 (6280 ± 70)

4 : W.K.102 (9360 ± 100)

TABLE 5.1 : Felsic mineralogy of three tephras from the Hauraki peat core (2-4 ϕ fraction)

| | Wt % Quartz | Wt % Anortho-clase | Wt % Plagio-clase | Wt % Glass and heavy minerals | Glass refractive index |
|---|---|---|---|---|---|
| Layer "a" (sugar-like tephra) | 22 | - | 45 | 33 | 1.496-1.500 |
| Layer "b" (white pumiceous ash and lapilli) | 16 | - | 23 | 61 | 1.497-1.498 |
| Layer "e" (graded, brown, ash and lapilli) | 18 | 24 | - | 58 | 1.510-1.511 |

TABLE 5.2 : Ferromagnesian mineralogy of three tephras from the Hauraki peat core (2-4 ϕ fraction)

| | Hypers-thene % | Cumming-tonite % | Horn-blende % | Augite % | Aegirine % | Others |
|---|---|---|---|---|---|---|
| Layer "a" (sugar-like tephra) | $73^{\pm}$ 8 ($2V_\alpha=61^o$) | 1 | $26^{\pm}$ 8 ($2V_\alpha=70^o$) | - | - | - |
| Layer "b" (white, pumiceous ash and lapilli) | $94^{\pm}$ 3 ($2V_\alpha=60^o$) | - | $5^{\pm}$ 2 ($2V_\alpha=74^o$) | 1 | - | - |
| Layer "e" (graded, brown ash and lapilli) | - | - | - | - | $96^{\pm}$ 3 | Cossyrite tuhualite olivine hypersthene |

Ferromagnesian mineral percentages include an estimate of error (determined because of the limited number of minerals available for counting) - error estimates calculated by the method of Van der Plas and Tobi (1965).

constituting only 40% of the 2-4 $\phi$ fraction, and a ferromagnesian mineral assemblage completely dominated by hypersthene. Layer "c", probably a tephra because of its relatively high proportion of heavy minerals, was not examined as extensively as the other tephras on account of the very low quantity of material present. However, the ferromagnesian mineral assemblage contained both hypersthene and hornblende. Layer "e" at a depth of 6 m, has distinctive graded bedding and brown colouration (Fig. 5.5).


FIGURE 5.5 : Layer "e" in the Hauraki peat core. The scale in the photograph is approximately 11 cm in length.

A 4 cm layer of peat collected immediately below the base of the ash and lapilli gave a radiocarbon age of 6280 years (θ = 70). Mineralogically, the tephra is quite unlike those above. It is peralkaline in composition, with abundant anorthoclase and quartz (42%) and a ferromagnesian mineral assemblage containing more than 95% aegirine with minor cossyrite, olivine and, very significantly, a single grain of tuhualite.

Pullar et al. (1977) examined a shallow peat core from the Hauraki swamp and discovered a layer of pumiceous ash (equivalent to layer "a" on Fig. 5.4) at a depth of 40-45 cm. This layer, which they called "reworked Taupo Pumice", was dated at between 350 and 800 years B.P., and contained hypersthene and hornblende in the ferromagnesian mineral assemblage. At the same site they dated and identified a layer of white pumiceous lapilli (equivalent to layer "b" on Fig. 5.4) as the Taupo Pumice (Table 1.1 p. 8 ) by the predominance of hypersthene in the ferromagnesian mineral assemblage (Ewart 1963).

However, the mineralogical characteristics of layers "a" and "b" (Tables 5.1 and 5.2) are too dissimilar for layer "a" to have been derived from layer "b", even following reworking. In particular, the quartz to plagioclase ratios are quite different, and layer "a" contains a considerable proportion of hornblende. Also, the two layers differ in composition (Table 5.3).

TABLE 5.3 : Elemental ratios of Si, K and Fe determined by XRF for layers "a" and "b" in the Hauraki peat core

| | $\frac{Si}{K}$ (cps) | $\frac{Fe}{Si}$ (cps) |
|---|---|---|
| Layer "a" ("sugar-like" tephra) | 1.42 ($\theta$ = 0.03) | 1.70 ($\theta$ = 0.01) |
| Layer "b" (white pumiceous lapilli) (Taupo Pumice) | 2.17 ($\theta$ = 0.08) | 2.14 ($\theta$ = 0.08) |

The mineralogical and chemical data presented above indicate that the sugar-like tephra is probably not reworked Taupo Pumice but represents a younger tephra between 350 and 800 years old. Pullar et al. (1977) have shown that the Kaharoa Ash is much more extensive than was previously thought, covering the entire Coromandel Peninsula and parts of Northland to a depth of at least 3 cm. They also dated the tephra and obtained ages ranging from 607 to 930 years B.P. and found it to be characterised by abundant biotite in the ferromagnesian mineral assemblage. Although Pullar et al. (1977) have concluded that the "sugar-like" tephra found in the Hauraki swamp is not the Kaharoa Ash because of the absence of biotite, the data presented in this thesis contradict this view and suggest that the deposit represents Kaharoa Tephra from which the biotite has been removed, perhaps as a result of deposition of the tephra under flooded conditions.

The 6280 year old graded brown coarse ash and very fine lapilli at 6 m depth in the peat, has a peralkaline composition as shown by its anorthoclase, aegirine, cossyrite and tuhualite mineral

assemblage, and is correlated with the peralkaline tephra occurring in field classes I and II in the Whangamata-Waihi region. The peralkaline mineralogy identifies the tephra's source as Mayor Island, the only known peralkaline Quaternary volcanism in New Zealand. The deposit is here named 'Whangamata Tephra Formation' (Wg). The name 'Whangamata Ash' utilised by McCraw (1975b) and other workers before that date should be replaced as it encompasses all components of field class II.

Buck (1978) in his examination of the pyroclastic deposits of Mayor Island, described a thick pumice-rich tephra (his lithotype 5) which he suggests would be the most likely correlative of the Whangamata Tephra. The deposit is the thickest single air-fall tephra on Mayor Island and has a ferromagnesian mineral assemblage similar to the Whangamata Tephra (approximately subequal amounts of aegirine and cossyrite with minor olivine - sample W12781), and is confined to the western side of the volcano, indicating that either the vent was inclined towards Whangamata or a strong easterly wind was blowing at the time of the pumice eruption.

## (B) TEPHRA STRATIGRAPHY OF THE TE PUKE REGION

As it is beyond the scope of this thesis to establish an accurate reference section in the Tauranga-Rotorua region, a composite column representing the Te Puke area has been constructed (see Fig. 5.9). Data were extracted from Howorth (1976) for the tephras older than and including the Kawakawa Tephra at a site near Otamarakau (site 113 in Fig. 5.6). Samples collected at Te Matai Rd (site 100) during the present survey gave information on the tephras younger than the Kawakawa Tephra. The stratigraphy of these younger tephras was established with the assistance of Dr W.A. Pullar by hand over hand mapping from the Rotorua region (particularly sites at Te Ngae, Maniatutu Rd and the Rotorua-Paengaroa highway) to Te Matai Rd (Fig. 5.6).

In the Bay of Plenty the Holocene tephra stratigraphy is less reliable than that of the older tephras because they are, in general, thinner and no detailed sections supported by mineralogical and chemical data are established for either the Rotorua Subgroup or the Okareka and Te Rere tephras (see Table 5.4). To improve the reliability of the stratigraphy of the younger part of the column at Te Matai Rd, samples were collected and the ferromagnesian mineral assemblages were examined (Table 5.5 and Fig. 5.8).

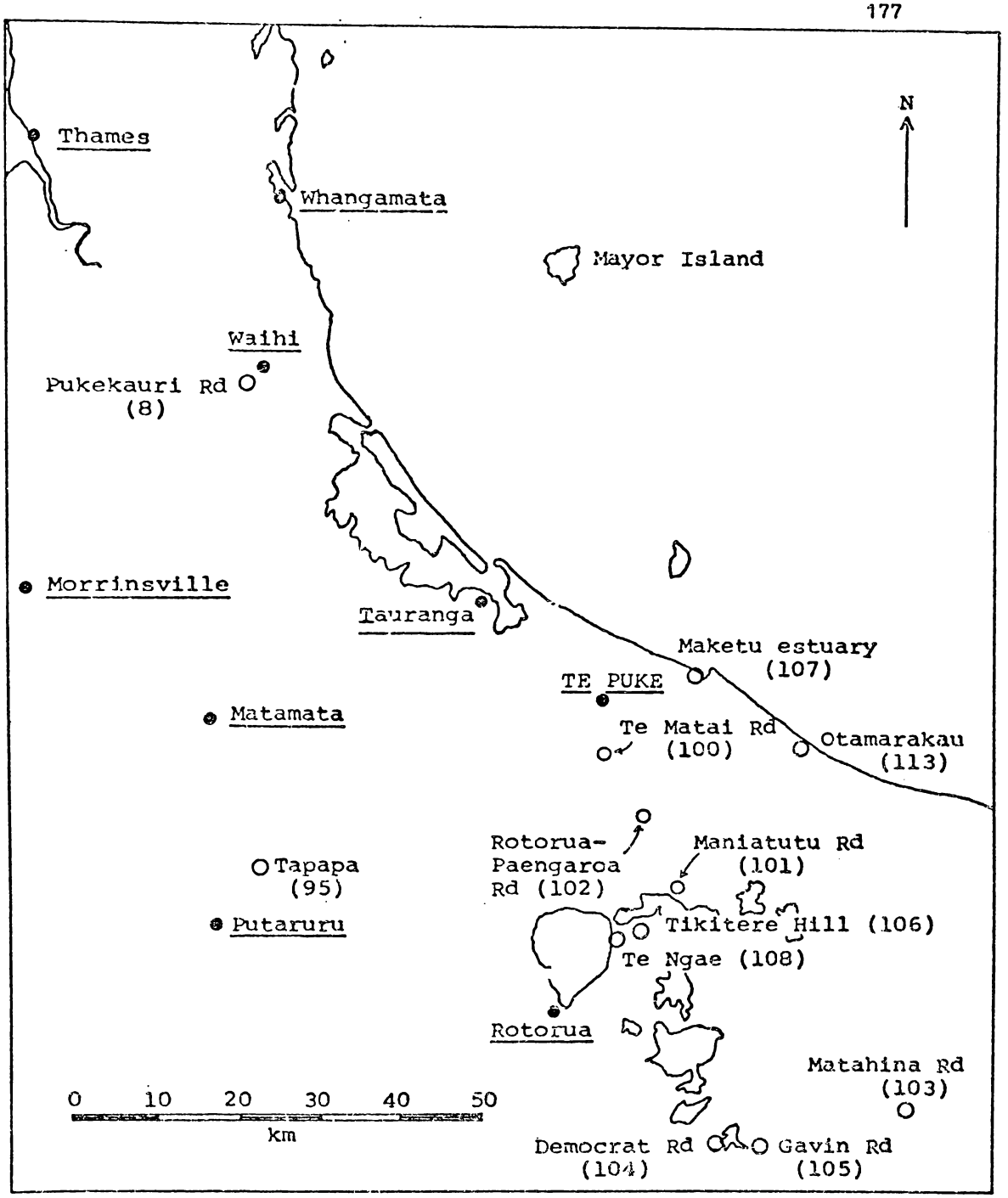


FIGURE 5.6 : Geographical location of sites and place names mentioned in the text. Site numbers are shown in parentheses, sections by open circles, and place names by closed circles.

TABLE 5.4 : Tephra symbols and ages used in Chapter 5.

Note on the Mamaku and Rotoma tephras.

There is considerable confusion in the literature regarding the age and stratigraphy of the Mamaku and Rotoma tephras (see below). Most workers favour the 7,000 year age for the Mamaku Ash, although Pullar and Heine (1971) suggest that the date may represent firing of vegetation on the Rotoma Ash surface and not an eruptive event. Unpublished work on the Haroharo complex has revealed that the deposit named the "Rotoma Ash" (Vucetich and Pullar 1964) contains two distinct tephras, which are here called "Rotoma Ash" and "Rotoma-2 Tephra" (Nairn, pers. comm.). Rotoma Ash is characterised by an abundance of cummingtonite in the ferromagnesian mineral assemblage and has been dated by Nairn at approximately 9,000 years B.P. Rotoma-2 Tephra is a younger tephra dominated by hypersthene and hornblende and contains only minor cummingtonite (see Table 5.7); its age is not yet known.

| Tephra | Radiocarbon age | Radiocarbon number | Where cited |
|---|---|---|---|
| Mamaku Ash | 7,050 ± 77 | NZ 1152 | Pullar et al. (1973)<br>McCraw (1975b)<br>Cole (1976)<br>Nathan (1976)<br>Nairn (1979,pers. comm.) |
| | 8,050 ± 105 | NZ 719 | Pullar & Heine (1971)<br>Cole (1972) |
| Rotoma Ash | 7,050 ± 77 | NZ 1152 | Pullar & Heine (1971) |
| | 7,330 ± 235 | NZ 1199 | Pullar et al. (1973)<br>Topping & Kohn (1973)<br>Vucetich & Pullar (1973)<br>McCraw (1975b)<br>Cole (1976) |
| | c.9,000 | | Nathan (1976)<br>Nairn (1979,pers. comm.) |

| Tephra | Symbol | Radiocarbon age (before 1950) | Radiocarbon number | Source |
|---|---|---|---|---|
| * Rotomahana Mud | Tr1 | 64 | - | |
| * Kaharoa Tephra | Ka | 930 ± 70 | NZ10 | Pullar et al. (1973) |
| Taupo Pumice | Tp | 1,819 ± 17 | Statistical mean of many dates | Healy (1964) |
| * Rotokawau Ash | Rw | ? | | |
| * Whakatane Ash | Wk | 5,180 ± 80 | NZ1066 | Pullar and Heine (1971) |
| Whangamata Tephra | Wg | 6,280 ± 70 | WK106 | This thesis |
| * Mamaku Ash | Ma | 7,050 ± 77 | NZ1152 | Pullar and Heine (1971) |
| Rotoma-2 Tephra | Rm2 | ? | | |
| * Rotoma Ash | Rm | c.9,000 | | Nairn, pers. comm. |
| * Waiohau Ash | Wh | 11,250 ± 200 | NZ568 | Pullar et al. (1973) |
| * Rotorua Ash | Rr | 13,450 ± 250 | NZ1615 | Pullar et al. (1973) |
| Okareka Ash | Ok | 20,700 ± 450 | NZ523 | Pullar and Heine (1971) |
| Te Rere Ash | Te | ? | | |
| Kawakawa Tephra | Kk | 19,850 ± 310 | NZ1056 | Pullar and Heine (1971) |
| Haupara Tephra | Hu | | | |
| Maketu Tephra | Mk | 30,100 - | | Pullar et al. (1973) |
| Tahuna Tephra | Ta | 42,000 | | |
| Ngamotu Tephra | Nt | | | |
| Rotoehu Ash | Re | 41,700 ± 3500 | NZ1126 | Pullar and Heine (1971) |

See note in the Table caption (opposite) on the Mamaku and Rotoma tephras. * Tephras comprise the Rotorua sub-group.

TABLE 5.5 : Ferromagnesian mineral abundances in the Rotorua Subgroup tephras of the composite Te Puke column (Te Matai Rd section).

| Tephra | Sample | Hypersthene % | Cummingtonite % | Hornblende % | Augite % | Hypersthene / Amphibole |
|---|---|---|---|---|---|---|
| Kaharoa Tephra Taupo Pumice | TM1 | 42 | 9 | 33 | 16 | 1.00 |
| ?Rotokawau, ?Whakatane, tephras | TM2 | 32 | 23 | 30 | 15 | 0.60 |
| Mamaku Ash | TM3 | 25 | 53 | 16 | 6 | 0.36 |
| Rotoma Ash | TM4 | 25 | 57 | 14 | 4 | 0.35 |
| ?Waiohau, Rotorua tephras | TM5 | 67 | 2 | 18 | 13 | 3.35 |

For stratigraphic position of samples see Fig. 5.9

The ferromagnesian mineral assemblages of the known calc-alkaline tephras likely to be represented in the Te Puke region are summarised in Table 5.6. Data are drawn from Ewart (1963, 1966), Cole (1970), Kohn (1973), Topping and Kohn (1973) and Howorth (1976) in addition to that from samples collected during this survey. Although eight groups of tephras have assemblages that are sufficiently unique to provide a means for their identification, only five individual tephras viz. Kaharoa, Taupo Pumice, Whakatane, Rotoma and Rotoehu tephras could be correlated with confidence, with the large group of hypersthene-rich tephras that lie between the Rotoma Ash and Rotoehu Ash indistinguishable from each other.

According to Pullar et al. (1977) the Kaharoa Tephra was deposited as a north westerly trending lobe completely blanketing the Coromandel Peninsula and Te Puke region. They identified the tephra on the basis of the biotite content of samples collected from peat swamps, and the titanomagnetite element chemistry. The ferromagnesian mineral assemblages of two samples of Kaharoa Tephra collected from the Maketu Estuary (site 107) and the Rotorua-Paengaroa highway (site 102) during the present survey, contained substantial amounts of biotite (e.g. Table 5.7). However, at Te Matai Rd, only nine km NNW of site 102, the Kaharoa Tephra is represented by fine white lapilli in a brown sandy loam matrix, with the bed containing only very rare biotite ( <1% - Table 5.5, Sample TM1). No biotite occurs in any of the other Te Matai Rd samples or in any of the Holocene and Late Pleistocene tephras on the Coromandel Peninsula. As Table 5.5 shows, the ferromagnesian mineral assemblage of TM1 is typical of Kaharoa Tephra, with the exception of the biotite content. It is therefore postulated that biotite in Kaharoa Tephra is depleted in the soil forming environment and is found only where conditions are favourable for its preservation i.e. in peat where it has fallen directly upon the surface of the swamp, or when buried by other tephras as at the Rotorua-Paengaroa site, or in rapidly accumulating sediments (as in the dune deposits at the Maketu Estuary).

Taupo Pumice is present in the Te Puke region and represented by white pumiceous lapilli scattered throughout the upper 60 cm of the Te Matai column.

TABLE 5.6 : Ferromagnesian mineral assemblages of calc-alkaline tephras that are potential contributors to the Te Puke column

| Tephra | Ferromagnesian mineral | Distinctive mineral(s) | Sites where the tephras were sampled | Supportive data |
|---|---|---|---|---|
| Kaharoa | Biotite, hypersthene, hornblende and minor augite | Biotite | Rotorua-Paengaroa Highway (site 102) | Cole (1970)<br>Pullar et al. (1977) |
| Taupo Pumice | Hypersthene and minor augite | Hypersthene | n.d.[1] | Ewart (1963) |
| Rotokawau | Hypersthene and hornblende + minor augite | | n.d. | Kohn (1973) |
| Whakatane | Hornblende, cummingtonite and hypersthene | Cummingtonite and hornblende | Gavin Rd (site 105)<br>Matahina Rd (site 103) | Kohn (1973)<br>Ewart (1966) |
| Mamaku | Hypersthene + minor hornblende | | Te Ngae (site 108)<br>Matahina Rd (site 103) | Kohn (1973) |
| Rotoma | Cummingtonite plus minor hypersthene + hornblende | Cummingtonite | Maniatutu Rd (site 101)<br>Rotorua-Paeng.Highway (site 102)<br>Matahina Rd (site 103) | <br>Ewart (1966)<br>Kohn (1973) |
| Waiohau | Hypersthene + hornblende | Hypersthene and hornblende | Democrat Rd (site 104) | Cole (1970) |
| Rotorua | Hypersthene + hornblende (tr.biotite and augite) | | Democrat Rd (site 104) | Kohn (1973)<br>Topping and Kohn (1973) |

| | | | | |
|---|---|---|---|---|
| Okareka | Hypersthene + hornblende | | Tapapa (site 95) | Kohn (1973) |
| Te Rere | Hypersthene + hornblende | | Tapapa (site 95) | Kohn (1973) |
| Kawakawa | Hypersthene, augite and hornblende | | n.d. | Topping and Kohn (1973) |
| Hauparu | Hypersthene, augite and hornblende | Hypersthene and Augite | Otamarakau (site 113) | Howorth (1976) |
| Maketu | Hypersthene + augite | | Otamarakau (site 113) | Howorth (1976) |
| Tahuna Ngamoto | Hornblende + hypersthene | Hornblende and Hypersthene | n.d. | Howorth (1976) |
| Rotoehu | Cummingtonite + minor hypersthene and hornblende | Cummingtonite | Matahina Rd (site 103) Tapapa (site 95) | Ewart (1966) |

[1] n.d. = not determined

TABLE 5.7 : Ferromagnesian mineral assemblages of selected calc-alkaline tephras in the Rotorua region (2-4 ϕ)

| Tephra | Site | Sample | Hypersthene % | Cummingtonite % | Hornblende % | Augite % | Biotite % | hypersthene / amphibole |
|---|---|---|---|---|---|---|---|---|
| Kaharoa Tephra | Rotorua-Paengaroa highway (site 102) | | 47 | 1 | 29 | 3 | 20 | 1.62 |
| Mamaku Ash | Te Ngae (site 108) | | 96 | - | 4 | - | - | 24.0 |
| | Maniatutu Rd (site 101) | S1* | 93 | 1 | 6 | - | - | 13.30 |
| Rotoma-2 Tephra | | S2* | 64 | 12 | 23 | 1 | - | 1.83 |
| Rotoma Ash | | S3* | 7 | 89 | 4 | - | - | 0.08 |
| | | S4* | 5 | 92 | 2 | 1 | - | 0.05 |
| | Matahina Rd (site 103) | | 12 | 83 | 4 | 1 | - | 0.14 |
| Rotoehu Ash | Matahina Rd (site 103) | Paleosol | 20 | 66 | 13 | 1 | - | 0.25 |
| | | 80-140 cm above base | 11 | 83 | 6 | - | - | 0.12 |

* For stratigraphic position of samples, see Fig. 5.8.

The Whangamata Tephra dated at 6,280 years B.P., is identified at Te Matai Rd by its aegirine content and is concentrated in the upper parts of the Rotoma Ash (Fig. 5.7).

The Rotoma Ash is characterised by the high proportion of cummingtonite in the ferromagnesian mineral assemblage and by its stratigraphic position with Whangamata Tephra. The only other cummingtonite bearing Holocene tephra is the Whakatane Ash (5,180 ± 80) which as it is younger than the Whangamata Tephra, must overlie it if it is present. Similarly, if the Mamaku Ash is present, it must lie between Whangamata Tephra and Rotoma Ash. The ferromagnesian mineral assemblages of selected Holocene tephras were examined at Maniatutu Rd (site 101) 19 km SE of Te Matai Rd, to clarify the stratigraphic relationships between the Mamaku and Rotoma tephras (Table 5.7 and Fig. 5.8). At Maniatutu Rd, the hypersthene-rich Mamaku Ash overlies Rotoma-2 Tephra containing hypersthene and hornblende, which in turn overlies Rotoma Ash, which is characterised by a high cummingtonite content. The substantial decrease in the amount of cummingtonite in the ferromagnesian mineral assemblage of the Rotoma Ash between Maniatutu Rd (c. 90%) and Te Matai Rd (c. 55%), is probably the result of mixing of younger, hypersthene-rich tephras with the cummingtonite-rich Rotoma Ash. The stratigraphic position of the Whangamata Tephra (Fig. 5.7) identifies these hypersthene-bearing tephras as the Mamaku and Rotoma-2 tephras. Because of the thinness of the Rotoma-2 Tephra at Maniatutu Rd, it is likely that the Mamaku Ash is the major hypersthene-rich component mixed with the Rotoma Ash at Te Matai Rd (Fig. 5.8).

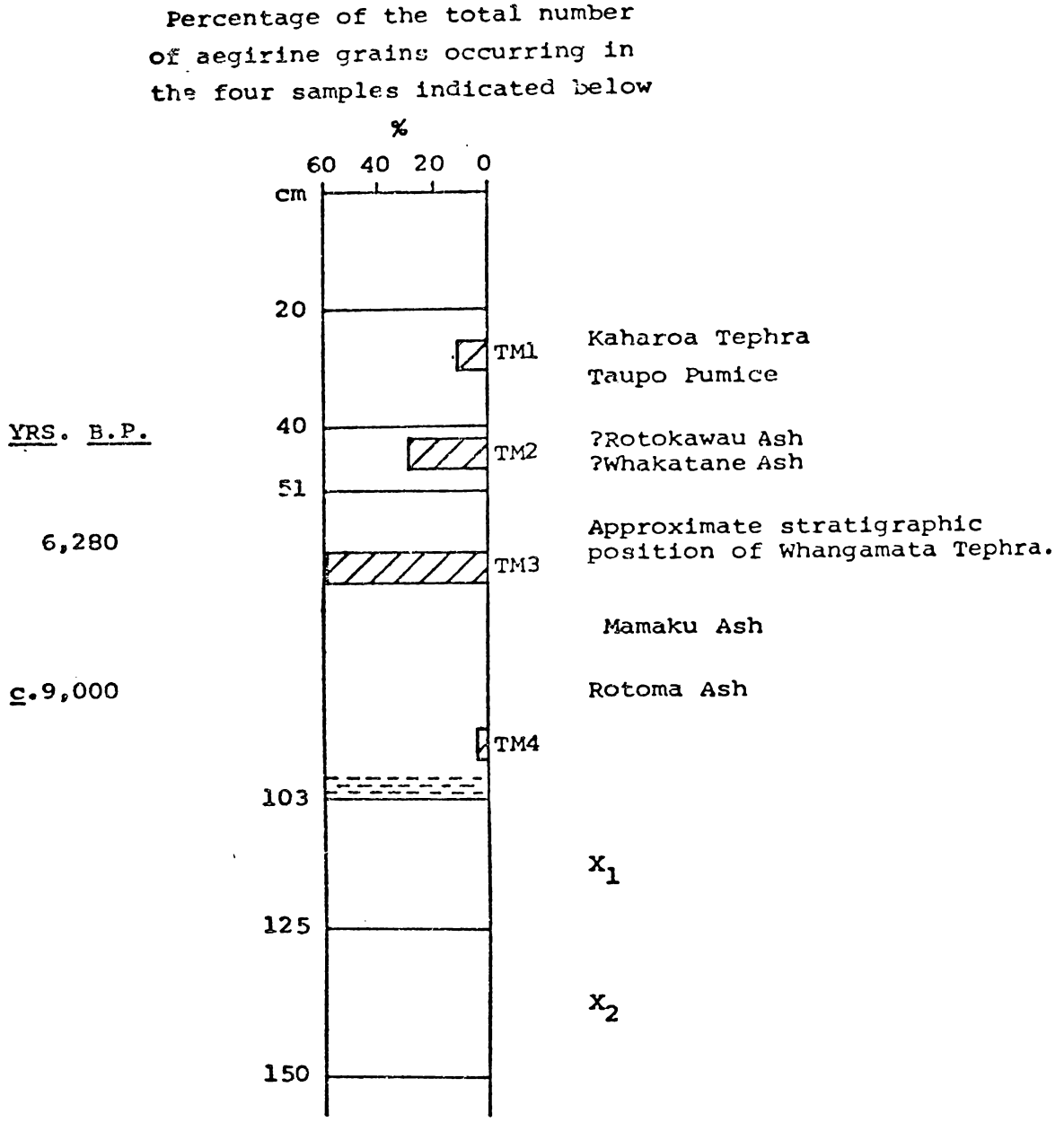


FIGURE 5.7 : Stratigraphic relationships of the Whangamata Tephra and Rotoma Ash at Te Matai Rd. The stratigraphic position of the Whangamata Tephra enables identification of the Rotoma Ash below, and also indicates that if the Mamaku Ash is present, it must lie between samples TM3 and TM4.

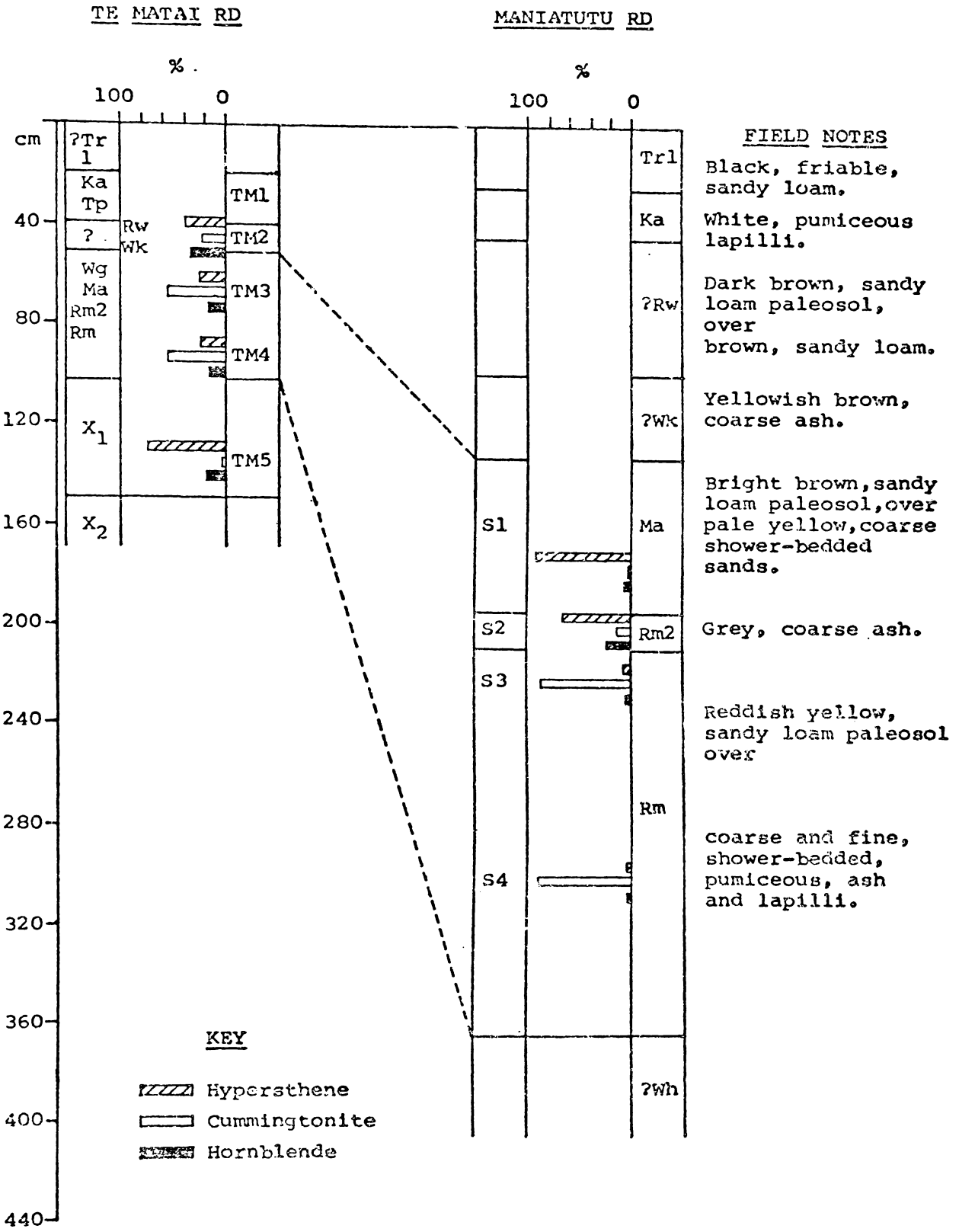


FIGURE 5.8 : Correlation of the Mamaku, Rotoma-2, and Rotoma tephras between Maniatutu Rd (site 101) and Te Matai Rd (site 100). The ferromagnesian mineral assemblages of the three tephras are also shown.
Te Matai samples are shown as TM1, TM2, TM3, TM4, and TM5
Maniatutu Rd samples are shown as S1, S2, S3, and S4.

The beds underlying the Rotoma Ash at Te Matai Rd have hypersthene-hornblende-augite ferromagnesian mineral assemblages (Table 5.5; sample TM5), which are characteristic of many tephras (e.g. Waiohau, Rotorua, Okareka, Te Rere and Kawakawa tephras). As it is beyond the scope of this thesis to establish a detailed stratigraphy in the Bay of Plenty, the five tephras characterised by hypersthene and hornblende-dominated ferromagnesian mineral assemblages, are grouped and termed the "X" tephras, i.e. X1, X2, X3 (see Figs. 5.7, 5.8, 5.9 etc).

Three Late Pleistocene tephras in the Te Puke region are possible contributors to the Coromandel tephra stratigraphy; the Hauparu, Maketu and Rotoehu tephras have a total thickness of 11 m at Otamarakau (5 m, 3 m and 3 m respectively), with the Hauparu and Maketu tephras characterised by a high augite content, and the Rotoehu Ash by a cummingtonite-dominated ferromagnesian mineral assemblage (Ewart 1966; Howorth 1976). Fig. 5.9 summarises the tephra stratigraphy of the Te Puke region.

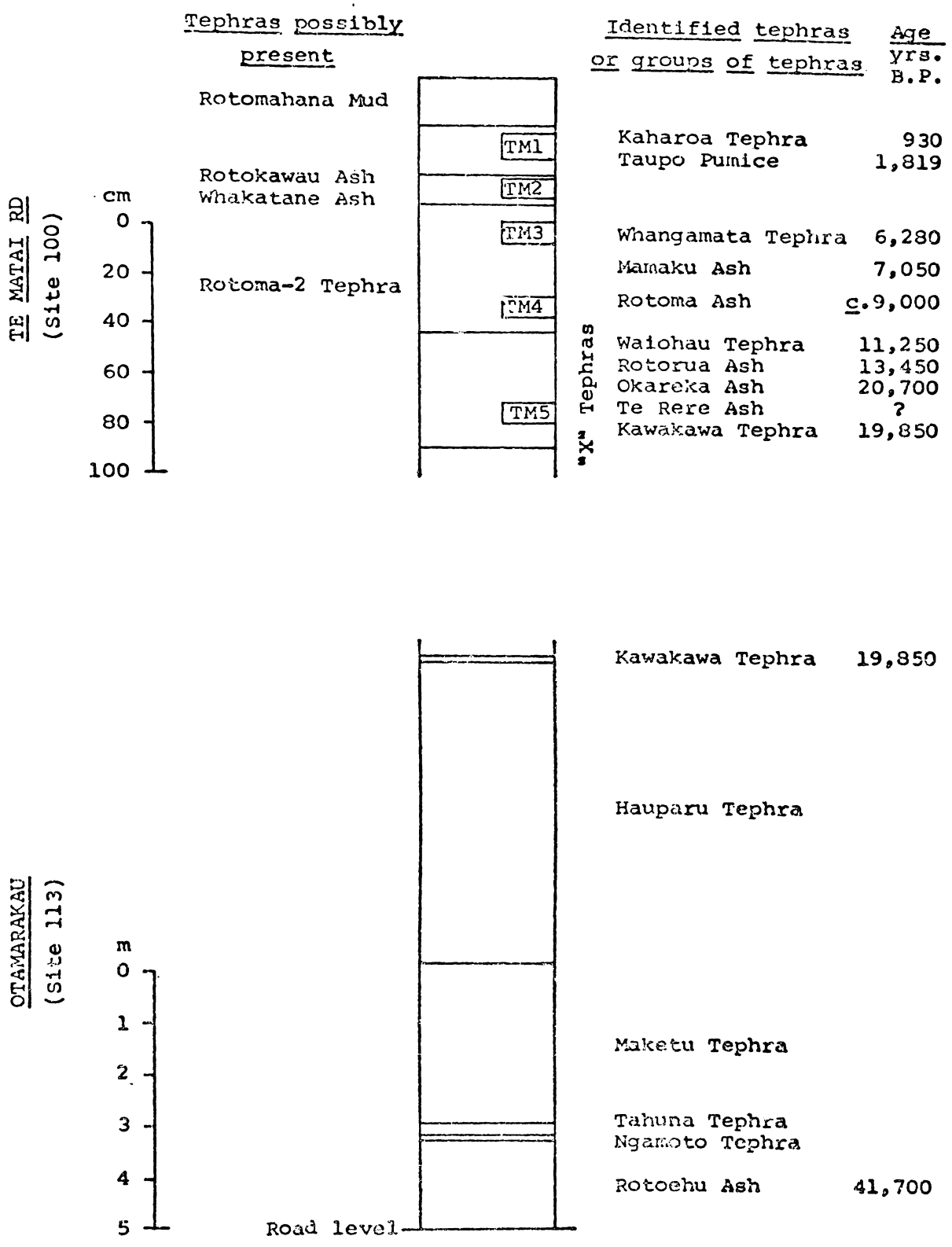


FIGURE 5.9 : A composite stratigraphic column of the Holocene and Late Pleistocene tephras in the Te Puke region. The field characteristics of the tephras at Te Matai Rd are described at the end of this thesis (p. 329). Otamarakau data after Howorth (1976).

## (C) CORRELATION OF TEPHRAS REPRESENTED AT THE TE PUKE STRATIGRAPHIC COLUMN WITH TEPHRAS FROM THE COROMANDEL PENINSULA

Stratigraphic columns at four sites spanning more than 70 km between Pukekauri Rd and Te Matai Rd were established to enable correlation of the Coromandel tephras with those represented in the Te Puke region (Fig. 5.10); these four sites represent an area which will be referred to in this report as the Katikati region. Ash shower maps (Pullar and Birrell 1973) show that the margins of many Central North Island tephras occur in the Katikati region and consequently as the distance increases northwards from Te Matai Rd, individual tephras thin considerably, and some occur in the more southern sites only. The tephras have thinned sufficiently north of Bethlehem for road cuttings to expose all the Holocene and Late Pleistocene tephras represented at that site. Tentative correlations between the known tephras from the Te Puke region and those contained in the Coromandel field classes, based upon field characteristics and stratigraphic position, are presented along with detailed pedological descriptions of the tephras at Reas Rd, Youngson Rd, Bethlehem, Ohauiti Rd and Te Matai Rd at the end of this thesis (Appendix F).

The Holocene and Late Pleistocene tephras in the Te Puke region have been correlated with those at Pukekauri Rd by field investigations aided by laboratory studies; in particular, particle size properties of the coarser than 4 $\emptyset$ fraction and the ferromagnesian mineral assemblages of selected samples, and the titanomagnetite element chemistry (Fig. 5.11).

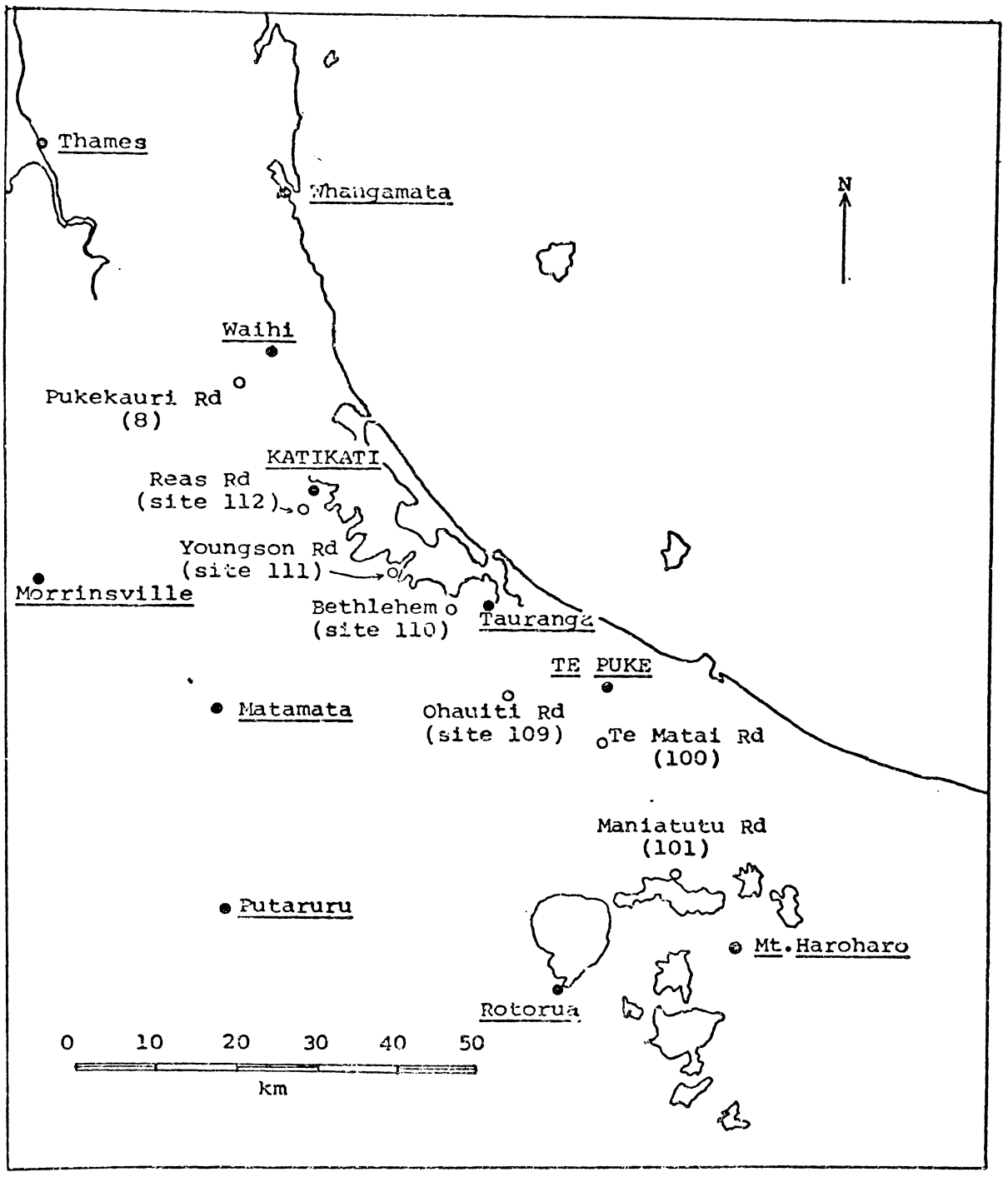


FIGURE 5.10 : Geographical location of sites and place names mentioned in the text. Site numbers are shown in parentheses, stratigraphic sections by open circles, and place names by closed circles.

FIGURE 5.11 : Holocene and Late Pleistocene tephra stratigraphy at Te Matai Rd, sites representing the Katikati region, and Pukekauri Rd. Correlation lines are based upon field and laboratory observations. Sample numbers and locations are shown on the right hand side of each stratigraphic column. Symbols "$X_1$", "$X_2$", etc. denote unidentified tephras from the group containing the Waiohau, Rotorua, Okareka, Te Rere, and Kawakawa tephras (see p.188). Full tephra names and ages are presented in Table 5.6 p.182.

1. read ?Rw
   ?Wk

2. read ?Trl
   ?Ka
   ?Tp
   ?Rw
   ?Wk

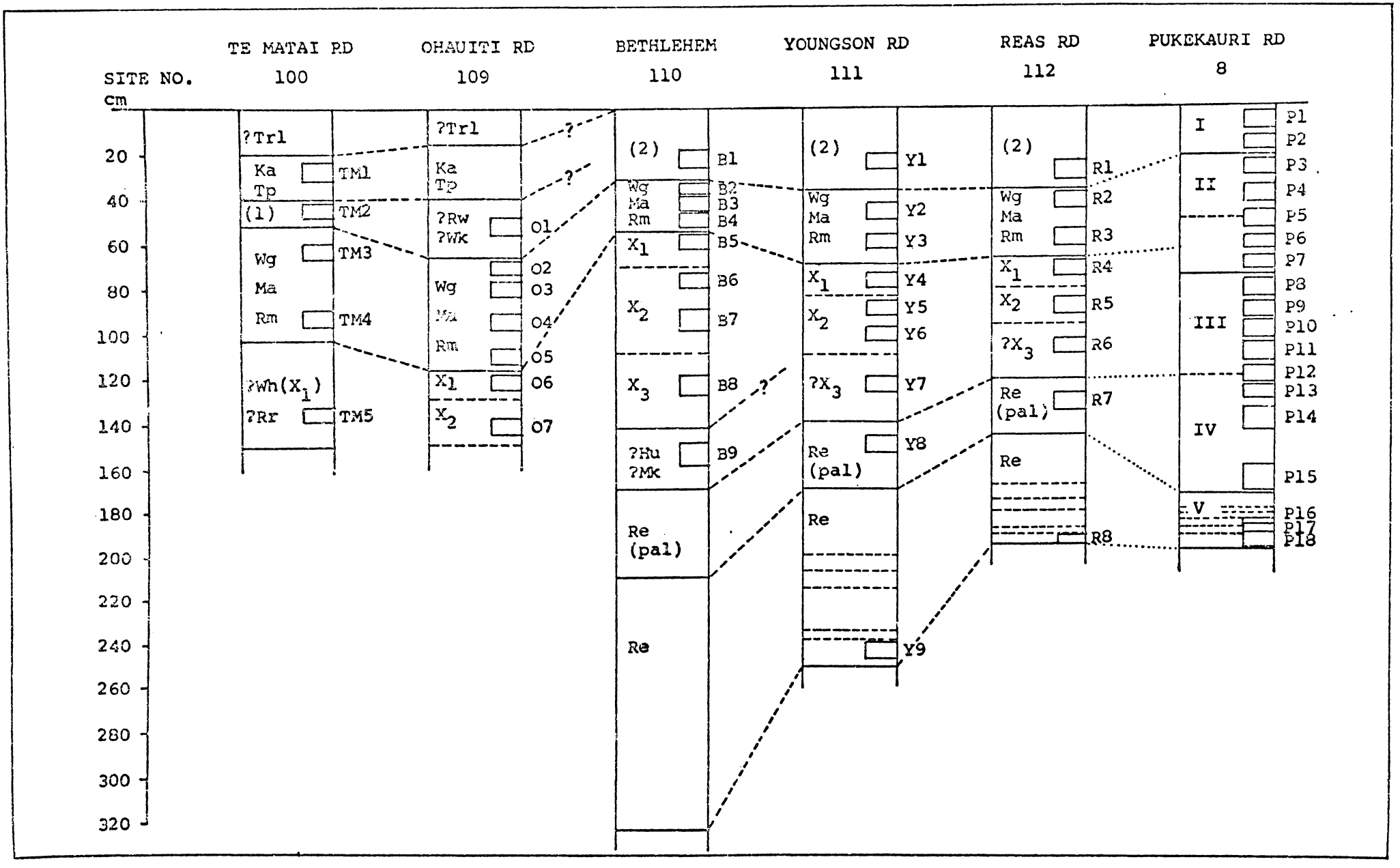
TE MATAI RD
OHAUITI RD
BETHLEHEM
YOUNGSON RD
REAS RD
PUKEKAURI RD
SITE NO.
100
109
110
111
112
8
cm
20
40
60
80
100
120
140
160
180
200
220
240
260
280
300
320
?Trl
Ka
Tp
(1)
Wg
Ma
Rm
?Wh(X1)
?Rr
TM1
TM2
TM3
TM4
TM5
?Rw
?Wk
O1
O2
O3
O4
O5
O6
O7
(2)
B1
B2
B3
B4
X1
B5
B6
X2
B7
X3
B8
?Hu
?Mk
B9
Re
(pal)
Y1
Y2
Y3
Y4
Y5
Y6
?X3
Y7
Y8
Y9
R1
R2
R3
R4
R5
R6
R7
R8
I
II
III
IV
V
P1
P2
P3
P4
P5
P6
P7
P8
P9
P10
P11
P12
P13
P14
P15
P16
P17
P18

Particle size parameters are presented in Appendix E, Table E.3 and summarised in Fig. 5.12; ferromagnesian mineral assemblages in Table 5.8 and Figs. 5.13, 5.15, 5.16 and 5.18; and the titanomagnetite element chemistry given in Appendix D, Table D2, and summarised in Figs. 5.14, 5.17 and 5.19.

(1) The Post-Whangamata Tephras

The Te Puke region contains up to five tephras that are less than 6,000 years in age; the Rotomahana Mud, Kaharoa Tephra, Taupo Pumice, Rotokawau Ash and Whakatane Ash, only two of which (the Kaharoa Tephra and Taupo Pumice) have been identified with confidence (Fig. 5.9 p.189).

The soil 'A' horizon at Te Matai Rd contains moderately coarse (less than 20 mm) brownish grey creampuffs, which may indicate remnants of the Rotomahana Mud (Vucetich and Pullar 1964). The creampuffs are no longer detectable at Ohauiti Rd and sites further north, although the distal component of the tephra is probably present in the uppermost parts of the tephra column.

Although Kaharoa Tephra can be recognised within the friable sandy loams constituting the upper 50 cm of the Te Matai Rd stratigraphic column, further north in the Katikati region its abundant brown pumice fragments become too fine to distinguish it from other tephras of sandy loam texture (e.g. Rotokawau Ash, Whakatane Ash). However, work on the Hauraki peat swamp and the isopach map of Pullar et al. (1977), strongly suggests that the Kaharoa Tephra was deposited in the Katikati region.

Taupo Pumice, characterised by its medium (less than 5 mm) white pumiceous lapilli, is the only Post-Whangamata tephra that can be recognised readily by its field characteristics at the sites north of Te Matai Rd.

Further characterisation of these younger tephras by laboratory techniques has not been attempted because of the thinness of the tephras involved and the degree of mixing they have undergone in the soil forming regime. It can be concluded that the sites in the Katikati region and field class I at Pukekauri Rd contain Taupo Pumice and probably Kaharoa Tephra, with possible additions from the Rotomahana Mud, Rotokawau Ash and Whakatane Ash.

(2) The Whangamata, Mamaku and Rotoma tephras

At Te Matai Rd, the Whangamata-Mamaku-Rotoma bed consists of 50 cm of pumiceous coarse loamy sand, the base of which is defined by a 3 cm layer of very coarse loamy sand. The bed is largely composed of the Mamaku and Rotoma tephras but, in addition, contains a small proportion of peralkaline material including aegirine, from the Whangamata Tephra.

Although the field properties of the Mamaku-Rotoma tephras change abruptly north of Ohauiti Rd, they are still recognisable at Reas Rd by their characteristic white pumiceous fragments. The tephras show a steady decrease in mean grain size between Ohauiti Rd and Reas Rd but become coarser at Pukekauri Rd as the proportion of Whangamata Tephra increases (samples O4, B3, Y3, R3, P3 and P4 in Fig. 5.12).

FIGURE 5.12 : Mean grain size of the coarser than 4 ∅ fraction of the Holocene and Late Pleistocene tephras at the Katikati sites and Pukekauri Rd. The width of each stratigraphic column represents a scale, shown by the Bethlehem site. Data from Appendix E (Fig. E.10). Parameters are summarised in Appendix E (Table E.3).

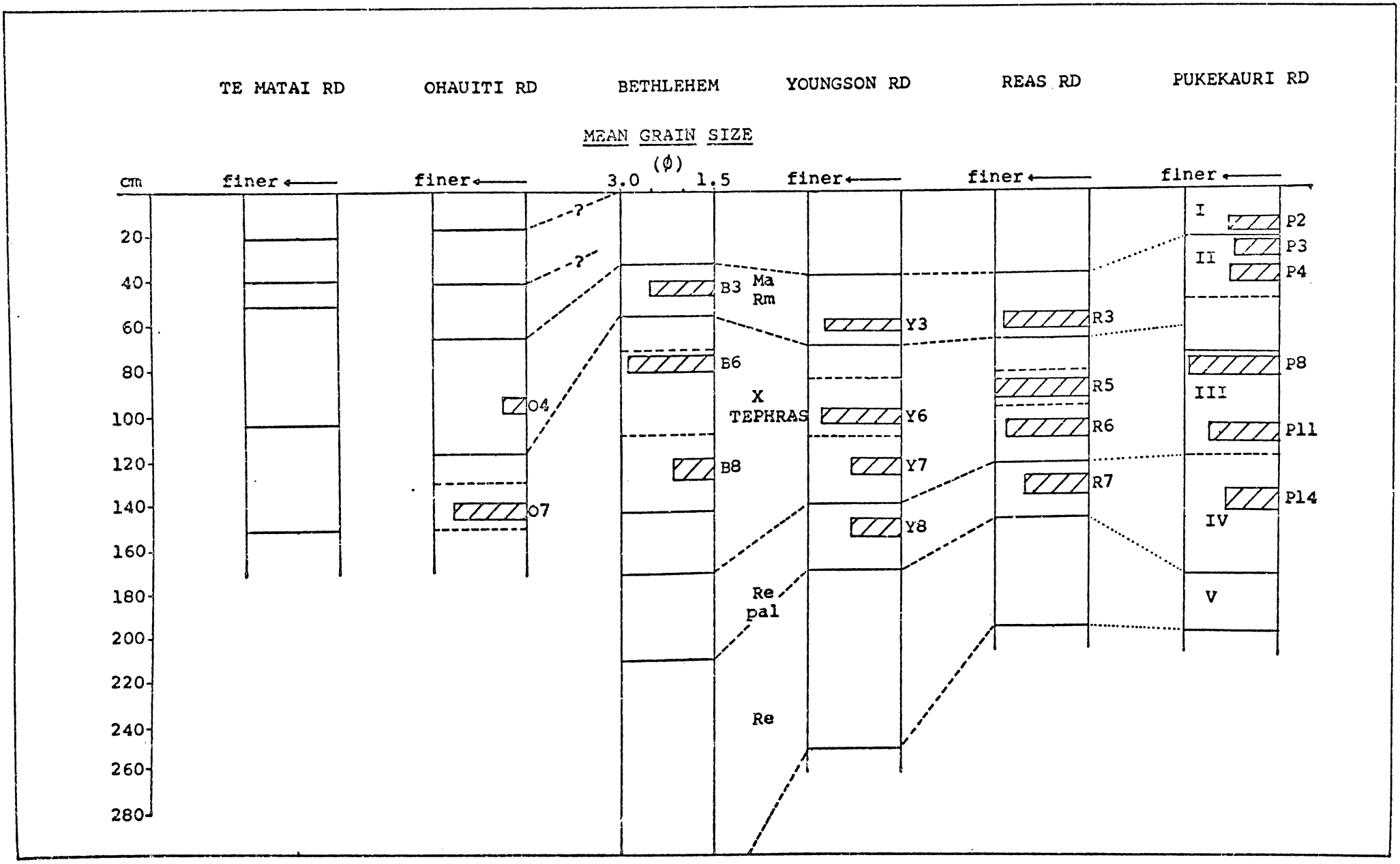
TE MATAI RD
OHAUITI RD
BETHLEHEM
YOUNGSON RD
REAS RD
PUKEKAURI RD
MEAN GRAIN SIZE
(ϕ)
3.0
1.5
cm
finer
20
40
60
80
100
120
140
160
180
200
220
240
260
280
?
?
O4
O7
B3
B6
B8
Ma
Rm
X
TEPHRAS
Re
pal
Re
Y3
Y6
Y7
Y8
R3
R5
R6
R7
I
II
III
IV
V
P2
P3
P4
P8
P11
P14

The ferromagnesian mineralogy of pure deposits of Mamaku Ash and Rotoma Ash and the mixed tephras in the Katikati region are shown in Fig. 5.13. The moderate cummingtonite content (c. 55%) of the Mamaku-Rotoma tephras at Te Matai Rd is maintained to Ohauiti Rd and then decreases considerably at Bethlehem and the more northern sites to approximately 20% of the ferromagnesian mineral assemblage, as the proportion of Rotoma Ash decreases. Correlation of the bed containing the Whangamata, Mamaku and Rotoma tephras between Te Matai Rd and the field class II samples of Pukekauri Rd is facilitated by the presence of aegirine, which increases in concentration progressively northwards from Te Matai Rd.

The titanomagnetite element chemistry of the Mamaku and Rotoma tephras progressively changes between Te Matai Rd and Reas Rd (Fig. 5.14) reflecting a decreasing proportion of Rotoma Ash in the bed with increasing distance north of Te Matai Rd. The deviation of the field class II titanomagnetite compositions from the linear sequence shown by the Mamaku-Rotoma tephras of the Katikati region, has resulted from the more significant influence of the Whangamata Tephra (represented in Fig. 5.14 by the sample OM3/4L) in field class II, which has resulted in a depression of the Ti/Mn and Ti/V ratios.

The particle size parameters, ferromagnesian mineralogy and titanomagnetite element chemistry all support the correlation of the Whangamata, Mamaku and Rotoma tephras with the three principal tephras constituting field class II on the Coromandel Peninsula (see Fig. 3.18 p. 96). Progressive changes in the amount of cummingtonite and in the titanomagnetite element ratios between Te Matai Rd and Pukekauri Rd indicate that the Mamaku Ash is more persistent northwards than the Rotoma Ash, and is the dominant calc-alkaline tephra of field class II.

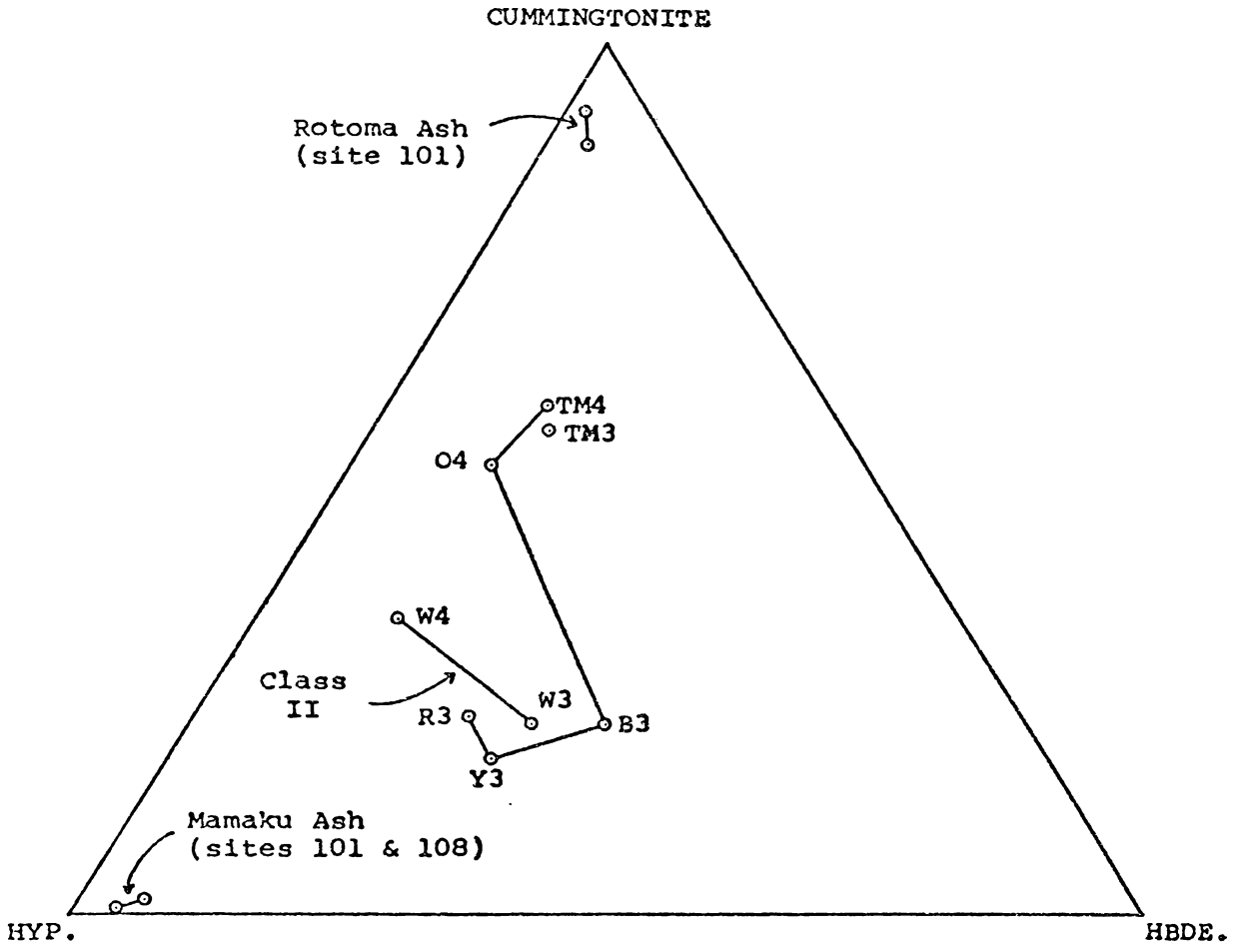


FIGURE 5.13 : Ferromagnesian mineral assemblages of Mamaku Ash and Rotoma Ash, the Mamaku-Rotoma beds in the Katikati region, and field class II samples.

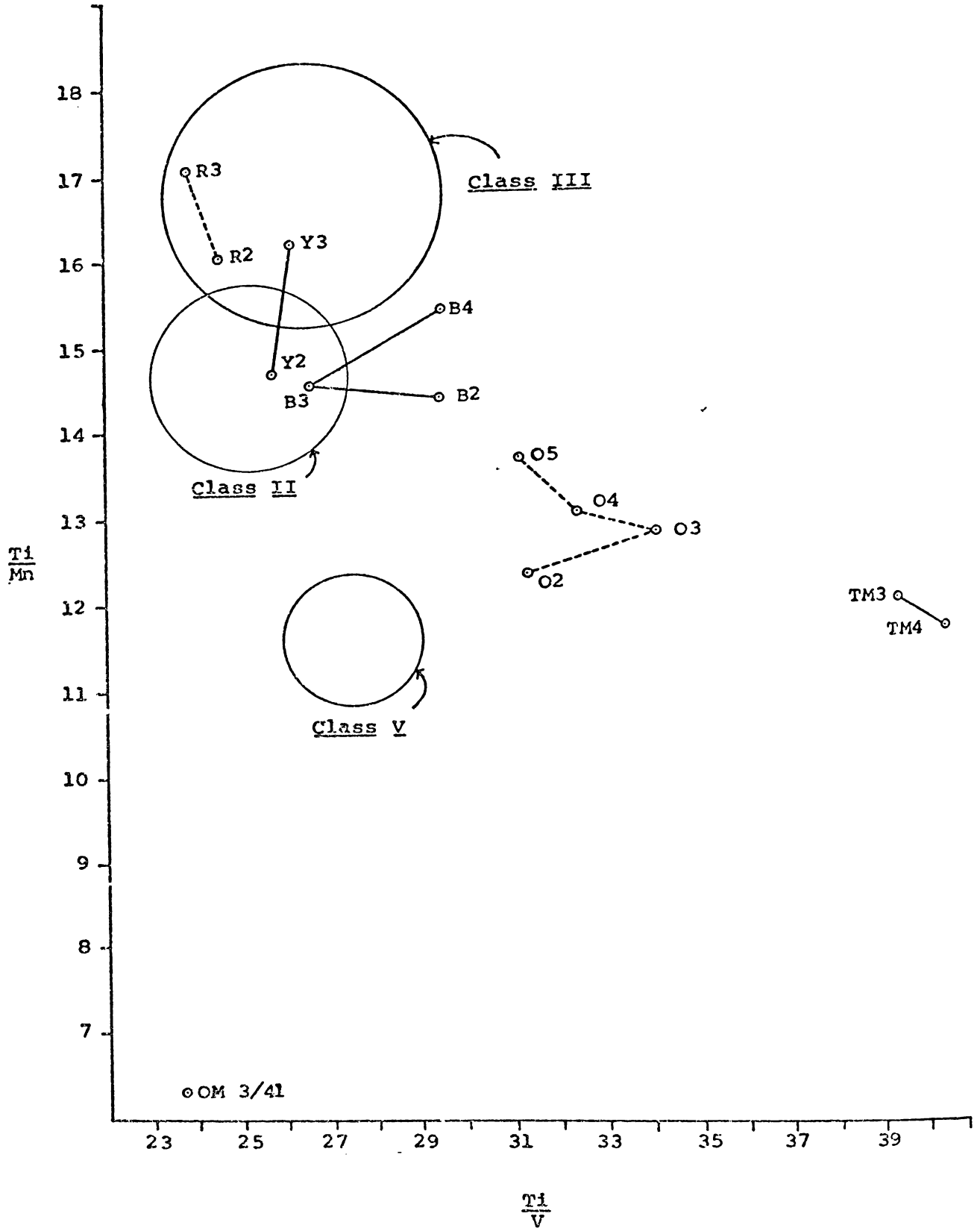


FIGURE 5.14 : Ratios of count rates of Ti, Mn and V from titanomagnetites extracted from the Mamaku-Rotoma tephras in the Katikati region. Samples are from Reas Rd(R2,R3); Youngson Rd(Y2,Y3); Bethlehem (B2,B3,B4); Ohauiti Rd(O2,O3,O4,O5); and Te Matai Rd(TM3,TM4). The coarser than -1ø fraction of OM3/4 is also shown (Old Mill-Class II). Circles encompass all samples from the Coromandel Peninsula for classes II, III and V, as shown in Appendix D (Fig. D.1 p. 299 ). The correct position of the circles representing classes II, III and V was ascertained by reanalysing samples from the Coromandel tephras, together with samples from the Katikati region.

(3) The "X" tephras

The beds underlying the Rotoma Ash at Te Matai Rd contain a group of tephras which are characterised by hypersthene, hornblende and augite ferromagnesian mineral assemblages; individual tephras, including the Waiohau Tephra, Rotorua Ash, Okareka Ash, Te Rere Ash and Kawakawa Tephra are not distinguished and they are termed the "X" tephras in this report (p.188). It is not known how many of the tephras listed above are grouped under the name "X" tephras, but at least two are defined at Te Matai Rd by a basal creampuff layer (see page 329). The heavy mineral contents of the "X" tephras at Bethlehem, Youngson Rd and Reas Rd all increase substantially with depth (Table 5.8), supporting the contention that more than one tephra is present. Whereas the upper samples constituting the "X" beds at Bethlehem, Youngson Rd and Reas Rd have an average of 6% heavy minerals in the 2-4 $\phi$ fraction, the lower samples average 17%, which suggests that as the "X" tephras are all rhyolitic, a considerable age difference exists between the various tephras which are represented.

The mean grain sizes of the tephras comprising the "X" beds at the sites in the Katikati region show a downward coarsening and a tendency to become finer grained towards Pukekauri Rd (samples O7, B6, B8, Y6, Y7, R5, R6, P8 and P11 in Fig. 5.12 p.196 ). However, at Pukekauri Rd this trend is not continued and the tephras of class III are significantly coarser than the Reas Rd samples.

The ferromagnesian mineral assemblages of the "X" tephras are remarkably constant, having high hypersthene/amphibole ratios and very low amounts of cummingtonite (less than 9%, - samples O7, B6,

TABLE 5.8 : Ferromagnesian mineral assemblages of selected samples from the Katikati region (2-4 Ø)

| Site | Sample | Hypersthene (%) | Cummingtonite (%) | Hornblende (%) | Augite (%) | Hypersthene / Amphibole | % heavy mins. in 2-4 Ø fraction |
|---|---|---|---|---|---|---|---|
| Reas Rd (site 112) | R3* | 46 | 20 | 22 | 12 | 1.08 | 3 |
| | R5 | 56 | 9 | 29 | 6 | 1.47 | 6 |
| | R6 | 61 | 9 | 24 | 6 | 1.84 | 12 |
| | R7 | 41 | 34 | 20 | 5 | 0.77 | 17 |
| Youngson Rd (site 111) | Y3* | 44 | 15 | 26 | 15 | 1.08 | 2 |
| | Y6 | 54 | 3 | 33 | 10 | 1.51 | 7 |
| | Y7 | 52 | 5 | 30 | 13 | 1.49 | 23 |
| | Y8 | 33 | 45 | 17 | 5 | 0.53 | 15 |
| | Y9 | 19 | 80 | 1 | - | 0.23 | n.d. |
| Bethlehem (site 110) | B5* | 35 | 19 | 35 | 11 | 0.65 | 2 |
| | B6 | 49 | 5 | 34 | 12 | 1.26 | 4 |
| | B8 | 48 | 3 | 38 | 11 | 1.16 | 17 |
| | B9 | 57 | 1 | 20 | 22 | 2.69 | n.d. |
| Ohauiti Rd (site 109) | O4* | 33 | 49 | 12 | 6 | 0.53 | 1 |
| | O7 | 49 | 4 | 35 | 12 | 1.24 | 3 |

n.d. = not determined

* aegirine is present in small amounts ( <1%)

B8, Y6, Y7, R5 and R6 in Figs. 5.15 and 5.16). Although these characteristics are shown clearly at all the sites in the Katikati region, they are not reproduced in the field class III deposits at Pukekauri Rd which have considerably lower hypersthene/amphibole ratios and moderate amounts of cummingtonite (samples P8 and P11 in Figs. 5.15 and 5.16).

The bulk titanomagnetite element chemistry for the "X" tephras in the Katikati region is less variable between sites than the Mamaku-Rotoma tephras, but exhibits a tendency for the Ti/Mn ratio to increase and the Ti/V ratio to decrease slightly between Ohauiti Rd and Reas Rd (Fig. 5.17). Extrapolation of this trend to the Pukekauri Rd site would give a composition significantly different from the field class III samples of the Coromandel Peninsula.

The mean grain size, ferromagnesian mineralogy (particularly the proportion of cummingtonite) and the titanomagnetite compositions all show that the "X" tephras at Te Matai Rd and at sites in the Katikati region, do not correlate directly with the field class III samples at Pukekauri Rd. The origins of the field class III deposit will be reviewed in the discussion at the end of this chapter.

(4) The Pre-Kawakawa tephras

At Bethlehem, the "X" tephras grade into 30 cm of bright brown coarse sandy loam which corresponds in stratigraphic position and field characteristics to either the Hauparu or Maketu tephras (Howorth 1976) (see also Birrell et al. 1977). Though clearly defined at Bethlehem, the bright brown tephra is unrecognisable in the Youngson Rd or Reas Rd columns. The deposit has a ferromagnesian

FIGURE 5.15 : Percentage cummingtonite in the ferromagnesian mineral fraction, and weight percent heavy minerals in the Holocene and Late Pleistocene tephras at the Katikati sites and Pukekauri Rd. Scales shown for the Bethlehem site.

1. % cummingtonite in the 2-4 Ø fraction of the ferromagnesian mineral assemblage.
2. Heavy minerals include opaque minerals and the ferromagnesian mineral assemblage (2-4 Ø fractions).

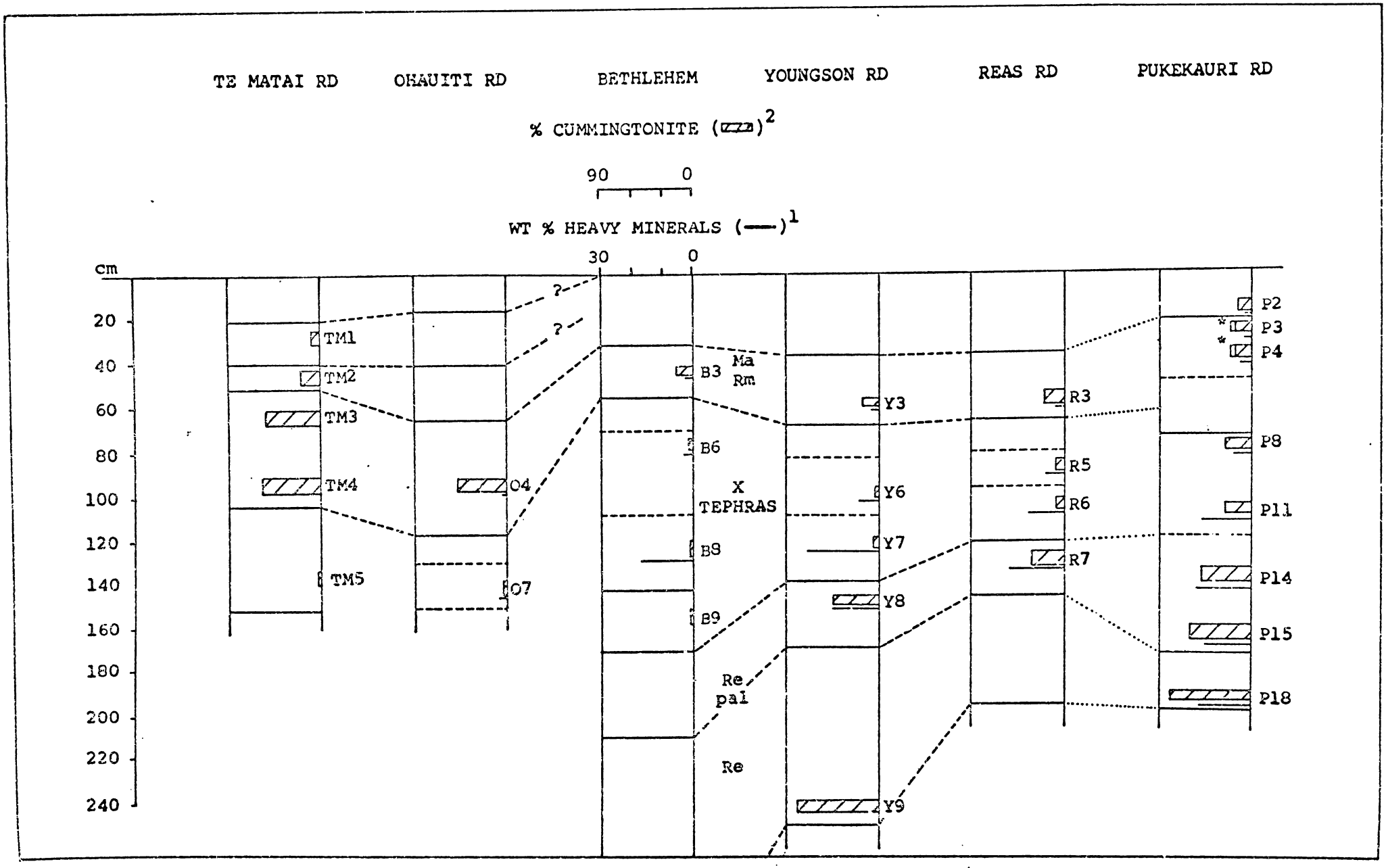
TE MATAI RD
OHAUITI RD
BETHLEHEM
YOUNGSON RD
REAS RD
PUKEKAURI RD
% CUMMINGTONITE (▨)2
90
0
WT % HEAVY MINERALS (—)1
30
0
cm
20
40
60
80
100
120
140
160
180
200
220
240
TM1
TM2
TM3
TM4
TM5
O4
O7
B3
B6
B8
B9
Ma
Rm
X
TEPHRAS
Re
pal
Re
Y3
Y6
Y7
Y8
Y9
R3
R5
R6
R7
P2
P3
P4
P8
P11
P14
P15
P18
?
?

FIGURE 5.16 : Hypersthene/Amphibole ratio in the Holocene and Late Pleistocene tephras at the Katikati sites and Pukekauri Rd. Scale shown for the Bethlehem site.

* Full bar length represents samples W3 and W4. The shorter bar length represents samples P3 and P4.

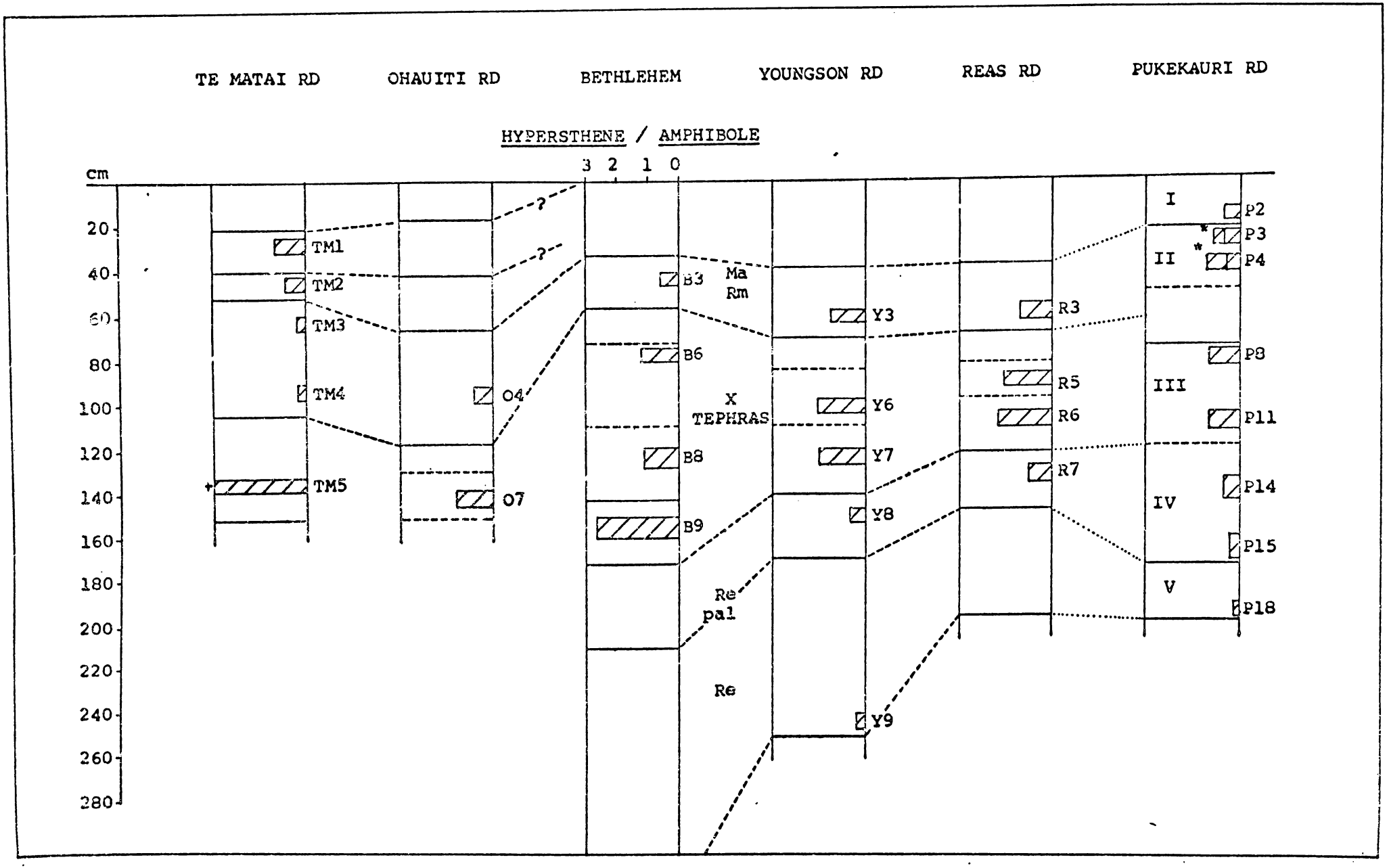
TE MATAI RD
OHAUITI RD
BETHLEHEM
YOUNGSON RD
REAS RD
PUKEKAURI RD
HYPERSTHENE / AMPHIBOLE
3 2 1 0
cm
20
40
60
80
100
120
140
160
180
200
220
240
260
280
TM1
TM2
TM3
TM4
TM5
O4
O7
B3
B6
B8
B9
Ma
Rm
X
TEPHRAS
Re
pal
Re
Y3
Y6
Y7
Y8
Y9
R3
R5
R6
R7
I
II
III
IV
V
P2
P3
P4
P8
P11
P14
P15
P18

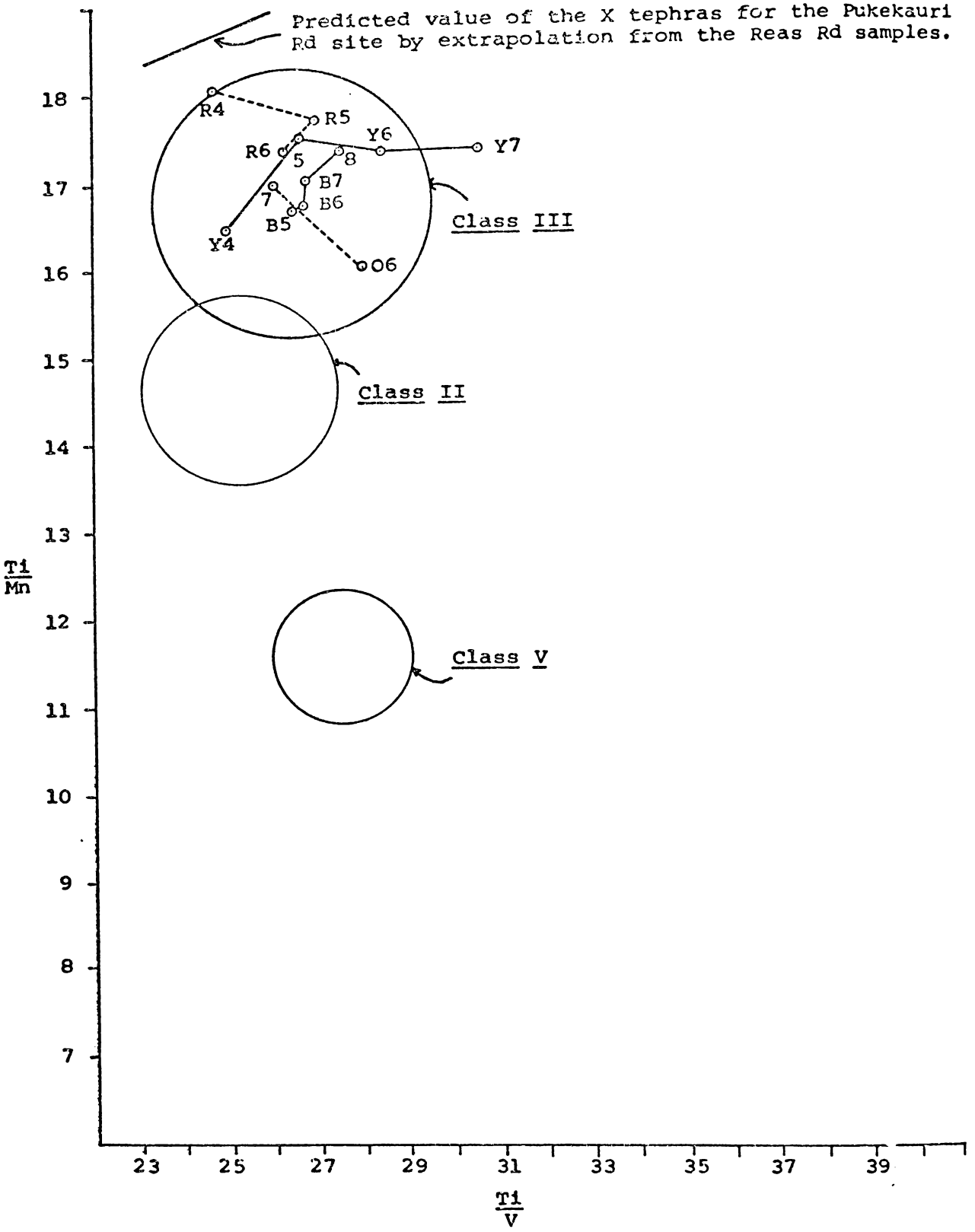


FIGURE 5.17 : Ratios of count rates of Ti, Mn and V from titanomagnetites extracted from the "X" tephras at the sites in the Katikati region. Samples from Reas Rd(R4,R5,R6); Youngson Rd(Y4,Y5,Y6,Y7); Bethlehem(B5,B6,B7,B8); and Ohauiti Rd(O5,O6). Circles encompass all samples from the Coromandel Peninsula sites for field classes II, III and V.

mineral assemblage consistent with the Hauparu tephra (Fig. 5.18B) and titanomagnetite characterised by an unusually high Ti/V ratio (sample B9 in Fig. 5.19). A sample representing the Hauparu Tephra was not collected at Youngson Rd and Reas Rd because of the inability to recognise it in the field and the wide sampling interval at these sites; however, the influence of the tephra is probably seen in sample Y7 in Fig. 5.19. Hauparu tephra is probably also present in the upper parts of field class IV (sample P13 in Fig. 4.22 p. 153), the titanomagnetites from which have a higher Ti/V ratio than the surrounding tephras (it was detected at Pukekauri Rd in preference to Reas Rd because of the closer sampling interval at Pukekauri Rd).

The base of the Late Pleistocene tephra column at Bethlehem, Youngson Rd and Reas Rd is defined by a brown sandy silt loam overlying multicoloured homogeneous and shower-bedded sands and loamy sands which contrast strongly with the underlying brown, clay-rich beds of the Hamilton Ash formation (Ward 1967). The tephra and its paleosol are represented at Pukekauri Rd by field classes V and IV respectively and can be correlated by their field characteristics, particularly the coarse grain size, prominent shower-bedding and stratigraphic relationship with the underlying deposits, with the Rotoehu Ash in the Te Puke region.

The ferromagnesian mineral assemblage of the Rotoehu Ash is dominated by cummingtonite which decreases in concentration in the paleosol, as hypersthene and hornblende become more prominent (Fig. 5.18A). The lower concentration of cummingtonite in the paleosol of the Rotoehu Ash is the result of contamination by a

A

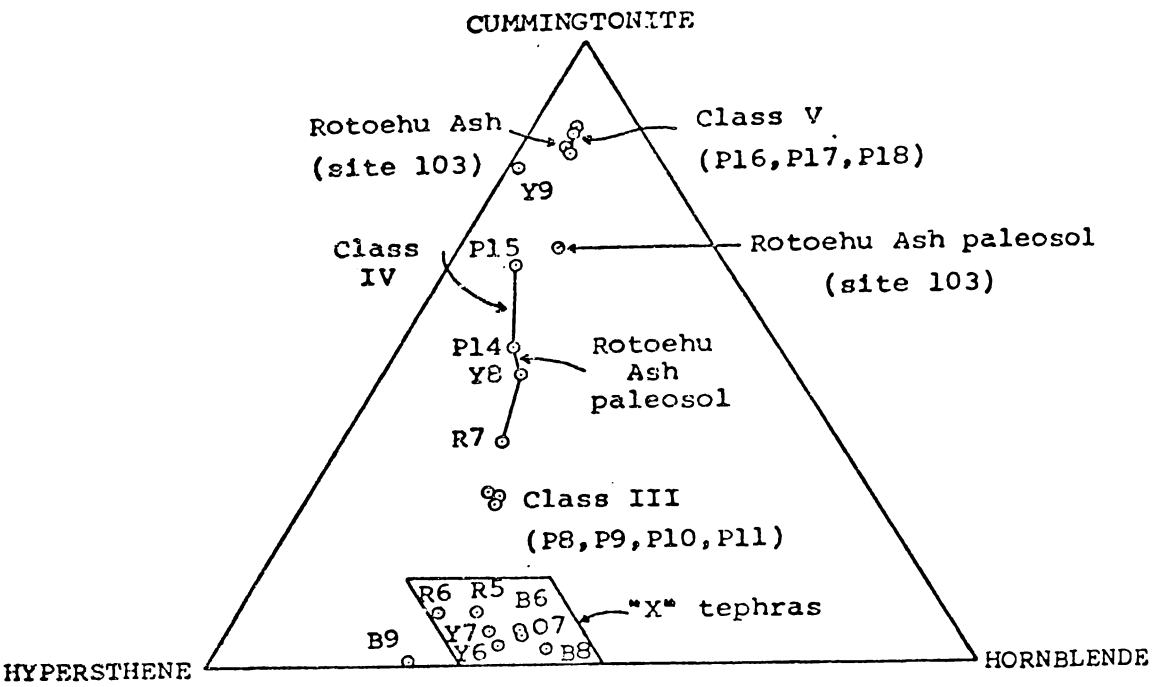


B

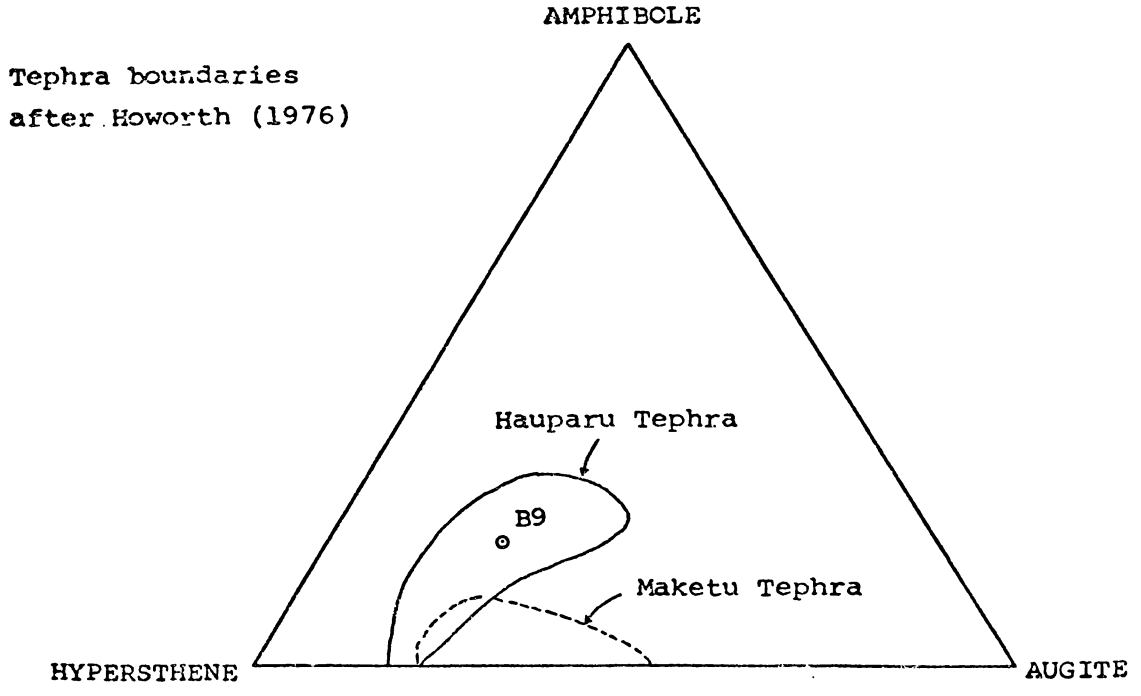


FIGURE 5.18 : Ferromagnesian mineral assemblages of tephras from the Katikati region and Pukekauri Rd.
A : "X" tephras, Class III samples, and Rotoehu Ash.
B : Characterisation of sample B9 (Hauparu Tephra).

younger, hypersthene and hornblende-bearing tephra, as demonstrated by electron microprobe analysis of titanomagnetite grains from field class IV (see Fig. 3.17 p. 89 ).

The titanomagnetites from the Rotoehu Ash and its paleosol have slightly lower Ti/Mn and Ti/V ratios than the corresponding samples from field classes V and IV (samples R8 and Y9, and R7 and Y8 in Fig. 5.19).

The high proportion of cummingtonite in the ferromagnesian mineral assemblage and titanomagnetite chemistry of the Rotoehu Ash and paleosol, confirm its correlation with field classes IV and V on the Coromandel Peninsula.

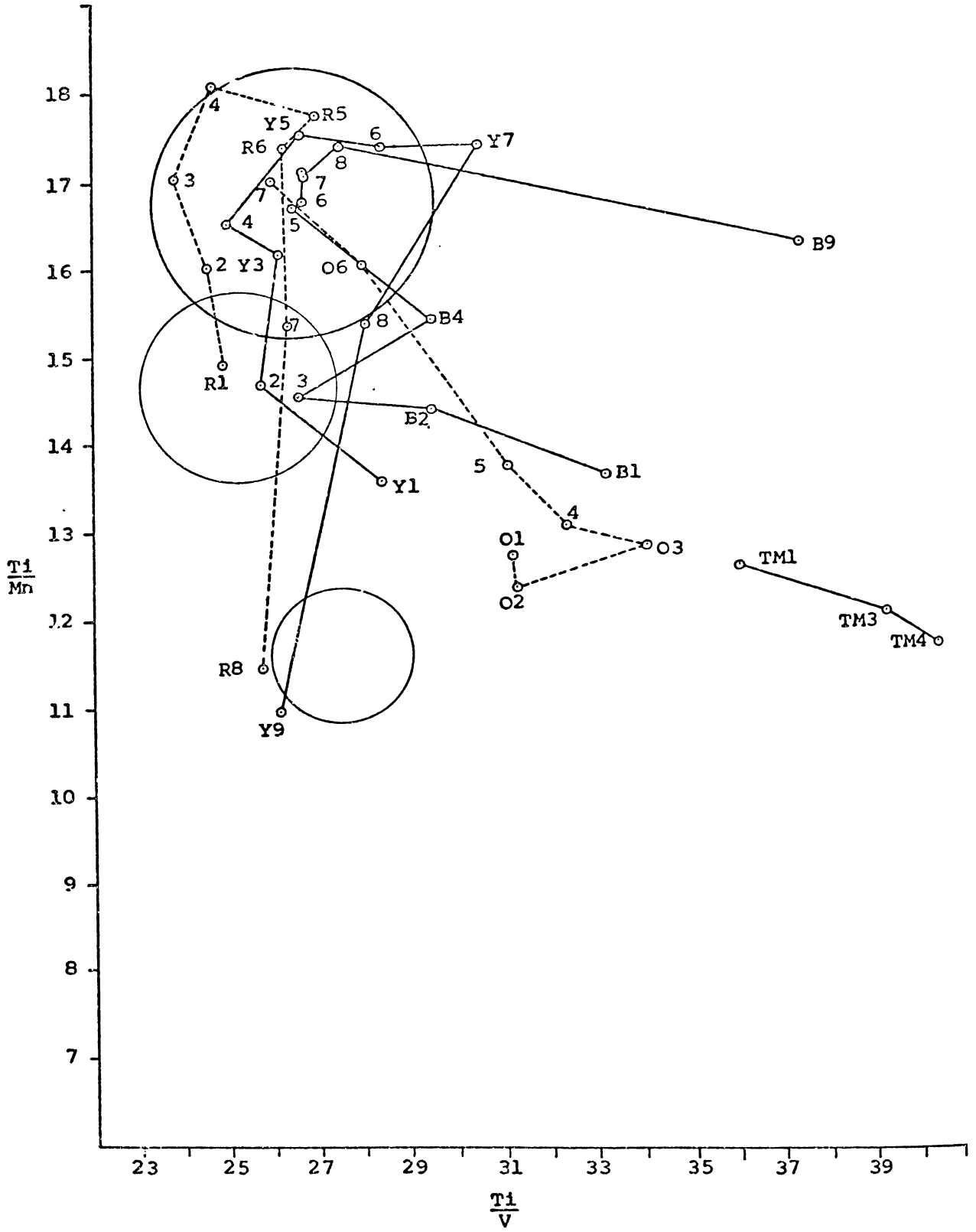


FIGURE 5.19 : Ratios of count rates of Ti, Mn and V from titanomagnetites extracted from the Holocene and Late Pleistocene tephras in the Katikati region. Samples are from Reas Rd (R1 to R8); Youngson Rd(Y1 to Y9); Bethlehem(B1 to B9); Ohauiti Rd(O1 to O7); and Te Matai Rd(TM1,TM3,TM4). Circles encompass all samples from the Coromandel Peninsula sites for field classes II,III and V.

## (D) DISCUSSION

### 1. Field class I

Correlation between Pukekauri Rd and Te Matai Rd lends support to the identification of Taupo Pumice and Kaharoa Tephra in class I. Whereas the former is a glass-rich coarse ash containing hypersthene and hornblende in the ferromagnesian mineral assemblage, the Taupo Pumice is represented by hypersthene-rich white pumiceous lapilli. The Whangamata Tephra, discussed below, also contributes to class I.

### 2. Field class II

The hypersthene-rich Mamaku Ash mixes with the cummingtonite-bearing Rotoma Ash between Maniatutu and Te Matai Rds and, as the mixed deposit thins north of Te Matai Rd, is supplemented by per-alkaline material from the Whangamata Tephra which thickens towards Whangamata.

### 3. Field class III

Three lines of evidence have shown that the "X" tephras in the Katikati region do not correlate with the Coromandel class III deposits; viz. the mean grain size, the proportion of cummingtonite in the ferromagnesian mineral assemblage and the titanomagnetite element chemistry. However, because of the comparable thicknesses of the "X" tephras at Reas Rd and the class III deposit at Pukekauri Rd (Fig. 5.11), the "X" tephras must be represented at Pukekauri Rd, contributing to the class III deposit in such a manner as to make their properties (as exhibited in the Katikati region) unrecognisable.

It is concluded from the mineralogical and chemical characteristics of the "X" tephras in the Katikati region and the class III deposit at Pukekauri Rd, that the "X" tephras are present in field class III in the form of a mixture with older tephras.

In the conclusions of Chapter 4 a model of tephra deposition and modification for field classes III to V was presented (Figs. 4.24 and 4.25, pp.157,9). In that model it was proposed that a hypersthene-hornblende dominated tephra (termed Tephra A) mixed with the class V tephra (Rotoehu Ash) to produce class IV, which was itself mixed with a second tephra (Tephra B), also hypersthene and hornblende-rich, to form class III. The characteristics of the "X" tephras and Hauparu Tephra are compared with tephras A and B in Fig. 5.20 and fit the model closely. It can therefore be concluded that field class V is represented solely by the Rotoehu Ash, field class IV by two mixed tephras (the Hauparu Tephra and the Rotoehu Ash), and field class III by three mixed tephras (the "X" tephras, the Hauparu Tephra and the Rotoehu Ash). Possible mechanisms of mixing of the "X", Hauparu and Rotoehu tephras, and the reason for the abruptness of the change from recognisable "X" tephras south of Katikati to the mixed class III deposit at Pukekauri Rd and sites further north are discussed below.

4. Field classes IV and V

Field classes IV and V correlate with the Rotoehu Ash and its paleosol with the latter diluted by the hypersthene-bearing Hauparu Tephra.

Table 5.9 lists the tephras present at the Pukekauri Rd reference site, and identifies the unknown Coromandel tephras in Figs. 3.18 p.96 , 4.24 p.157 , and 4.25 p.159 .

TABLE 5.9 : Identification of the unknown tephras presented in Chapters 3 and 4 of this thesis

| Tephra | Identification of unknown tephras in the Figures as indicated below | |
|---|---|---|
| | Fig. 3.18 p.96 | Fig. 4.24 p.157 Fig. 4.25 p.159 |
| Kaharoa Ash | Tephra J | |
| Taupo Pumice | Tephra I | |
| Whangamata Tephra | Tephra F | |
| Mamaku Ash | Tephra G | |
| Rotoma Ash | Tephra H | |
| "X" tephras | Tephra E | Tephra B |
| Hauparu Tephra | Tephra C | Tephra A |
| Rotoehu Ash | Tephras A,B and D | |

## 5. Possible mechanisms of mixing of thinly bedded tephras

Between Bethlehem and Waihi each of the "X", Hauparu, and Rotoehu tephras become finer grained and thin substantially (Fig. 5.22, p.222). In addition the "X" tephras, which occur as a discrete unit in the Katikati region, mix with the Hauparu and Rotoehu tephras to form the Silty bed (class III) at all sites north of Reas Rd. The sudden transition between the recognisable "X" tephras south of Katikati and the composite class III deposits at Pukekauri Rd suggests that the mixing processes operating north of Katikati are either associated with tephra thicknesses and depths of burial, or with climatic controls.

FIGURE 5.20 : Ferromagnesian mineralogy and titanomagnetite compositions for field classes III to V, and calculated characteristics of component tephras A and B, compared with the proposed correlatives, the Hauparu Tephra and "X" tephras respectively. (See Fig. 4.26 p.161).

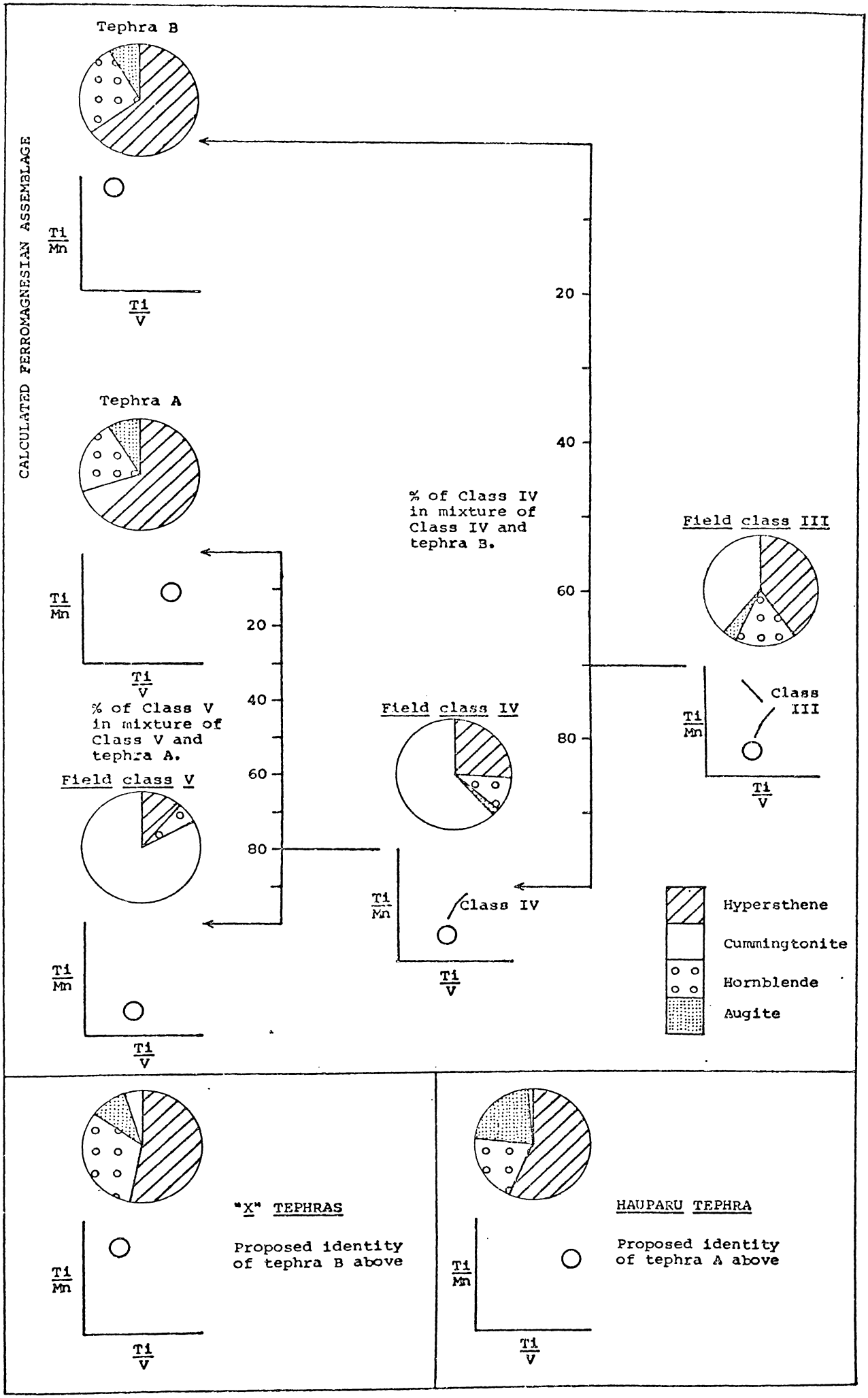
CALCULATED FERROMAGNESIAN ASSEMBLAGE
Tephra B
Tephra A
Ti/Mn
Ti/V
20
40
60
80
% of Class IV in mixture of Class IV and tephra B.
% of Class V in mixture of Class V and tephra A.
Field class III
Field class IV
Field class V
Class III
Class IV
Hypersthene
Cummingtonite
Hornblende
Augite
"X" TEPHRAS
Proposed identity of tephra B above
HAUPARU TEPHRA
Proposed identity of tephra A above

(a) The influence of tephra thicknesses on the mixing of tephras.

Tephra thicknesses might cause the change in character of the "X" tephras north of Reas Rd in two main ways. First, the mixing mechanism may only be effective in shallow depths. Where the "X" tephras are thick (south of Reas Rd), the mixing would be confined to the "X" tephras; where they are thinner (north of Reas Rd), the Hauparu and Rotoehu tephras would also be included. However, as Fig. 5.22 shows, there is very little difference in the combined thicknesses of the "X", Hauparu, and Rotoehu tephras between Reas Rd and region 6 (the Waihi Basin), which suggests that this factor alone is inadequate to explain the sudden mixing of the three tephras.

The second way in which tephra deposits may have contributed to the formation of the mixed Silty bed is through its effect on vegetation. If vegetation and/or its associated fauna are the mixing agents, then the area between Reas Rd and Pukekauri Rd might correspond to the boundary between complete destruction of the vegetation by the "X" tephras to the south and only partial destruction to the north. The "X" tephras may therefore have been preserved as a discrete layer south of Reas Rd but incorporated into the Hauparu and Rotoehu tephras at Pukekauri Rd under the influence of the preserved vegetation. Vucetich and Pullar (1963) estimated that about 45 cm of cold tephra are required to completely destroy vegetation. This estimate is supported by Nicholls (1963) who concluded that a hail of volcanic lapilli will have little effect upon indigenous high forest unless it is .. " more than a few feet deep or hot enough to kill vegetation outright " (p. 64). The "X" tephras decrease in thickness from 89 cm at Bethlehem to 55 cm at

Reas Rd. If Vucetich and Pullar's estimate is approximately correct, then Reas Rd approximates the boundary between total destruction (to the south) and partial destruction (to the north) of vegetation by the eruption. This hypothesis is dependent upon the "X" tephras having a minimum thickness of about 45 cm at Reas Rd and is not applicable if they are composed of two or more tephras of lesser thickness. Little more can be added in support or denial of this hypothesis as the number of tephras comprising the "X" tephras is at present unresolved.

(b) The influence of climate on the mixing of tephras

Climate may exert an indirect influence on the tephra stratigraphy through its control on the distribution and type of vegetation. Each of the Climap Report (1976), Luz (1977), McGlone et al. (1978) and Wilson (1978) have suggested that while temperatures in the southern half of the North Island and in the South Island dropped by about 6 $^{o}$C during glacial times, the temperatures in the northern half of the North Island were depressed by no more than 4 $^{o}$C, with a steep latitudinal temperature gradient between 37$^{o}$-38 $^{o}$S. The region between 37$^{o}$-38$^{o}$S has been climatically sensitive to flora in the past, with many species being limited to north of this latitudinal range. . Thus Allan (1961) lists:

Kauri (Agathis australis) - found from North Cape (34$^{o}$ 22' S lat.) to Maketu/Kawhia (38 $^{o}$S lat.)

Taraire (Beilschmiedia tarairi) - found from North Cape (34$^{o}$ 22' S lat.) to East Cape/Raglan (37$^{o}$ 50' S lat.)

Litsea calicaris - found from North Cape (34$^{o}$ 22' S lat.) to 38 $^{o}$S lat.

Tawari (Ixerba brexioides) - Hokianga (35$^{o}$ 30'S lat.) to a little south of 38 $^{o}$S lat.

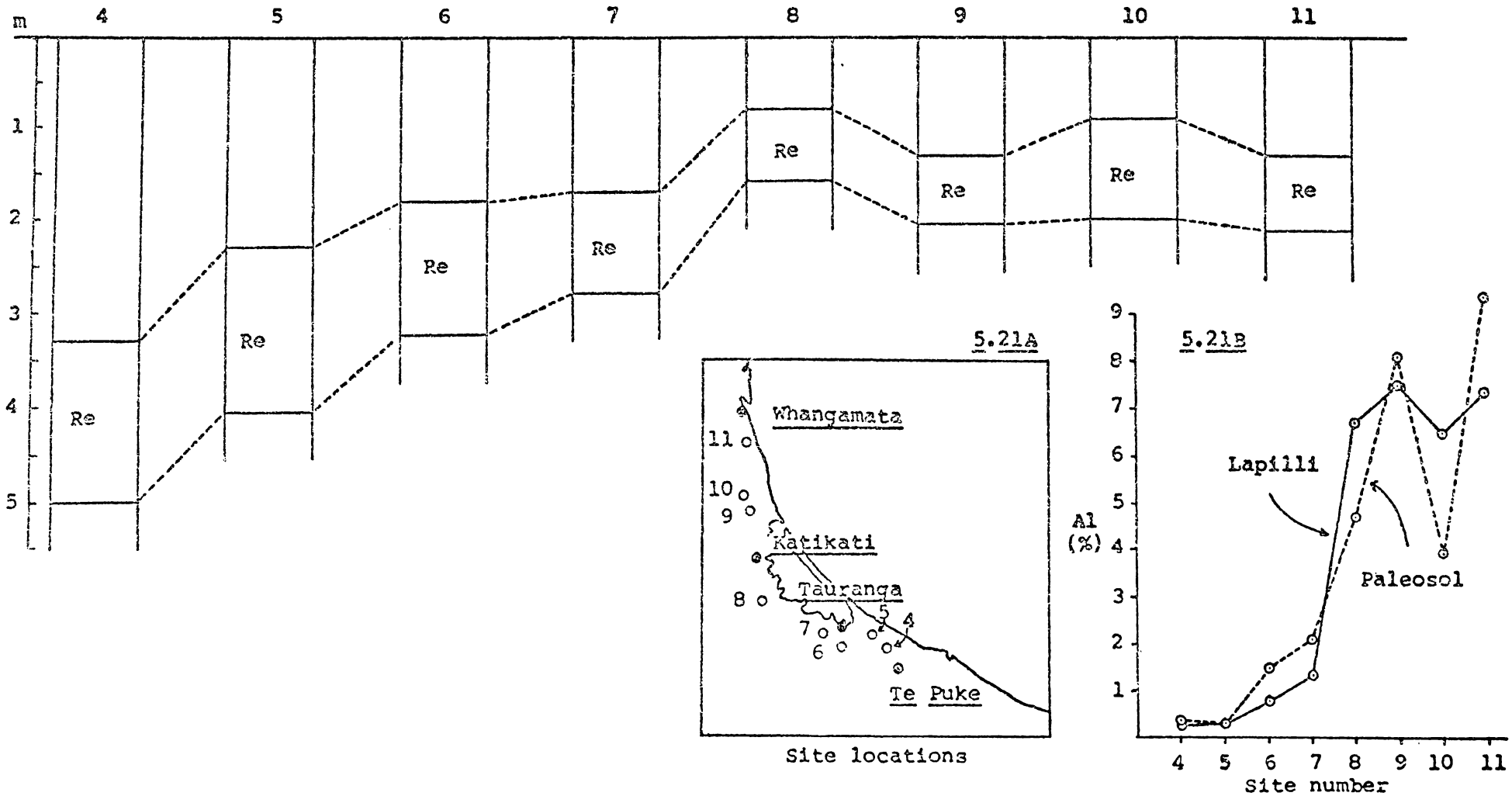


FIGURE 5.21: Thickness of the Rotoehu Ash (paleosol and lapilli) and overlying tephras, and the percentage Tamm extractable Al for the Rotoehu Ash at 8 sites between Te Puke and Whangamata. Site numbers and all data from Birrell et al.(1977).

Monoao (Dacrydium kirkii) - found from Hokianga (35° 30' S lat.) to Auckland City (lat. 37 °S)

Toatoa (Phyllocladus glaucus) - found from lat. 35 °S to lat. 38 °S.

In addition, Wilson (1978) estimates that the southern limit of continuous forest during glacial times was approximately 37° 30' (Fig. 5.23 p. 222).

Birrell et al. (1977) - Fig. 5.21, determined the Tamm-extractable Al, Fe and Si in the Rotoehu Ash and its paleosol at eight sites between Te Puke and Whangamata (Fig. 5.21A) in order to evaluate the degree of weathering that the tephra had undergone at each site. They found a sharp rise in the element concentrations north of site 7 (e.g. % Al in Fig. 5.21B) and considered sites 8 to 11 to be more weathered than the sites further south. They attributed the stronger weathering in the more northern sites to a prolonged absence of cover deposits and the influence of past warmer climates. The coincidence of a stronger weathering regime as indicated by the Rotoehu Ash with a change in the effectiveness of mixing processes in the Katikati region (Fig. 5.23), suggests that climate or more likely vegetation may be responsible for the mixing processes.

Little is known about the Late Quaternary vegetation patterns on the Coromandel Peninsula, but considering the temperature changes noted above and the ameliorating maritime influences it is most likely that a complete forest cover characterised the region (McGlone 1973). The Late Quaternary vegetation patterns of the Katikati-Tauranga region are also unknown. McGlone et al. (1978) examined pollen from three peat deposits in the Hamilton Basin and suggested

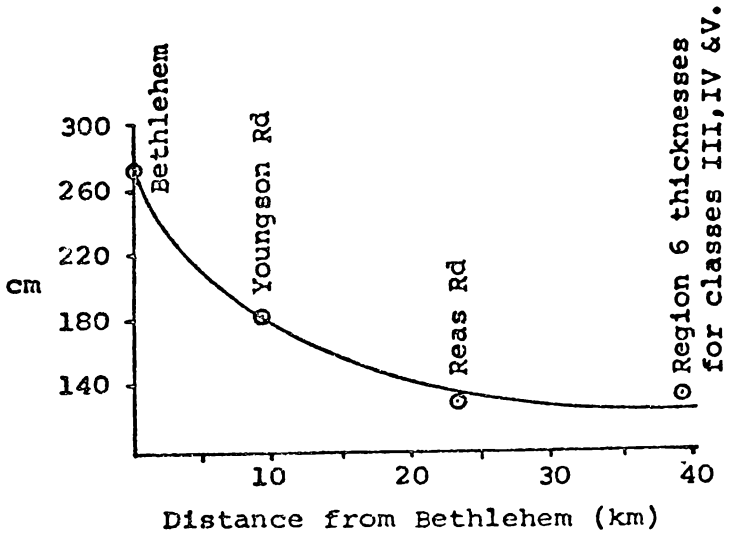


FIGURE 5.22 : Variation in the total thickness of the "X", Hauparu, and Rotoehu tephras at Bethlehem, Youngson Rd, Reas Rd, and the Waihi plain, with the latter represented by the Region 6 thicknesses of classes III to V (see Figs. 2.10 and 2.15, p. 29 , and p. 39 .

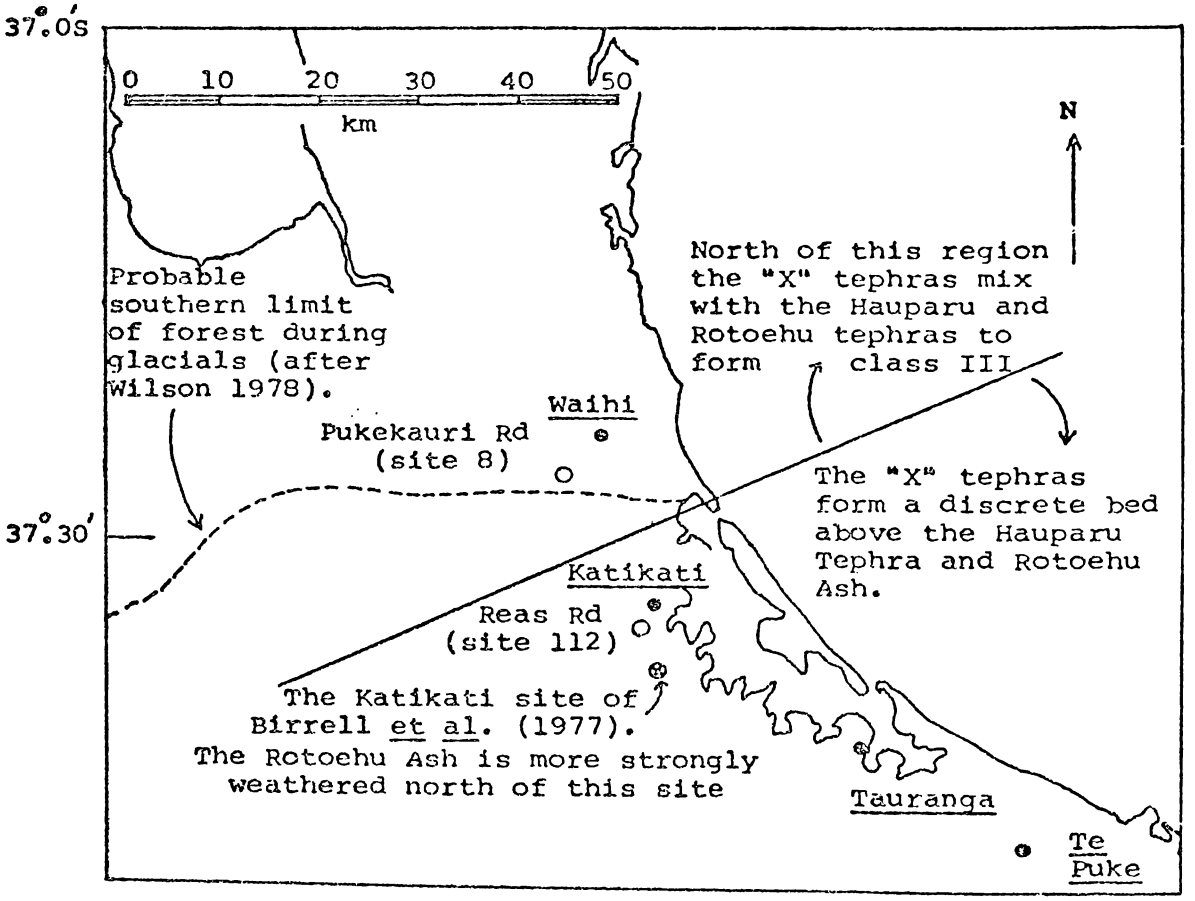


FIGURE 5.23: Summary of the vegetational and geological changes occurring in the region between Katikati and Pukekauri Rd.

that between 20,000 and 16,000 years B.P. this basin was dominated by scrub, grassland and swamp with only small areas of forest confined to the surrounding stable hills. They attributed the lack of forest in the Hamilton Basin to a climatic regime characterised by cold, dry winter months and having high intensity cyclonic rain-storms in summer, with droughts, severe frosts and high winds. Forest growth was restricted to sheltered areas. The similarity in latitude between the Hamilton Basin and the Katikati-Tauranga region lends some support to the possibility that the continuous forest cover of the Coromandel Peninsula may have changed into scrubland south of the Pukekauri Rd site.

The processes causing the mixing of the "X", Hauparu, and Rotoehu tephras on the Coromandel Peninsula may therefore be connected with a forest vegetation and associated fauna. Dudas and Harward (1975) suggested that the uprooting of trees was a major mechanism for mixing ash soils in the forested areas they examined. However at their sites a microrelief of mounds and pits usually occurred; no such evidence exists within the Silty bed on the Coromandel Peninsula. It is therefore doubtful whether such a mechanism has operated in this case.

Other possible mixing agents include soil fauna, and movement of soil particles within the vertical and horizontal cracks that are characteristic of the subsoils of allophane-rich yellow brown loams (N.Z. Soil Bureau 1968; Plate 33, Vol. 2).

There is presently insufficient evidence to define more closely the environment or mechanism by which the "X", Hauparu, and Rotoehu tephras have combined to form the Silty bed on the Coromandel Peninsula.

However a change in vegetation cover and associated fauna from forest to scrubland between Pukekauri Rd and Reas Rd is considered to be the most likely explanation.

## E. HISTORY OF TEPHRA DEPOSITION ON THE COROMANDEL PENINSULA IN THE LATE QUATERNARY

The Late Quaternary tephra sequence on the Coromandel Peninsula consists of at least nine separate tephras whose names and stratigraphic relationships are compared with the terminology of previous workers in Table 5.10.

TABLE 5.10 : Tephra stratigraphy of Late Quaternary tephras on the Coromandel Peninsula as established by previous workers and this thesis

| McCraw (1975a and b) | Birrell *et al.* (1977) | Pullar *et al.* (1977) | This thesis |
|---|---|---|---|
| Taupo Pumice | Whangamata Ash | Kaharoa Ash | Kaharoa Tephra and Taupo Pumice |
| | | Taupo Pumice | |
| Whangamata Ash | | | Whangamata Tephra, Mamaku Ash and Rotoma Ash |
| Whangamata Lapilli | | | |
| friable silt loam | ?Okareka Ash | | "X" tephras, Hauparu Tephra and Rotoehu Ash |
| "Lumpy bed" | Rotoehu Ash (paleosol) | | Hauparu Tephra and Rotoehu Ash |
| Compact fine sand | Rotoehu Ash | | Rotoehu Ash |

Approximately 40,000 years B.P. Mt Haroharo in the Rotorua district (Fig. 5.10 p.191) erupted in a series of pulses of varying magnitude depositing shower-bedded ash and lapilli of the Rotoehu Ash over an area of more than 50,000 $km^2$, including the full length of the Coromandel Peninsula. Soil formation on the Rotoehu Ash was eventuallyinterrupted, after about 10,000 years, when the Hauparu Tephra derived from a vent close to the northern shores of Lake Rotoehu was deposited in the Bay of Plenty and Coromandel regions. South of Bethlehem this tephra was sufficiently thick to bury the Rotoehu soil, but further north it became incorporated into the soil and is not represented as a separate tephra.

During or soon after the peak of the last major cold period (20,000-18,000 years B.P.), at least two fine grained tephras erupted from either the Taupo or Okataina Volcanic Centres (Fig. 1.2 p.5) depositing material over a large part of the Central Volcanic Region and on the Coromandel Peninsula at least as far north as Whitianga. The tephras, which are unidentified and termed the "X" tephras in the Katikati region, include representatives of older eruptions (i.e. approximately 20,000 years B.P. - e.g. the Okareka, Te Rere or Kawakawa tephras), and younger eruptions (i.e. approximately 14,000-11,000 years B.P. - e.g. Rotorua or Waiohau tephras). South of Katikati these tephras are preserved as a discrete bed above the Hauparu Tephra. Further north however, they are intimately mixed with the Hauparu Tephra and the upper parts of the Rotoehu Ash, forming the Silty bed on the Coromandel Peninsula.

Between 9,000 and 7,000 years B.P., under conditions of ameliorating climate, the Mamaku Ash and Rotoma Ash were erupted from

the Okataina Volcanic Centre and approximately 30 cm of tephra was deposited over the southern half of the Coromandel Peninsula. About 1,000 years later, the peralkaline Whangamata Tephra was erupted from Mayor Island and deposited tephra in two lobes, a coarse lobe of pumiceous ash and lapilli up to 60 cm thick extending between Whangamata and Thames on the Coromandel Peninsula, and a fine ash lobe extending to the south and southwest of the Peninsula, in the Bay of Plenty and Waikato regions. As the Whangamata, Mamaku and Rotoma tephras were deposited within a relatively short period of time (c. 3,000 years) and occur within the soil forming zone, the tephras on the Peninsula were thoroughly mixed by soil forming processes, but not incorporated into class III below.

Although the distal portion of many post-Whangamata tephras probably fell over the Coromandel Peninsula, they are not recognisable except for the conspicuous pumiceous lapilli of the Taupo Pumice eruption (1,819 years B.P.), and the coarse pumiceous ash of the Kaharoa Tephra (930 years B.P.).

# POSSIBLE FUTURE WORK

The results of this study suggest several profitable lines of research that might be considered for future investigations.

1. The effectiveness of vegetation and soil fauna in translocating inorganic material within the soil forming regime.
2. The tephra stratigraphy of the Bay of Plenty region, including identification of the "X" tephras.
3. Investigation of the Holocene tephra stratigraphy within the Hamilton Basin by detailed sampling of peat lakes.
4. Examination of sediment cores from the Hauraki Gulf and Pacific Ocean (between Whangamata and Mayor Island), with a purpose of elucidating tephra stratigraphy and sedimentation patterns of the ocean adjacent to the Coromandel Peninsula.

# REFERENCES

ALLAN, H.H. 1961: Flora of New Zealand. Volume 1. Govt Printer, Wellington, New Zealand. 1085 p.

BAUMGART, I.L. 1954: Some ash showers of the Central North Island. N.Z. Journal of Science and Technology 35(6): 456-68.

BIRRELL, K.S. 1974: Effect of pretreatment with hydrogen peroxide on composition of clay fractions extracted from organic horizons of andosols. Transactions 10th International Congress Soil Science VII: 179-87.

BIRRELL, K.S.; PULLAR, W.A.; SEARLE, P.L. 1977: Weathering of Rotoehu Ash in the Bay of Plenty district. N.Z. Journal of Science 20: 303-10.

BOND, A.; SPARKS, R.S.J. 1976: The Minoan eruption of Santorini, Greece. Journal of the Geological Society of London 132: 1-16.

BORCHARDT, G.A.; HARWARD, M.E. 1971: Trace element correlation of volcanic ash soils. Soils Science Society of America. Proceedings 35: 626-30.

BRITISH STANDARDS INSTITUTION 1967: "Methods of testing soils - for civil engineering purposes". British Standard 1377. 234 p.

BUCK, M.D. 1978: Pyroclastic deposits on Mayor Island, Bay of Plenty, New Zealand. (Unpublished M Sc thesis lodged in the Library, University of Waikato, Hamilton, New Zealand).

CARMICHAEL, I.S.E. 1963: The occurrence of magnesian pyroxenes and magnetite in porphyritic acid glasses. Mineralogical Magazine 33(16): 394-403.

———————— 1967: The iron-titanium oxides of salic volcanic rocks and their associated ferromagnesian silicates. Contributions to Mineralogy and Petrology 14: 36-64.

CARMICHAEL, I.S.E.; TURNER, F.J.; VERHOOGEN, J. 1974: "Igneous Petrology". McGraw-Hill. 739 p.

CLIMAP PROJECT MEMBERS 1976: The surface of the ice-age Earth. Science 191: 1131-7.

COLE, J.W. 1970: Description and correlation of Holocene volcanic formations in the Tarawera-Rerewhakaaitu region. Transactions of the Royal Society of N.Z. (Earth Sciences) 8(7): 93-108.

———— 1972: Distribution of high-alumina basalts in the Taupo Volcanic Zone. Geology Department, Victoria University of Wellington, Publication No.1.

———— 1976: Rhyolitic volcanism on Mt Tarawera. Pp 19-21 in Nathan, S. (ed.) Volcanic and geothermal geology of the Central North Island, New Zealand. 25th International Geological Congress - Excursion Guide No. 55A and 56C.

CORTES, A.; FRANZMEIER, D.P. 1972: Weathering of Primary minerals in volcanic ash-derived soils of the Central Cordillera of Colombia. Geoderma 8(2/3): 165-76.

DAVOREN, A. 1978: A survey of New Zealand peat resources. Water and Soil Technical Publication 14 157 pp.

DUDAS, M.J.; HARWARD, M.E. 1975: Inherited and detrital 2:1 type phyllosilicates in soils developed from Mazama Ash. Soil Science Society of America. Proceedings 39: 571-7.

EATON, G.P. 1964: Windborne volcanic ash: A possible index to polar wandering. Journal of Geology 72(1): 1-35.

EDWARDS, A.P.; BREMNER, J.M. 1967: Dispersion of soil particles by sonic vibration. Journal of Soil Science 18(1): 47-63.

EWART, A. 1963: Petrology and petrogenesis of the Quaternary pumice ash in the Taupo area, New Zealand. Journal of Petrology 4(3): 392-431.

———— 1965: Mineralogy and petrogenesis of the Whakamaru Ignimbrite in the Maraetai area of the Taupo Volcanic Zone, New Zealand. N.Z. Journal of Geology and Geophysics 8(4): 611-679.

———— 1966: Review of mineralogy and chemistry of the acidic volcanic rocks of Taupo Volcanic Zone, New Zealand. Bulletin Volcanologique 29: 147-72.

———— 1968: The petrography of the Central North Island rhyolitic lavas. Part 2 - Regional petrography including notes on associated ash-flow pumice deposits. N.Z. Journal of Geology and Geophysics 11(2): 478-545.

———— 1971: Notes on the chemistry of ferromagnesian phenocrysts from selected volcanic rocks, Central Volcanic Region. N.Z. Journal of Geology and Geophysics 14(2): 323-40.

EWART, A.; GREEN, D.C.; CARMICHAEL, I.S.E.; BROWN, F.H. 1971: Voluminous low temperature rhyolitic magmas in New Zealand. Contributions to Mineralogy and Petrology 33: 128-44.

EWART, A.; TAYLOR, S.R.; CAPP, A.C. 1968: Geochemistry of the pantellerites of Mayor Island, New Zealand. Contributions to Mineralogy and Petrology 17: 116-40.

FISHER, R.V. 1961: Proposed classification of volcaniclastic sediments and rocks. Geological Society of America Bulletin 72: 1409-1414.

———— 1964: Maximum size, median diameter, and sorting of tephra. Journal of Geophysical Research 69(2): 341-55.

———— 1966: Textural comparison of John Day Volcanic Siltstone with loess and volcanic ash. Journal of Sedimentary Petrology 36(3): 706-718.

FOLK, R.L. 1966: A review of grain-size parameters. Sedimentology 6: 73-93.

———— 1968: "Petrology of Sedimentary Rocks". Hemphill's 170 p.

FOLK, R.L.; WARD, W.C. 1957: Brazos River Bar: A study in the significance of grain size parameters. Journal of Sedimentary Petrology 27(1): 3-26.

GEORGE, W.O. 1924: The relation of the physical properties of natural glasses to their chemical composition. Journal of Geology 32(5): 353-72.

GRANGE, L.I. 1931: Volcanic-ash showers. A geological reconnaissance of volcanic-ash showers of the central part of the North Island. The N.Z. Journal of Science and Technology 12(4): 228-40.

GRANT-TAYLOR, T.L.; RAFTER, T.A. 1962: New Zealand radiocarbon age measurements -5. N.Z. Journal of Geology and Geophysics 5: 331-59.

HEALY, J. 1964: Part 1 - Dating of the younger volcanic eruptions of the Taupo region. Pp 7-42 in "Stratigraphy and chronology of Late Quaternary volcanic ash in Taupo, Rotorua and Gisborne districts". N.Z. Geological Survey Bulletin n.s. 73.

HENDY, C.H.; WILSON, A.T. 1968: Paleoclimatic data from speleothems. Nature 219(5149): 48-51.

HODDER, A.P.W. 1974: The use of physical and chemical techniques in the identification of tephra in the North Island, New Zealand. (Unpublished Ph.D. thesis lodged in the Library, University of Waikato, Hamilton, New Zealand).

———— 1978: Refractive index and hydration of rhyolitic glass from Holocene tephras, North Island, New Zealand. N.Z. Journal of Geology and Geophysics 21: 155-66.

HODDER, A.P.W.; WILSON, A.T. 1976: Identification and correlation of thinly bedded tephra: The Tirau and Mairoa ashes. N.Z. Journal of Geology and Geophysics 19(5): 663-82.

HOWORTH, R. 1975: New formations of Late Pleistocene tephras from the Okataina Volcanic Centre, New Zealand. N.Z. Journal of Geology and Geophysics 18(5): 683-712.

———— 1976: Late Pleistocene tephras of the Taupo and Bay of Plenty regions. (Unpublished Ph.D. thesis lodged in the Library, Victoria University of Wellington, New Zealand).

HOWORTH, R.; RANKIN, P.C. 1975: Multi-element characterisation of glass shards from stratigraphically correlated rhyolitic tephra units. Chemical Geology 15: 239-50.

HUME, T.M. 1978: Clay petrology of Mesozoic to Recent sediments of Central Western North Island of New Zealand. (Unpublished Ph.D. thesis lodged in the Library, University of Waikato, Hamilton, New Zealand).

HUTTON, C.O. 1956: Re-examination of the mineral tuhualite. Mineralogical Magazine 31: 96-106.

INMAN, D.L. 1952: Measures for describing the size distribution of sediments. Journal of Sedimentary Petrology 22(3): 125-45.

JESSEN, M.R. 1977: Horotiu and Waihou silt loams - A comparative study. (Unpublished M.Sc. thesis lodged in the Library, University of Waikato, Hamilton, New Zealand).

JOWSEY, P.C. 1966: An improved peat sampler. The New Phytologist 65(2): 245-48.

KADDAH, M.T., 1974: The hydrometer method for detailed particle-size analysis: 1. Graphical interpretation of hydrometer readings and test of method. Soil Science 118(2): 102-8.

KIRKMAN, J.H. 1975: Clay mineralogy of some tephra beds of Rotorua area, North Island, New Zealand. N.Z. Soil News 23(4): 127-9.

KITTLEMAN, L.R. 1973: Mineralogy, correlation, and grain-size distributions of Mazama Tephra and other post-glacial pyroclastic layers, Pacific Northwest, Geological Society of America Bulletin 84: 2957-80.

KOHN, B.P. 1970: Identification of New Zealand tephra-layers by emission spectrographic analysis of their titanomagnetites. Lithos 3: 361-8.

———— 1973: Some studies of New Zealand Quaternary pyroclastic rocks. (Unpublished Ph.D. thesis lodged in the Library, Victoria University of Wellington, New Zealand).

KOHN, B.P.; GLASBY, G.P. 1978: Tephra distribution and sedimentation rates in the Bay of Plenty, New Zealand. N.Z. Journal of Geology and Geophysics 21(1): 49-70.

KRUMBEIN, W.C. 1936: Application for logarithmic moments to size frequency distribution of sediments. Journal of Sedimentary Petrology 6: 35-47.

KUNO, H.; ISHIKAWA, T.; KATSUI, Y.; YAGI, K.1 YAMASAKI, M.; TANEDA, S. 1964: Sorting of pumice and lithic fragments as a key to eruptive and emplacement mechanism. Japanese Journal of Geology and Geography 35: 223-8.

LIPMAN, P.W. 1971: Iron-titanium oxide phenocrysts in compositionally zoned ash-flow sheets from Southern Nevada. Journal of Geology 79: 438-56.

LOWE, D.J. (in prep.): Origin and composite nature of Late Quaternary airfall deposits, Hamilton Basin. (Unpublished M.Sc. thesis lodged in the Library, University of Waikato, Hamilton, New Zealand).

LUZ, B. 1977: Late Pleistocene paleoclimates of the South Pacific based on statistical analysis of planktonic foraminifers. Palaeogeography, Palaeoclimatology, Palaeoecology 22: 61-78.

MARSHALL, P. 1932: Notes on some volcanic rocks of the North Island, New Zealand. N.Z. Journal of Science and Technology 13: 198-202.

———— 1936: Geology of Mayor Island. Transactions of the Royal Society N.Z. 66: 337-45.

McCRAW, J.D. 1968: Soils. Pp 21-39 in "Land Inventory Survey, Ohinemuri County". N.Z. Department of Lands and Survey.

———— 1975a: Soil. Pp 30-38 in "Land Inventory Survey, Coromandel-Thames Counties". N.Z. Department of Lands and Survey.

———— 1975b: Quaternary airfall deposits of New Zealand. Pp 35-44 in Suggate, R.P.; Creswell, M.M. (eds). "Quaternary Studies (INQUA)". Royal Society of N.Z. Bulletin 13.

McCRAW, J.D.; WHITTON, J.S. 1971: Soils of Mayor Island, Bay of Plenty, New Zealand. N.Z. Journal of Science 14(4): 1009-25.

McGLONE, M.S. 1973: Vegetation changes in the Otiran and Aranuian. International Union for Quaternary Research, IX International Congress. Pp 13-19.

McGLONE, M.S.; NELSON, C.S.; HUME, T.M. 1978: Palynology, age and environmental significance of some peat beds in the Upper Pleistocene Hinuera Formation, South Auckland, New Zealand. Journal of the Royal Society of N.Z. 8(4): 385-93.

NASMITH, H.; MATHEWS, W.H.; ROUSE, G.E. 1967: Bridge River Ash and some other Recent ash beds in British Columbia. Canadian Journal of Earth Sciences 4: 163-70.

NATHAN, S. 1976: Outline of geology. Pp 10-14 in Nathan, S. (ed) Volcanic and geothermal geology of the Central North Island, New Zealand. 25th International Geological Congress-Excursion guide No. 55A and 56C.

NELSON, C.S.; COCHRANE, R.H.A. 1970: A rapid X-ray method for the quantitative determination of selected minerals in fine-grained and altered rocks. Tane 16: 151-62.

NEW ZEALAND METEOROLOGICAL SERVICE. 1966: Summaries of climatological observations at New Zealand stations to 1960. N.Z. Meteorological Service Miscellaneous Publication 122. 59 p.

NEW ZEALAND SOIL BUREAU. 1968: Soils of New Zealand. Part 2 N.Z. Soil Bureau Bulletin 26(2): 39-49.

NICHOLLS, J.L. 1963: Vulcanicity and indigenous vegetation in the Rotorua district. Proceedings of the N.Z. Ecological Society 10: 58-65.

NICHOLLS, J.; CARMICHAEL, J.S.E. 1969: Peralkaline acid liquids: A petrological study. Contributions to Mineralogy and Petrology 20: 268-94.

NORRISH, K.; HUTTON, J.T. 1969: An accurate X-ray spectrographic method for the analysis of a wide range of geological samples. Geochimica et Cosmochimica Acta 33: 431-53.

PRYOR, W.A.; HESTOR, N.C. 1969: X-ray diffraction analysis of heavy minerals. Journal of Sedimentary Petrology 39: 1384-9.

PULLAR, W.A. 1967: Volcanic ash beds in the Waikato District. Earth Science Journal 1(1): 17-36.

PULLAR, W.A.; BIRRELL, K.S. 1973: Age and distribution of Late Quaternary Pyroclastic and associated cover deposits of the Rotorua and Taupo area, North Island, New Zealand. N.Z. Soil Survey Report 1.

PULLAR, W.A.; BIRRELL, K.S.; HEINE, J.C. 1973: Named tephras and tephra formations occurring in the Central North Island, with notes on derived soils and buried paleosols. N.Z. Journal of Geology and Geophysics 16(3): 498-518.

PULLAR, W.A.; HEINE, J.C. 1971: Ages, inferred from $^{14}C$ dates, of some tephra and other deposits from Rotorua, Taupo, Bay of Plenty, Gisborne and Hawke's Bay Districts. Radiocarbon Users Conference, Wellington, 1971: 117-38.

PULLAR, W.A.; KOHN, B.P.; COX, J.E. 1977: Air-fall Kaharoa Ash and Taupo Pumice, and sea-rafted Loisels Pumice, Taupo Pumice, and Leigh Pumice in northern and eastern parts of the North Island, New Zealand. N.Z. Journal of Geology and Geophysics 20(4): 697-717.

RANKIN, P.C. 1973: Correlation of volcanic glasses in tephras and soils using micro-element compositions. N.Z. Journal of Geology and Geophysics 16(3): 637-41.

RIGG, G.B.; GOULD, H.R. 1957: Age of Glacier Peak eruption and chronology of post-glacial peat deposits in Washington and surrounding areas. American Journal of Science 255: 341-63.

ROSS, C.S.; SMITH, R.L. 1955: Water and other volatiles in volcanic glasses. American Mineralogist 40: 1071-89.

---------- 1961: Ash-flow tuffs: their origin, geologic relations and identification. U.S. Geological Survey Professional Paper 366.

SALTER, R.T. 1979: A pedological study of the Kauroa Ash Formation at Woodstock. (Unpublished M.Sc. thesis lodged in the Library, University of Waikato, Hamilton, New Zealand).

SELBY, M.J.; PULLAR, W.A.; McCRAW, J.D. 1971: The age of Quaternary surfaces at Waihi Beach. Earth Science Journal 5(2): 106-12.

SINGER, M.; UGOLINI, F.C.; ZACHARA, J. 1978: In situ study of podzolization on tephra and bedrock. Journal of Soil Science of America 42: 105-11.

SKINNER, D.N.B. 1976: Sheet N40 and part sheets N35, N36 and N39 Northern Coromandel (1st edition). "Geological map of New Zealand 1:63 360" Map (1 sheet) and notes (28 p.). N.Z. Department of Scientific and Industrial Research, Wellington.

SMITH, D.G.W.; WESTGATE, J.A. 1969: Electron probe technique for characterising pyroclastic deposits. Earth and Planetary Science Letters 5: 313-9.

SMITH, H.W.; Okazaki, R.; KNOWLES, C.R. 1977a: Electron microprobe data for tephra attributed to Glacier Peak, Washington. Quaternary Research 7: 197-206.

1977b: Electron microprobe analysis of glass shards from tephra assigned to Set W, Mount St Helens, Washington. Quaternary Research 7: 207-17.

SMITH, J.V.; GAY, P. 1958: The powder patterns and lattice parameters of plagioclase feldspars. II. Mineralogical Magazine 31(240): 744-62.

STEEN, V.C.; FRYXELL, R. 1965: Mazama and Glacier Peak pumice glass: uniformity of refractive index after weathering. Science 150: 878-80.

TAYLOR, N.H. 1933: Soil processes in volcanic ash-beds. The volcanic ash-beds of the northern King Country and their secondary alumina minerals. N.Z. Journal of Science and Technology 14(4): 193-202.

———— 1953: The soil pattern. Pp 11-12 in Baylis, G.T.S. (Chairman) "The ecological significance of the Central North Island ash showers". Report of second annual meeting of N.Z. Ecological Society.

TAYLOR, N.H.; POHLEN, I.J. 1962: Soil Survey Method. N.Z. Soil Bureau Bulletin 25. 242 p.

THORARINSSON, S. 1954: II, 3. The tephra-fall from Hekla on March 29th, 1947: Pp 1-68 in Einarsson, T.; Kjartansson, G.; Thorarinsson, S. (eds) "The eruption of Hekla, 1947-48". Societas Scientiarum Islandica, Reykjavik.

TOPPING, W.W. 1972: Burrell lapilli eruptives, Mount Egmont, New Zealand. N.Z. Journal of Geology and Geophysics 15(3): 476-90.

TOPPING, W.W.; KOHN, B.P. 1973: Rhyolitic tephra marker beds in the Tongariro area, North Island, New Zealand. N.Z. Journal of Geology and Geophysics 16(3): 375-95.

TUTTLE, O.F.; BOWEN, N.L. 1958: Origin of granite in the light of experimental studies in the system $NaAlSi_3O_8$ - $KAlSi_3O_8$ - $SiO_2$ - $H_2O$. Geological Society of America Memoir 74.

VAN DER PLAS, L.; TOBI, A.C. 1965: A chart for judging the reliability of point counting results. American Journal of Science 263: 87-90.

VLADIMIROV, V.YE. 1968: Study of the effect of acoustic vibrations on the physicochemical properties of a soil suspension. Soviet Soil Science 5: 654-59.

VUCETICH, C.G.; PULLAR, W.A. 1963: Ash beds and soils in the Rotorua district. Proceedings of the New Zealand Ecological Society 10: 65-72.

---------- 1964: Part 2 - Stratigraphy of Holocene ash in the Rotorua and Gisborne districts. Pp 43-80 in "Stratigraphy and chronology of Late Quaternary volcanic ash, in Taupo, Rotorua and Gisborne districts". N.Z.Geological Survey Bulletin n.s. 73.

---------- 1969: Stratigraphy and chronology of Late Pleistocene volcanic ash beds in Central North Island, New Zealand. N.Z. Journal of Geology and Geophysics 12(4): 784-837.

WALKER, G.P.L. 1971: Grain-size characteristics of pyroclastic deposits. Journal of Geology 79: 696-714.

WALKER, G.P.L.; WILSON, L.; BOWELL, E.G. 1971: Explosive volcanic eruptions - I. The rate of fall of pyroclasts. Geophysical Journal of Royal Astronomical Society 22: 377-83.

WARD, W.T. 1967: Volcanic ash beds of the Lower Waikato Basin, North Island, New Zealand. N.Z. Journal of Geology and Geophysics 10(4): 1109-35.

WATSON, J.R. 1971: Ultrasonic vibration as a method of soil dispersion. Soils and Fertilisers 34(2): 127-34.

WELLMAN, H.W. 1962: Holocene of the North Island of New Zealand: a coastal reconnaissance. Transactions of the Royal Society of N.Z. (Geology)1(5): 29-99.

WESTGATE, J.A.; FULTON, R.J. 1975: Tephrostratigraphy of Olympia interglacial sediments in South-central British Columbia, Canada. Canadian Journal of Earth Science 12: 489-502.

WILCOX, R.E. 1965: Volcanic ash chronology. Pp 807-16 in "The Quaternary of the United States, VII INQUA Congress." Princeton Press, New York.

WILLETT, R.W. 1950: The New Zealand Pleistocene snowline, climatic conditions and suggested biological effects. N.Z. Journal of Science and Technology 32 B(1): 18-48.

WILLIAMS, H.; McBURNEY, A.R. 1969: "An investigation of volcanic depressions - Part 2". N.A.S.A. publication, Houston, Texas, 92 pp.

WILSON, A.T. 1978: The glacial history of New Zealand. Unpublished manuscript.

WRIGHT, J.B.; LOVERING, J.F. 1965: Electron-probe micro-analysis of the iron-titanium oxides in some New Zealand iron sands. Mineralogical Magazine 35: 604-21.

# APPENDIX A

## NOTES ON PETROGRAPHY AND MINERALOGY

Appendix A includes petrological and mineralogical information not presented elsewhere, and which has been removed from the main text to improve continuity between chapters. It contains petrological descriptions of pumice, of rock fragments and of volcanic glass particles as well as descriptions and optical data for seventeen minerals contained within the five field classes at Pukekauri Road.

All optical data were determined by petrological microscope and the universal stage. 2V measurements have an estimated error of $\pm 2^{o}$. Refractive indices, determined by immersion oils, have an estimated error of $\pm$ 0.003. X-ray diffraction data were gathered on a Philips X-ray diffraction spectrometer.

## PETROGRAPHY

### (a) Pumice

Acid pumices are confined to the younger tephras (field classes I and II) and are subdivided into two categories on the basis of colour.

#### (i) Yellow orange pumice

Fine and very fine pumice, yellow orange in colour occurs commonly in class I samples and very commonly within class II. The pumice has a low to moderate concentration of 0.1-0.2 mm in

diameter vesicles, thin walls and frequently shows strong flow-banding. The phenocryst content is very low and dominated by anorthoclase.

(ii) White pumice

Medium and fine white pumice is common in field class I. Its white colouration and transparency indicates that the pumice is less weathered and younger than that described above. The pumice has a moderate concentration of 0.05-0.10 mm in diameter vesicles, thin walls, sometimes shows flow-banding and contains a predominantly plagioclase phenocryst content.

(b) Rock fragments

Grey and white rock fragments are common in all the Pukekauri Road samples. Generally the rock fragments are composed of a glassy ground mass with isolated anhedral zones of devitrified glass and scarce altered plagioclase phenocrysts.

(c) Volcanic Glass

(i) Obsidian

Pale green, transparent, sub-rounded obsidian fragments are common in the younger tephras (field classes I and II); in some cases the obsidian is vesiculated and shows flow-banding textures, crystallites and microlites of ? plagioclase composition.

(ii) Colourless glass

Ross (1928 ; in Ewart 1963) recognised three habits of glass shards in rhyolitic tephras; curved fragments representing glass which originally enclosed rounded bubbles and consisting of curved

fragments of the bubble wall, which may be Y-shaped where three bubbles were in close contact. (Fig. A.1a); platy fragments of almost flat glass plates, formed by the fragmentation of the walls which enclosed large, flattened, lens-shaped vesicles (Fig. A.1b); pumiceous fragments of fibrous glass (Fig. A.1c). All three types of glass shards and many intermediate forms have been recognised in the Pukekauri Road tephras. Fibrous pumiceous fragments (type c) predominate in field classes I and II and platy fragments in classes III, IV and V. The scarcity of curved and pumiceous fragments in the three older field classes suggests that either pumice was not a major component of the tephras, or, more likely, the finer more curved fragments have been removed by weathering. The volcanic glass content decreases with increasing age, from very abundant in the younger tephras to very common lower in the profile.

Refractive indices were determined for selected samples in order to detect any major differences between tephras; results are shown in Table A.1.

TABLE A.1: Refractive indices for volcanic glasses from the Pukekauri Rd tephras

| Sample | Field class | Range in refractive index |
|---|---|---|
| P1 | I | 1.495 - 1.512 |
| P3 | II | 1.496 - 1.512 |
| P10 | III | 1.492 - 1.495 |
| P15 | IV | 1.495 - 1.498 |
| P17 | V | 1.495 - 1.496 |

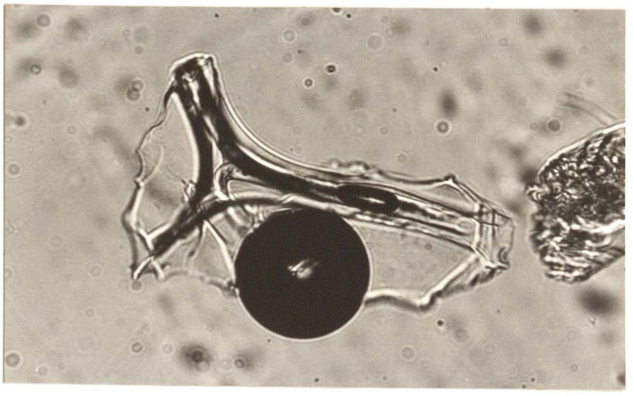

(a)

Curved fragments

Y-shaped fragments of glass where three bubbles were in close contact.
Sample P3, x220.

(b)

Platy fragments

Flat glass plates enclosing lens-shaped vesicles.
Sample P3, x160.

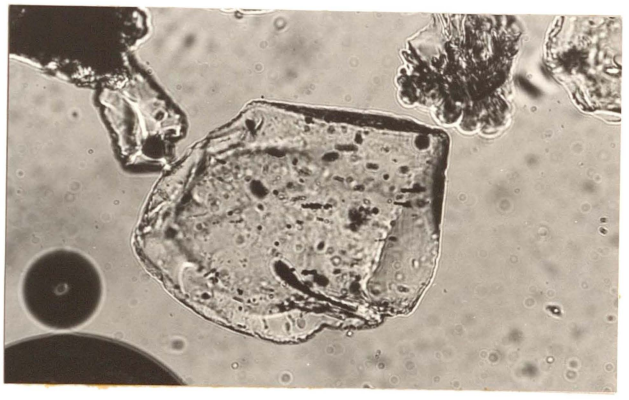

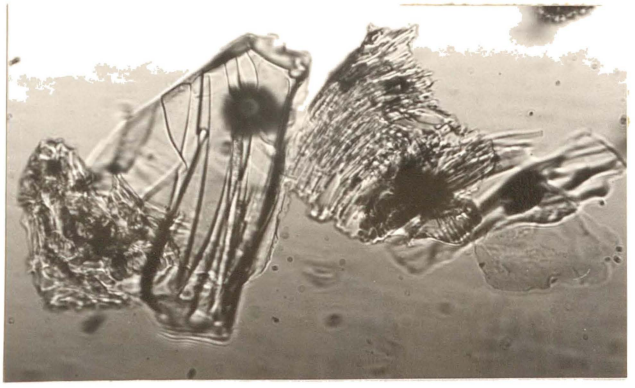

(c)

Pumiceous fragments

Fibrous pumiceous glass.
Sample P3, x160.

FIGURE A.1 (a-c) : Photomicrographs of volcanic glasses representing the three dominant forms found in the Coromandel tephras.

Only curved or platy glass fragments were used in the refractive index measurements as Ewart (1963) demonstrated that other forms of glass had more variable refractive indices. The range of refractive index shown by the Coromandel tephras (1.492–1.512) is considerably higher than that recorded by Ewart (1963) for the Taupo Ash shower sequence (1.496–1.502).

George (1924) has provided a useful method for determining the approximate silica content of volcanic glass by means of its refractive index; two major factors must be considered when applying this method:

(i) Water content of glasses. Many authors (e.g. Ewart 1963; Ross and Smith 1955, 1961; Wilcox 1965) have demonstrated the relationship between refractive index and water content. Ross and Smith (1955) showed that the presence of 1% water would lower the estimated $SiO_2$ content by approximately 2%. Ewart (1963) found that the weathered pumiceous glasses (distinguished by the presence of brown staining) contained the highest water contents and also the highest refractive indices.

(ii) Iron oxidation states. Ross and Smith (1961) indicated that if a glass has any appreciable proportion of iron, the different states of oxidation will have a marked effect on the indices of refraction. In order to test the accuracy of the technique, data from two groups of tephras of different ages were examined and shown in Tables A.2 and A.3.

Despite the considerable variation in the water contents of the Taupo Ash sequence (Ewart 1963), there is a good correlation

TABLE A.2 - Calculated $SiO_2$ contents from refractive index measurements on glasses from the Taupo Ash Shower sequence.

| SAMPLE | $SiO_2$ (anal.) % [1] | average r.i. [1] | r.i. ($\sigma$) | $SiO_2$ (calc.) % [2] | $\Delta SiO_2$ (anal.-calc.) | $\Delta SiO_2$ % [3] |
|---|---|---|---|---|---|---|
| Taupo Lapilli (Member 3) | 71.2 | 1.501 | $2.12 \times 10^{-3}$ | 71.6 | -0.4 | -0.6 |
| Member 5 | 71.9 | 1.502 | $1.41 \times 10^{-3}$ | 71.3 | +0.6 | +0.8 |
| Member 8 | 71.3 | 1.502 | $7.07 \times 10^{-4}$ | 71.1 | +0.2 | +0.3 |
| Member 14d (upper) | 71.9 | 1.501 | $1.41 \times 10^{-3}$ | 71.8 | +0.1 | +0.1 |
| Member 14d (lower) | 71.9 | 1.498 | $1.41 \times 10^{-3}$ | 72.5 | -0.6 | -0.8 |
| Waimihia (Member 15) | 70.5 | 1.498 | $1.41 \times 10^{-3}$ | 72.5 | -2.0 | -2.8 |
| Member 19W | 70.8 | 1.503 | $1.41 \times 10^{-3}$ | 71.0 | -0.2 | -0.3 |
| Member 24 (upper) | 71.3 | 1.502 | 0.0 | 71.3 | 0.0 | 0.0 |
| Member 25 (upper) | 71.3 | 1.503 | 0.0 | 71.0 | +0.3 | +0.4 |
| Member 25 (lower) | 71.3 | 1.502 | 0.0 | 71.3 | 0.0 | 0.0 |

1 Data from Ewart (1963)

2 By the method of George (1924)

3 Anal.-Calc./Anal.(%).

between the refractive index and the $SiO_2$ content, with a maximum error of 2.8%. The technique is also applicable to older tephras, for example the Rotoehu Ash (Table A.3), the $SiO_2$ contents of which can be estimated to within 3% of the true value.

TABLE A.3: Calculated $SiO_2$ contents from refractive index measurements on glasses from the Rotoehu Ash

| | $SiO_2$ (anal.) % 1 | average r.i. 2 | r.i. | $SiO_2$ (calc.) % 3 | $SiO_2$ (anal.-calc.) | $SiO_2$ % 4 |
|---|---|---|---|---|---|---|
| Rotoehu Ash (42,000 yrs B.P.) | 70.4 | 1.498 | $5.2 \times 10^{-4}$ | 72.3 | -1.9 | -2.7 |

1. Data from Kohn (1973)
2. Data from Hodder (1974)
3. By the method of George (1924)
4. Anal. - Calc./Anal.

It is therefore concluded that estimations of $SiO_2$ content determined from refractive index measurements of volcanic glasses are possible even in moderately aged tephras, provided that the glasses are not strongly weathered and are colourless, thereby indicating a low iron content. The red-brown colouration of many of the glasses from classes I and II renders them unsuitable for the application of this technique. However, the glasses of the older field classes complying with the provisions outlined above, allow estimations of composition to be made (Table A.4) and show that the tephras of these classes are predominantly, if not completely, rhyolitic in composition.

TABLE A.4: Calculated $SiO_2$ contents of volcanic glasses from refractive index measurements of field classes III, IV and V at Pukekauri Rd

| Sample | r.i. | $SiO_2$ (calc.) % 1 | $SiO_2$ (Calc.) Mean (%) |
|---|---|---|---|
| P 10 (F.C.III) | 1.492 - 1.495 | 74.5 - 73.7 | 74.1 |
| P 15 (F.C. IV) | 1.495 - 1.498 | 73.7 - 72.5 | 73.1 |
| P 18 (F.C. V) | 1.495 - 1.496 | 73.7 - 73.3 | 73.5 |

1. By the method of George (1924)

## MINERALOGY

### (a) Plagioclase Feldspar

Plagioclase is the most commonly occurring mineral in all the samples examined, increasing in concentration within the sand fractions from very common in classes I and II to very abundant in field classes III, IV and V.

Plagioclase was identified optically and confirmed by routine X-ray diffraction analysis and has a composition of andesine (An 38-48), calculated from optical data by the Michel-Levy method. This is comparable with central North Island volcanic rocks, which have Ca-oligoclase to andesine compositions of An 25-46. The structural state of the plagioclase was determined by the X-ray

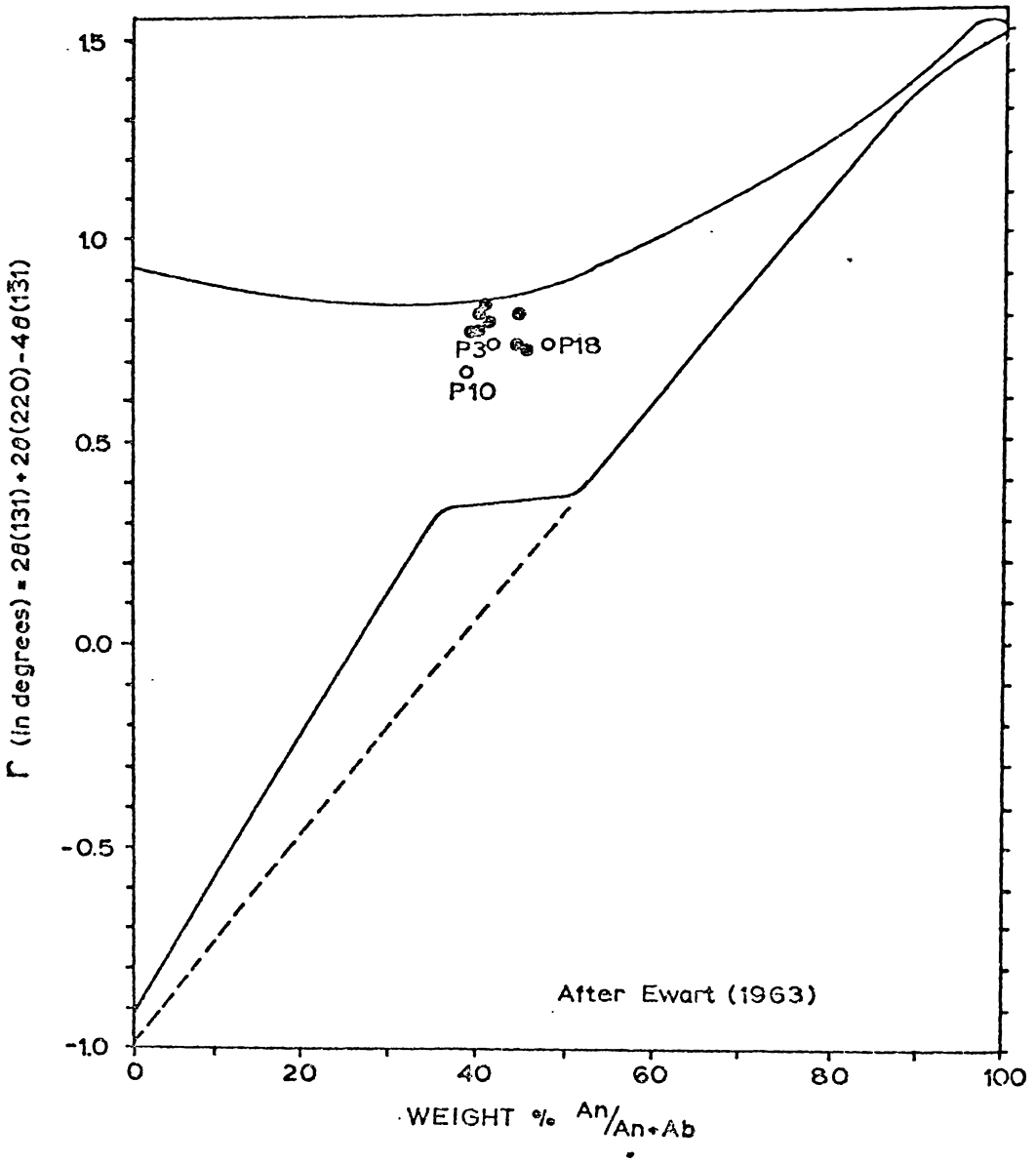


FIGURE A.2 : Structural state of plagioclases from the Coromandel tephras at Pukekauri Rd.

● plagioclase from the Taupo Ash sequence (Ewart 1963)

○ plagioclase from the Pukekauri Rd site (F.C.II P3; F.C.III P10; F.C.V P18)

powder method of Smith and Gay (1958), and was found to be the high temperature disordered state (Fig. A.2).

Plagioclase occurs as fresh, euhedral or subhedral grains commonly exhibiting simple and multiple twinning and containing inclusions of glass and euhedral magnetite crystals. Optic axial angles were determined for plagioclases from three field classes, with results shown in Table A.5. The very high coefficient of variation shown for P10 (22%) suggests that the plagioclase from field class III may fall into two populations derived from separate sources.

TABLE A.5: Plagioclase optic axial angles for Field Classes II, III and V at Pukekauri Rd

| Field Class | Sample | Range of 2V (2V $\gamma$) | Number of Measurements (n) | Mean ($\bar{x}$) | Standard deviation ($\sigma$) | Coefficient of variation (C) % |
|---|---|---|---|---|---|---|
| II | P3 | 94 - 104 | 4 | 98 | 4.2 | 4.3 |
| III | P10 | 68 - 117 | 9 | 92 | 20.2 | 22.0 |
| V | P18 | 92 - 105 | 5 | 98 | 5.1 | 5.2 |

(b) Anorthoclase

The potassic feldspar anorthoclase occurs only in the two younger field classes, commonly in field class I and very common in field class II.

Anorthoclase was identified by its optical properties and confirmed by X-ray diffraction analysis. Its composition was determined by the X-ray method of Tuttle and Bowen (1958), which

requires the accurate measurement of the difference between the position of the $\bar{2}01$ anorthoclase peak and the $10\bar{1}0$ quartz peak and is applicable only when the feldspar is sufficiently homogenized. Anorthoclase was concentrated from two field class II samples and X-rayed in triplicate, firstly as untreated powders and secondly heated to over 900 $^{o}$C to allow homogenization of separate phases, should they exist. The $\bar{2}01$ anorthoclase peak was not affected by the heating, indicating that the feldspar was not submicroscopically exsolved. A mean Or content of Or29 (range Or31-Or27) derived from the $\delta\ \bar{2}01$ values for the untreated powders when plotted against 2V confirmed the mineral as anorthoclase. Optic axial angles determined from two field class II samples, ranged from $2V\alpha = 44^{o} - 48^{o}$.

Anorthoclase occurs as fresh euhedral or subhedral crystals which frequently show simple twinning and contains common euhedral magnetite and glass inclusions.

Anorthoclase from field class II differs from that examined by Ewart et al(1968) from Mayor Island pantelleritic lavas, as the Mayor Island phenocrysts have a higher Or content (Or36-43) and are sub-microscopically exsolved.

(c) Quartz

Quartz which was identified by its optical properties and by standard XRD techniques, is present in all field classes but becomes more abundant in classes III to V. Quartz varies from anhedral to subhedral transparent crystals which occur in all five field classes, to 1-3 mm diameter white and pink anhedral, irregular crystals contained within classes I and II.

(d) Hypersthene

Hypersthene is present in all tephras and is abundant in the ferromagnesian mineral fraction of class III, very common in classes I, II and IV, and common in class V. Hypersthene occurs as stubby, partially rounded prisms (Fig. A.3a), often containing inclusions of magnetite. It is weakly to moderately pleochroic from bottle green to greenish-orange, shows no compositional zoning, and some grains appear to be strained as indicated by wavy extinctions. 2V determinations indicate two groups of hypersthene compositions: one hypersthene is more Mg-poor ($2V\alpha$ = 58-62°, average 60°, composition En 64-68) and is found in all field classes, while the other hypersthene is relatively Mg-rich ($2V\alpha$ = 63-65°, average 64°, composition En 69-71.) Optic axial angles and compositions for hypersthene, hornblende and cummingtonite in field classes I - V are summarised in Table A.6 - the two types of hypersthene are labelled OpxA and OpxB respectively. The presence of both OpxA and OpxB in class III suggests that it may be a mixture of two or more tephras. Hypersthene phenocrysts from the Taupo Ash shower sequence exhibit lower Mg contents from those indicated above (En 48-64; Ewart 1963). Individual members of the recently renamed Mangaoni Lapilli Formation have compositions more like the Coromandel tephras (En 65-72; Howorth 1976).

(e) Augite

Augite is in highest concentration in field classes I and II where it is very common in the ferromagnesian mineral fraction, and decreases in the older classes, being common in class III, rare in

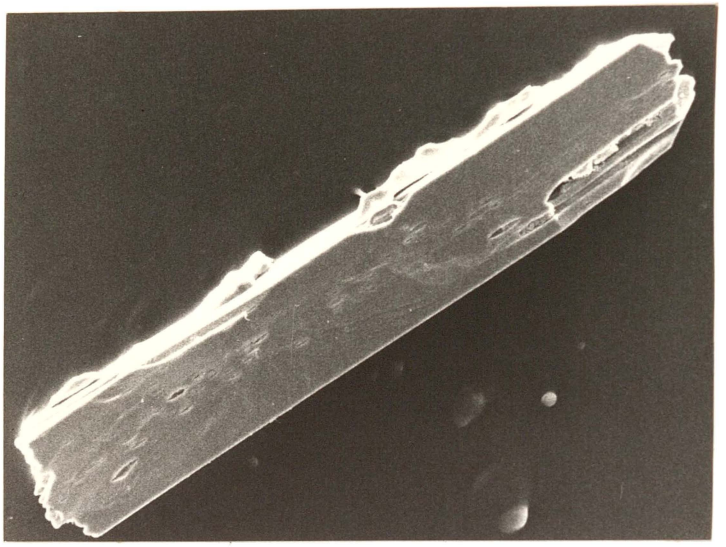

(a)
HYPERSTHENE
Sample P12
(x180)

(b)
AEGIRINE
Sample P4
(x320)

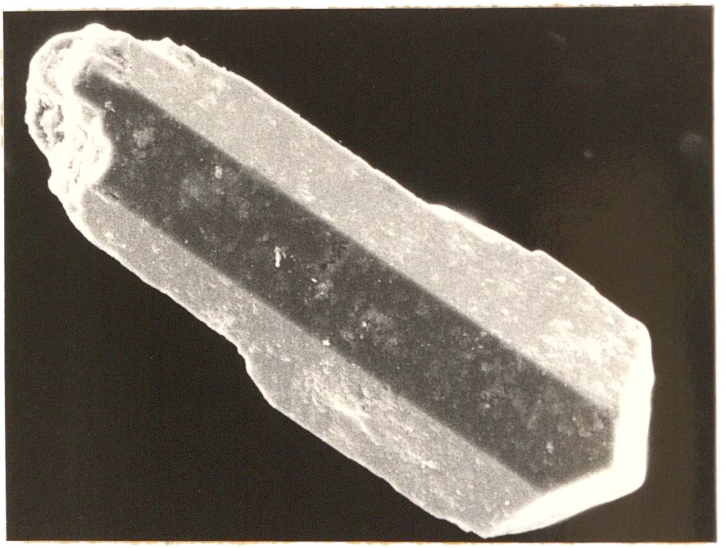

FIGURE A.3 (a-d) : Electron-micrographs of the dominant ferromagnesian minerals from the Coromandel tephras at Pukekauri Rd.

(c)
HORNBLENDE
Sample P8
(x110)

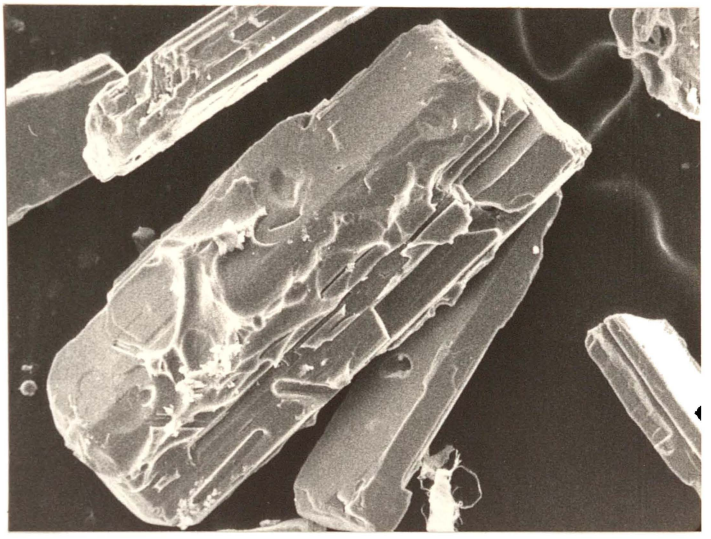

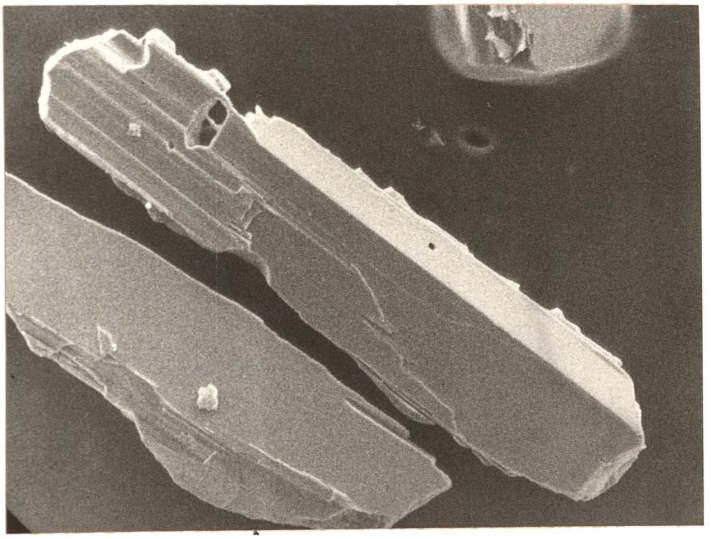

(d)
CUMMINGTONITE
Sample P16
(x120)

class IV and absent from class V. It forms colourless to pale green, stubby, rounded prisms which for any sample, are always smaller than the accompanying hypersthene grains. Inclusions are rare, with small glass blebs occasionally being present. $2V\gamma = 48^{o}$, which is similar to that in augites from the Taupo Ash shower sequence ($2V\gamma = 45\text{–}48^{o}$; Ewart 1963).

(f) Aegirine

Aegirine is common in the ferromagnesian mineral fraction of classes I and II but is absent from classes III, IV and V. It occurs mostly as stout prisms (Fig. A.3b) or slender needles commonly surrounded by an envelope of glass. Aegirine is strongly pleochroic from a deep emerald green to yellow-green, and simple twinning is common. No further optical properties could be obtained because of grain orientation and the extreme body colours. The presence of considerable amounts of aegirine in an otherwise calc-alkaline mineral suite indicates dual sources for field classes I and II; this is discussed further in Chapter 3.

(g) Hornblende

Common hornblende is present in all samples from Pukekauri Rd and is abundant in the ferromagnesian mineral fraction of classes I and II, very common in classes III and IV and common in class V. The elongated, euhedral prismatic crystals (Fig. A.3c) are moderately pleochroic with a pleochroic formula $\alpha$ = pale greenish brown, $\beta$ = brown green and $\gamma$ = olive green, $z\wedge c = 14^{o}$, $2V\gamma$ varies from $67\text{–}83^{o}$ (average $75^{o}$) and contain rare magnetite inclusions. Twinning is rare.

(h) Cummingtonite

Cummingtonite is represented in all field classes and increases in concentration markedly in the older tephras; it is very common in the ferromagnesian mineral fraction of classes I, II and III, very abundant in class IV and extremely abundant in field class V. Cummingtonite has been identified by optical properties in conjunction with X-ray diffraction data. A sample of cummingtonite estimated to be 95% pure, was mounted as a smear and compared with cummingtonite extracted from pumice of the Rotoiti Breccia Formation. The diffraction patterns were identical, with the three major peaks at 8.35 Å (100%), 3.07 Å (96%) and 3.26 Å (44%) confirming its identification.

Cummingtonite usually occurs as euhedral, elongated prismatic crystals (Fig. A.3d), often twinned and commonly containing euhedral magnetite and occasionally hypersthene inclusions. Pleochroism is weak with $\alpha (= \beta)$ = pale orange green, $\gamma$ = pale green and $z \wedge c = 20^{o}$. Cummingtonite is distinguishable from hypersthene by its cloudy green colouration compared with the transparent green of hypersthene, its higher birefringence and extinction angle. Hornblende typically exhibits darker body colours and a lower birefringence compared with cummingtonite. $2V\gamma$ ranges from 86-94° (average 89°) (see Table A.6) with an estimated composition of En39-13 (average En 29), indicating that the mineral is iron-rich and mostly lying within the cummingtonite field with a low proportion of minerals occupying the grunerite field.

TABLE A.6 - Summary of optic axial angles and compositon data for Field Classes I - V at Pukekauri Rd.

| SAMPLE | MINERAL | 2V RANGE | MEAN ($\bar{X}$) | STD. DEVN. ($\sigma$) | COEFF. OF VARTN. (C) % | NO. OF SMPLS (n) | COMPOSITION RANGE (En) | COMP. MEAN (En) |
|---|---|---|---|---|---|---|---|---|
| P1 (FC I) | OpxA | 58 - 61 | 59 | 1.2 | 2.0 | 5 | 64 - 67 | 65 |
| | HBDE | 67 - 83 | 76 | 6.1 | 8.0 | 5 | | |
| | CGTE | 86 - 94 | 89 | 3.4 | 3.8 | 5 | 39 - 13 | 29 |
| P3 (FC II) | OpxA | 58 - 62 | 60 | 1.1 | 1.8 | 9 | 64 - 68 | 66 |
| | HBDE | 72 - 75 | 73 | 1.3 | 1.8 | 5 | | |
| | CGTE | 88 - 91 | 89 | 1.3 | 1.5 | 5 | 33 - 23 | 29 |
| P8 (FC III) | OpxA | 58 - 62 | 60 | 1.5 | 2.5 | 6 | 65 - 67 | 66 |
| | OpxB | 63 - 64 | 63 | 0.6 | 0.9 | 3 | 69 - 70 | 69 |
| | HBDE | 71 - 76 | 74 | 2.1 | 2.8 | 6 | | |
| | CGTE | 87 - 93 | 89 | 3.0 | 3.4 | 5 | 36 - 16 | 29 |
| P10 (FC III) | OpxA | 59 - 62 | 60 | 0.8 | 1.3 | 7 | 65 - 68 | 66 |
| | OpxB | 64 - 65 | 64 | 0.5 | 0.8 | 3 | 70 - 71 | 71 |
| | HBDE | 72 - 77 | 75 | 2.3 | 3.1 | 5 | | |
| | CGTE | 86 - 90 | 88 | 1.8 | 2.0 | 5 | 39 - 27 | 32 |
| P15 (FC IV) | OpxA | 58 - 60 | 59 | 0.5 | 0.8 | 5 | 64 - 66 | 65 |
| | HBDE | 68 - 82 | 76 | 5.4 | 7.1 | 5 | | |
| | CGTE | 84 - 94 | 90 | 4.1 | 4.6 | 5 | 45 - 13 | 27 |
| P17 (FC V) | OpxA | 58 - 61 | 60 | 1.1 | 1.8 | 6 | 64 - 67 | 66 |
| | HBDE | 68 - 82 | 76 | 5.4 | 7.1 | 5 | | |
| | CGTE | 84 - 94 | 90 | 4.1 | 4.6 | 5 | 45 - 13 | 27 |
| average for all samples | OpxA | 58 - 62 | 60 | 0.4 | 0.7 | 38 | 64 - 68 | 66 |
| | OpxB | 63 - 65 | 64 | 0.8 | 1.3 | 6 | 69 - 71 | 70 |
| | HBDE | 67 - 83 | 75 | 3.8 | 5.1 | 31 | | |
| | CGTE | 86 - 94 | 89 | 3.1 | 3.5 | 30 | 39 - 13 | 29 |

(i) Unknown pyroxene (? Hedenbergite)

A euhedral to subhedral, slightly pleochroic pale greenish-brown pyroxene was found in samples from field class II. The colour, moderately high extinction angle ($30^{o}$), high 2V ($2V\gamma = 59^{o}$) indicates that it may be close to hedenbergite in composition.

(j) Oxyhornblende

Minor amounts of oxyhornblende occur in the younger tephras at Pukekauri Road, within field classes I and II. It occurs as elongated, subhedral, dark red crystals, strongly pleochroic from $\alpha$ = yellow, $\beta$ = yellowish-red and $\gamma$ = dark red, $z \wedge c = 2^{o}$, and $2V\alpha = 80^{o}$.

(k) Riebeckite

Two types of riebeckite have been identified: One type was found in classes I and II occurring as small anhedral crystals, very dark in colour and strongly pleochroic from pale violet to azure blue. The second type is confined to field class IV and occurs as elongated, subhedral prisms showing strong pleochroism from pale bluish green to azure blue and $2V\alpha = 67^{o}$, $z \wedge c = 0^{o}$.

(l) Tuhualite

Tuhualite was first described by Marshall (1932) from Mayor Island, with further mineralogical data given by Marshall (1936 ) and Hutton (1956). It was found only in field class II as two small anhedral grains. The crystals were strongly pleochroic with a pleochroic formula $\alpha$ = pale pink, $\beta$ = light pinkish purple and

$\gamma$ = dark purple and $2V\gamma = 52^{o}$, properties which are optically identical with those given by Hutton (1956) and confirm the mineral as tuhualite.

(m) Cossyrite

Very dark red crystals of cossyrite occur in field classes I and II as scarce components of the ferromagnesian mineral fraction.

(n) Olivine

Small colourless to very pale green subhedral crystals of olivine are rare in field classes I and II.

(o) Zircon

Rare, euhedral, prismatic zircon crystals are present in all field classes.

(p) Vermiculite

Large, brown subhedral to anhedral flakes from field class IV were X-rayed and identified as vermiculite through the collapse of the 14 $\overset{o}{A}$ basal reflection upon heating. Identification was confirmed by density measurements ($d \simeq 2.5$) and 2V ($2V\alpha = 0\text{-}2^{o}$). Cortez and Franzmeier (1972) reported vermiculite in acid volcanic ashes from the Colombian Andes mountains and considered it to be an alteration product of biotite or phlogopite.

(q) Oxide minerals

The term "oxide minerals" used in this section refers to opaque minerals of the $FeO - Fe_2O_3 - TiO_2$ system. Of the three major solid

solution series that exist in this system, two are found in the Coromandel tephras: the magnetite-ulvospinel series and the hematite-ilmenite series. As magnetites from New Zealand low temperature rhyolitic magmas analysed by Ewart et al. (1971) were all found to be titaniferous and more correctly termed "titanomagnetite", it is highly likely that magnetites from the Coromandel tephas also fit into this category.

(1) Titanomagnetite

Titanomagnetite is the most prevalent oxide mineral in the Coromandel tephras and is abundant in the heavy mineral fraction of all five field classes. The majority of crystals occur as octahedra modified by small rhombic dodecahedral faces, apparently little affected by weathering (Fig. A.4). Under reflected light titanomagnetite is creamy white and bireflectance is absent (Fig. A.5a).

While the majority of titanomagnetite crystals examined were microscopically homogeneous, a small percentage of grains exhibited exsolution and replacement textures. Three varieties of exsolution textures are present:

(i) Rarely, under very high magnification (X 1000), small black lamellae of aluminous spinel were observed lying parallel to the cubic (100) planes of the host titanomagnetite (Fig. A.5b).

(ii) Hematite lamellae occur as narrow lines or broad bands generally exsolved along the octahedral (111) directions of the host titanomagnetite (Fig. A.5b). Hematite is characterised by its bluish white appearance when compared with titanomagnetite and its distinct bireflectance and strong anisotropism.

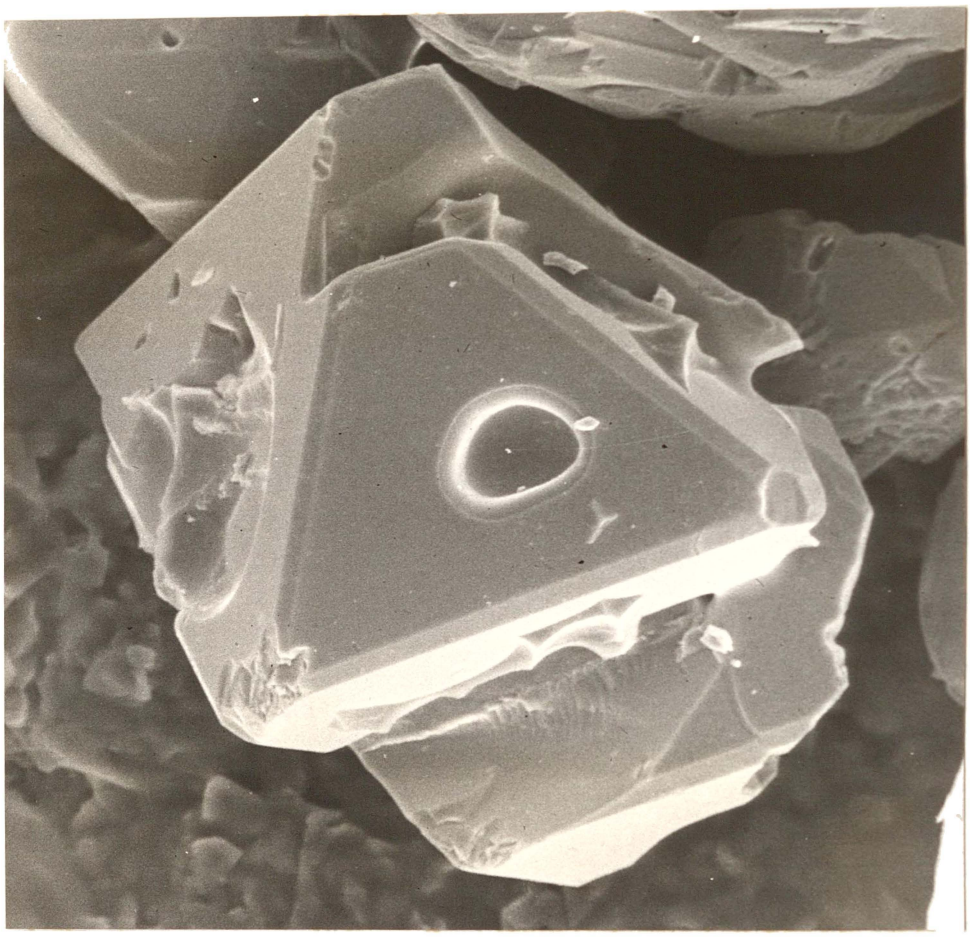

FIGURE A.4 : Titanomagnetite octahedron showing vesicle, and euhedral cavities formerly occupied by inclusions or intergrown minerals.
Sample P15, x270.

(a)
Microscopically homogeneous t-magnetite crystal (light grey) with included marcasite (white) and apatite (dark grey).
plane polarised light, x350.

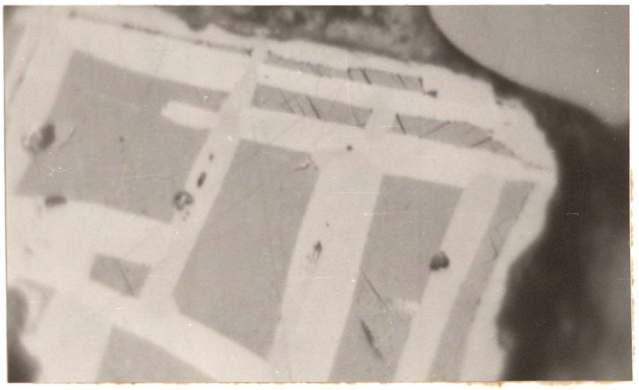

(b)
Exsolved hematite lamellae (white) in titanomagnetite (grey). Black aluminous spinels exsolved parallel to the cubic planes (100) are seen in the centre of the micrograph.
plane polarised light, oil immersion, x1000.

(c)
Titanomagnetite (pale grey) with exsolved lens-shaped ilmenite lamellae (dark grey) exsolved along (111) directions.
partially crossed nicols, oil immersion, x1000.

FIGURE A.5 (a-c) : Exsolution textures of titanomagnetite. All micrographs from sample P10 (field class III).

(iii) Lens-shaped ilmenite exsolution lamellae parallel octahedral (111) planes and have been identified as ilmenite from their creamy colour, strong bireflectance, anisotropism and their brownish tink in oil (Fig. A.5c).

Three kinds of replacement textures of titanomagnetite have been observed:

(i) Replacement of the titanomagnetite host by hematite (martitisation), proceeding from the margin of the titanomagnetite grain and leaving an unaltered core (Fig. A.6a).

(ii) Rarely, titanomagnetite was found replaced by goethite; remnants of titanomagnetite aligned parallel to the cubic (100) planes occur right to the crystal edge.

(iii) The third replacement texture is very similar to the martitisation textures, with a core of titanomagnetite surrounded by a bluish white strongly fractured mineral, identified by its isotropism as maghemite (Fig. A.6b).

The most common inclusions in titanomagnetite are apatite (occurring as hexagonal prisms and acicular crystals - Fig. A.5a), marcasite, pyrite and a variety of silicates (Fig. A.6c).

2. Ilmenite.

Scarce, euhedral crystals of ilmenite occur in all field classes. The mineral is greyish white under reflected light, exhibits moderate bireflectance and strong anisotropism (Fig. A.6c).

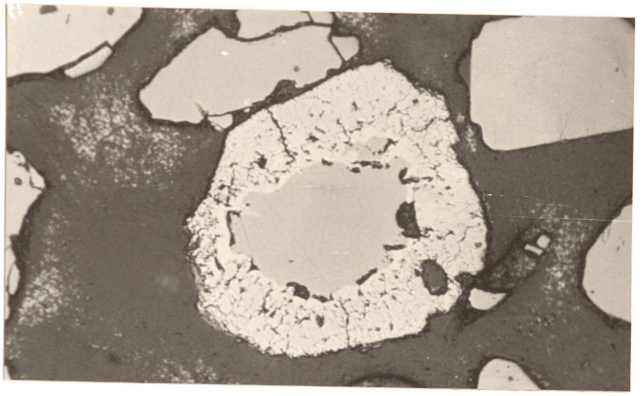

(a)
Martitisation
Titanomagnetite (grey) forms the central core and is surrounded by a rim of hematite (white) plane polarised light, x350, sample P10.

(b)
Core of titanomagnetite (grey) surrounded by replacement material (white) - probably maghemite.
plane polarised light, x350, sample P15

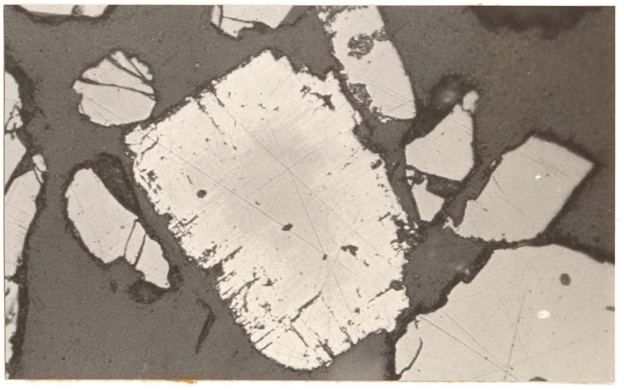

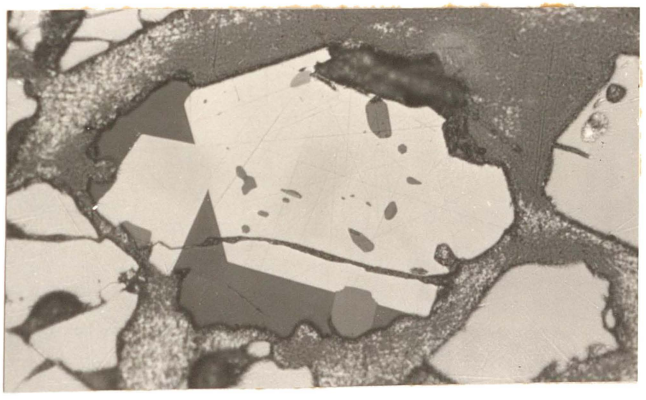

(c)
Ilmenite grain (white) with siliceous inclusions (grey) plane polarised light x350, sample P15.

FIGURE A.6 (a-b) : Replacement texture of titanomagnetite.

(c) : Ilmenite grain with siliceous inclusions.

# APPENDIX B

## METHODOLOGY

### (1) Sample Preparation

The high content of organic carbon in the soil horizons of many New Zealand andosols necessitates pretreatment of samples for any laboratory examination requiring size fractionation of its constituents (Birrell 1974). Although clay mineral damage through oxidation by hydrogen peroxide has been well documented in the literature (e.g. Birrell 1974), it was necessary to remove organic matter from all samples lying within either the A or B soil horizons, to achieve complete dispersion. Dispersion of the tephras was effected by exposing them to ultra-sonic vibrations but, unlike many other workers (e.g. Edwards and Bremner 1967; Vladimirov 1968; Watson 1971) who found that a dispersing agent was unnecessary when using ultra-sonic vibrations, a stable suspension could only be maintained in an acid medium of pH 3.

A probe type ultra-sonic vibrator was used for full dispersion of the samples. An evaluation of the extent of decomposition of primary minerals by the probe was made by exposing separate samples of whole tephra and of part of a silt fraction (4.5-7 Ø) to vibrations of varying periods and monitoring any changes in particle size. The influence of vibration time and water to solid ratio on the whole sample was tested using sample P18 which was slurried, split and treated in three different ways (Table B1 and Fig. B1a). A vibration time of six minutes was found necessary to ensure adequate

TABLE B.1 : Influence of vibration treatment of varying times on whole sample and silt fraction of sample P18 (F.C.V)

| SAMPLE | size fraction subjected to probing | treatment | size fraction determined | Mz (ϕ) | $\sigma_G$ (ϕ) | degree of dispersn. |
|---|---|---|---|---|---|---|
| 1 | whole tephra sample | 3 mins. probe water/solid=5 | coarser than 4ϕ | 2.30 | 0.77 | poor |
| 2 | | 6 mins. probe water/solid=5 | | 2.29 | 0.79 | Excellent |
| 3 | | 6 mins. probe water/solid=10 | | 2.26 | 0.78 | Excellent |
| 4 | 4.5 - 7ϕ | untreated sample | 4.5 - 7ϕ | 5.90 | 0.83 | n.a.[1] |
| 5 | | probed for additional 3mins | | 5.85 | 0.95 | n.a. |
| 6 | | probed for additional 6mins | | 5.89 | 1.03 | n.a. |

1 : Not applicable

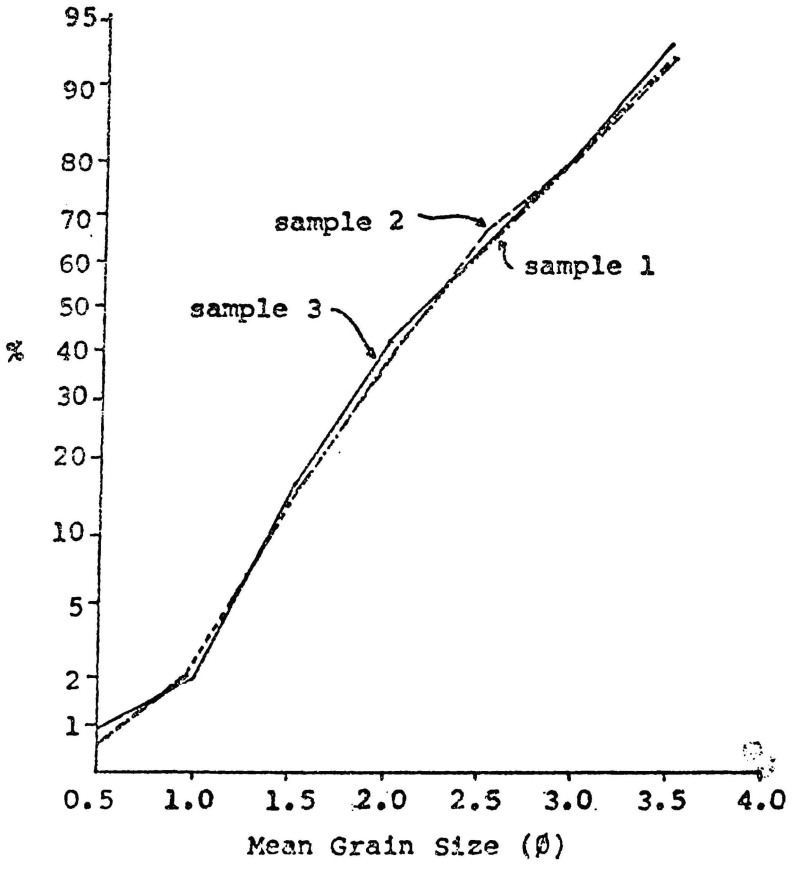


FIGURE B1.a: Influence of vibration treatment on the <4Ø fraction of P18.

Sample 1 : 3 mins. vibration; water/solid = 5
Sample 2 : 6 mins. vibration; water/solid = 5
Sample 3 : 6 mins. vibration; water/solid = 10
(Grain size parameters summarised in Table B1)

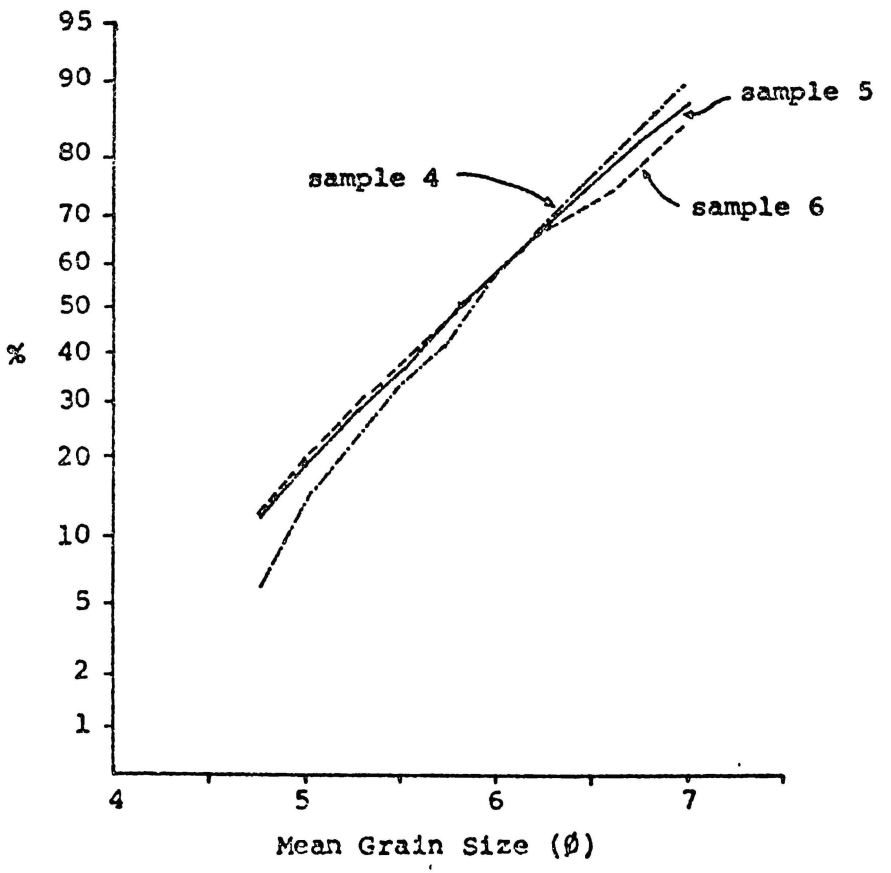


FIGURE B1.b: Influence of vibration treatment on the 4.5-7Ø fraction of P18.

Sample 4 : untreated sample
Sample 5 : Exposed to 3 mins. vibration
Sample 6 : Exposed to 6 mins. vibration
(Grain size parameters summarised in Table B1)

dispersion of the silt and clay sized material and a water to solid ratio of ten was adopted, neither of which significantly altered the sand fraction particle size distribution. As the experiment aimed at evaluating the influence of vibration treatment on primary material, the 4.5-7Ø sample from P18 (separated from sample 3 in Table B1) was probed to ensure that the sample was free of clay minerals. This clay-free sample was then utilised as a standard to monitor the influence of additional probing and is labelled "untreated sample" (sample 4) in Table B1. This procedure is likely to underestimate the influence of ultra-sonic vibrations on the silt fraction, as that portion of sample 4 most susceptible to physical decomposition will have already been destroyed by the earlier treatment. Exposure of the silt fraction to probing for six minutes caused little variation in the mean grain size but produced a higher sorting coefficient (Table B1). On the basis of the above data, all samples were dispersed by exposure to vibration treatment for six minutes, using a water to solid ratio of ten and a dispersent of HCl at a pH of 3. A flow chart outlining laboratory procedure for sample preparation is given in Fig. B2.

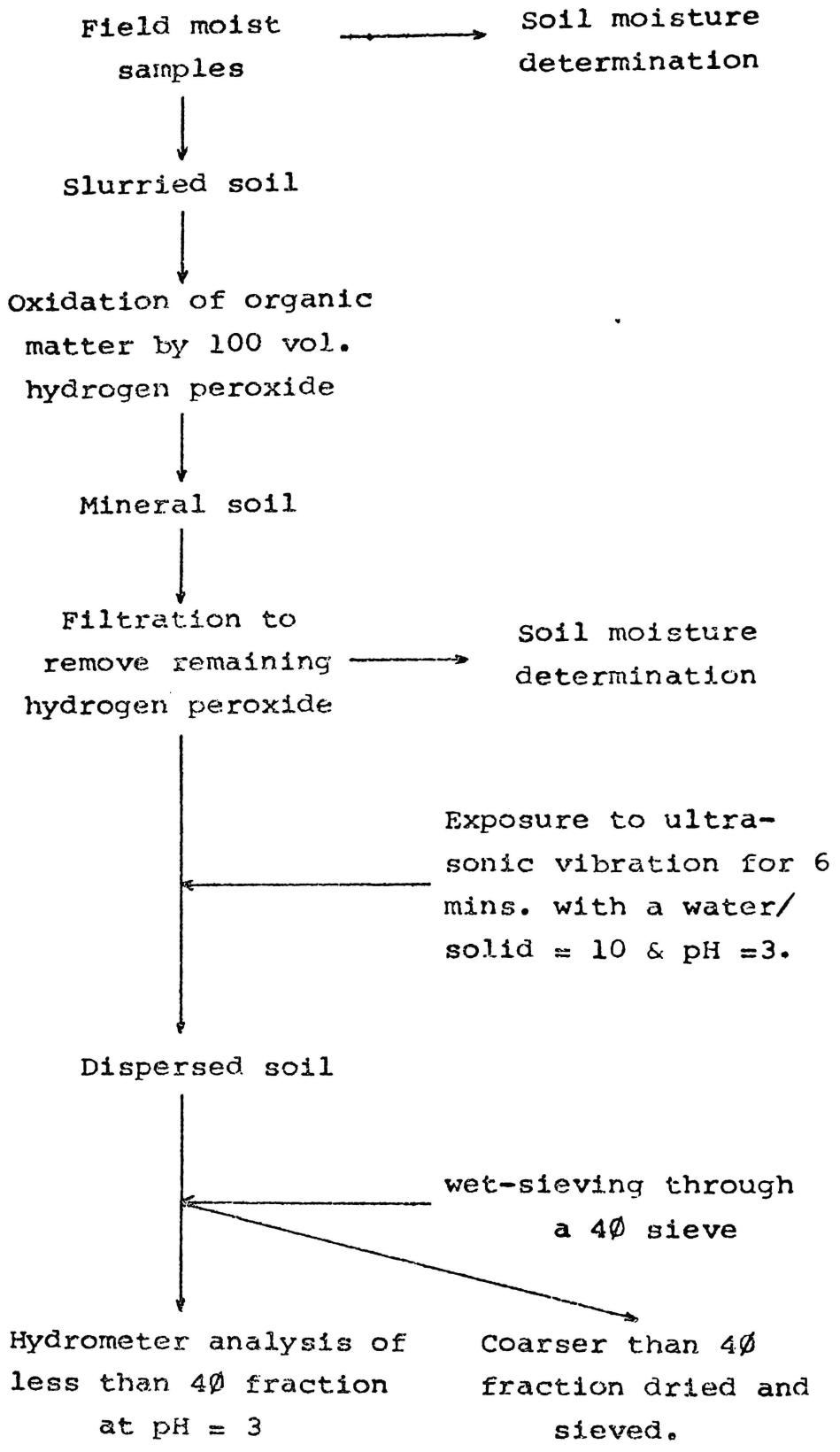


FIGURE B2 : Flow chart for preparation of samples for size fractionation.

(2) Particle Size Analysis

Clay and silt particle size distributions were obtained by hydrometer using the standard method of the British Standards Institution (B.S. 1377; 1967). The hydrometers and cylinders used in the determinations were calibrated to calculate effective depth and the soil dispersed in distilled water brought to a pH of 3 by dilute hydrochloric acid. Corrections were made for temperature and density of the settling medium. The use of dilute hydrochloric acid to give an acid pH caused considerable problems during the analyses. The problem occurred with samples rich in allophane in which the density of the settling medium changed with time as the acid stripped Fe and Al ions from clay minerals. Density corrections were made 24 hours after settling began by extracting an aliquot of supernatant material, removing suspended colloids by super centrifuge, and measuring liquid density by specific gravity bottle. The density corrections thus applied are accurate only for measurements made after a considerable time interval from initial sedimentation (and are therefore excessive for earlier measurements). Duplicate analyses indicate an experimental error of between 5 and 10%, a margin also supported by the work of Kaddah (1974).

Particles coarser than 4 Ø were dry sieved at $\frac{1}{2}$Ø intervals on an Endocott test sieve shaker for a period of ten minutes. Duplicate measurements on two samples over a time interval of six months indicated an experimental error for the mean grain size and standard deviation of less than 1%.

Statistical parameters used in this study are those of Inman (1952) and Folk and Ward (1957) and are summarised in Tables B2 and B3.

TABLE B2: Statistical parameters, their value and meaning

| Name | Symbol | Value | Meaning |
|---|---|---|---|
| Phi | $\phi$ | $\phi = -\log_2$(dia. in mm) | A logarithmic measure of grain size diameter |
| Phi Mean (Folk and Ward 1957) | $M_z\phi$ | $M_z\phi = \frac{\phi(16+50+84)}{3}$ | An average size of the sediment as influenced by the source environment and energy level of transporting fluid |
| Phi Deviation Measure (Sorting) (Inman 1952) | $\theta\phi$ [1] (or $\theta_G\phi$) | $\theta_G\phi = \frac{\phi(84-16)}{2}$ | Standard deviation. A measure of the deviation of the population from a log-normal distribution. |

[1] Symbol after Folk (1968)

TABLE B3: Scale for Sorting (Standard deviation) - $\phi$ after Folk (1968)

| Sorting Term | Symbol | (Units) |
|---|---|---|
| very well sorted | v.w.s. | |
| | | 0.35 |
| well sorted | w.s. | |
| | | 0.50 |
| moderately well sorted | m.w.s. | |
| | | 0.71 |
| moderately sorted | m.s. | |
| | | 1.00 |
| poorly sorted | p.s. | |
| | | 2.00 |
| very poorly sorted | v.p.s. | |
| | | 4.00 |
| extremely poorly sorted | e.p.s. | |

Table 84: Terminology and grain size limits for pyroclastic fragments, and proposed divisions for the Lapilli size fraction

| Pyroclastic Fragments[1] | | Grade Size (mm) | Grade Size (Ø diameters) |
|---|---|---|---|
| Blocks and bombs | Coarse | 256 | -8 |
| | Fine | 64 | -6 |
| Lapilli | Very coarse | 32 | -5 |
| | Coarse | 16 | -4 |
| | Medium | 8 | -3 |
| | Fine | 4 | -2 |
| | Very fine | 2 | -1 |
| Ash | Coarse | 1/16 | 4 |
| | Fine | | |

1 Main subdivisions after Fisher (1961)

(3) Semi-quantitative Analysis of Felsic Minerals by X-ray diffraction (X.R.D.)

(after the method of Nelson and Cochrane 1970).

Instrument settings and calibration

Analyses were carried out on a Philips XRD using nickel-filtered copper radiation generated at approximately 35 kV and 15 mA with $1^{o}$ divergence and scatter slits and 0.1 mm receiving slit, a scanning speed of $2^{o}$ 2 θ per minute, a chart speed of 20 mm per minute, a time constant of four seconds, a rate meter setting of 400 counts per second, and using a circular rotating sample holder. The machine was calibrated daily by adjusting the power supply to the X-ray tube in order to maintain a constant peak height for the 4.26 Å quartz peak from a quartz standard. Samples were ground for three minutes in a ring mill until they passed through a 4.5 ϕ (44 μm) sieve.

Construction of standard curves

Standard powders were prepared by thorough mixing of minerals largely derived from the Coromandel tephras. Two groups of standards were made up, one dominated by plagioclase and the other by anorthoclase. Plagioclase was concentrated from a class V sand fraction which, from microscope point-counting contained 83% plagioclase and 17% quartz. Pure anorthoclase was extracted from the 0-2 ϕ (1000-250 μm) fraction of a class II deposit near Whangamata. Rhyolitic glass was derived from crushed obsidian. Quartz was obtained from the plagioclase quartz class V sand fraction mentioned above, augmented by quartz from a reef at Te Aroha.

In order to assess the influence of heavy mineral abundances on the background levels of diffractometer traces (c.f. Nelson and Cochrane 1970), four samples with heavy mineral fractions ranging from 2-22 wt. % were examined (Table 8.4b).

TABLE 84b : The influence of heavy mineral content on the background levels of X-ray diffraction traces

| Sample (2-4Ø) | | Heavy Mineral Abundance (Wt. %) | QUARTZ | | PLAGIOCLASE | |
|---|---|---|---|---|---|---|
| | | | Peak height | Back-ground | Peak height | Back-ground |
| I | P1 | 2 | 5 | 9.5 | 10 | 8.0 |
| III | P10 | 14 | 5 | 7.5 | 20 | 7.0 |
| III/IV | P12 | 21 | 4 | 7.5 | 31 | 7.0 |
| III/IV | P13 | 22 | 6 | 7.0 | 27 | 7.5 |

Table 8 4b indicates that there is no correlation between a high heavy mineral content and high background intensities. Entire sand fractions (i.e. heavy plus light minerals) were therefore utilised in determining the relative abundances of quartz, feldspar and volcanic glass.

The composition and peak height above background for eight standards are shown in Table B5. Standard curves used to determine the weight percentage of quartz, plagioclase and anorthoclase in the Coromandel tephra samples are given in Figs. B3-B5.

Intensity-concentration curves have also been constructed for plagioclase and quartz by Nelson and Cochrane (1970) and Hume (1978). The plagioclase curve utilised in this thesis indicates a considerably higher plagioclase content for any peak height than does the curve of Nelson et al. This difference may be due to variations in plagioclase composition (Nelson et al., oligoclase; this thesis, andesine), or it may reflect the influence of large amounts of volcanic glass diluting the plagioclase in the curve of Figure B4. The quartz curves are comparable where the quartz concentration exceeds 10% by weight, but when it is lower, the curve shown in Figure B3 has a significantly lower quartz concentration and does not pass through the origin of the graph. The very high proportion of glass may also explain the unusual departure of the quartz curve from a straight line relationship.

TABLE 85: Standard mixtures run in triplicate and peak intensities for quartz, plagioclase and anorthoclase

| Standard Number | | Mineral Content (Wt. %) | Peak Height above Background ($\pm 1\sigma$) |
|---|---|---|---|
| | Plagioclase[1] | 12 | $8 \pm 1$ |
| 1 | Quartz[2] | 5 | $4 \pm 0.5$ |
| | Glass | 83 | - |
| | Plagioclase | 25 | $23 \pm 3$ |
| 2 | Quartz | 11 | $5 \pm 0.5$ |
| | Glass | 64 | - |
| | Plagioclase | 39 | $37 \pm 3$ |
| 3 | Quartz | 17 | $9 \pm 1$ |
| | Glass | 44 | - |
| | Plagioclase | 54 | $48 \pm 3$ |
| 4 | Quartz | 23 | $15 \pm 1.5$ |
| | Glass | 23 | - |
| | Anorthoclase[3] | 15 | $11 \pm 2$ |
| 5 | Quartz | 5 | $4 \pm 0.5$ |
| | Glass | 80 | - |
| | Anorthoclase | 30 | $23 \pm 3$ |
| 6 | Quartz | 10 | $6 \pm 1$ |
| | Glass | 60 | - |
| | Anorthoclase | 45 | $35 \pm 4$ |
| 7 | Quartz | 15 | $8 \pm 1$ |
| | Glass | 40 | - |
| | Anorthoclase | 60 | $51 \pm 4$ |
| 8 | Quartz | 20 | $13 \pm 1.5$ |
| | Glass | 20 | - |

1. Peak height above background at 3.19 Å ($28.0^\circ$ 2θ)
2. Peak height above background at 4.26 Å ($20.8^\circ$ 2θ)
3. Peak height above background at 3.24 Å ($28.5^\circ$ 2θ)

FIGURE B3: Intensity - concentration curve for quartz. (400 cps)

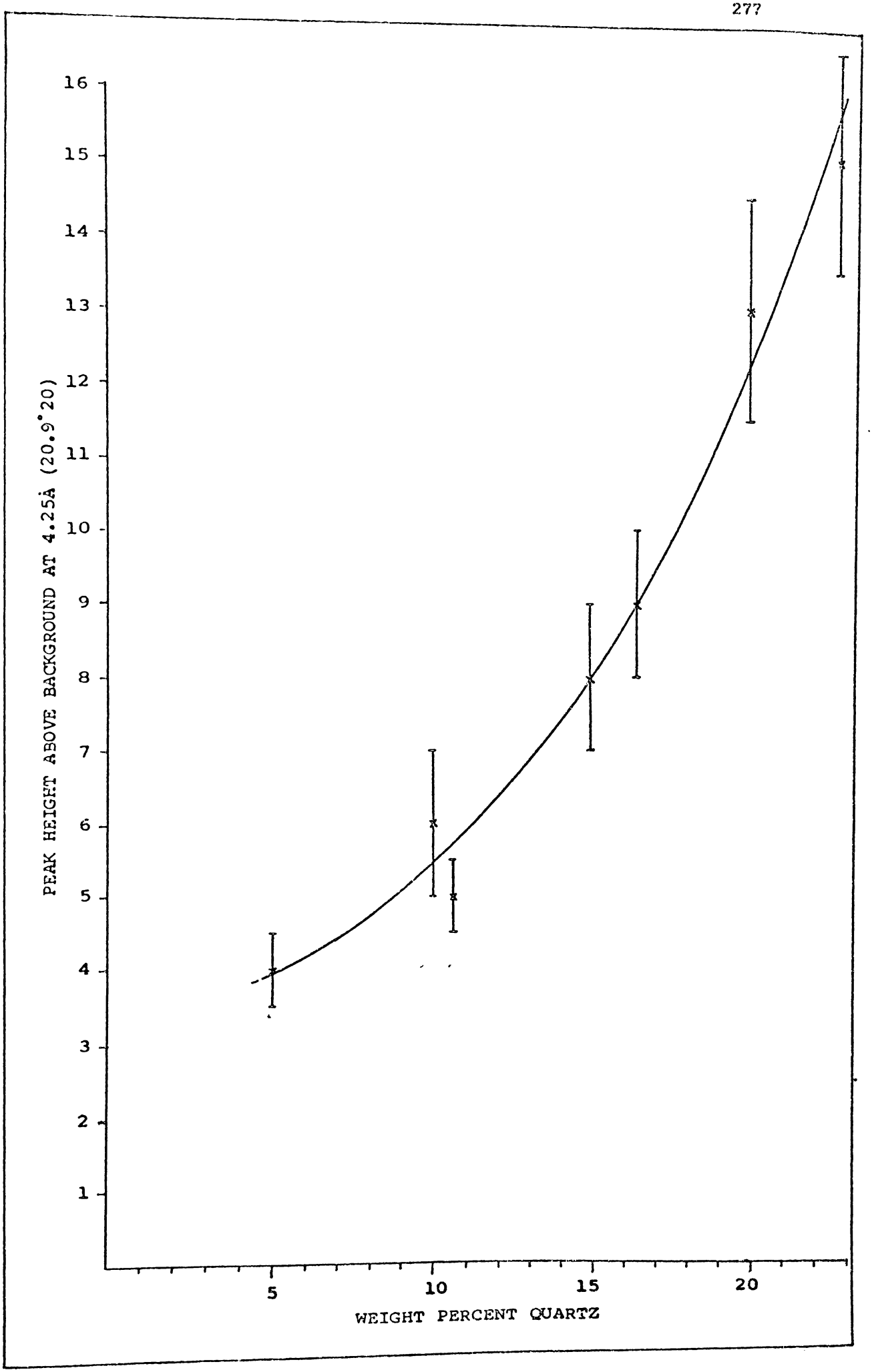
PEAK HEIGHT ABOVE BACKGROUND AT 4.25Å (20.9°2θ)
16
15
14
13
12
11
10
9
8
7
6
5
4
3
2
1
5
10
15
20
WEIGHT PERCENT QUARTZ

FIGURE B4: Intensity - concentration curve for plagioclase. (400 cps)

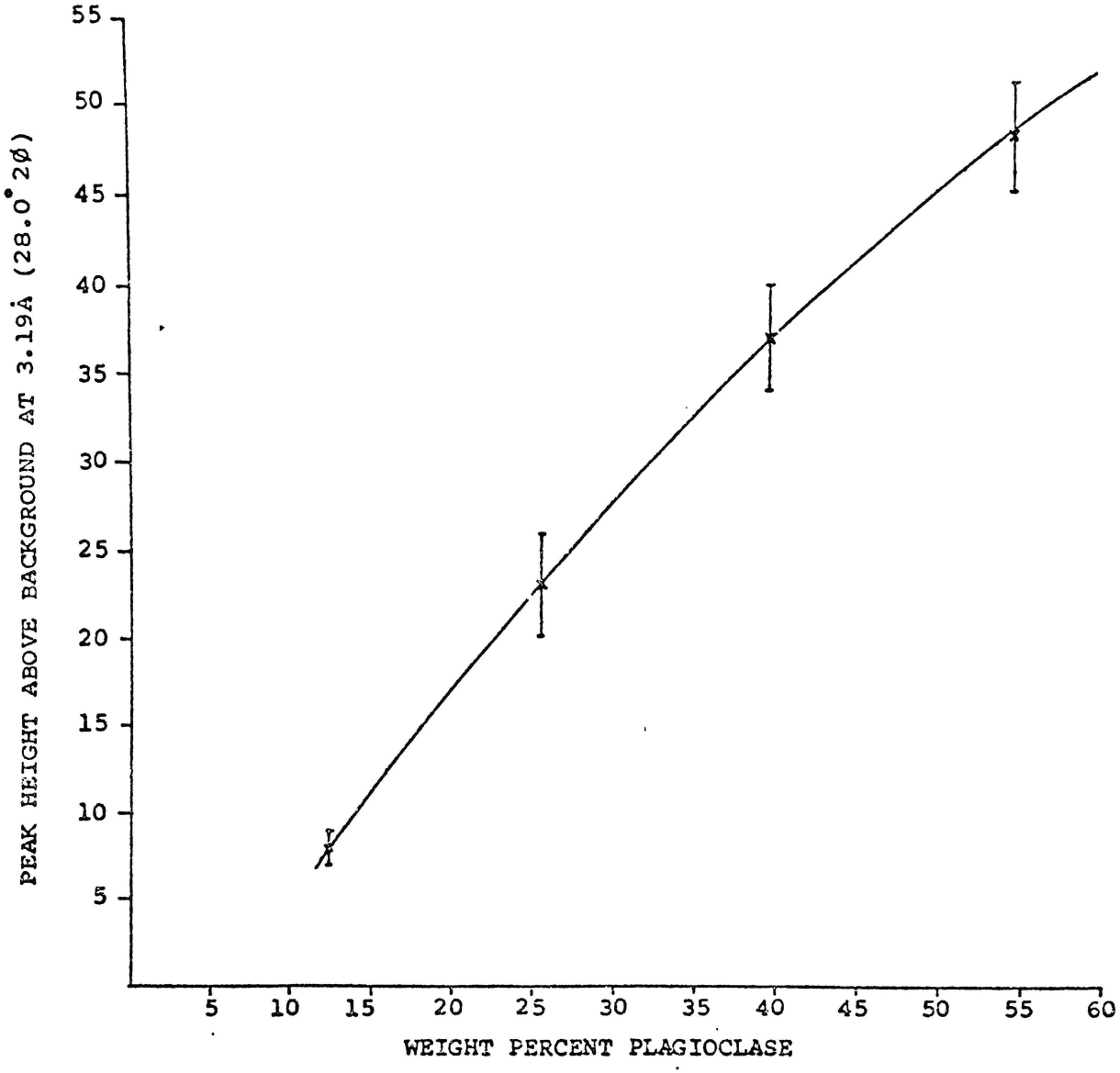
PEAK HEIGHT ABOVE BACKGROUND AT 3.19Å (28.0° 2Ø)
55
50
45
40
35
30
25
20
15
10
5
5 10 15 20 25 30 35 40 45 50 55 60
WEIGHT PERCENT PLAGIOCLASE

FIGURE B5: Intensity - concentration curve for anorthoclase. (400 cps)

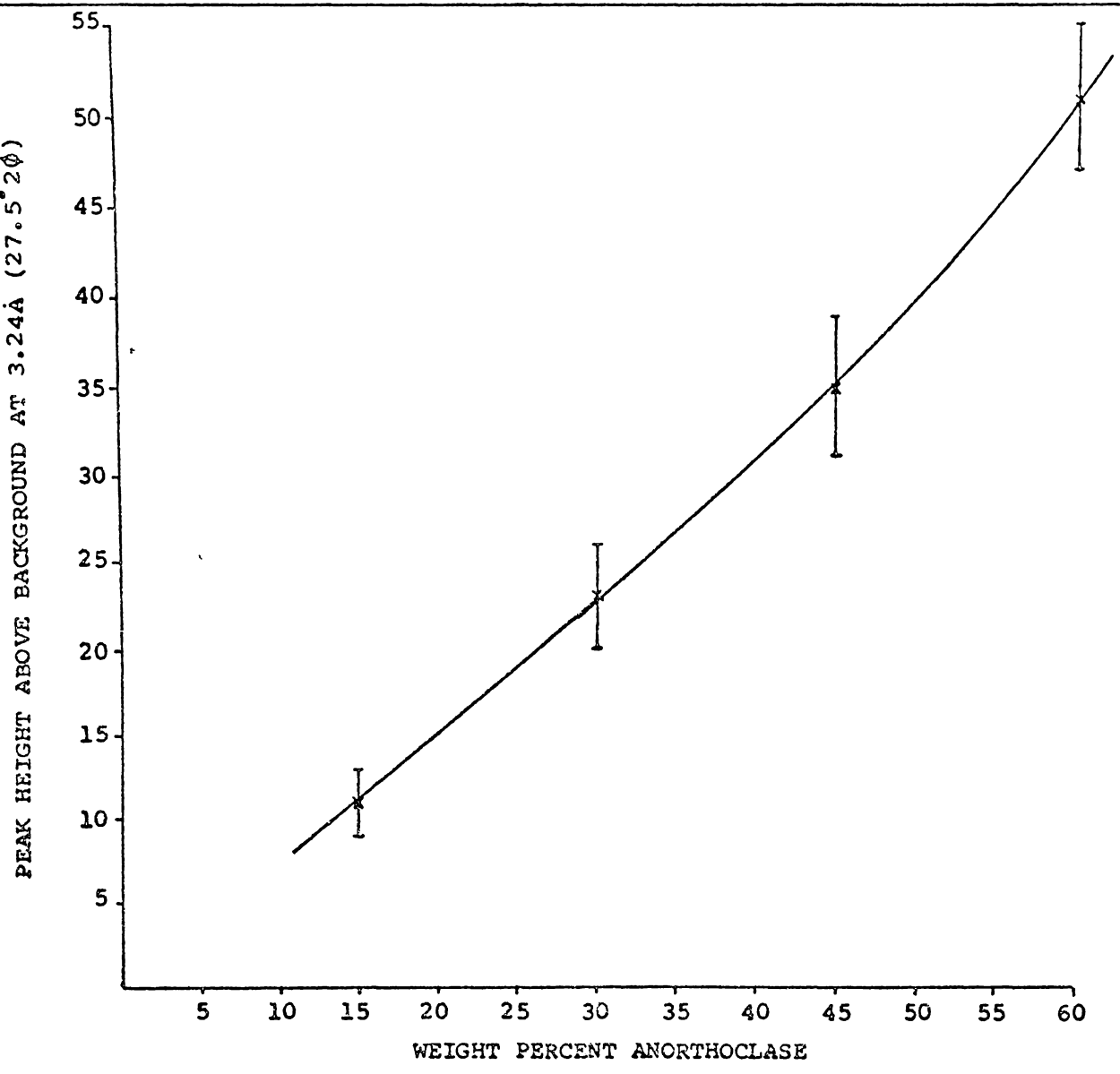
PEAK HEIGHT ABOVE BACKGROUND AT 3.24Å (27.5°2ϕ)
55
50
45
40
35
30
25
20
15
10
5
5
10
15
20
25
30
35
40
45
50
55
60
WEIGHT PERCENT ANORTHOCLASE

FIGURE B6 : Logarithmic plot of the X-ray spectrum of titanomagnetite from field class V (P18) identifying peaks from the main elements and showing Regional and Local background positions.

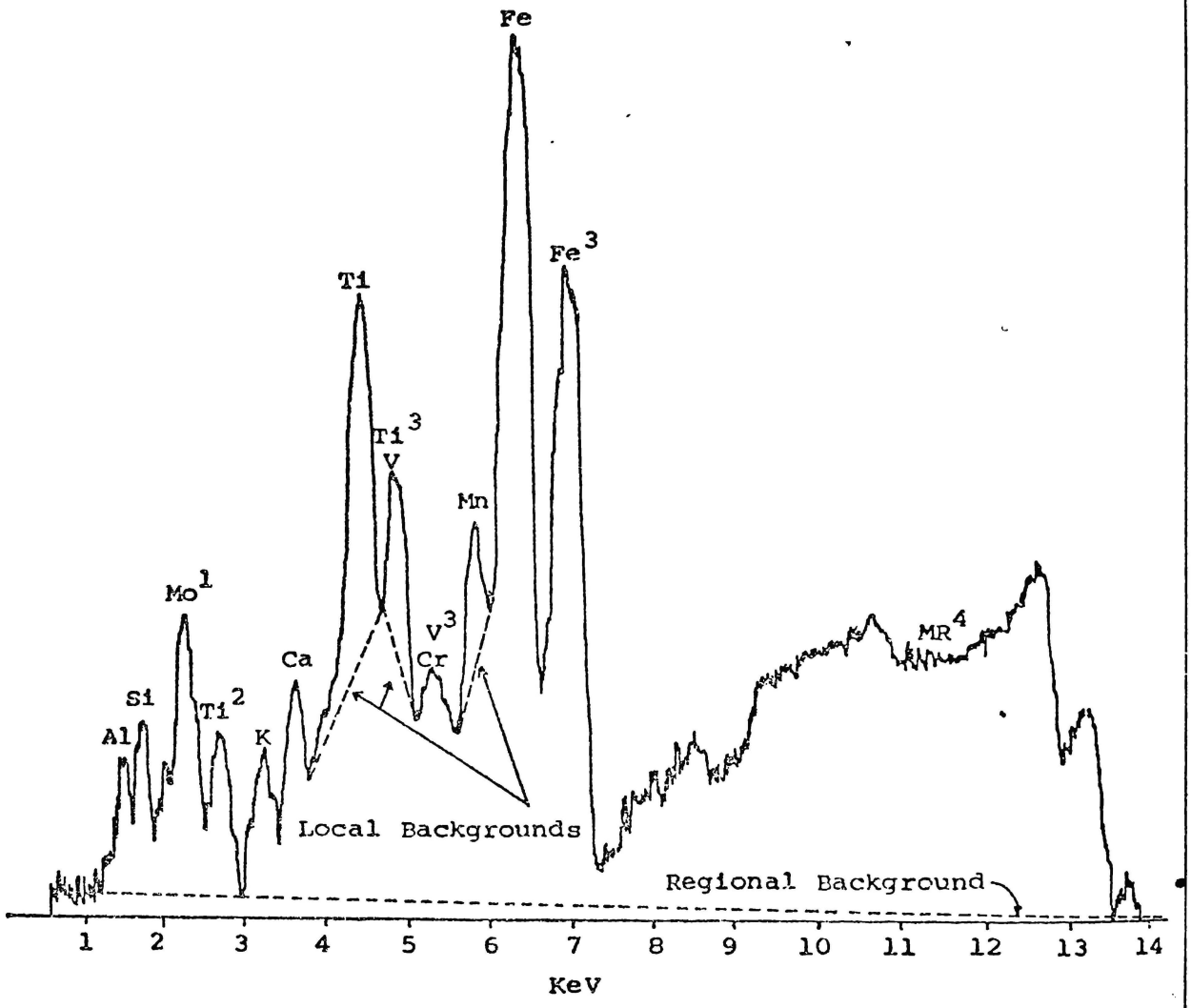


NOTE : 1 . Mo (Lα)
2 . Ti escape peak
3 . Element K (β)
4 . MR = Monitoring Region

All peaks are K (α) unless otherwise indicated.

(4) Elemental analyses of Titanomagnetite by X-ray fluorescence (X.R.F.)

Sample preparation

Large quantities of oven-dried samples were ground lightly in a ring-mill to release enclosed titanomagnetite crystals. Impure titanomagnetite concentrates were obtained by extraction with a magnet under water. Purification and grinding of the samples were completed in two steps: by moderate grinding in an agate mortar and multiple extraction under acetone followed by extreme grinding and multiple extraction until the magnetites had an estimated purity in excess of 99%. Powdered titanomagnetites were covered with mylar film and analysed using the conditions described below.

Experimental conditions

Analyses were carried out using an energy dispersive X-ray fluorescence (Ortec 6110) with a Si (Li) detector and a multichannel analyser interfaced with a 16K word PDP 11/05 computer. The excitation conditions consisted of unfiltered radiation from a molybdenum anode operated at 15 kV and 20 mA with the sample irradiated under a vacuum of approximately 6 MPa. Samples were analysed automatically in groups of eight accompanied by four standards, inserted to detect any machine drift.

Kohn (1970) found that combinations of the ratios of Ti, V, Mn and Co served to identify each of the tephras he examined. A typical X-ray spectrum for titanomagnetite extracted from the Coromandel tephras indicates that the concentration of Co was too low to permit measurement by this method (Fig. B6). Although all peak intensities for the nine elements shown in Fig. B6 were

recorded, the experimental conditions were established by utilising ratios of the fluorescent intensities of Ti, V and Mn. Machine conditions and sample matrices were monitored by counting a narrow band of channels devoid of spectra from the sample between 11.41 and 11.59 KeV. The interference of TiKβ on VKα was overcome by peak stripping techniques involving the analysis of pure $TiO_2$.

The peak intensity to background ratio has considerable influence upon the sensitivity and reproducibility of results and is controlled principally by the positioning of the background levels, which can be either regional or local (Fig. B6). The influence of both regional and local background positions was determined experimentally from two samples (P9, P16) which were repeatedly analysed for each background position (Table B6).

TABLE B6: The influence of the peak to background ratio on the reproducibility and sensitivity of results

| Background Position | Sample | Elemental Ratio | Number of Analyses | Mean | Standard Deviation | Coefficient of variation (%) |
|---|---|---|---|---|---|---|
| Regional | P16 | Ti/V | 10 | 26.26 | 1.09 | 4.17 |
| | | Ti/Mn | 10 | 11.34 | 0.15 | 1.36 |
| | P9 | Ti/V | 10 | 25.53 | 0.57 | 2.22 |
| | | Ti/Mn | 10 | 17.69 | 0.24 | 1.38 |
| Local | P16 | Ti/V | 10 | 26.99 | 1.45 | 5.38 |
| | | Ti/Mn | 10 | 11.35 | 0.10 | 0.88 |
| | P9 | Ti/V | 10 | 25.50 | 0.46 | 1.80 |
| | | Ti/Mn | 10 | 17.50 | 0.22 | 1.28 |

The peak to background ratio showing the highest coefficient of variation is Ti/V and thus the background position which provides the best reproducibility for this ratio (i.e. regional background) has been used.

The optimum counting time was derived in a similar manner to that outlined above. One sample (P18) was analysed twelve times without disturbing the powder, for three different time intervals - 100, 200 and 400 seconds (Table B7).

TABLE B7: The influence of optimum counting time on reproducibility of results - utilising sample P18

| Counting Time (seconds) | Elemental Ratio | Number of Analyses | Mean | Standard Deviation | Coefficient of variation (%) |
|---|---|---|---|---|---|
| 100 | Ti/V | 12 | 29.36 | 2.72 | 9.27 |
| | Ti/Mn | 12 | 10.71 | 0.17 | 1.61 |
| 200 | Ti/V | 12 | 28.09 | 1.07 | 3.83 |
| | Ti/Mn | 12 | 10.73 | 0.18 | 1.70 |
| 400 | Ti/V | 12 | 28.69 | 0.96 | 3.34 |
| | Ti/Mn | 12 | 10.68 | 0.12 | 1.13 |

A counting time of 400 seconds was selected since this time interval resulted in ratios showing the lowest coefficients of variation.

The reproducibility of the Ti, V and Mn fluorescent intensity ratios for two samples (P8, P18) was examined by multiple analysis of powders freshly packed prior to each analysis (Table B8).

TABLE B8: Influence of repacking of powdered samples on reproducibility of results

| Sample | Elemental Ratio | Number of Analyses | Mean | Standard Deviation | Coefficient of variation (%) |
|---|---|---|---|---|---|
| P8 | Ti/V | 16 | 24.01 | 0.65 | 2.72 |
| | Ti/Mn | 16 | 18.14 | 0.22 | 1.22 |
| P18 | Ti/V | 16 | 28.95 | 0.96 | 3.30 |
| | Ti/Mn | 16 | 10.94 | 0.15 | 1.35 |

Note 1) Counting time = 400 seconds, using regional background positions.

The coefficients of variation obtained above have been used to calculate the standard deviations for samples P8 and P18 in Fig.3.12 (p.79)

Although ground titanomagnetite powders were utilised in preference to glass discs because the equipment for their manufacture was not available, it is unlikely that the use of solid solutions would have improved the usefulness of the method. Norrish and Hutton (1969) point out that errors in analysing powders arise from the mineralogical heterogeneity of the rock samples; these errors are obviously not applicable to the finely ground pure titanomagnetites used in this study. As the technique was designed as an aid in the correlation of deposits in closely spaced stratigraphic columns, elemental concentrations were not required. The use of fluorescent intensities of various elements rather than their concentrations avoids matrix effects and the need for dilution, which reduces the

sensitivity of the method for trace elements. The statement of Smith and Westgate (1969) concerning the use of elemental analyses for the identification and characterisation of ash deposits is applicable here:

"Furthermore, if compositions are not required, simple identifications can be made on the X-ray count rate alone, thereby making it unnecessary to use standards of known composition, and also avoiding the calculations of element concentrations. Such a procedure would lend itself very readily to automation." (p.318).

5. Elemental analysis of individual titanomagnetite grains by Electron Microprobe Analysis (E.M.)

Samples of titanomagnetite grains were polished, gold coated and then irradiated under a JEOL-JSM 35 scanning electron microscope fitted with an ORTEC energy dispersive electron microprobe. Operating conditions were an accelerating voltage of 25 KV, specimen absorbed current $6 \times 10^{-10}$A, 1300 times magnification and 40 second counting time.

Intensities of Fe and Ti measured on a multi-channel analyser were determined by partial integration of peak counts, with the energy range integrated approximately equal to the sum of the intensities of all channels within the full width at half the maximum intensity i.e. the FWHM (Fig. B7).

An Sn standard analysed over 40 times during the period of analysis to monitor operating conditions, had a coefficient of variation of 1.61% associated with the mean of a ratio of the 3.52 KeV

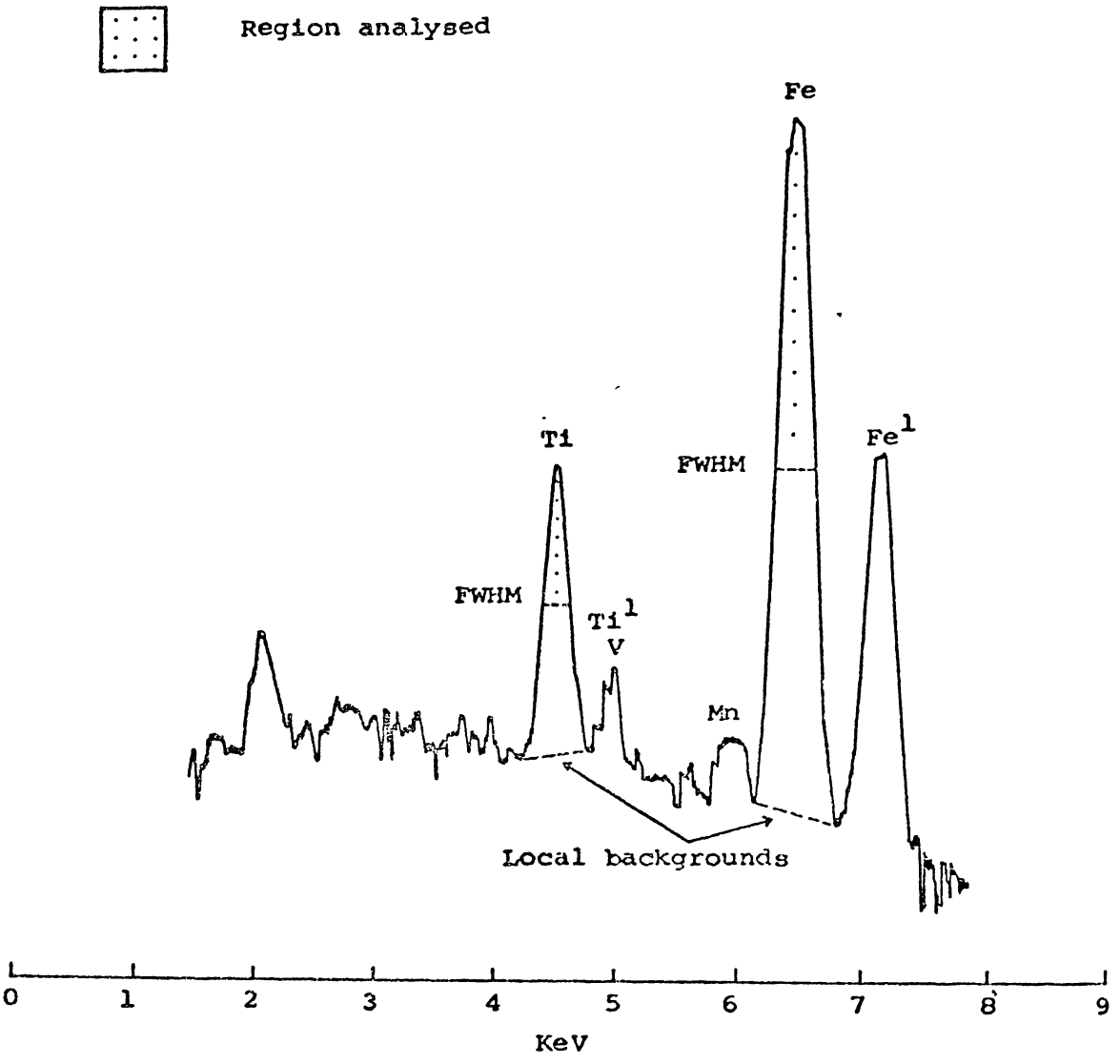


FIGURE B7 : Logarithmic plot of the X-ray spectrum of titanomagnetite from field class V (K10) identifying peaks from the main elements as analysed by electron microprobe.

Note : 1. Element K(β)
All peaks are K(α) unless otherwise indicated.

channel over the total counts from the FWHM.

Unmixed titanomagnetite grains were detected and avoided by their extreme Fe/Ti ratios as compared with the ratios normally exhibited by homogeneous grains (Fig. B8 ).

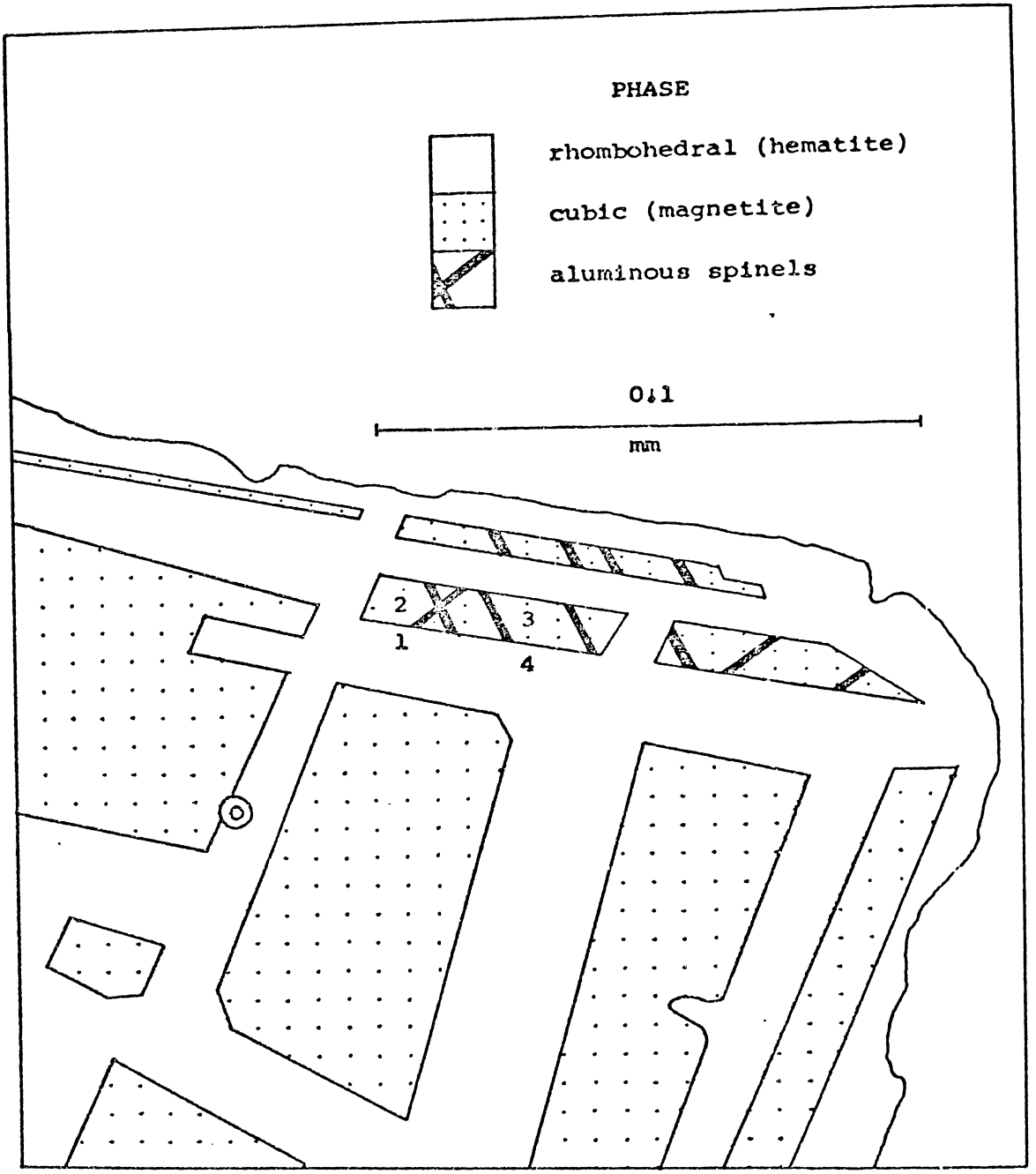


FIGURE B8 : Exsolved titanomagnetite grain analysed to enable identification of nonhomogeneous grains under the SEM. (Fe/Ti ratio for homogeneous grains =4.0-7.8)

Analysis points : (1) rhombohedral phase (Fe/Ti = 3.94)
(2) cubic phase (Fe/Ti = 14.81)
(3) cubic phase (Fe/Ti = 14.14)
(4) rhombohedral phase (Fe/Ti = 3.74)

(Note : Fe/Ti equals the total counts of Fe accumulated in 40 seconds divided by those for Ti)

## 6. Evaluation of techniques for characterising composite tephra deposits

One of the aims of this thesis was to establish new techniques to facilitate correlation of tephras within mixed tephra beds and to discriminate between individual tephras within such mixtures. Two new techniques have been presented.

1. Elemental analysis of bulk concentrations of titanomagnetite

The elemental analysis of finely ground, purified titanomagnetite separates by XRF has proved to be a rapid and effective means of correlating tephras between sites and for distinguishing individual tephras within a stratigraphic sequence. Since the technique was developed it has been utilised successfully in other tephra studies carried out at the University of Waikato, namely on studies of the Horotiu and Waihou silt loams by Jessen (1977), the Kauroa Ash by Salter (1979), the Late Quaternary tephra cover of the Hamilton Basin by Lowe (in prep.) and the Hamilton Ash Formation by Shepherd (in prep.).

The use of elemental ratios instead of elemental concentrations, while simplifying the procedure, does have the disadvantage of producing data that cannot easily be used by other workers. However, published titanomagnetite element concentrations can only be utilised for correlation purposes if they come from pure tephra deposits; the majority of tephras in this study are composite units so that absolute concentrations would be of little real value.

2. Elemental analysis of single grains of titanomagnetite

The successful application of elemental analysis of single titanomagnetite crystals in tephra studies has also been demonstrated. Electron microprobe analysis of sectioned and polished titanomagnetite grains has enabled the determination of the number of tephras present in mixed tephra deposits and also an estimate of their relative proportions. The major disadvantage of using the electron microprobe for this purpose is the long time required to examine each sample; if 50 grains are analysed per sample, approximately two hours of machine time are involved.

# APPENDIX C

## NUMBER, NAME AND LOCATION OF SITES REFERRED TO IN THE TEXT, AND NZMS 1 MAP EDITIONS

| Site Number | Site Name | Grid Reference |
|---|---|---|
| 1 | Tauranga highway | N53/416865 |
| 2 | Athenree subway | N53/365878 |
| 3 | Woodlands Rd | N53/342858 |
| 4 | Waimata Rd | N53/343865 |
| 5 | Waihi Beach corner | N53/422934 |
| 6 | Waihi Beach | N53/397923 |
| 7 | Tauranga Rd | N53/341939 |
| 8 | Pukekauri Rd | N53/303921 |
| 9 | Waitawheta | N53/263901 |
| 10 | Paeroa-Waihi highway | N53/310938 |
| 11 | Rawhiti Rd | N53/186825 |
| 12 | Rahu Rd | N53/225918 |
| 13 | Ngatitangata Rd | N53/394973 |
| 14 | Corner Heard and Trig Rds | N53/381958 |
| 15 | Thames-Paeroa highway | N53/170018 |
| 16 | Komata Reef Rd | N53/229995 |
| 17 | Waitakauri Valley | N53/272014 |
| 18 | Waihi-Whangamata highway | N53/384026 |
| 19 | Hikutaia Valley (1) | N53/229067 |
| 20 | Hikutaia Valley (2) | N53/244061 |
| 21 | Maratoto Valley | N53/245057 |
| 22 | State highway 25 | N53/373091 |
| 23 | Whangamata dump | N49/345150 |
| 24 | Ash type site | N49/343179 |
| 25 | Old Mill site | N49/345218 |
| 26 | Whangamata pub. | N49/340211 |
| 27 | Kopu 2 | N49/074198 |
| 28 | Kopu-Hikuai Rd (1) | N49/078205 |
| 29 | Kirikiri stream | N49/104225 |
| 30 | Kopu-Hikuai Rd (2) | N49/122233 |
| 31 | Kopu-Hikuai summit | N49/165250 |
| 32 | Kauaeranga Valley | N49/108263 |
| 33 | Tararu Valley | N49/045314 |
| 34 | Tairua river (1) | N49/235258 |
| 35 | Tairua river (2) | N49/234260 |

| Site Number | Site Name | Grid Reference |
|---|---|---|
| 36 | Hikuai Valley Rd | N49/232268 |
| 37 | Kopu site | N49/252285 |
| 38 | Kopu-Whangamata junction | N49/373317 |
| 39 | Tairua forest | N49/293304 |
| 40 | Opoutere Beach | N49/368298 |
| 41 | Ohui Beach | N49/366321 |
| 42 | Opoutere | N49/373337 |
| 43 | Hikuai-Pauanui Rd | N49/333359 |
| 44 | Tairua mill | N49/320370 |
| 45 | Pinnacles hut | N49/206378 |
| 46 | Tairua cemetery | N44/337412 |
| 47 | Tairua town | N44/340425 |
| 48 | Tairua-Whitianga highway | N44/330453 |
| 49 | Whitianga-Tairua Rd | N44/310474 |
| 50 | Dalmeny corner-Tairua | N44/306480 |
| 51 | Boat Harbour Rd (1) | N44/294518 |
| 52 | Boat Harbour Rd (2) | N44/285511 |
| 53 | Boat Harbour Rd (3) | N44/284522 |
| 54 | Coroglen-Dalmeny corner | N44/193518 |
| 55 | Topps Rd | N44/190533 |
| 56 | Whitianga-Coroglen Rd | N44/180528 |
| 57 | Kaimarama-Coroglen Rd (1) | N44/176538 |
| 58 | Whitianga | N44/158585 |
| 59 | Kaimarama-Coroglen Rd (2) | N44/158586 |
| 60 | Kaimarama-Coromandel Rd (1) | N44/127598 |
| 61 | Kaimarama-Coromandel Rd (2) | N44/033660 |
| 62 | Ohaka beach | N44/205662 |
| 63 | Wharekaho beach (1) | N44/215668 |
| 64 | Wharekaho beach (2) | N44/214668 |
| 65 | Whitianga-Kuaotunu highway | N44/218699 |
| 66 | Kuaotuna | N40/158723 |
| 67 | Whangapoua Rd | N40/105714 |
| 68 | Te Rerenga | N40/098722 |
| 69 | Te Rerenga-Whangapoua Rd | N40/098727 |
| 70 | Coromandel-Te Rerenga Rd | N40/076718 |

| Site Number | Site Name | Grid Reference |
|---|---|---|
| 71 | Whangapoua Beach | N40/110772 |
| 72 | Coromandel township | N40/006704 |
| 73 | Coromandel-Colville | N39/967760 |
| 74 | Kennedy Bay-Waikawau Bay Rd | N40/048894 |
| 75 | Waikawau Bay (1) | N40/027906 |
| 76 | Waikawau Bay (2) | N40/035906 |
| 77 | Waiaro site | N39/936916 |
| 78 | Waiaro Bay | N39/924926 |
| 80 | Parihaka Rd (Tairua forest) | N49/244165 |
| 81 | Mayor farm | N49/377118 |
| 82 | Whangamata reservoir | N49/355158 |
| 83 | Moana point | N49/345195 |
| 84 | Whangamata south | N49/348148 |
| 85 | Neavesville | c.N49/200215 |
| 86 | Tairua forest | N49/335195 |
| 87 | Ohui | N49/320347 |
| 90 | Welches Rd | N56/755781 |
| 91 | Rototuna | N56/776535 |
| 92 | Kakepuku | N74/792136 |
| 93 | Taotaoroa | N66/167335 |
| 95 | Tapapa | N66/372215 |
| 100 | Te Matai Rd | N67/779387 |
| 101 | Maniatutu Rd | N76/887199 |
| 102 | Rotorua-Paengaroa highway | N67/846298 |
| 103 | Matahina Rd | N86/192886 |
| 104 | Democrat Rd | N86/934824 |
| 105 | Gavin Rd | N86/995824 |
| 106 | Tikitere Hill | N76/828133 |
| 107 | Maketu Estuary | N59/910495 |
| 108 | Te Ngae | N76/792114 |
| 109 | Ohauiti Rd | N67/656460 |
| 110 | Bethlehem | N58/590579 |
| 111 | Youngson Rd (formerly Crapps Rd) | N58/496614 |
| 112 | Reas Rd | N57/379725 |
| 113 | Otamarakau | N68/052407 |

MAP EDITIONS FOR THE 1:63 360 TOPOGRAPHICAL MAP SERIES (NZMS 1)

| | | |
|---|---|---|
| N39 | – | 3rd Ed. (1974) |
| N40 | – | 3rd Ed. (1974) |
| N44 | – | 4th Ed. (1972) |
| N49 | – | 3rd Ed. (1967) |
| N53 | – | 3rd Ed. (1965) |
| N56 | – | 3rd Ed. (1965) |
| N57 | – | 4th Ed. (1974) |
| N58 | – | 3rd Ed. (1965) |
| N59 | – | 2nd Ed. (1967) |
| N65 | – | 4th Ed. (1974) |
| N66 | – | 4th Ed. (1971) |
| N67 | – | 2nd Ed. (1965) |
| N68 | – | 2nd Ed. (1967) |
| N74 | – | 3rd Ed. (1974) |
| N76 | – | 2nd Ed. (1964) |
| N86 | – | 2nd Ed. (1968) |

# APPENDIX D

## TITANOMAGNETITE ELEMENT RATIOS FOR THE COROMANDEL TEPHRAS, AND TEPHRAS FROM THE KATIKATI REGION

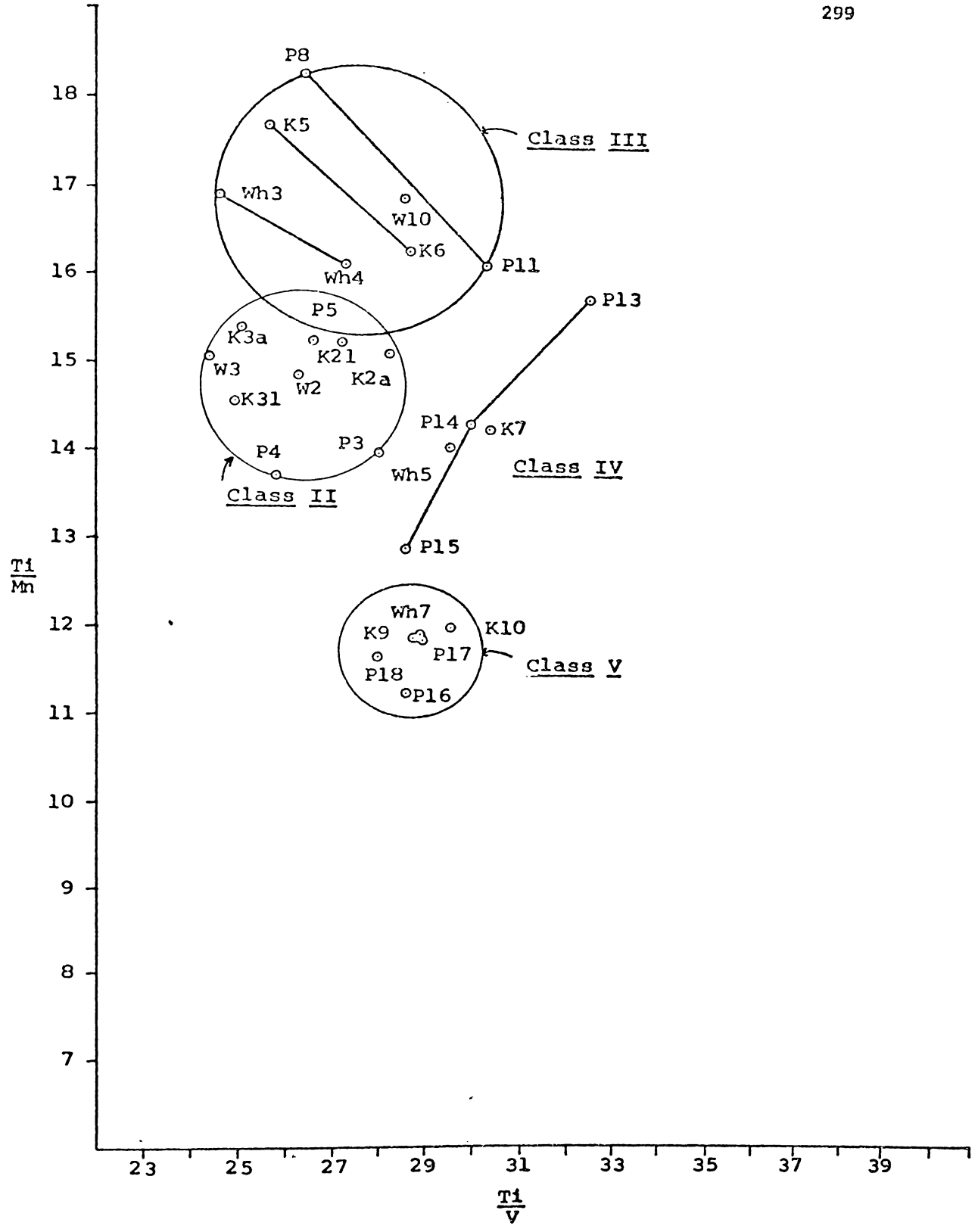


FIGURE D.1 : Summary of the ratios of count rates of Ti, Mn and V from titanomagnetites extracted from field classes II to V from the major sites on the Coromandel Peninsula. Samples from Pukekauri Rd(P3,P4,P5,P8,P11,P13,P14,P15,P16,P17,P18), Waihi Beach(W2,W3,W10), Kopu(K2a,K21,K3a,K31,K5,K6,K7,K9, K10), and Whitianga (Wh3,Wh4,Wh5,Wh7). Circles encompass all samples from the Coromandel Peninsula sites for field classes II, III and V.

TABLE D.1 : Ti/V AND Ti/Mn ratios of titanomagnetites analysed by XRF, for sites 8, 37, 6 and 58.

| Site | Sample | Ti/V | Ti/Mn |
|---|---|---|---|
| Pukekauri Rd (site 8) | P1 | 32.6 | 14.1 |
| | P2 | 32.2 | 13.7 |
| | P3 | 28.0 | 14.0 |
| | P4 | 25.8 | 13.8 |
| | P5 | 26.6 | 15.3 |
| | P6 | 26.5 | 16.9 |
| | P7 | 26.7 | 17.9 |
| | P8 | 26.4 | 18.3 |
| | P9 | 26.7 | 17.8 |
| | P10 | 27.0 | 17.1 |
| | P11 | 30.4 | 16.2 |
| | P12 | 29.8 | 16.2 |
| | P13 | 32.4 | 15.8 |
| | P14 | 29.8 | 14.3 |
| | P15 | 28.5 | 12.9 |
| | P16 | 28.6 | 11.2 |
| | P17 | 28.9 | 11.9 |
| | P18 | 28.0 | 11.6 |
| Kopu (site 37) | K2Ash (K2A) | 28.3 | 15.1 |
| | K2 lapilli (K2L) | 27.2 | 15.3 |
| | K3Ash (K3A) | 25.1 | 15.4 |
| | K3 lapilli (K3L) | 25.0 | 14.6 |
| | K5 | 25.7 | 17.7 |
| | K6 | 28.6 | 16.3 |
| | K7 | 30.3 | 14.3 |
| | K9 | 28.7 | 11.9 |
| | K10 | 29.5 | 12.1 |
| | Kcmpf | 28.6 | 11.9 |

| Site | Sample | Ti/V | Ti/Mn |
|---|---|---|---|
| Waihi Beach (site 6) | W2 | 26.3 | 14.9 |
| | W3 | 24.5 | 15.1 |
| Whitianga (site 58) | Wh3 | 24.6 | 16.9 |
| | Wh4 | 27.3 | 16.2 |
| | Wh5 | 29.5 | 14.1 |
| | Wh7 | 28.9 | 11.9 |
| Old Mill (site 25) | OM3/4 lapilli (OM3/4L) | 23.7 | 6.3 |

TABLE D.2 : Ti/V and Ti/Mn Ratios of titanomagnetites, analysed by XRF, for sites 112, 111, 110 and 100.

| Site | Sample | Ti/V | Ti/Mn |
|---|---|---|---|
| Reas Rd (site 112) | R1 | 24.9 | 15.0 |
| | R2 | 24.6 | 16.1 |
| | R3 | 23.8 | 17.1 |
| | R4 | 24.6 | 18.2 |
| | R5 | 26.9 | 17.8 |
| | R6 | 26.3 | 17.4 |
| | R7 | 26.4 | 15.4 |
| | R8 | 25.8 | 11.5 |
| Youngson Rd (site 111) | Y1 | 28.4 | 13.6 |
| | Y2 | 25.7 | 14.7 |
| | Y3 | 26.1 | 16.2 |
| | Y4 | 25.0 | 16.5 |
| | Y5 | 26.6 | 17.6 |
| | Y6 | 28.3 | 17.4 |
| | Y7 | 30.4 | 17.4 |
| | Y8 | 28.0 | 15.4 |
| | Y9 | 26.2 | 10.9 |
| Bethlehem (site 110) | B1 | 33.2 | 13.7 |
| | B2 | 29.4 | 14.5 |
| | B3 | 26.5 | 14.6 |
| | B4 | 29.5 | 15.5 |
| | B5 | 26.4 | 16.8 |
| | B6 | 26.6 | 16.8 |
| | B7 | 26.7 | 17.1 |
| | B8 | 27.4 | 17.4 |
| | B9 | 37.3 | 16.4 |

| Site | Sample | Ti/V | Ti/Mn |
|---|---|---|---|
| Ohauiti Rd (site 109) | 01 | 31.2 | 12.8 |
| | 02 | 31.3 | 12.4 |
| | 03 | 34.1 | 12.9 |
| | 04 | 32.4 | 13.2 |
| | 05 | 31.1 | 13.7 |
| | 06 | 28.0 | 16.2 |
| | 07 | 26.0 | 17.1 |
| Te Matai Rd (site 100) | TM1 | 36.1 | 12.7 |
| | TM3 | 39.4 | 12.1 |
| | TM4 | 40.5 | 11.8 |

# APPENDIX E

## PARTICLE SIZE DATA AND PARAMETERS

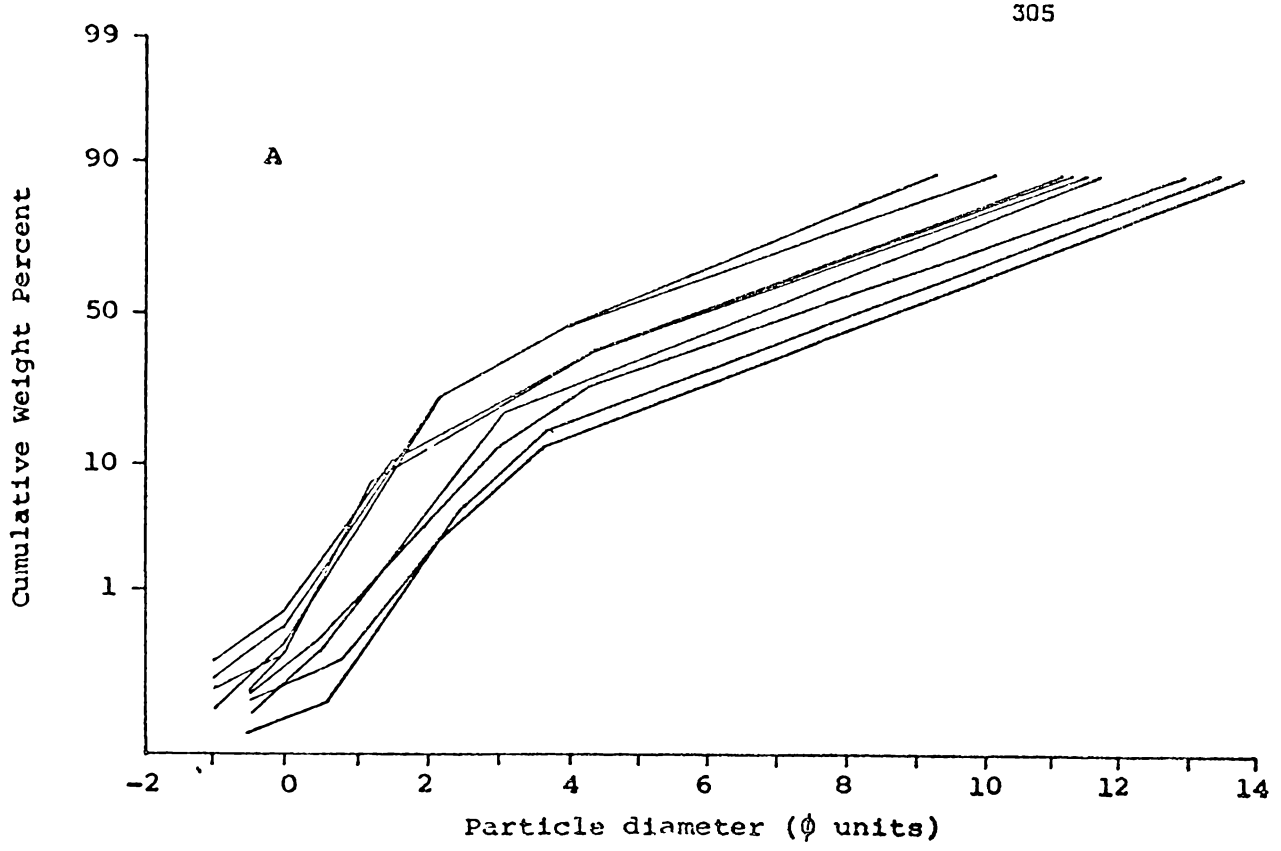


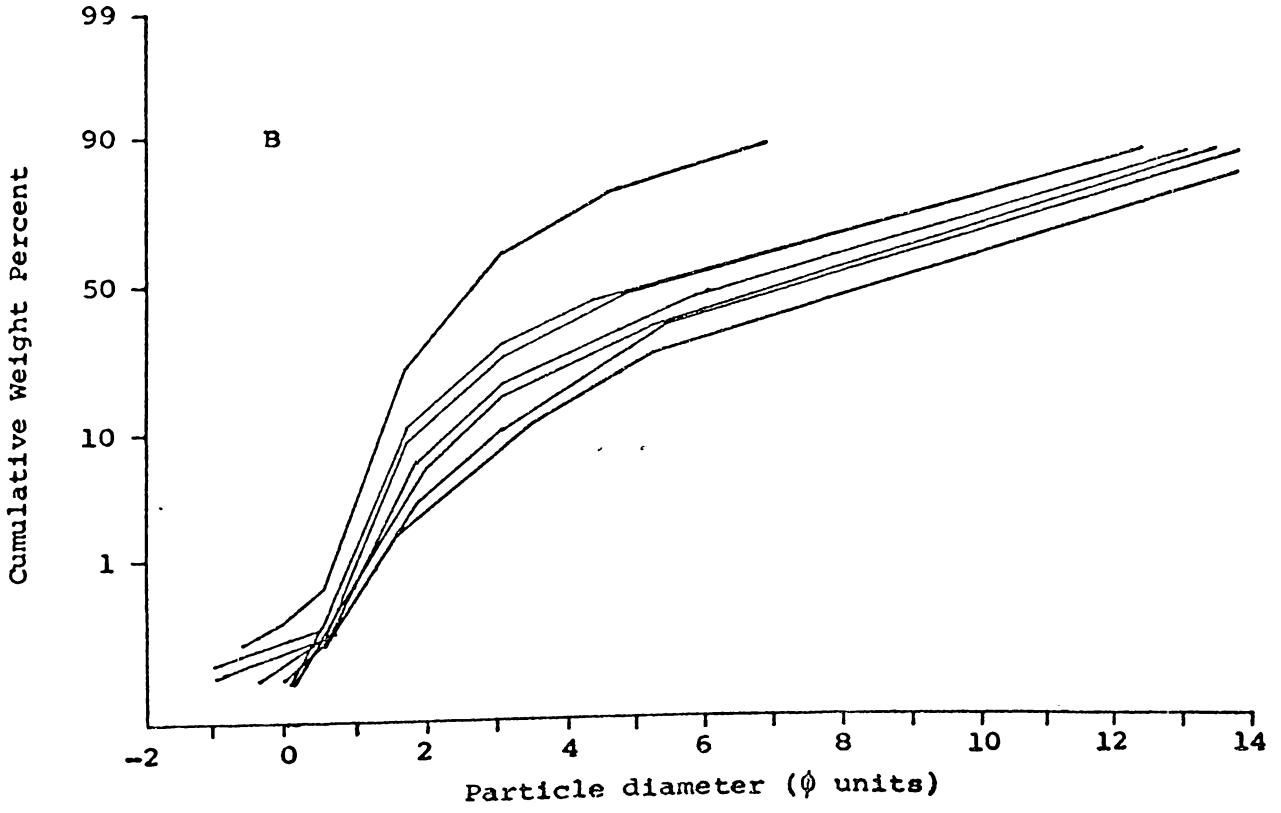


FIGURE E.1 : Particle size curves for the Pukekauri Rd. tephras.
A : Samples P1,P2,P3,P4,P5,P6,P7,P8, and P9
B : Samples P10,P11,P12,P13,P14,P15, and P18
Individual samples are not labeled because of the similarity in their grain size distributions.

FIGURE E.2 : Histograms of the particle size distributions of the Pukekauri Rd tephras. Samples P1,P4,P10,P15 and P18.

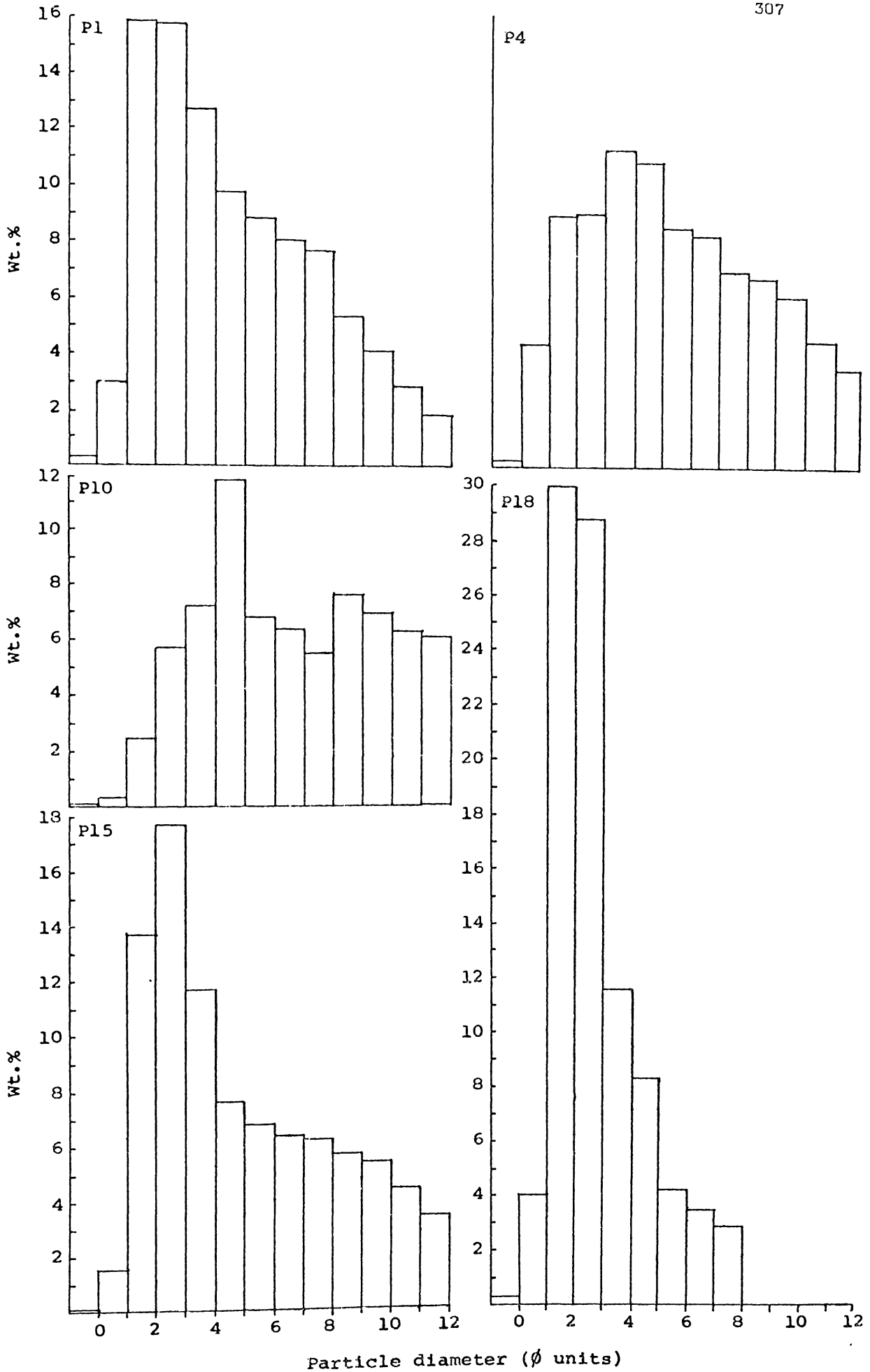
P1
P4
P10
P18
P15
Wt.%
Particle diameter (Ø units)

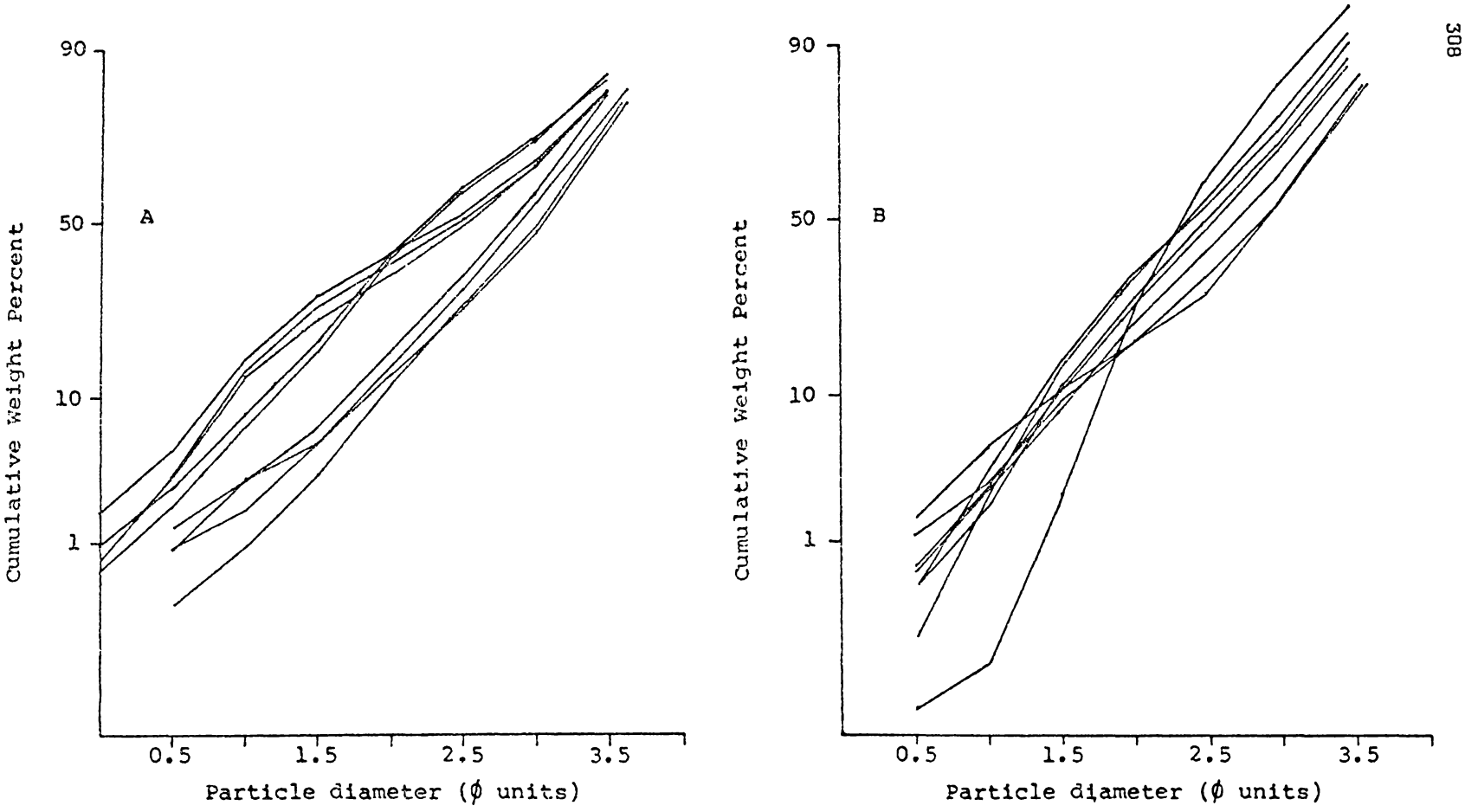


FIGURE E.3 : Particle size curves for the coarser than 4ϕ fraction of the Pukekauri Rd. tephras.
A : Samples P1,P2,P3,P4,P5,P6,P7,P8,P9
B : Samples P10,P11,P12,P13,P14=P15,P16,P17,P18
Individual samples are not labeled because of the similarity in their grain size distributions.

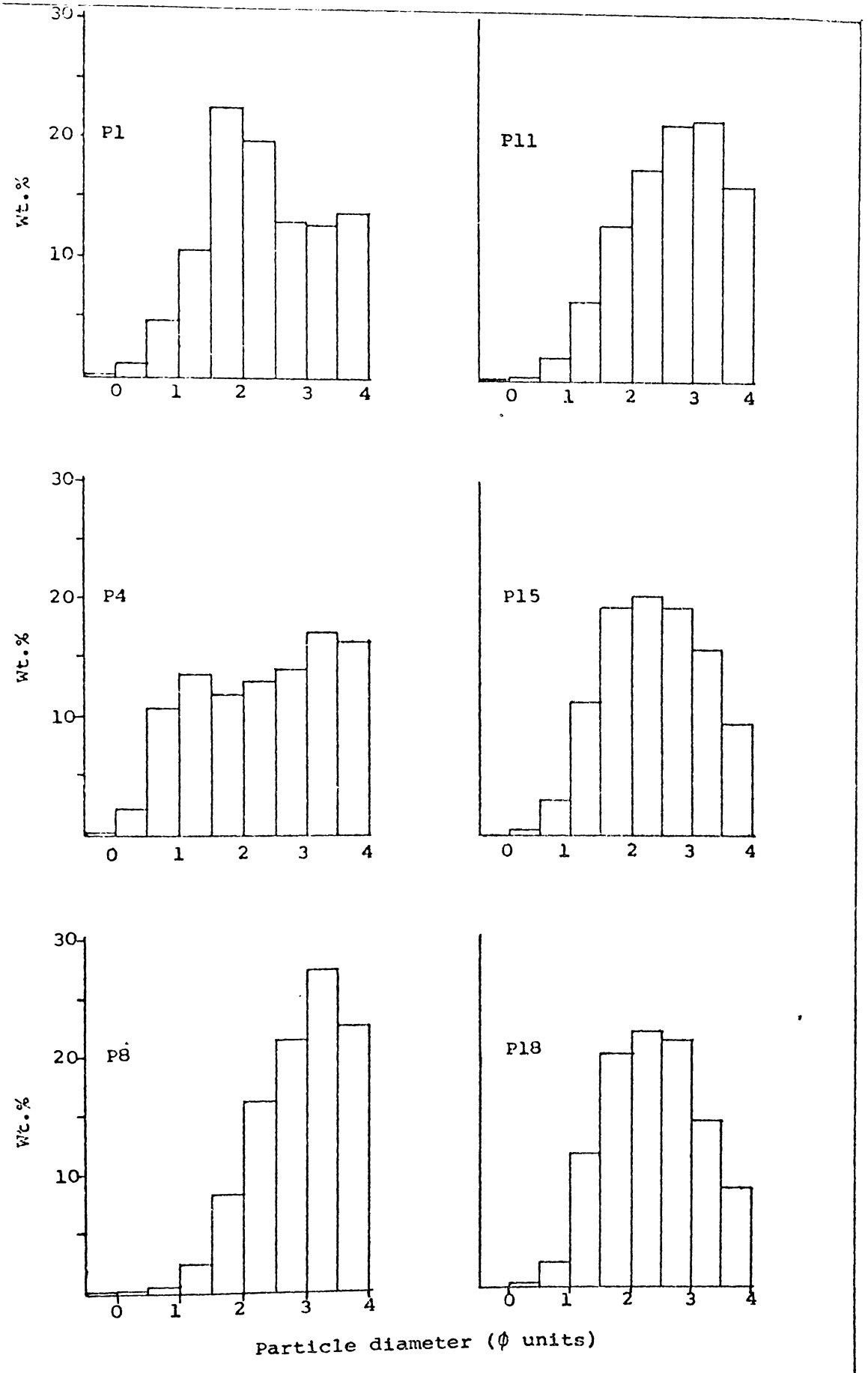


FIGURE E.4 : Histograms of the particle size distributions of the coarser than 4ϕ fraction of Pukekauri Rd. samples P1, P4, P8, P11, P15, P18.

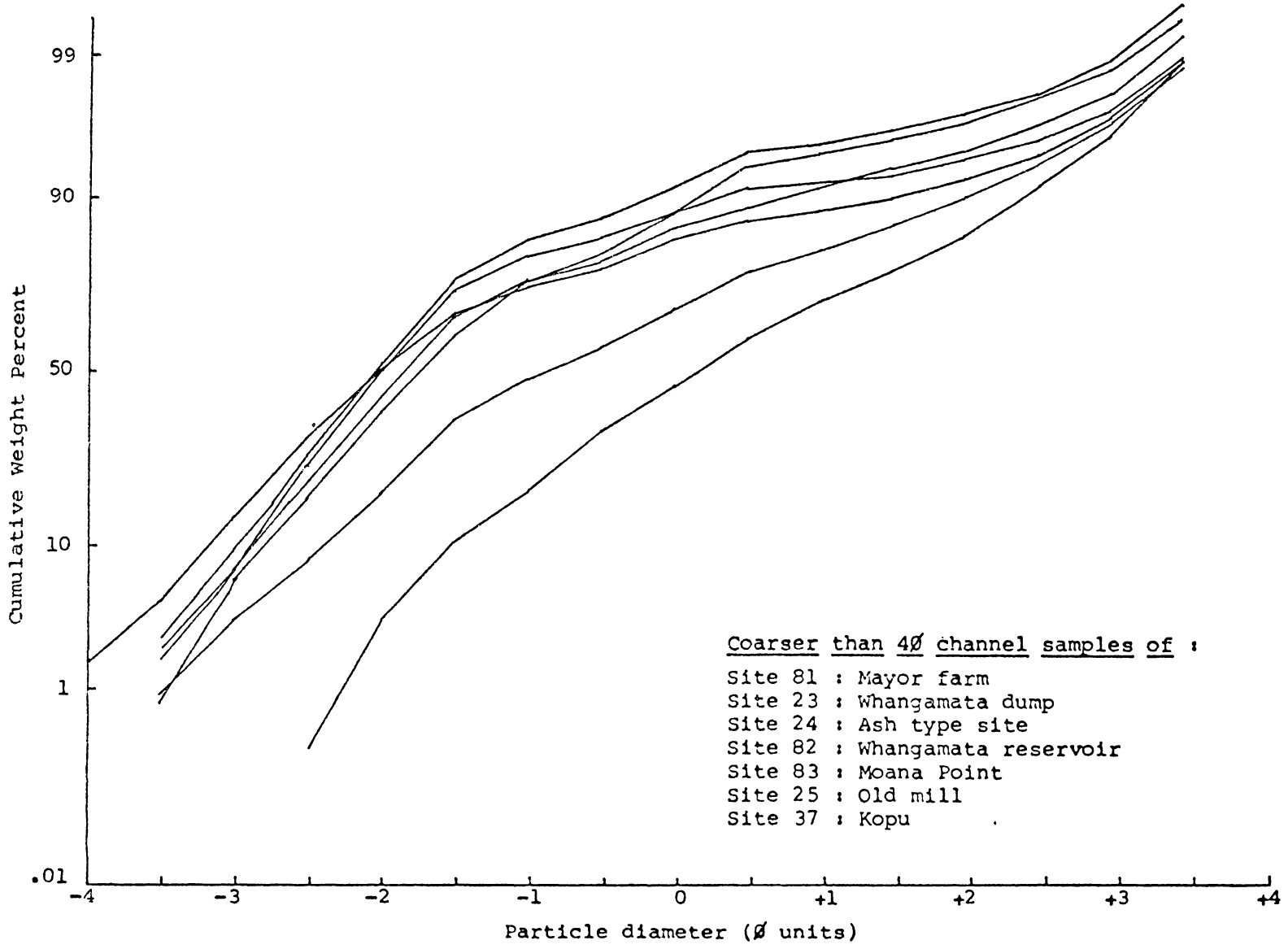


FIGURE E.5 : Cumulative frequency curves of the coarser than 4Ø fraction of class II channel samples from the greater Whangamata area.(see Fig. 4.3).

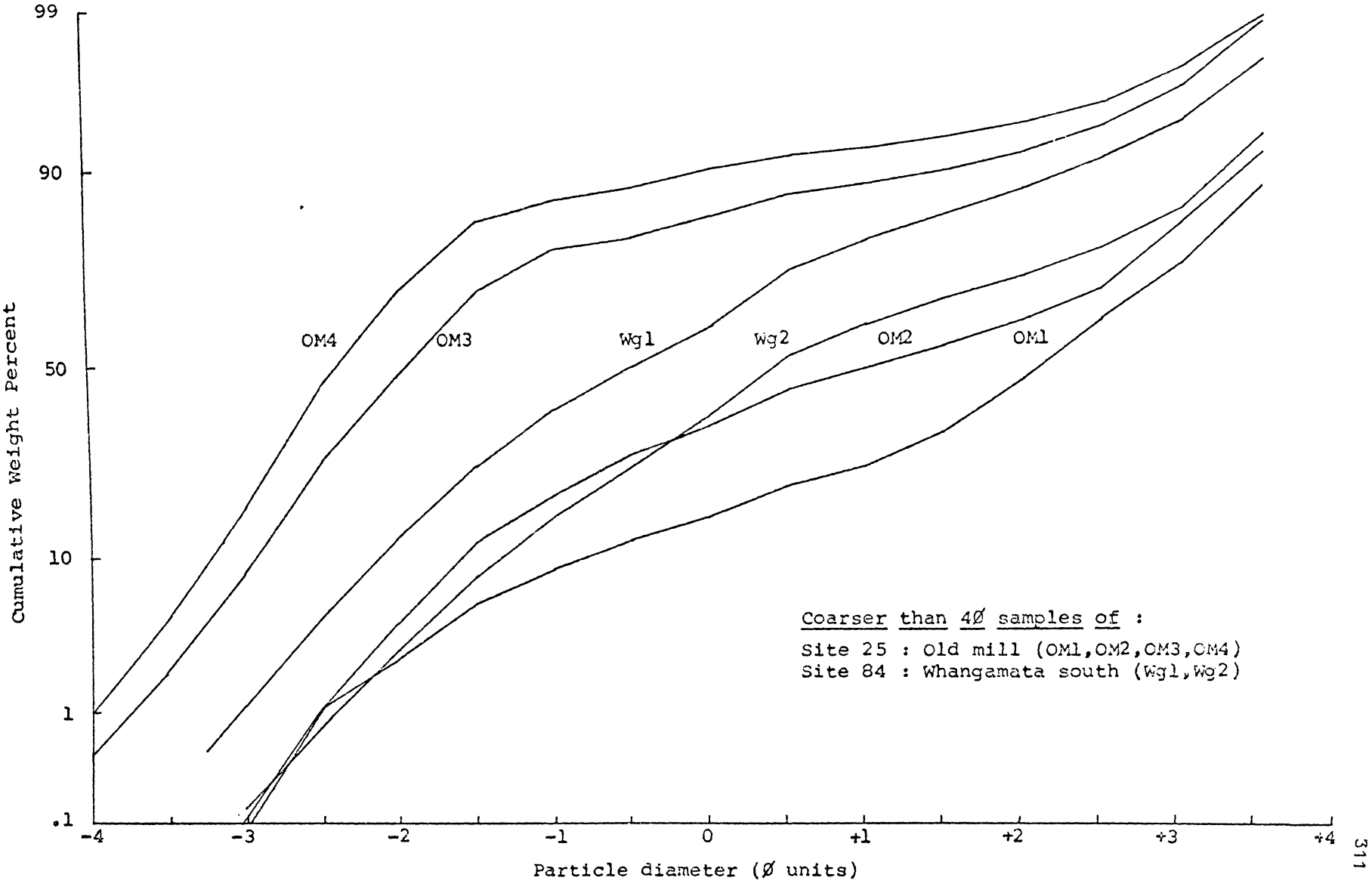


FIGURE E.6 : Cumulative frequency curves for the coarser than 4Ø fraction of field class II samples from sites 25 and 84. (see Fig.4.5).

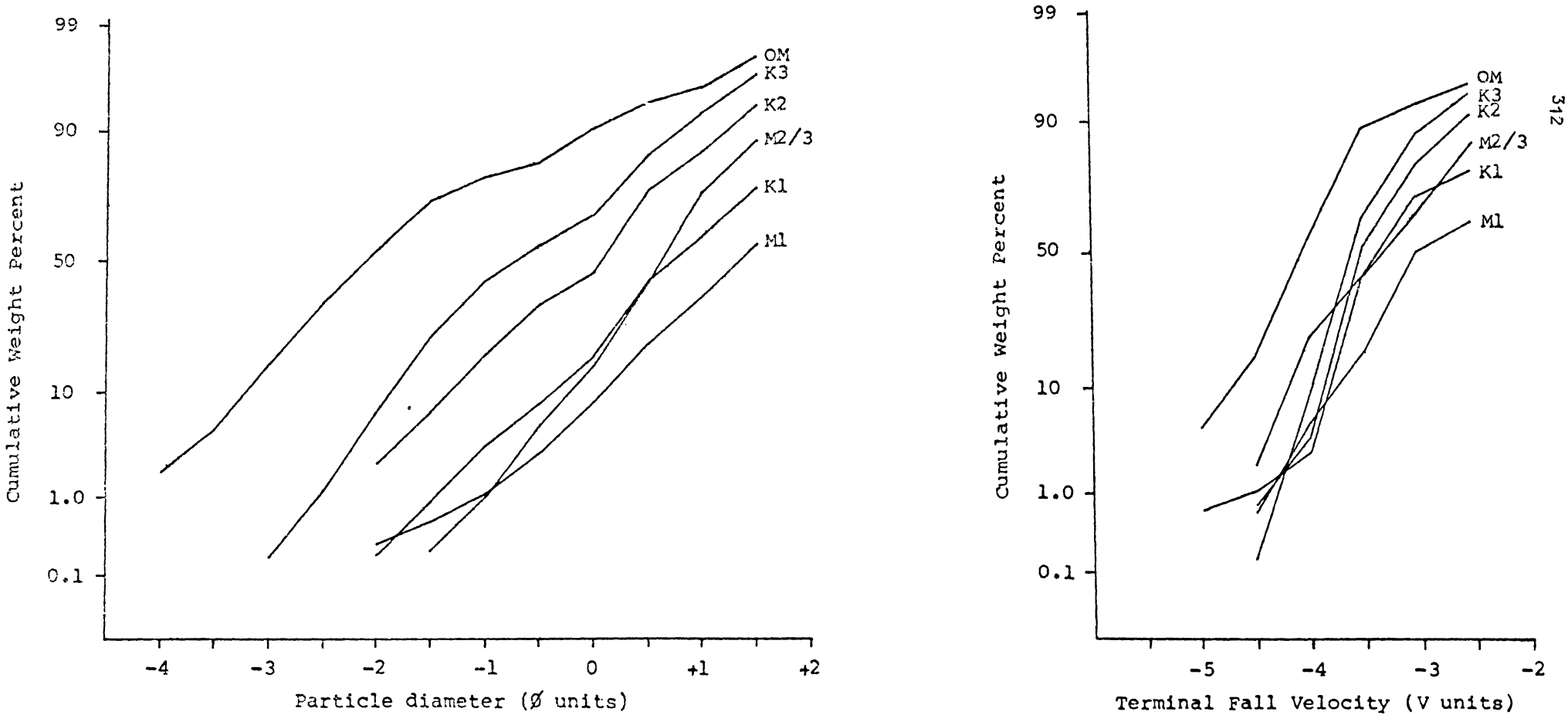


FIGURE E.7 : Particle size and Terminal fall velocity cumulative frequency curves for the coarser than 2Ø fraction of class II samples from the greater Whangamata area (see Figs. 4.6 and 4.7 ).

Note : $\emptyset = -\log_2 d$ , where d equals particle diameter in mm.

$V = -\log_2 \overline{TV}$ , where $\overline{TV}$ equals the terminal velocity in meters per second.

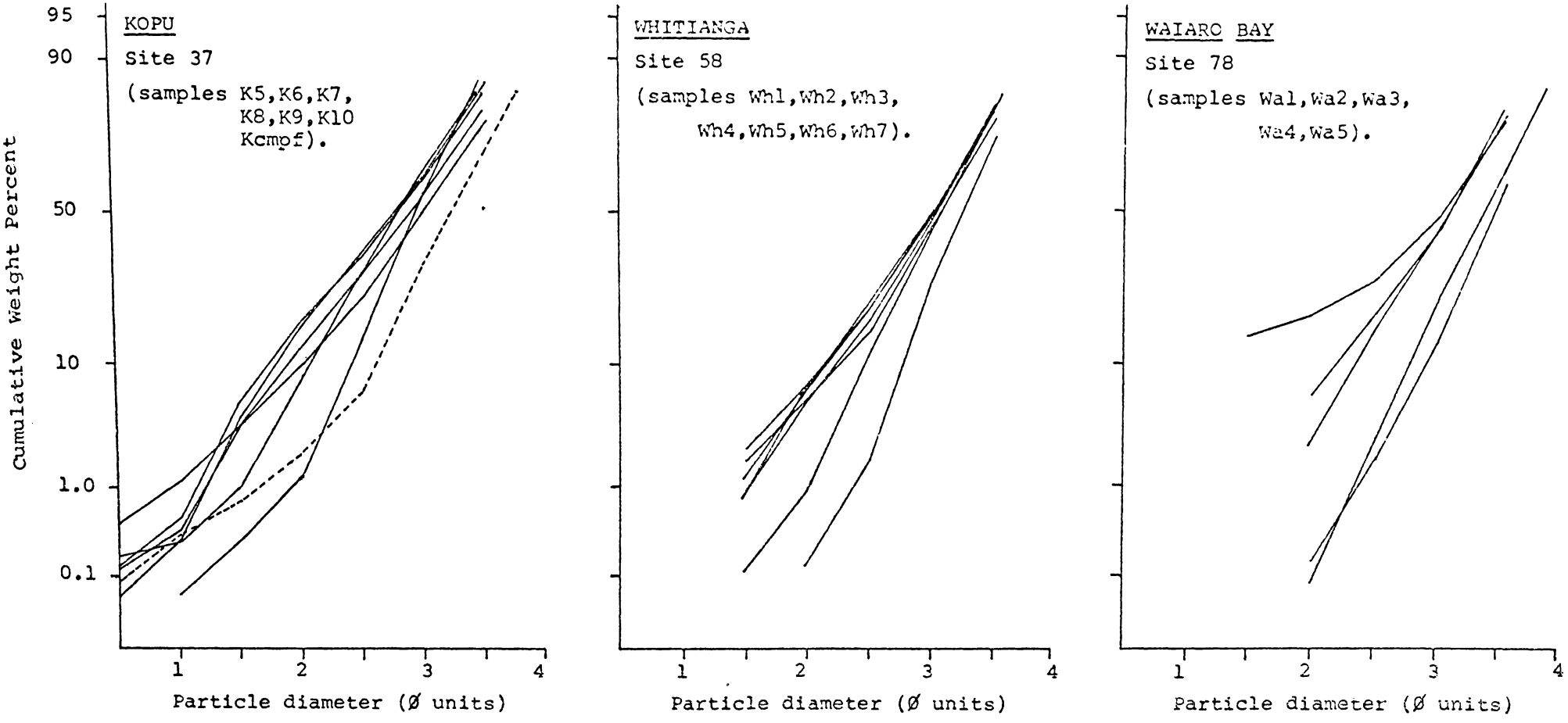


FIGURE E.9 : Particle size cumulative frequency curves of the coarser than 4Ø fraction of class III to V samples from Kopu, Whitianga and Waiaro Bay sites.(see Fig.4.16 p 139).

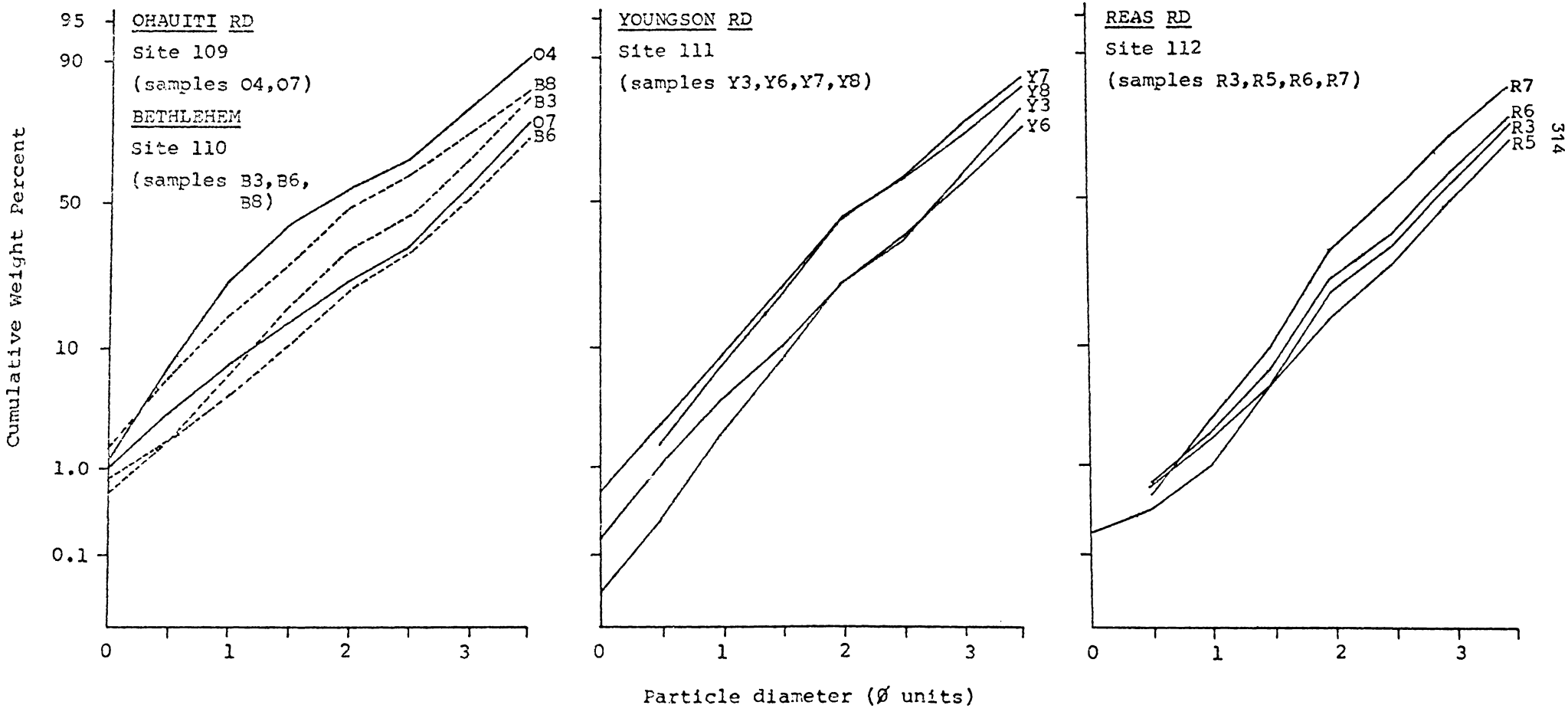


FIGURE E.10 : Particle size cumulative frequency curves for the coarser than 4Ø fraction of selected samples from the Katikati region (see 5.12).

TABLE E.1 : Weight percentage sand, silt and clay, and mean grain size for the tephras at the Pukekauri Rd stratigraphic column

| Sample | | Wt % Sand | | Wt % Silt | | Wt % Clay | | Mean grain size ($M_z$ Ø) |
|---|---|---|---|---|---|---|---|---|
| | | <4 Ø | >20 μm | 4–8Ø | 20–2μm | >8 Ø | <2 μm | |
| I | P1 | 48 | 64 | 35 | 24 | 17 | 12 | 4.75 |
| | P2 | 48 | 62 | 31 | 23 | 21 | 15 | 4.99 |
| I/II | P3 | 35 | 51 | 36 | 27 | 29 | 22 | 5.92 |
| II | P4 | 35 | 52 | 36 | 25 | 29 | 23 | 5.99 |
| | P5 | 35 | 51 | 37 | 27 | 28 | 22 | 5.98 |
| II/III | P6 | 28 | 43 | 37 | 30 | 35 | 27 | 6.61 |
| | P7 | 25 | 39 | 34 | 27 | 41 | 34 | 7.29 |
| III | P8 | 19 | 30 | 33 | 30 | 48 | 40 | 7.85 |
| | P9 | 16 | 26 | 31 | 30 | 53 | 44 | 8.33 |
| | P10 | 17 | 32 | 32 | 25 | 51 | 43 | 8.47 |
| | P11 | 21 | 40 | 37 | 24 | 42 | 36 | 7.67 |
| III/IV | P12 | 27 | 41 | 33 | 25 | 40 | 34 | 7.25 |
| | P13 | 30 | 46 | 34 | 24 | 36 | 30 | 6.75 |
| IV | P14 | 39 | 55 | 31 | 21 | 30 | 24 | 6.00 |
| | P15 | 44 | 56 | 27 | 20 | 29 | 24 | 5.81 |
| V | P18 | 75 | 86 | 19 | 9 | 6 | 5 | 3.10 |

Grain size divisions are after Folk (1968) - in phi units, and the New Zealand Soil particle size classes (in μm).

TABLE E.2 : Mean grain size and sorting coefficient (graphic standard deviation) for the coarser than 4 Ø fraction of the tephras at Pukekauri Rd

| Sample | | Mean Grain size ($M_Z$ Ø) | Graphic Standard Deviation (σ Ø) |
|---|---|---|---|
| I | P1 | 2.36 | 0.97 |
| | P2 | 2.31 | 0.98 |
| I/II | P3 | 2.27 | 1.24 |
| II | P4 | 2.35 | 1.21 |
| | P5 | 2.38 | 1.16 |
| II/III | P6 | 2.75 | 0.77 |
| | P7 | 2.85 | 0.78 |
| III | P8 | 2.94 | 0.75 |
| | P9 | 2.93 | 0.78 |
| | P10 | 2.81 | 0.86 |
| | P11 | 2.68 | 0.86 |
| III/IV | P12 | 2.55 | 0.83 |
| | P13 | 2.50 | 0.83 |
| IV | P14 | 2.40 | 0.86 |
| | P15 | 2.40 | 0.86 |
| V | P16 | 2.79 | 0.88 |
| | P17 | 2.41 | 0.56 |
| | P18 | 2.38 | 0.81 |

TABLE E.3 : Mean grain size and sorting coefficient (graphic standard deviation) for the coarser than 4 Ø fraction of selected samples from the Katikati region

| Site | Sample | Mean grain size ($M_z$ Ø) | Standard deviation ($O_G$ Ø) |
|---|---|---|---|
| Reas Rd (site 112) | R3 | 2.87 | 0.96 |
| | R5 | 2.99 | 0.94 |
| | R6 | 2.83 | 0.96 |
| | R7 | 2.56 | 0.91 |
| Youngson Rd (site 111) | Y3 | 2.76 | 0.91 |
| | Y6 | 2.81 | 1.04 |
| | Y7 | 2.34 | 0.99 |
| | Y8 | 2.33 | 1.09 |
| Bethlehem (site 110) | B3 | 2.52 | 1.05 |
| | B6 | 2.85 | 1.06 |
| | B8 | 2.17 | 1.23 |
| Ohauiti Rd (site 109) | O4 | 1.89 | 1.17 |
| | O7 | 2.70 | 1.08 |

# APPENDIX F

## REFERENCE SECTIONS

A. LATE QUATERNARY TEPHRAS OF THE COROMANDEL PENINSULA

B. LATE QUATERNARY TEPHRAS OF THE KATIKATI AND TE PUKE REGIONS

REFERENCE SECTIONS : A

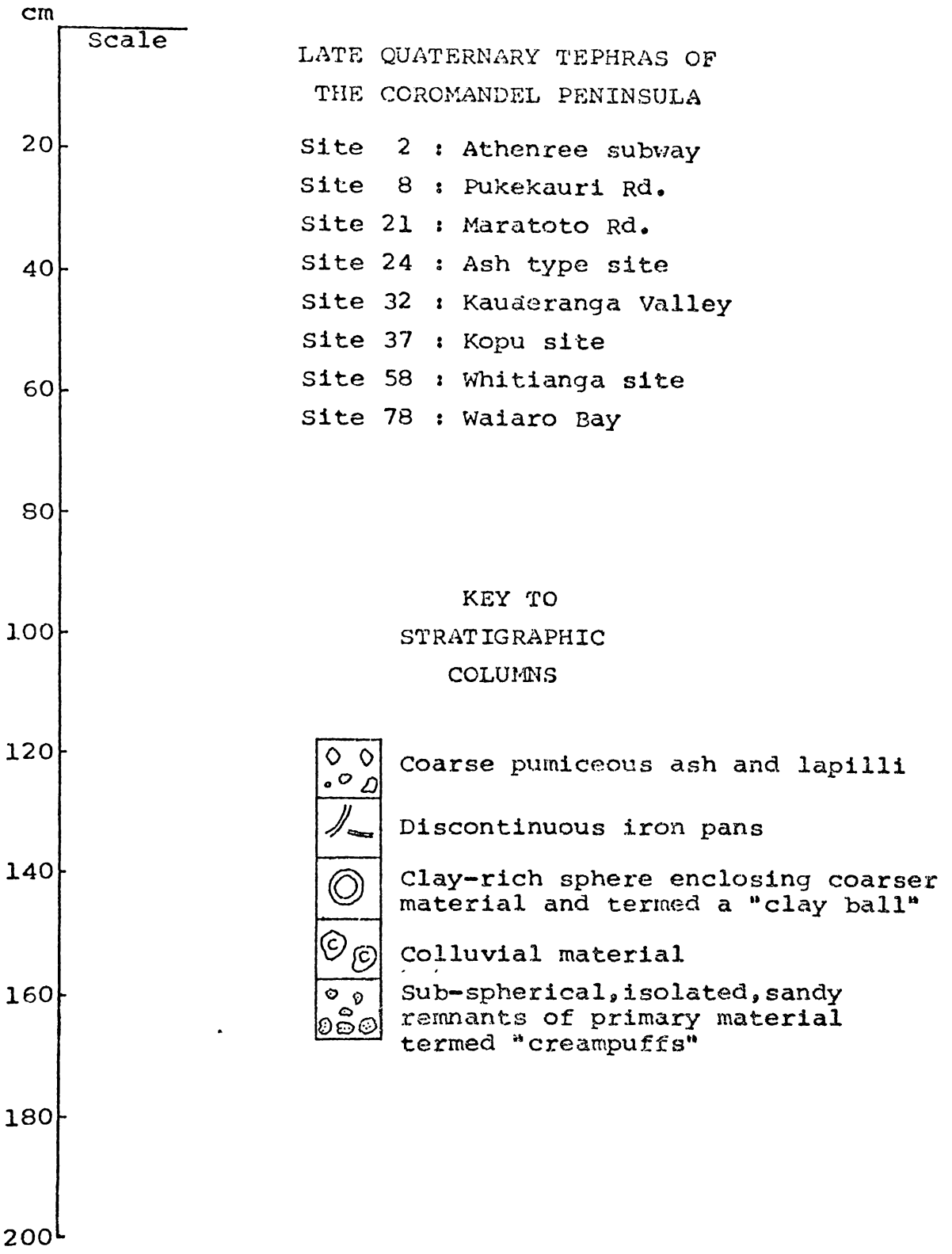


Note : The word "strongly" when applied to descriptions of soil structure, is often abbreviated to "str."

SITE 2 : ATHENREE SUBWAY (N53/365878)

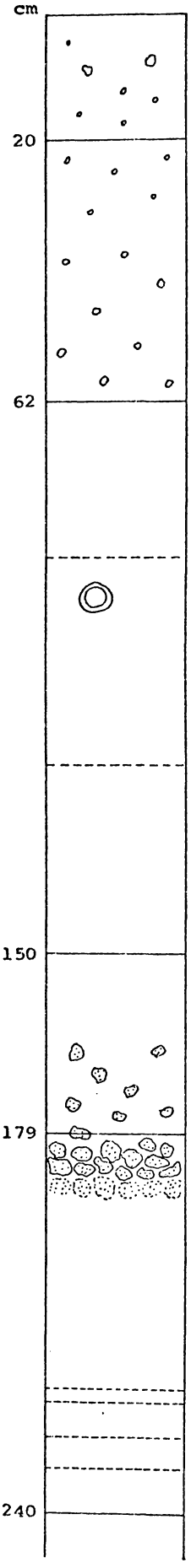

| | cm | |
|---|---|---|
| FIELD CLASS I | 0 | Black (10YR 2/2) sandy silt loam; friable; strongly developed fine and medium granular structure crushing to crumb; few fine (<1mm) orange yellow pumice grains; few medium (<5mm) white pumice grains; many fine roots; distinct boundary, |
| FIELD CLASS II | 20 | Bright brown (7.5YR 5/8) to yellowish brown (10YR 5/8) sandy silt loam; slightly sticky; friable to slighty firm; moderately developed medium and fine nutty structure with some coarse blocks all crushing moderately easily to fine crumb; many fine (<1mm) orange yellow pumice grains; few roots; indistinct boundary, |
| | 62 | Yellowish brown (10YR 5/6) silt loam; slightly sticky; slightly to moderately firm; moderately developed medium blocky structure with a few coarse blocks; many red-stained root channels; indistinct boundary, |
| FIELD CLASS III | 87 | Bright yellowish brown (10YR 6/6) silt loam; slightly sticky; moderately firm; weakly developed coarse and medium blocky structure; many root channels present; indistinct boundary, |
| | 120 | Bright yellowish brown (10YR 6/6) fine silt loam; slightly sticky; moderately firm to firm; very weakly developed coarse blocky structure tending towards massive; few small (<3mm) orange mottles increasing in concentration with depth; few dead roots; distinct boundary, |
| FIELD CLASS IV | 150 | Bright yellowish brown (10YR 6/6) silty sandy loam; slightly sticky; firm; weakly developed coarse blocky structure tending to massive; few dead roots; discontinuous mottle zone in upper 10cm; weathered surface characterised by clear crystals and redder colours; abundant creampuffs of sandy loam texture concentrated near the base; diffuse boundary, |
| | 179 | Bright yellowish brown (10YR 6/6) sandy loam matrix surrounding abundant creampuffs of sand and loamy sand texture; over |
| FIELD CLASS V | | Homogeneous and multiple-bedded sands and loamy sands; firm to very firm; massive crushing to single grain structure; distinct boundary, |
| | 240 | Pale blue clay |

SITE 8 : PUKEKAURI RD. (N53/303931)

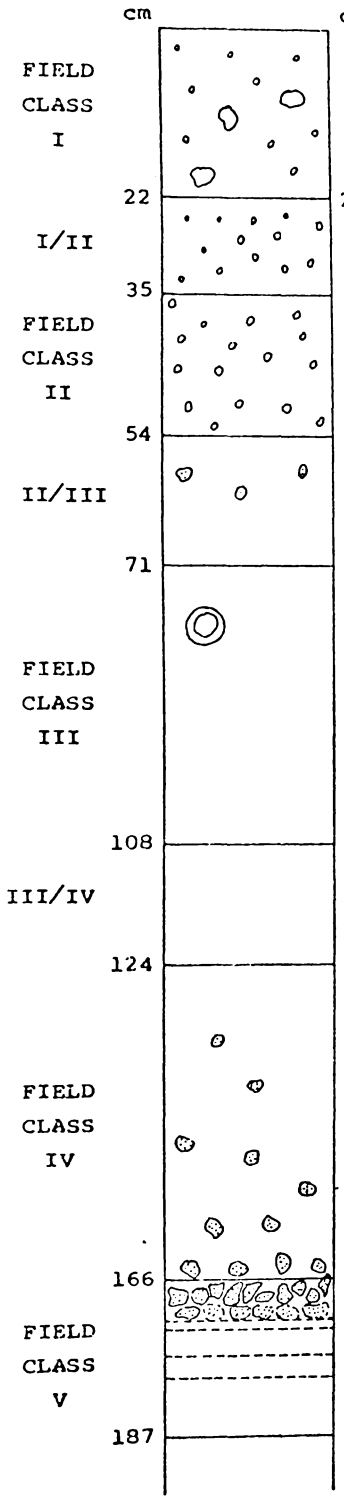


Brownish black (10YR 2/3) sandy loam; friable; strongly developed fine granular structure with some crumb; few medium (<5mm) white pumice grains (?Tp); many small (<1mm) orange yellow pumice grains increasing in concentration downwards; many fine roots; indistinct mixed boundary,

Yellowish brown (10YR 5/6) coarse sandy loam; friable; str. developed medium crumb and fine granular structure; abundant orange yellow pumice grains; indistinct boundary,

Bright brown (7.5YR 5/8) to yellowish brown (10YR 5/8) silty sandy loam; slightly sticky; friable; moderately developed fine crumb and medium to coarse nutty structure; many roots; abundant small (<3mm) orange yellow pumice grains; indistinct boundary,

Bright yellowish brown (10YR 6/8) fine sandy silt loam; fiable to slightly firm; moderately developed medium nutty structure with some crumb and minor coarse nuts; few medium (<10mm) grey creampuffs of fine sandy loam texture; distinct boundary,

Bright brown (7.5YR 5/8) to yellowish brown (10YR 5/8) silt loam; friable to slightly firm; moderately developed medium and coarse blocky structure with some nuts; few dead roots; minor clay balls; indistinct boundary,

Yellowish brown (10YR 5/8) silt loam; slightly sticky; slightly firm to friable; moderately developed fine, medium and coarse blocky structure; few dead roots; indistinct boundary,

Yellowish brown (10YR 5/8) silty sandy loam; slightly to moderately sticky; moderately firm to firm; weakly to moderately developed medium and coarse blocky structure; moderately abundant creampuffs, sandy loam to sand in texture, increasing in concentration with depth; weathered surfaces exhibit bright brown (7.5YR 5/8) colours and are flecked by fine (<1mm) clear crystals; diffuse boundary,

Homogeneous sandy loams, loamy sands and sands overlying shower-bedded sands; distinct boundary,

Grey mottled clay

SITE 21 : MARATOTO VALLEY (N53/245056)

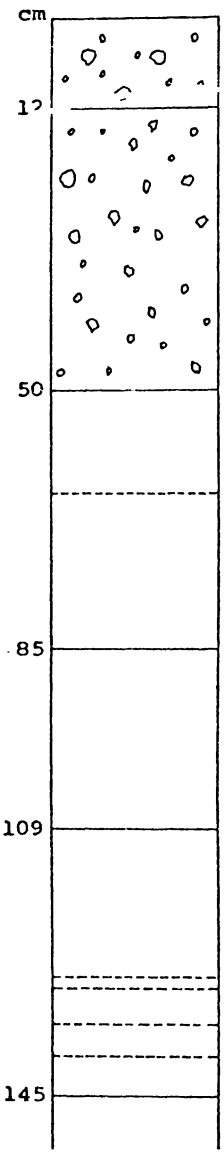

| | cm | | |
|---|---|---|---|
| FIELD CLASS I | 12 | 12 | Brownish black(7.5YR 2/2) sandy loam; very friable; strongly developed very fine crumb structure; few (<2mm) white pumice grains(?Tp); few medium (1cm) clear crystals-colluvium?; few small orange pumice grains; abundant roots; distinct boundary, |
| FIELD CLASS II | 50 | 50 | Brown (7.5YR 4/6) and dark brown (7.5YR 3/4) changing with depth into bright brown (7.5YR 5/8) silt loam; slightly gritty; friable; moderately developed medium nutty and fine crumb structure breaking easily into single grain; abundant to diffuse,small (<1mm) discrete pumice grains; moderate roots; indistinct boundary, |
| FIELD CLASS III | 85 | 64<br>85 | Bright brown (7.5YR 5/6) to yellowish brown (10YR 5/6) fine gritty silt loam; slightly firm; moderately developed medium and coarse blocky structure; few indistinct,medium (5-8mm) creampuffs; few to many roots; indistinct boundary,<br><br>Yellowish brown (10YR 5/6) to brown (10YR 4/6) silt loam; slightly sticky; moderately firm; moderately developed medium and coarse blocky structure; few root channels; indistinct boundary, |
| FIELD CLASS IV | 109 | 109 | Yellowish brown (10YR 5/8) sandy loam; firm; massive to weakly developed coarse and fine nutty to blocky structure; creampuffs become abundant with depth-sandy loam in texture, very firm; exposed surfaces flecked by clear crystals; diffuse boundary, |
| FIELD CLASS V | 145 | 145 | Multicoloured homogeneous and shower-bedded sandy loams, loamy sands and sands; firm;massive;distinct boundary,<br><br>Pallid blue clay |

SITE 24 : ASH TYPE SITE (N49/343179)

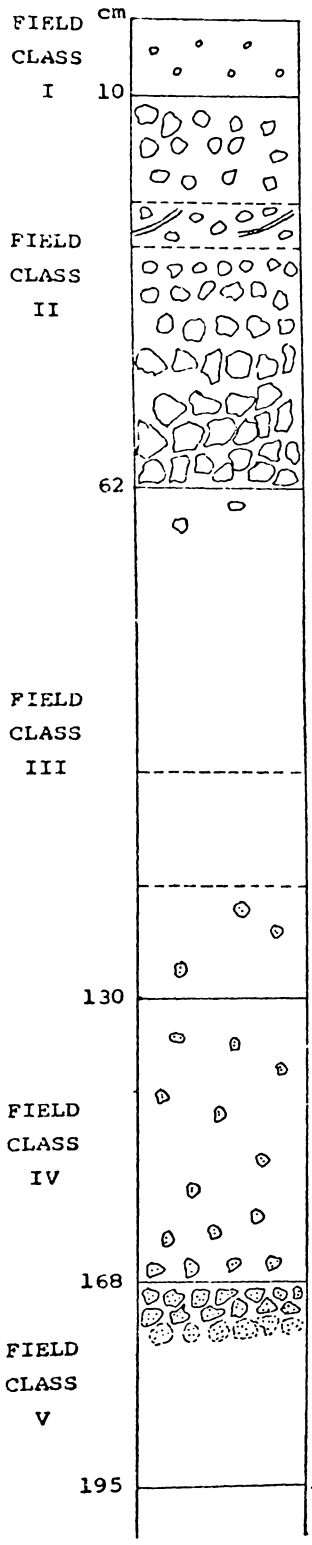


Black (10YR 1.7/1) gritty sandy loam; very friable; moderately to str. developed medium to fine crumb structure with some coarse granules; abundant 1-2mm clear crystals giving a "sugary" appearance; abundant fine and medium roots; many small (<3mm) orange pumice grains; variable thickness (10-20cm); distinct boundary,

Dull yellowish brown (10YR 5/4) coarse to fine lapilli and coarse pumiceous sand; very friable to loose; lapilli very easily crushed and often in an "egg-cup" structure; variable thickness (0-40cm); distinct boundary,

Dull yellowish brown (10YR 5/4) and dark reddish brown (5YR 3/6) coarse lapilli in a loamy matrix; friable; lapilli moderately firm; many small, discontinuous iron pans; indistinct boundary,

Dark reddish brown (5YR 3/6) very coarse lapilli (<30mm); lapilli weakly cemented insitu but loose on digging; lapilli firm to very firm; single-grained structure; lapilli external surface dark reddish brown in colour, internally bright brown (7.5YR 5/8); moderately abundant green obsidian fragments (average 3-8mm); distinct boundary but isolated lapilli occur in the upper 10cm of the silty bed below; lapilli normally graded,

Yellowish brown (10YR 5/6) clayey silt loam; slightly sticky; slightly firm to friable; moderately developed fine and medium nutty structure crushing to weakly developed crumb; few dead bracken roots; indistinct boundary,

Yellowish brown (10YR 5/6) slightly gritty silt loam; friable to slightly firm; moderately developed fine and medium nutty structure crushing to weakly developed crumb; indistinct boundary,

Yellowish brown (10YR 5/6) gritty silt loam; slightly firmer consistence; other properties as above; few grey creampuffs of fine sandy loam texture; distinct boundary,

Bright brown (7.5YR 5/8) to yellowish brown (10YR 5/8) silt loam; slightly firm; moderately developed medium and coarse nutty to blocky structure; the abundant creampuffs have bright brown (7.5YR 5/8) exteriors and bright yellowish brown (10YR 6/6) interiors,<5cm in diameter,and are very firm to firm coarse sandy loams; creampuff concentration increases with depth; indistinct boundary,

Generally, bright yellowish brown (10YR 6/6) sandy loams loamy sands and sands; firm; weakly to moderately developed coarse blocky structure breaking with some pressure to single grain; bright brown (7.5YR 5/8) staining around blocks; variable thickness; distinct wavy boundary,

Grey-brown clay

## SITE 32 : KAUAERANGA VALLEY (N49/108263)

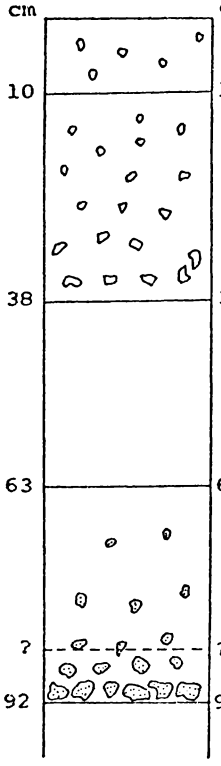


FIELD CLASS I

Brownish black (10YR 3/2) gritty silt loam; very friable; moderately developed fine crumb structure with a few medium nuts; few small orange pumice grains; abundant roots; indistinct boundary,

FIELD CLASS II

Brown (7.5YR 4/6) gritty silt loam; friable; moderately developed fine crumb structure with many medium nuts breaking with slight pressure to fine crumb; abundant small (<3mm) rotten yellow orange pumice grains; moderate roots; indistinct boundary,

FIELD CLASS III

Yellowish brown (10YR 5/8) silt loam; friable; slightly sticky; slightly firm; moderately developed medium and fine nutty structure with some fine crumb; indistinct boundary,

FIELD CLASSES IV & V

Yellowish brown (10YR 5/8) silt loam; friable to firm; moderately sticky; str. developed fine to medium nutty structure with some minor fine crumbs changing with depth to a weakly to moderately developed fine nutty and fine crumb structure; many small grey and yellow creampuffs becoming abundant with depth and of fine sandy silt loam texture; no clear division between field classes IV and V; distinct boundary below the creampuff zone,

Blue fine silt.

SITE 37 : KOPU SITE (N49/252285)

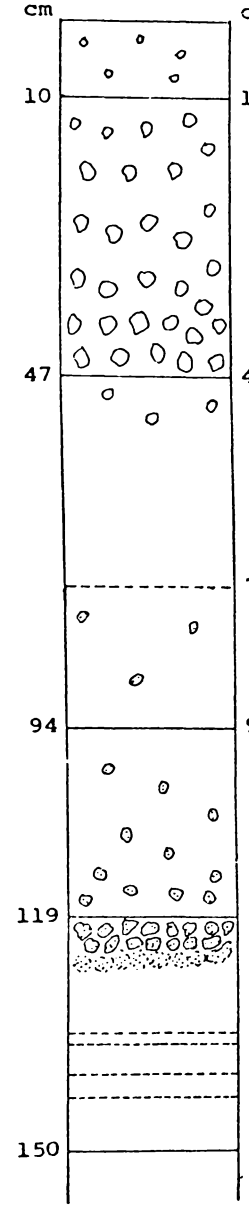

| | cm | | cm | |
|---|---|---|---|---|
| FIELD CLASS I | | | | Dark brown (7.5YR 3/3) sandy loam; very friable; strongly developed fine crumb structure with a few medium granules; many roots; abundant small (< 3mm) orange yellow pumice grains; indistinct boundary, |
| | 10 | | 10 | |
| FIELD CLASS II | | | | Reddish brown (5YR 4/6) to brown (7.5YR 4/6) gravelly pumice (<10mm); pumice coherent insitu; friable; moderately to str. developed fine and medium nutty structure crushing readily to fine and medium crumb; consistence becomes friable to slightly firm with depth; indistinct boundary, |
| | 47 | | 47 | |
| FIELD CLASS III | | | | Yellowish brown (10YR 5/6) very greasy silt loam; moderately firm; weakly to moderately developed medium and coarse nutty structure; few isolated red brown pumice grains; indistinct boundary, |
| | | | 75 | |
| | | | | Yellowish brown (10YR 5/8) silt loam; slightly firm; moderately developed medium and fine nutty structure crushing to weakly developed crumb; few indistinct grey creampuffs; indistinct boundary, |
| | 94 | | 94 | |
| FIELD CLASS IV | | | | Approximately equal amounts of matrix and creampuff. Matrix - Orange (7.5YR 6/8) to bright yellowish brown (10YR 6/8) medium to coarse sandy loam; slightly firm to friable; weakly developed coarse nutty structure breaking to blocky; Creampuffs - Bright yellowish brown (10YR 6/8) medium to coarse sandy loam; slightly sticky; very firm; |
| | 119 | | 119 | diffuse boundary, |
| FIELD CLASS V | | | | Bright yellowish brown (10YR 6/8) sandy loams and sands; very firm; weakly developed coarse blocky structure breaking to massive; distinct boundary, |
| | 150 | | 150 | Blue grey clay |

## SITE 58 : WHITIANGA SITE (N44/158585)

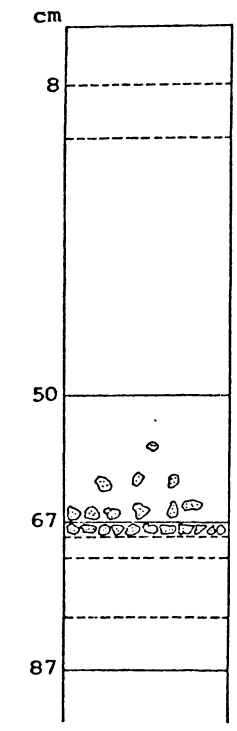


Black (7.5YR 2/1) silt loam; friable; weakly developed fine nutty structure; many roots; indistinct boundary,

Dark brown (10YR 3/4) silt loam; very friable; moderately developed fine and medium nutty structure; few roots; indistinct boundary,

Yellowish brown (10YR 5/8) to bright yellowish brown (10YR 6/8) clayey silt loam; friable to firm; moderately developed fine and medium nutty structure; indistinct boundary,

Bright brown (7.5YR 5/8) to bright yellowish brown (10YR 6/8) sandy silt loam; firm to very firm; diffuse boundary,

Compact grey and yellow shower-bedded sands; sharp boundary,

Grey clay

SITE 78 : WAIARO BAY (N39/924926)

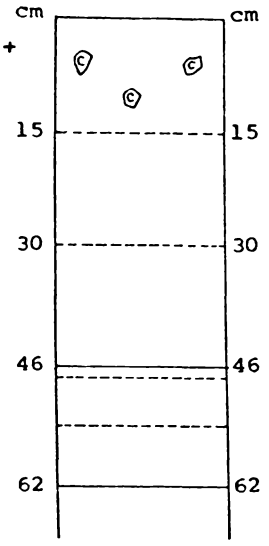


Brownish black (10YR 3/2) clay loam; friable to firm; moderately developed medium nutty structure with some granules; many roots; many coarse (<20mm) pebbles (?Colluvium); indistinct boundary,

Yellowish brown (10YR 5/6) clay loam; firm; bank exposures show coarse prisms which break readily to a moderately developed nutty structure; few roots; indistinct boundary,

Bright yellowish brown (10YR 6/6) clay loam; friable to firm; structureless; diffuse boundary,

Compact grey and yellow loamy sands

White clay

REFERENCE SECTIONS : B

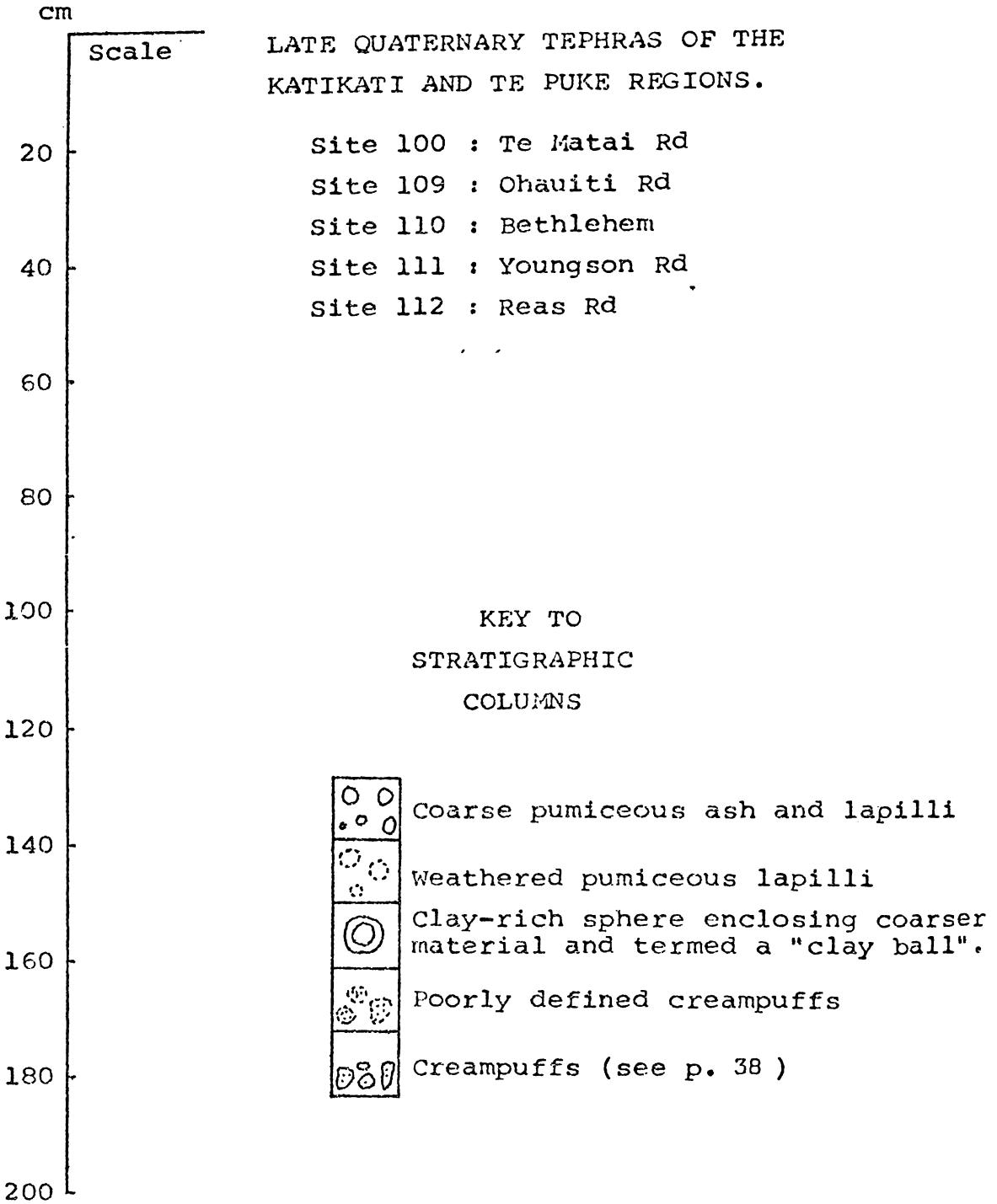

SITE 100 : TE MATAI RD (N67/779387)

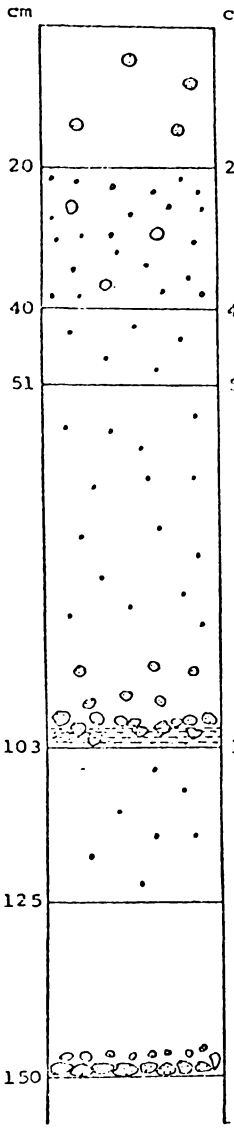


Black (7.5YR 2/1) sandy loam; very friable; strongly developed medium crumb and fine granular structure; many fine (<2mm) brown pumice grains increasing in concentration with depth; few moderately coarse (<20mm) brownish grey (7.5YR 5/1) creampuffs of sandy loam texture; many fine roots; distinct boundary,

Brown (10YR 4/4) coarse sandy loam (? loamy sand); very friable; strongly developed medium and coarse crumb structure crushing easily to single grain; abundant small (<2mm) brown pumice grains; few medium (<5mm) white pumice grains (?Tp) throughout; many fine roots; indistinct boundary,

Brown (10YR 4/6) sandy loam; friable; strongly developed medium and fine granular and medium crumb structure, tending toward single grain; abundant small (<2mm) brown pumice grains; diffuse boundary (gradational)

Yellowish brown (10YR 5/8) coarse sandy loam; friable; moderately developed medium and coarse nutty structure crushing readily to crumb; grading into

bright yellowish brown (10YR 6/8) coarse loamy sand; friable; weakly developed coarse nutty structure tending towards single grain; abundant medium (<3mm) pumice grains increasing in concentration with depth; many creampuffs increasing in concentration towards the sandy base of medium to coarse sandy loam texture; grading into

3cm (100 - 103cm) of bright yellowish brown (10YR 6/8) very coarse loamy sand; friable; weakly developed coarse nutty structure tending to single grain; diffuse boundary,

Brown (10YR 4/6) sandy loam and sandy silt loam; slightly sticky; weakly to moderately developed coarse and medium blocky structure; many white, small (<1mm) grains diminishing with depth; many moderately stained root channels; indistinct boundary,

Bright brown (7.5YR 5/8) to yellowish brown (10YR 5/8) sandy silt loam; slightly sticky; slightly firm; moderately developed coarse blocky and nutty structure; abundant red root channels; abundant bright yellowish brown (10YR 6/8) creampuffs of fine sandy loam texture, at the base (140 - 150cm); indistinct boundary,

Upper Quaternary tephras

## SITE 109 : OHAUITI RD (N67/656460)

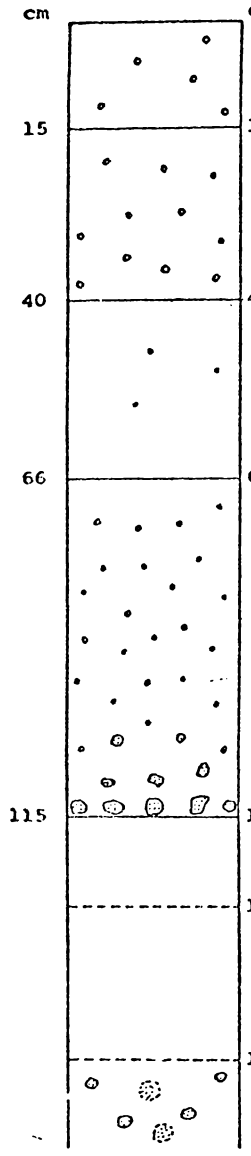


Black (7.5YR 2/1) gritty sandy loam; friable; strongly developed very fine crumb structure; abundant small (<1mm) grey pumice grains throughout; bed of variable thickness; few white pumice grains (<5mm) throughout; distinct boundary.

Dark brown (7.5YR 3/4 - 10YR 3/4) loamy sand; extremely friable (loose); single grained structure; abundant distinct, fine (<1mm) pumice grains; few fine and medium roots; distinct boundary.

Bright brown (7.5YR 5/6) to yellowish brown (10YR 5/6) sandy silt loam; friable; moderately developed fine, medium and coarse nutty structure; few small (<1mm) white pumice grains; indistinct boundary.

Yellowish brown (10YR 5/6) coarse loamy sand; slightly to moderately firm; moderately developed medium and coarse nutty and fine crumb structure; minor clay balls; abundant small (<1mm) white pumice grains throughout; few creampuffs near the base; indistinct boundary.

Brown (10YR 4/6) sandy silt loam; slightly firm; moderately developed medium and coarse blocky structure; few small (1-2mm) black crystals scattered throughout; indistinct boundary.

Characteristics as above. with the particle size becoming finer giving a slightly sticky silt loam; indistinct boundary.

Brown (7.5YR 4/6) gritty silt loam; moderately sticky; weakly developed coarse and fine blocky structure; abundant very weathered coarse orange pumice grains and pale grey coarse sandy creampuffs.

SITE 110 : BETHLEHEM (N50/590579)

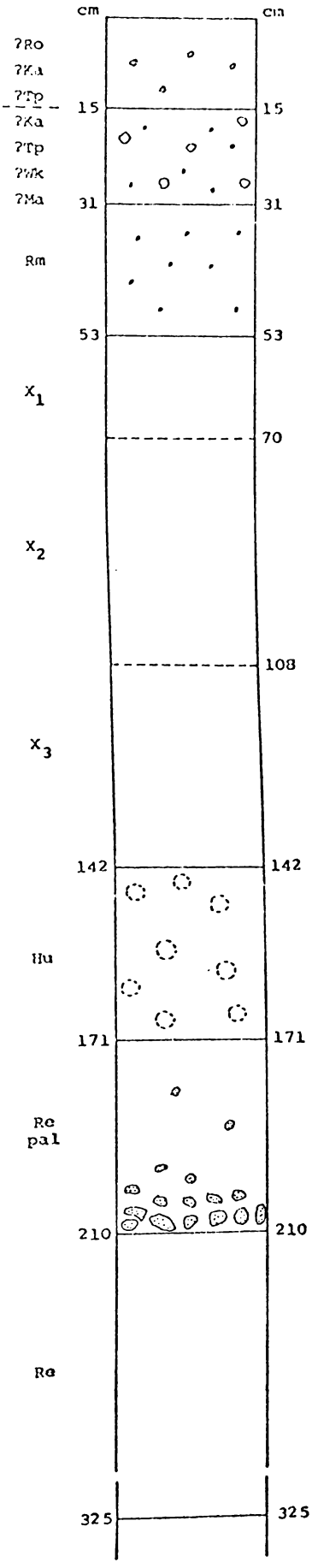


Black (5YR 1.7/1) sandy loam; very friable; moderately developed very fine crumb structure; abundant small (<2mm) pumice grains; abundant roots; distinct variable boundary.

Dark brown (7.5YR 3/4) gritty sandy loam; very friable; strongly developed very fine crumb structure; abundant 1-2mm pumice grains concentrated in pockets; few coarse pumice grains (3-4mm); few to many roots; distinct boundary.

Brown (7.5YR 4/6 - 10YR 4/6) silty sandy loam; friable; moderately developed coarse blocks and fine and very fine crumb structure; abundant small (<1mm) pumice grains throughout; many fine roots; weathered surface shows abundant white flecks (?pumice); indistict boundary.

Bright brown (7.5YR 5/6) sandy-silt loam; friable; moderately developed medium and coarse blocky structure; few roots; indistinct boundary.

Dull yellowish brown (10YR 5/4) to yellowish brown (10YR 5/6) silt loam; slightly sticky; friable; structure as above; few roots; indistinct boundary.

Properties as above, slightly firmer consistence; distinct boundary.

Bright brown (7.5YR 5/8) coarse sandy loam; friable; weakly to moderately developed medium and coarse nuts and blocks, crushing readily to coarse crumb structure; few roots; bed appearance suggests deeply weathered orange pumiceous lapilli; distinct boundary.

Yellowish brown (10YR 5/6) sandy silt loam; slightly sticky; friable to slightly firm; weakly developed medium and coarse nutty structure with some fine blocks; abundant pumice grains (<2mm) increasing in concentration with depth; many root channels; diffuse boundary.

Homogeneous and shower-bedded coarse lapilli and ash; loose consistence; massive; distinct boundary.

Brown clay

## SITE 111 : YOUNGSON RD (N58/496614)

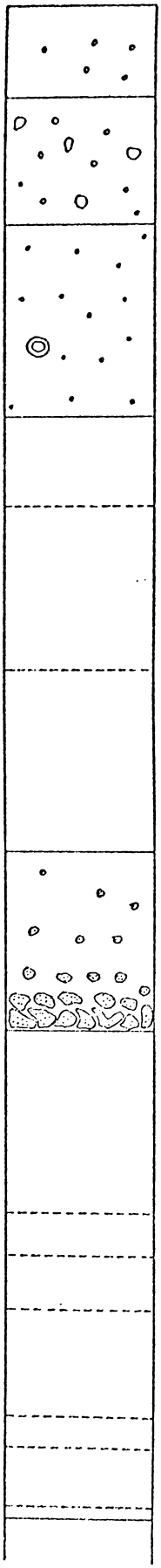

| | cm | |
|---|---|---|
| ?Ka<br>Tp | 15 | Black (5YR 1.7/1) gritty sandy loam; friable; moderately developed fine and medium crumb structure; few whitish yellow pumice grains (<10mm); many very fine (<1mm) white crystals throughout; many roots; distinct boundary, |
| ?Tp<br>?Wk<br>?Ma | 36 | Brown (7.5YR 4/4) coarse sandy loam; very friable (loose); strongly developed fine and very fine crumb structure; abundant 1-2mm yellow pumice grains throughout; many roots; many charcoal fragments; indistinct variable boundary, |
| Rm | 68 | Yellowish brown (10YR 5/6) sandy silt loam; slightly sticky; friable to slightly firm; weakly to moderately developed medium and fine blocky structure crushing readily to some fine crumbs; few roots; abundant fine (<1mm) white flecks (?pumice) especially on weathered faces; few clay balls present; indistinct boundary, |
| $X_1$ | 83 | Bright brown (7.5YR 5/8) to yellowish brown (10YR 5/8) silt loam; slightly sticky; friable; weakly to moderately developed coarse and medium blocky structure; few roots; indistinct boundary, |
| $X_2$ | 110 | |
| $X_3$ | 140 | Yellowish brown (10YR 5/6) silt loam; other properties as above; indistinct boundary, |
| Re pal | 170 | Brown (7.5YR 4/6-10YR 4/6) sandy silt loam; slightly firm; weakly to moderately developed coarse nuts and medium to fine blocks; creampuffs increasing in size and concentration with depth; weathered surfaces characterised by abundant, loose, clear and white crystals; diffuse boundary, |
| Re | 251 | Multi-coloured homogeneous sands and shower-bedded sands and loamy sands; firm; single grained structure; distinct boundary, |
| | | Brown clay (undifferentiated brown tuffs) |

SITE 112 : REAR RD (N57/379725)

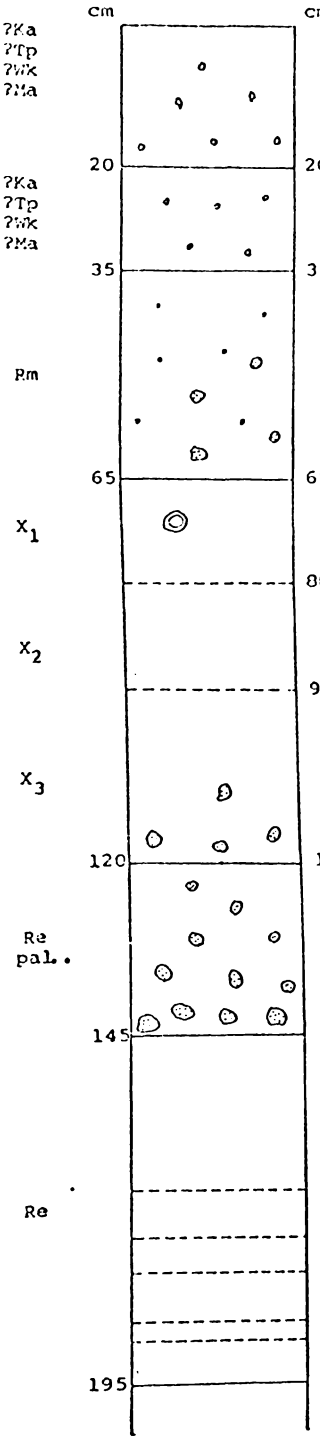


Black (5YR 1.7/1) gritty sandy loam; very friable; moderately developed medium and fine crumb structure; few pale yellowish white pumice grains (2-5mm); many coarse, medium and fine roots; distinct boundary,

Dark brown (10YR 3/3) sandy loam; very friable; moderately developed fine crumb structure; few pale white pumice grains in concentrated pockets (?Tp); many roots; indistinct boundary,

Bright brown (7.5YR 5/6) to brown (7.5YR 4/6) sandy silt loam; very friable to friable; moderately developed fine crumb structure; few fine (<1mm) white specks (? pumice grains) throughout; few greyish creampuffs (<2cm) of fine sandy texture throughout; few medium and fine roots; on external surfaces of cuttings, abundant fine (<1mm) pumice grains occur; indistinct boundary,

Yellowish brown (10YR 5/8) silt loam; friable; weakly developed medium and fine nuts crushing to fine crumb structure; few fine roots; few coarse clay balls ( approx. 2cm); indistinct boundary,

Brown (10YR 4/6) fine silt loam; friable to firm; remaining characteristics as above,

Brown (10YR 4/6) fine silt loam (slightly higher clay content than above); moderately firm to firm; structure as above;
115 - 120 cm : few reddish brown (5YR 4/6) coarse sandy creampuffs, Fe stained; indistinct boundary,

Brown (7.5YR 4/6) sandy loam; friable to firm; weakly to moderately developed fine and medium blocky structure; abundant coarse sandy creampuffs increasing in concentration with depth; diffuse boundary; external surface characterised by coarse columnar structure and abundant clear and white crystals,

Variably coloured shower-bedded coarse to fine sands; some exhibiting slight cohesion; firm; single grained structure; few infilled large plant channels; sharp boundary,

Brown sticky sand

# A : COROMANDEL TEPHRAS

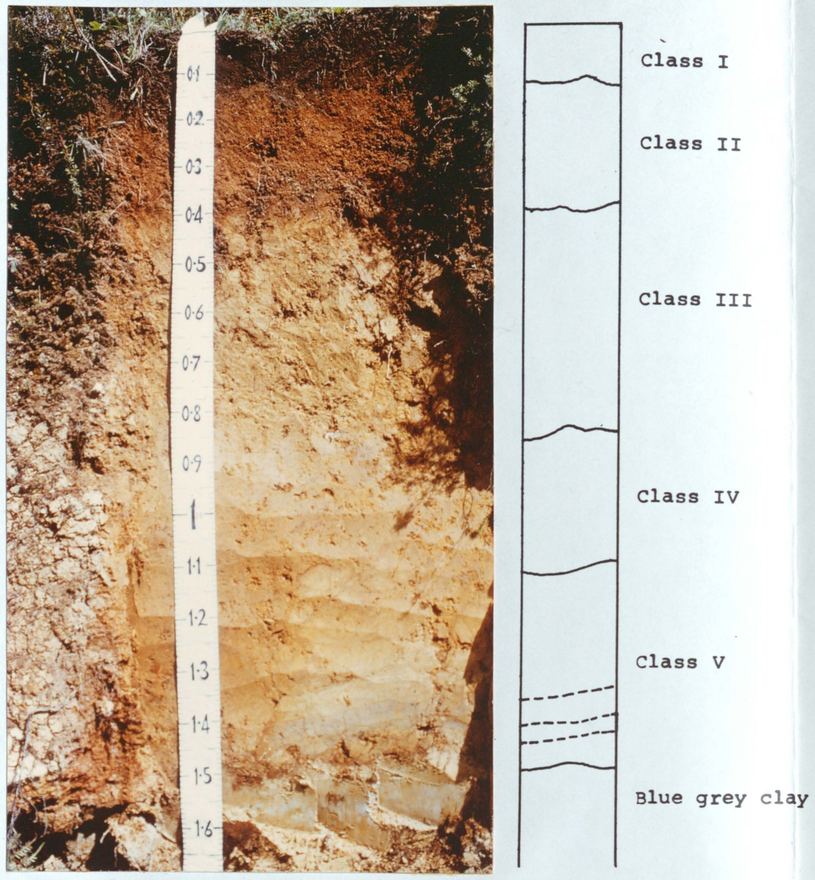


FIELD CLASS CHARACTERISTICS AT THE KOPU SITE

| Field Class | Field Name | Extent of distribution on the Peninsula | Generalised Field Characteristics | | | | |
|---|---|---|---|---|---|---|---|
| | | | Average range in thickness | Colour | Texture | Consistence | Structure |
| I | Recent bed | South of Whenuakite and beyond the southern boundary | 0-20 cm | Black | Gritty sandy loam | Very friable | Mod. developed fine crumb or fine granular structure |
| II | Pumiceous bed | South of Tairua and beyond the southern boundary | 0-60 cm | Dark reddish brown and dull yellowish brown lapilli | Coarse, fine, and very fine pumiceous lapilli | Loose | Massive (single grain) |
| | | | | Bright brown to yellowish brown ash | Coarse ash | Friable | Mod. developed fine crumb and and medium nutty structure |
| III | Silty bed | South of Whitianga and beyond the southern boundary | 32-57 cm | Yellowish brown to bright yellowish brown | Silt loam to clay loam | Friable to firm | Moderately developed medium nutty or blocky structure |
| IV | Lumpy bed | The entire length of Coromandel Peninsula at least as far north as Waiaro Bay | 18-40 cm | Yellowish brown to bright brown | Sandy loam to clay loam | Firm | Weakly to moderately developed coarse blocky structure |
| V | Shower-bedded class | | 13-40 cm | Bright yellow to grey, green and orange | Shower-bedded and massive sands and loamy sands | Firm to very firm | Massive (single grain) |

GENERALISED FIELD CLASS CHARACTERISTICS

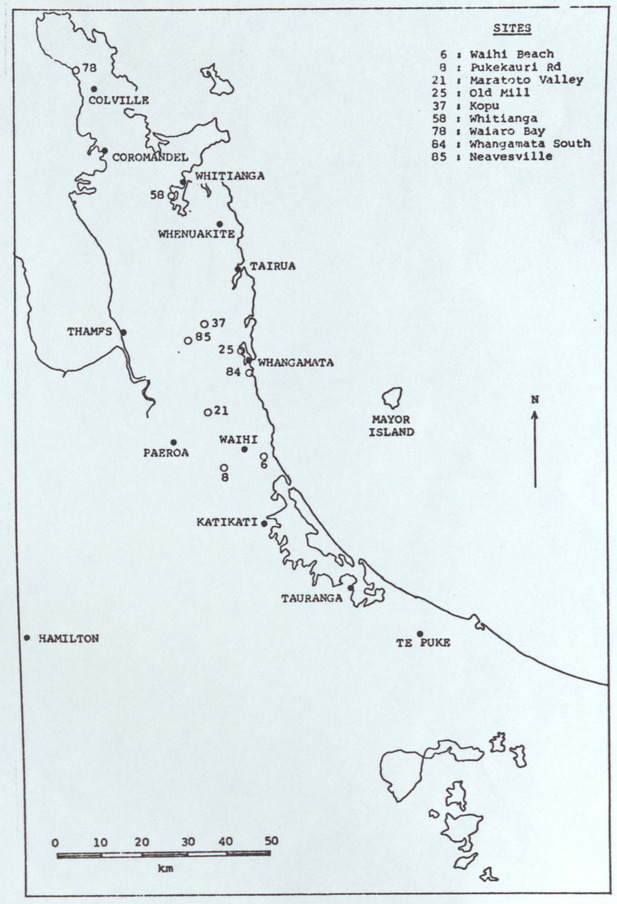


LOCALITY MAP

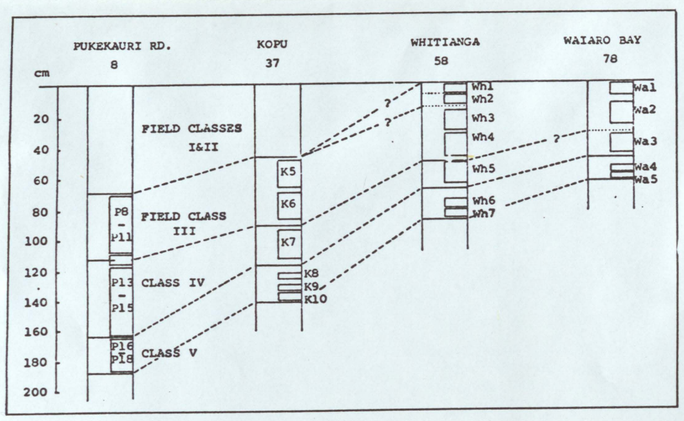


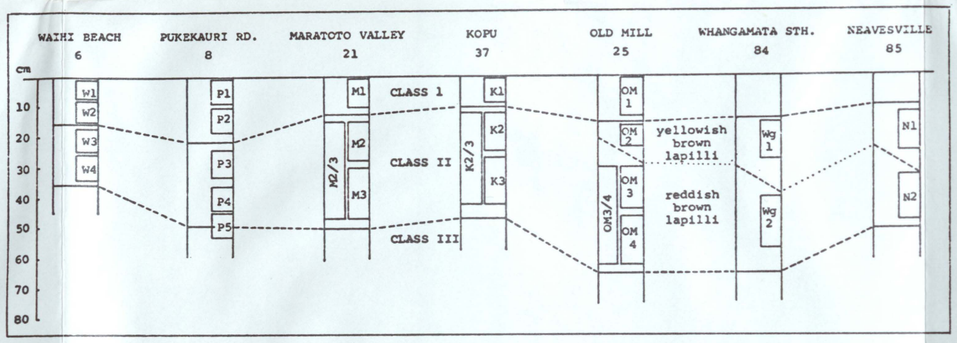


FIELD CLASSES, SAMPLE LOCATIONS, AND BED THICKNESSES

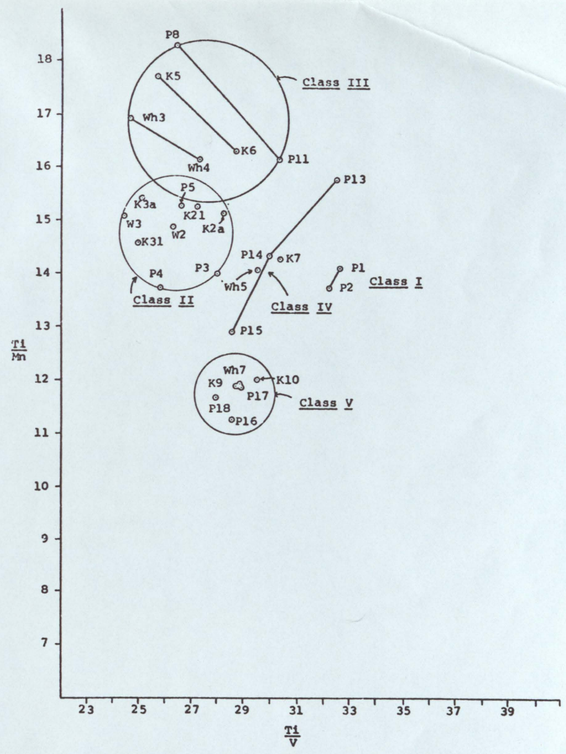


MULTI-PARTICLE TITANOMAGNETITE CHEMISTRY

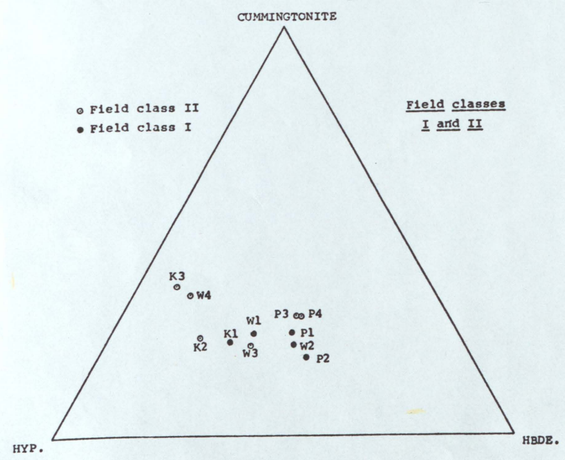


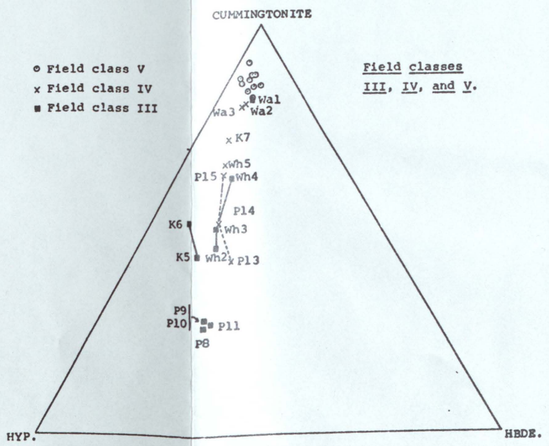


FERROMAGNESIAN MINERALOGY

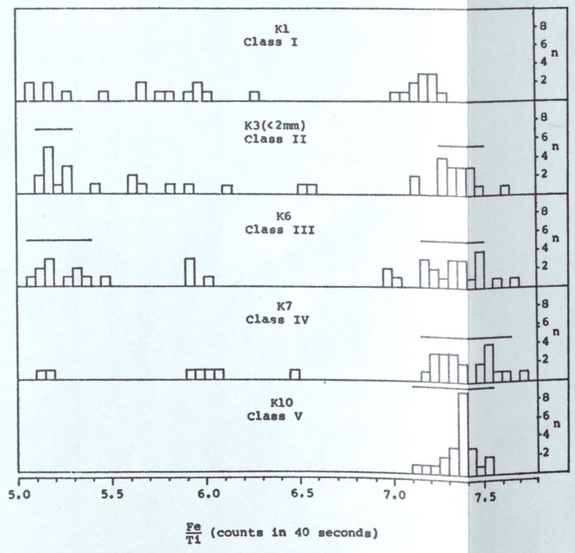


SINGLE-PARTICLE TITANOMAGNETITE CHEMISTRY

# B : KATIKATI-TE PUKE TEPHRAS

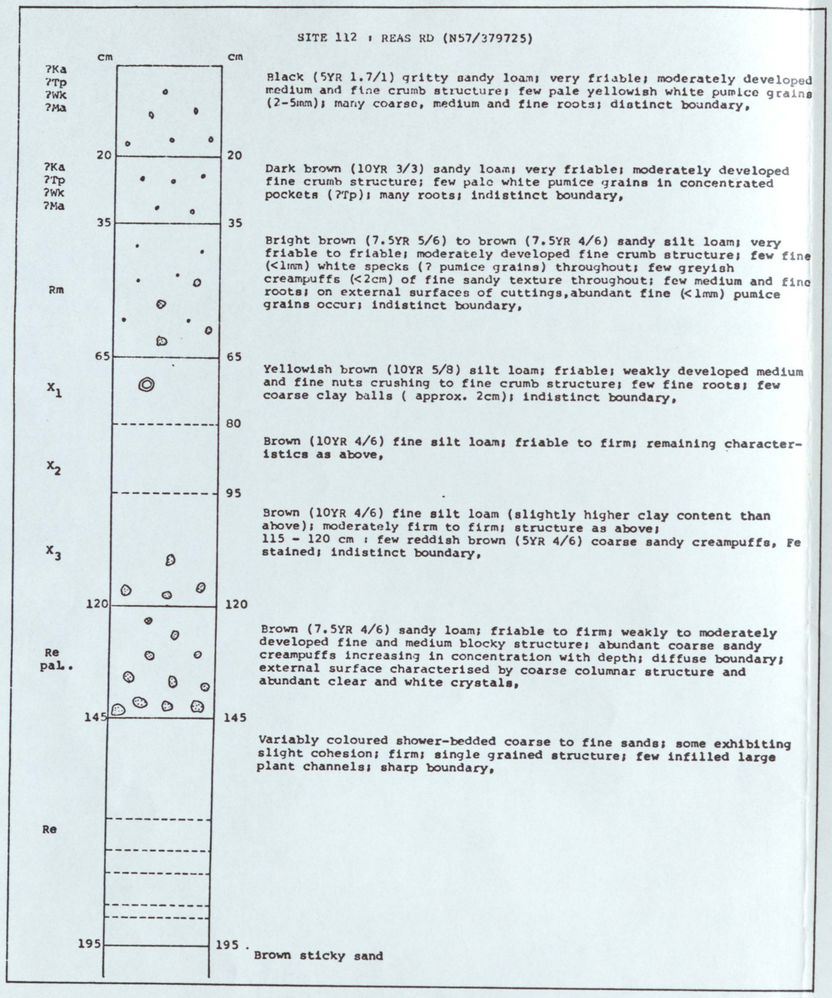


FIELD CLASS CHARACTERISTICS AT REAS RD

| Tephra | Symbol | Radiocarbon age (before 1950) | Radiocarbon number | Source |
|---|---|---|---|---|
| Rotomahana Mud | Trl | 64 | - | |
| Kaharoa Tephra | Ka | 930 ± 70 | NZ10 | Pullar et al. (1973) |
| Taupo Pumice | Tp | 1,819 ± 17 | Statistical mean of many dates | Healy (1964) |
| Rotokawau Ash | Rw | ? | | |
| Whakatane Ash | Wk | 5,180 ± 80 | NZ1066 | Pullar and Heine (1971) |
| Whangamata Tephra | Wg | 6,280 ± 70 | WK106 | This thesis |
| Mamaku Ash | Ma | 7,050 ± 77 | NZ1152 | Pullar and Heine (1971) |
| Rotoma-2 Tephra | Rm2 | ? | | |
| Rotoma Ash | Rm | c.9,000 | | Nairn, pers. comm. |
| Waiohau Ash | Wh | 11,250 ± 200 | NZ568 | Pullar et al. (1973) |
| Rotorua Ash | Rr | 13,450 ± 250 | NZ1615 | Pullar et al. (1973) |
| Okareka Ash | Ok | 20,700 ± 450 | NZ523 | Pullar and Heine (1971) |
| Te Rere Ash | Te | ? | | |
| Kawakawa Tephra | Kk | 19,850 ± 310 | NZ1056 | Pullar and Heine (1971) |
| Haupara Tephra | Hu | | | |
| Maketu Tephra | Mk | 30,100 - | | Pullar et al. (1973) |
| Tahuna Tephra | Ta | 42,000 | | |
| Ngamotu Tephra | Nt | | | |
| Rotoehu Ash | Re | 41,700 ± 3500 | NZ1126 | Pullar and Heine (1971) |

NAMED TEPHRAS AND THEIR AGES

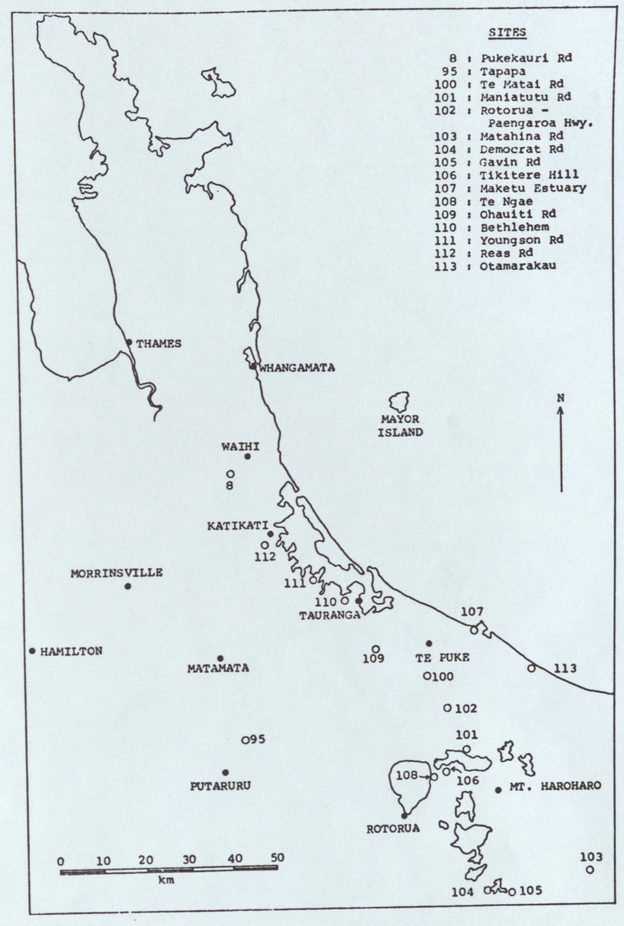


LOCALITY MAP

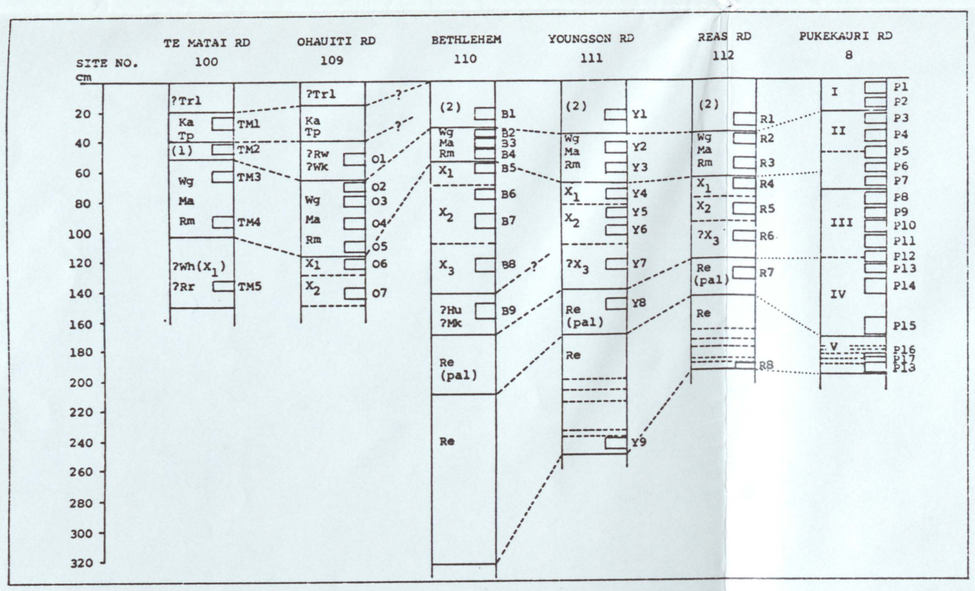


TEPHRA SAMPLE LOCATIONS AND BED THICKNESSES

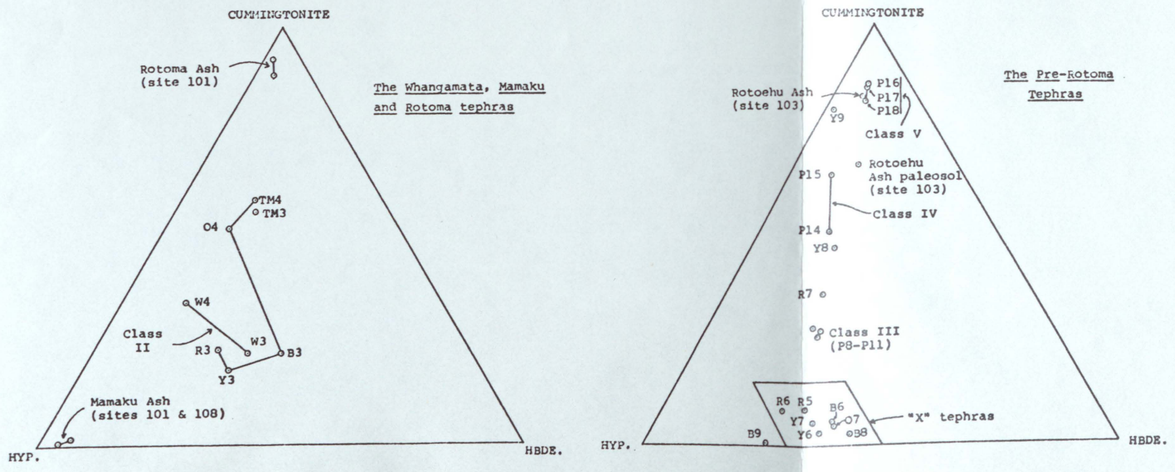


FERROMAGNESIAN MINERALOGY

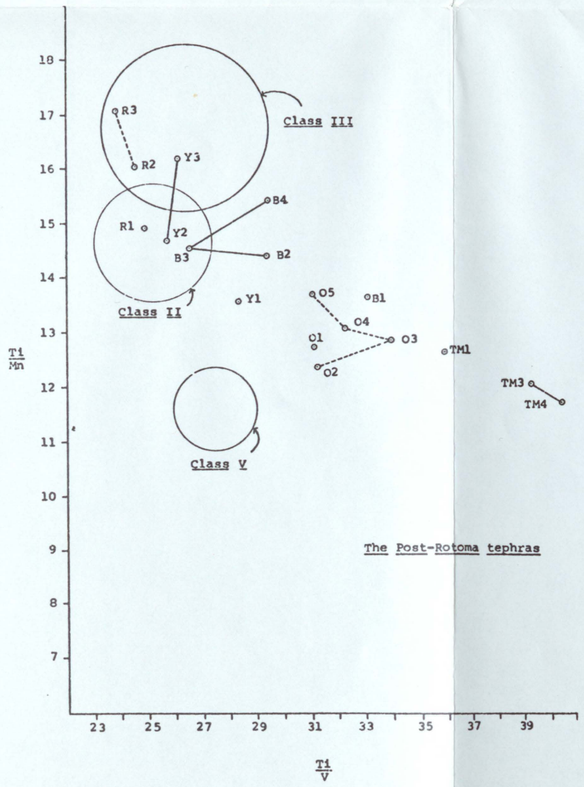


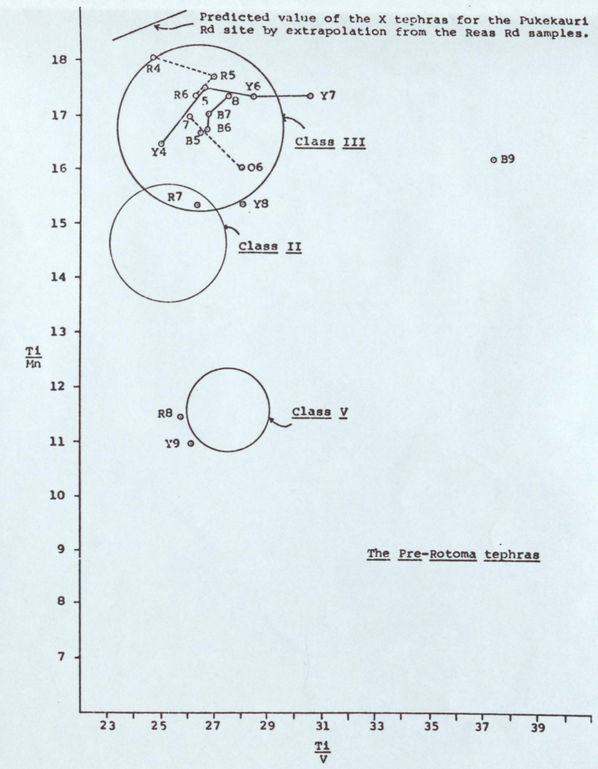


TITANOMAGNETITE CHEMISTRY